Climate variability and extremes in the Okavango River Basin, southern Africa

By

Oliver Moses

Supervisors:

Prof. Chris J.C. Reason

Dr. Ross C. Blamey

Thesis presented for the degree of **Doctor of Philosophy** in the Department of Oceanography, Faculty of Science,

University of Cape Town

June 2023

Funding

I sincerely thank the University of Botswana for funding my PhD.

Plagiarism declaration

I know the meaning of plagiarism and declare that all the work in the thesis, save for that which is properly acknowledged, is my own. This thesis contains less than 80,000 words including appendices, bibliography, footnotes, tables and equations, and has less than 150 Figures.

I confirm that I have been granted permission by the University of Cape Town's Doctoral Degrees Board to include the following publication(s) in my PhD thesis, and where co-authorships are involved, my co-authors have agreed that I may include the publication(s):

Moses, O., Blamey, R.C., Reason, C.J.C., 2022. Relationships between NDVI, river discharge and climate in the Okavango River Basin region. *International Journal of Climatology* 42(2), 691-713.

Moses, O., Blamey, R.C., Reason, C.J.C., 2022. Extreme rainfall events over the Okavango River basin, southern Africa. *Accepted, Weather and Climate Extremes*.

Moses, O., Blamey, R.C., Reason, C.J.C., 2022. Drought metrics and temperature extremes over the Okavango River basin, southern Africa, and links with the Botswana High. *Under Review, International Journal of Climatology*.

Signature: Signed by candidate **Date:** 2 June 2023

Student Name: Oliver Moses **Student Number:** MSSOLI001

Abstract

The Okavango River Basin (ORB) located in southern Africa is a region of highly sensitive and biodiverse ecosystems. It spans Angola, Namibia and Botswana, with the world-famous Okavango Delta located in the latter country. The ecosystems depend on the highly seasonal ORB streamflow, which is also the major source of freshwater for the rural population, most of whom depend on subsistence farming. Climate variability and extremes such as droughts, hot days and extreme rainfall events are not well understood over this region. Also, the relationship between climate and other aspects like vegetation and river discharge are not well understood. To contribute to a better understanding of this relationship, the thesis investigated relationships between rainfall, temperature, Normalized Difference Vegetation Index (NDVI) and river discharge, and their interannual variability and trends.

It was found that at monthly and seasonal time scales, NDVI spatial patterns are closely related to those of rainfall than temperature. The NDVI-rainfall and NDVI-temperature relationships differ north of 18.9°S where rainfall is higher than to its south. Correlations between NDVI and rainfall show lags of 1-2-months. Large areas across the region show significant warming trends in all seasons but mainly in October-December (OND), as well as wetting mainly in the north. The warming trend may imply more evaporation and desiccation which may exacerbate extreme event impacts such as severe droughts. Interannual variability of rainfall, NDVI and temperature is pronounced with significant correlations with El Niño-Southern Oscillation (ENSO), the subtropical Indian Ocean Dipole (SIOD) and the Botswana High for rainfall and temperature, and for NDVI with ENSO. The temperature (rainfall) correlations with ENSO and the Botswana were positive (negative), with the SIOD they were negative (positive), and the NDVI-ENSO correlations were negative. On longer time scales, the wet 2006-2013 period was analysed relative to much drier 1999-2005 epoch for OND. The 2006-2013 wetter conditions appear linked to La Niña Modoki conditions, regional circulation differences and warmer sea surface temperature near Angola.

Extreme rainfall events over the ORB were analysed. The analysis was performed within a larger region in western central southern Africa (WCSA), given that many rainfall events extend beyond river basin boundaries. Focus was placed on extreme rainfall events accumulated over 1-day (DP1) and 3-days (DP3), during the main rainy season, January-

April (JFMA). Due to data sparsity, the Climate Hazards Group Infrared Precipitation with Station data (CHIRPS) were used to identify these events.

It was found that contributions of DP1 and DP3 events to JFMA rainfall totals are, on average, ~10% and ~17%, respectively, but in some years their contributions exceed 30%. Most of the events result from tropical-extratropical cloud bands, with tropical lows being also important. Interannual variability in extreme events is substantial and appears linked to ENSO and the Botswana High. Although ENSO influences the extreme events and rainfall totals more generally over southern Africa, by far the neutral JFMA 2017 season experienced the wettest conditions over the world-famous Okavango Delta region. Factors that contributed to these heavy rains included a deeper Angola Low, weaker mid-level Botswana High and anomalous westerly moisture fluxes from the tropical southeast Atlantic during January – early March. The second most intense rainfall event occurred on April 22nd, resulting from a cut-off low. DP1 frequencies show significant increasing trends, and similarly, rain-days and rain totals over many areas. These trends have important implications for agricultural and water management as well as wildlife conservation in the ORB.

To contribute to a better understanding of drought over the ORB region, the thesis analysed various drought metrics. These include a Cumulative Drought Intensity (CDI) index, based on the product of maximum dry spell duration and maximum temperature anomaly, and the Standardised Precipitation-Evapotranspiration Index (SPEI). Strong horizontal gradients in frequencies of dry spells and hot days were found to shift south over the ORB from August to November as the tropical rain-belt shifts increasingly south of the equator, the Congo Air Boundary declines and the Botswana High strengthens and shifts southwestwards. By December, the tropical gradient in dry spell frequencies is unnoticeable while that across the Limpopo River and southern ORB region, where the Botswana High is centred, stands out. On seasonal time scales, October-November 2013-2021 is particularly hot and dry over the Okavango Delta region. The thesis provided evidence that this hot and dry epoch is related to a stronger and southward shifted Botswana High and reduced low-level moisture convergence. On interannual time scales, there were strong relationships with the Botswana High, and to lesser extent ENSO. A strong drying-warming trend was found in the early summer, linked to a significant strengthening of the Botswana High. These trends, in conjunction with the Coupled Model Intercomparison Project Phase 6 (CMIP6) projected early summer drying over southern Africa found in the literature, may impact severely on the sensitive ecosystems of the ORB, and on water availability as well as subsistence farming in the region.

Acknowledgements

Many thanks to the University of Botswana for funding my PhD. To my supervisors, Prof. Chris J.C. Reason and Dr. Ross C. Blamey, many thanks for your support, hard work and tireless guidance throughout my PhD. To the staff and fellow students of the Oceanography Department, thank you all for your support. In particular, Dr. Raymond Roman, thanks so much for your IT support. To my friend Lynnette, many thanks to you and your family for making my stay in Cape Town an enjoyable one by assisting me in various ways, like storing my luggage at your place when I had visited my family in Botswana, and at times, you took me to the airport. To my Botswana friends, Ian and Shadrack, and many others, thank you for your support. To my family, I cannot thank you enough, but thank you for taking care of family projects while I was busy studying, which otherwise would have collapsed.

Last but not least, I would like to thank the various organisations that provided datasets used in the analysis. The datasets are provided in the following websites:

CHIRPS https://www.chc.ucsb.edu/data/chirps
PERSIANN-CDR https://chrsdata.eng.uci.edu
NCEP circulation fields and OLR https://www.psl.noaa.gov/data/gridded
NDVI https://ecocast.arc.nasa.gov/data/pub/gimms/3g.v1
2m air temperature https://psl.noaa.gov/data/gridded/data.ghcncams.html
Niño 3.4 index https://origin.cpc.ncep.noaa.gov
Topographical data https://www.ngdc.noaa.gov/mgg/global
River discharge www.okavangodata.ub.bw/ori
SASSCAL http://data.sasscal.org
GridSat https://www.ncei.noaa.gov/data/geostationary-ir-channel-brightness-temperature-gridsat-b1/access
IBTrACS https://www.ncdc.noaa.gov/ibtracs
TRMM https://disc.gsfc.nasa.gov/datasets
ERA5 data https://cds.climate.copernicus.eu
SPEI http://spei.csic.es/index.html
NOAA Optimally Interpolated SST
https://psl.noaa.gov/data/gridded/data.noaa.oisst.v2.highres.html

The Botswana and Namibia Meteorological Services provided station data, the South African Weather Service provided synoptic weather maps, and the Botswana Disaster Management Office provided flood impact data.

List of Tables

List of Figures

Table of Contents

Chapter 1: Introduction

The Okavango River Basin (ORB) (blue polygon in **Figure 1.1b**), stretching from Angola through Namibia to Botswana, contains unique rivers in the sense that it does not flow into the ocean, but it terminates in the latter country. The basin water is lost in various ways such as through evapotranspiration and infiltration to be part of underground water (McCarthy and Metcalfe, 1990; Murray-Hudson et al., 2006). The terminal section of the ORB contains the world-famous Okavango Delta, which is a United Nations Educational, Scientific and Cultural Organization (UNESCO) site, and it is also a Ramsar site, well-known for its highly biodiverse and sensitive ecosystems (Murray-Hudson et al., 2006; UNESCO, 2014). These ecosystems crucially depend on the highly seasonal streamflow originating mainly in the Angolan Highlands (high rainfall zone) shown in **Figure 1.2**, which receives higher rainfall than the Okavango Delta region located in Ngamiland district (**Figure 1.2**) in northwestern Botswana (low rainfall zone) (McCarthy et al., 2003; Andersson et al., 2003, 2006; Kgathi et al., 2006; Murray-Hudson et al., 2006). The ORB streamflow is also a critically important source of freshwater for the rural population, most of whom rely on subsistence farming as it is the case over southern Africa generally. Previous studies indicated that future development initiatives in the ORB riparian states (Andersson et al., 2006; Kgathi et al., 2006; Hughes et al., 2011), as well as population growth (Weinzierl and Schilling, 2013), are likely to increase water extraction from the ORB, hence there is need to better understand the climate of this basin.

Most of southern Africa (except the far southwest and the south coast of South Africa) experiences rainfall from October to March or April. Rainfall totals range from ~1000 mm/year in the Angolan Highlands to ~450 mm/year in the Okavango Delta located in Ngamiland district (see **Figures 1.1b** and **1.2** for locations). Generally, temperatures are high particularly over Botswana where daily maximums can exceed 42°C (Moses and Gondwe, 2019).

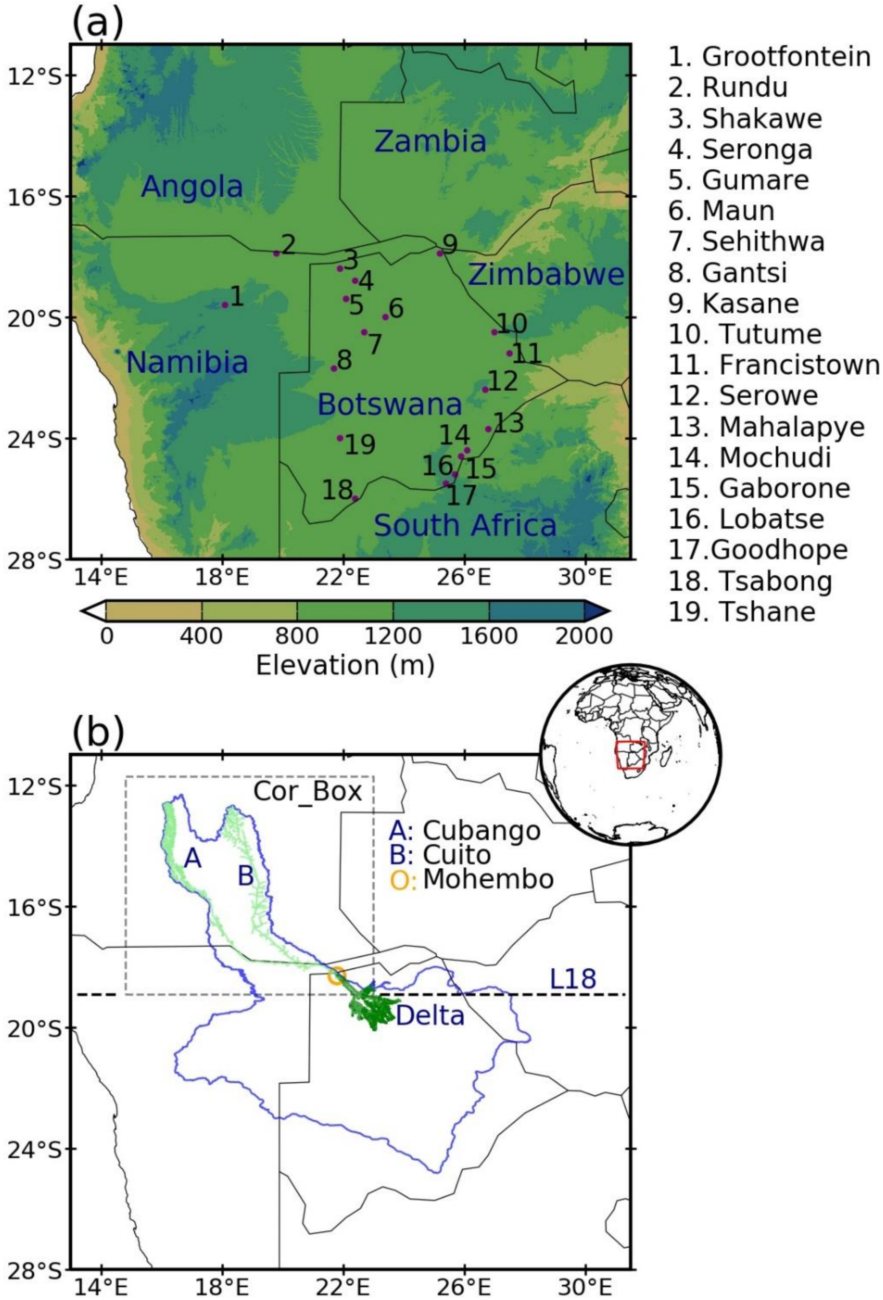

Figure 1.1 (a) The ORB region (11°-28°S, 13°-31.5°E), its surface elevation and the selected rainfall stations numbered 1 to 19 (full names shown on the right of the figure). (b) The spatial extent of the Okavango River catchment (blue polygon) and the location of the Okavango Delta and the two main rivers, the Cubango and Cuito (denoted by “A” and “B”, respectively). The circle just to the north of the Delta denotes Mohembo hydrological station. “L18” is the 18.9°S latitude dividing the study area into high and low rainfall zones. Cor_Box (11.7°-18.9°S, 14.8°-23°E) is the area mainly upstream of Mohembo which includes the northern Okavango catchment. This figure is discussed further in Chapter 4.

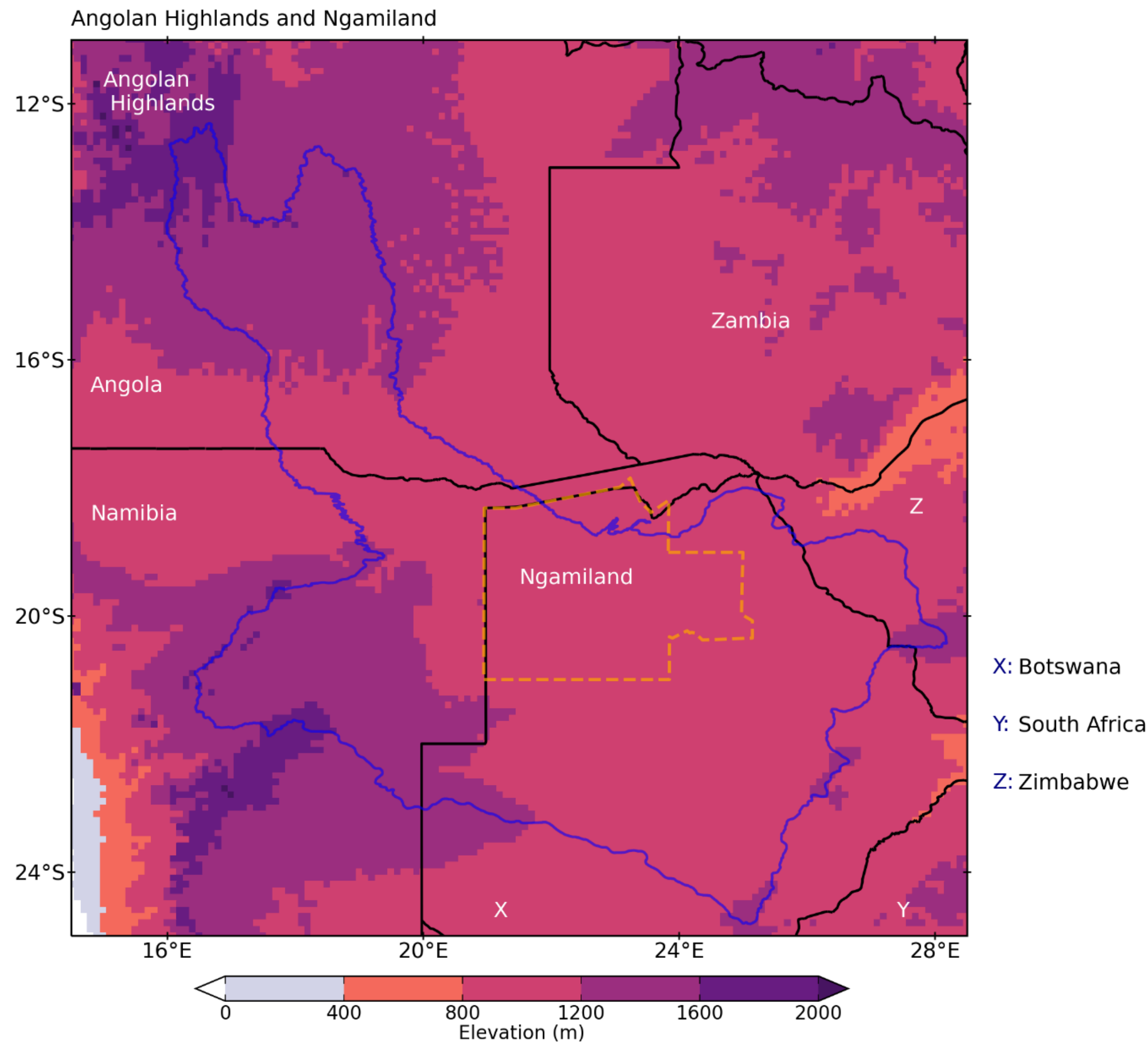

Figure 1.2 Locations of the Angolan Highlands and Ngamiland district in northwestern Botswana.

Rainfall is caused mainly by tropical-extratropical cloud bands, also known locally as tropical-temperate troughs (Harrison, 1984; Hart et al., 2010, 2013, 2018; Macron et al., 2014), which are triggered by the Angola Low by providing the moisture at early stage of their development (Munday and Washington, 2017; Crétat et al., 2018). Other important systems contributing to rainfall include mesoscale convective systems (MCSs; Blamey and Reason, 2012, 2013; Morake et al., 2021) and tropical lows (Munday and Washington, 2017; Howard et al., 2019; Howard and Washington, 2020; Rapolaki et al., 2019, 2020). However, contribution of these systems to rainfall over the ORB region has not been given much attention.

There is large climate variability over both space and time in southern Africa generally, with recurring climate extremes such as temperature extremes (hot days, heat waves), droughts and floods induced by extreme rainfall events (e.g., Tyson, 1986; Richard and Poccard, 1998; Mulenga et al., 2003; Rouault and Richard, 2003; Cook et al., 2004; Reason et al., 2005, 2006; Conway et al., 2015; Meque et al., 2022), which may be worsened by climate change (IPCC, 2013, 2021; Engelbrecht et al., 2015; Munday and Washington, 2019; Wainwright et al., 2021). The large climate variability in the region impacts rain-fed subsistence farming and water availability.

Climate variability also has impacts on other aspects of the environment such as vegetation, which are expressed in different ways across southern Africa. For instance, in the ORB region, such impacts are reflected in vegetation patterns, which are thought to reflect those in rainfall and the hydrological conditions (Murray-Hudson et al., 2006; Revermann et al., 2016). However, it is not well understood whether climate influences on vegetation in the drier regions in the south of the ORB are different from those in the wetter regions in the north. The Normalised Difference Vegetation Index (NDVI; Tucker et al., 1991; 2005; Pinzon and Tucker, 2014) is commonly used (Malo and Nicholson, 1990; Davenport and Nicholson, 1993; Farrar et al., 1994; Nicholson and Farrar, 1994; Richard and Poccard, 1998; Camberlin et al., 2007; Martiny et al., 2010; Richard et al., 2012) to assess vegetation characteristics such as photosynthetic activity (greenness or brownness).

Factors contributing to climate variability in southern Africa are complex. They include sea surface temperature (SST) anomalies in the neighbouring Indian and Atlantic oceans or in the remote tropical Pacific. El Niño-Southern Oscillation (ENSO) in the tropical Pacific is known to be the main interannual climate mode affecting southern Africa (Lindesay, 1988; Reason et al., 2000; Reason and Jagadheesha, 2005; Blamey et al., 2018; Hart et al., 2018). However, ENSO impacts may vary across the subcontinent. Not much attention has been paid to ENSO impacts on droughts, temperature extremes and extreme rainfall events over the ORB region. This could have been due to the tremendous lack of high-resolution observational data in this region, particularly in Angola which was ravaged by civil war for 27 years until 2002 (Andersson et al., 2006; Hammond, 2011). Satellite-based data products are now available for use and have been used successfully in southern Africa (e.g., Mahlalela et al., 2020; Thoithi et al., 2021; Meque et al., 2022). Other climate modes such as the subtropical Indian Ocean Dipole (SIOD; Behera and Yamagata, 2001; Reason, 2001a, the Southern Annular Mode

(SAM; Gillett et al., 2006) and the Benguela Niño (Rouault et al., 2003a; Hansingo and Reason, 2009) may also affect the region on interannual scales.

ENSO drives variability of the South Indian Convergence Zone (SIOCZ; Cook, 2000; Lazenby et al., 2016). This SIOCZ is a large-scale austral summer rainfall feature extending across southern Africa into the southwest Indian Ocean, which provides the majority of southern African rainfall (Cook, 2000; Lazenby et al., 2016). Variability of the SIOCZ is not only driven by ENSO but also by the subtropical Indian Ocean Dipole (SIOD; Lazenby et al., 2016). ENSO may impact other regional circulation systems like the mid-level Botswana High, which tends to suppress (enhance) rainfall when it is strong (weak) due to increased (reduced) subsidence over the region (Reason, 2016; Driver and Reason, 2017). The Botswana High forms at mid-levels (500 hPa), thermally induced in response to heat released by high rainfall over the Congo Basin (Reason, 2016; Driver and Reason, 2017). It starts to appear in August, strengthens through spring and by December it is strongly expressed over southern Africa (Reason, 2016; Driver and Reason, 2017). This high-pressure system weakens in March. Driver and Reason (2017) found the Botswana High to have a relationship with dry spell frequencies over southern Africa, but this relationship has not been emphasised over the ORB. There is need to better understand this relationship because dry spell frequency is an important aspect of the rainy season which may affect crop growth (Usman and Reason, 2004; Reason et al., 2005).

Other important factors contributing to climate variability over southern Africa include the Congo Air Boundary through its meridional seasonal shifts. It has long been known that this boundary is generated when the low-level westerlies which originate as recurved Atlantic southeasterlies, meet with the low-level easterly trade winds from the Indian Ocean (Taljaard, 1972; Torrance, 1979). It manifests in southern Africa mainly between late winter and early spring, and it exhibits intra-seasonal fluctuations north and south that can be associated with rainfall variability (Torrance, 1979; Taljaard, 1986). Howard and Washington (2019, 2020) showed that the Congo Air Boundary marks the location of the southern edge of the African tropical rain-belt. However, a possible link between meridional seasonal shifts of the Congo Air Boundary and dry spell frequencies has not been given a close consideration.

Evidence of warming trends (Barros and Field, 2014; Engelbrecht et al., 2015; Maúre et al., 2018; Meque et al., 2022) and early summer drying (IPCC, 2021; Munday and Washington, 2019; Wainwright et al., 2021) over southern Africa has been provided. These trends may have adverse impacts on rain-fed subsistence farming, water availability and ecosystems in the region, motivating this study to assess these trends over particular regions in southern Africa.

The principal aim of the thesis is to better understand potential relationships between climate, photosynthetic vegetation activity (represented by NDVI) and river discharge over the ORB region, as well as climate variability and extremes (droughts, hot days and extreme rainfall events), during the extended austral summer (October-April) rainfall season, within the period 1981-2021. Note that because rainfall events by their nature can extend over a larger region than the ORB, the analysis of rainfall extremes is computed for a larger domain, called western central southern Africa (WCSA), which includes the ORB within it. The thesis also aims to better understand potential links of these variables with climate modes such as ENSO and regional systems such as the Botswana High, as well as trends. These aims are achieved by addressing the following questions:

Chapter 4:

- How are the NDVI and river discharge influenced by rainfall and temperature variability in the ORB region?
- Are relationships between the NDVI and rainfall/temperature in the high rainfall zone statistically different from those on the low rainfall zone?
- Do large-scale climate modes, such as ENSO, impact strongly on NDVI, river discharge, temperature and rainfall in the ORB region?

Chapter 5:

- What are the characteristics of extreme rainfall events over the WCSA?
- What are the most important weather systems driving these events?
- What proportion of these extreme events contribute to summer rainfall totals?
- What are the factors that might have contributed to the severe floods that occurred over the Okavango Delta region (Ngamiland) during the summer of 2017?

Chapter 6:

- How do spatial mean patterns in dry spell frequencies and in hot days vary seasonally, and are there relationships with the African tropical rain-belt, Congo Air Boundary and the Botswana High?
- How do drought metrics and hot day frequencies vary interannually, and do they show significant trends?
- Do these variables have relationships with climate modes such as ENSO?

The thesis is organised as follows. **Chapter 2**, presented next, gives a review of relevant literature. **Chapter 3** describes data and methods used. **Chapter 4** has already been published, **Chapters 5** has been accepted for publication whereas and **Chapter 6** have been submitted to journals for publication. These three chapters are included in the thesis as published or submitted, and they address the questions posed therein. Word-for-word of some material may occur in the thesis to preserve fidelity of the papers. **Chapter 7**, presented last, gives a summary and conclusions of the thesis as a whole.

Chapter 2: Literature Review

The climate of subtropical southern Africa (area south of 10°S) is characterised by a strong seasonal cycle (Tyson, 1986; Mason and Jury, 1997; Reason et al., 2006). Except for the south-western Cape and the southern Cape coastal region which experience rainfall in austral winter and throughout the year, respectively, most of subtropical southern Africa experiences rainfall usually from October to March or April, which is mostly convective. May-September is typically dry over the latter region. Important regional atmospheric circulation systems as well as weather systems that influence the weather and climate of southern Africa are discussed in *Section 2.1*.

Subtropical southern Africa also experiences highly variable weather and climate, both spatially and temporally, with occurrences of droughts, temperature extremes and floods resulting from extreme rainfall events being common (Tyson, 1986; Mason and Jury, 1997; Cook et al., 2004; Reason et al., 2006; Lyon, 2009; Meque et al., 2022). Impacts of this variability are manifested in various ways such as relationships in the variability of climatic variables and vegetation patterns reviewed in *Section 2.5*. Climate variability in the ORB and in subtropical southern Africa in general, is driven by conditions in the surrounding Indian and Atlantic Oceans, discussed in *Section 2.2*, and those in the remote tropical Pacific, discussed in *Section 2.3*. Other factors contributing to this variability include topography and geographic location between the tropics and the midlatitudes. Thus, the climate of the region is complex, responding to several factors that interact with each other on different time scales (Allan et al., 2003; Reason and Rouault, 2002; Reason et al., 2006), hence it is not well understood. Also, significant trends in rainfall and temperature have been found previously over southern Africa, discussed in *Section 2.4*.

2.1 Regional atmospheric circulation and weather systems of importance

Important regional atmospheric circulation systems as well as weather systems that influence the weather and climate of southern Africa are discussed. The SIOCZ is an important large-scale austral summer rainfall feature with a northwest-southeast diagonal orientation, extending from the southern African continent into the southwest Indian Ocean over the southeast coast from 10°-40°S to 0°-60°E (Cook 1998, 2000). Interannual shift in its position dominates austral summer climate variability over southern Africa and the southwestern Indian Ocean (Cook, 2000). The SIOCZ is driven by the circulation around the Angola Low and the South Indian High, and an additional influx from the northwestern region, all (these three moisture flux pathways) of which converge at 850 hPa to form this feature (Cook, 2000; Lazenby et al., 2016). The SIOCZ is significantly correlated with ENSO and the SIOD at the 95% confidence interval (Lazenby et al., 2016).

The Inter-Tropical Convergence Zone (ITCZ) (**Figure 2.1**), which is distinct from the SIOCZ (Cook, 2000), also plays an important role in defining the climate of subtropical southern Africa through its meridional displacement (e.g., Tyson, 1986; van Heerden and Taljaard, 1998; Cook et al., 2004; Reason et al., 2006). From September, the ITCZ starts to shift from north of the equator towards southern Africa. It reaches its southernmost position in February when it lies across Madagascar and Mozambique Channel, with north easterly monsoon towards Tanzania which then recurves over northern Mozambique and the Channel as northwesterlies towards Madagascar. Droughts can occur over subtropical southern Africa if the ITCZ does not shift as far south as usual, whereas if it shifts further south than usual, wet summers can occur due to heavier and more persistent rains (Cook et al., 2004). From March, the ITCZ retreats northwards such that by May, it lies north of the equator with strong southeasterly flow along the Tanzanian and northern Mozambique coasts.

The ITCZ extends its meridional arm through the Congo Basin, which is a high rainfall region. Over its seasonal cycle, the Congo Air Boundary (CAB) shifts from this Congo Basin in spring to western Zambia/central Angola (north of the ORB) in early summer where it eventually breaks down (Howard and Washington, 2019). The CAB is traditionally defined as the location where the low-level westerlies which originate from the Atlantic as recurved southeasterlies, converge with the low-level easterly trade winds from the Indian Ocean (Taljaard, 1972; Torrance, 1979). More recently, using a novel algorithm to understand the regional circulation complexities, Howard and Washington (2019) included the humidity component to this definition, and defined the CAB as a band of surface humidity gradient and/or near-surface wind convergence located at the northern edge of the easterly Indian Ocean trade winds and the southern edge of the low-level westerlies. These authors found the CAB to be an indicator of the location of the southern edge of the African tropical rain-belt. Note that Thompson (1965) and Torrance (1979) made a clear delineation between the CAB and the ITCZ, and that Leroux (2001) described that moving polar highs may play a role in controlling the anomalous movement of the CAB.

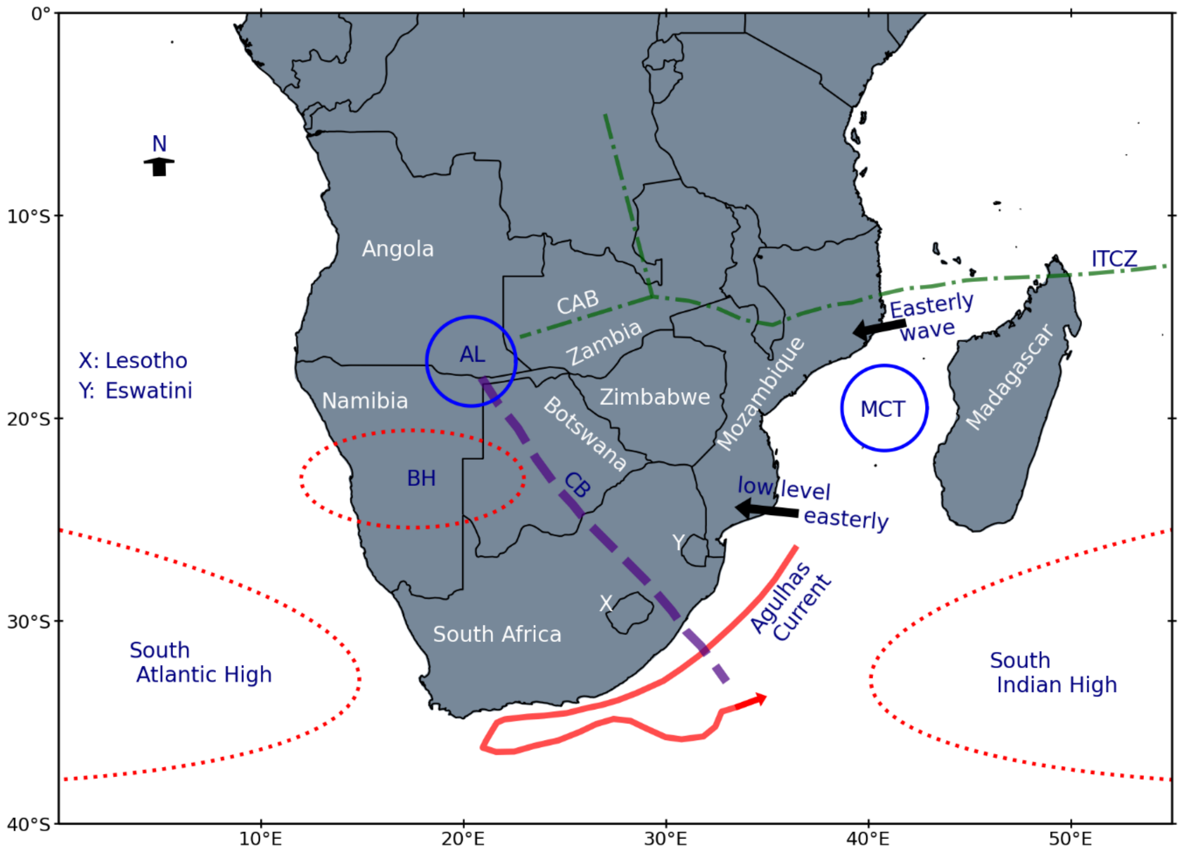

Figure 2.1 A schematic [adapted from Driver and Reason (2017)] showing common synoptic features that influence the weather and climate of southern Africa during summer. These features are labelled and are discussed in the text. They include the Botswana High (BH), Angola Low (AL), tropical-extratropical cloud bands (CB), the ITCZ over the western Indian Ocean, Congo Air Boundary (CAB), South Atlantic High (St. Helena High), South Indian High (Mascarene High), Mozambique Channel Trough (MCT), Agulhas Current, tropical low-level easterlies and easterly waves.

Over its seasonal cycle, the CAB prevents incursion of unstable moist Congo air into subtropical southern Africa until it breaks down in November/December, after which more rainfall occurs over many subtropical areas (Dunning et al., 2016; Howard and Washington, 2019) including the ORB. Thus, the CAB plays a crucial role in the climate of subtropical southern Africa through its meridional seasonal shifts. However, as indicated earlier, a potential link between seasonal shifts of this boundary and patterns in dry spells has not been given much attention.

It is worth noting that use of the ITCZ paradigm over the African landmass has been criticised by Nicholson (2018). The author argues that as the surface wind convergence maxima and the locations of rainfall maxima do not coincide, the traditional model of trade wind convergence setting the location of rainfall does not hold. Howard and Washington (2019) showed that over the tropical rain-belt, the relative humidity features very little gradient and is typically > 95%, reflecting that little wind convergence is required to reach saturation, which is in support of Nicholson (2018). However, Howard and Washington (2019) demonstrated that surface wind convergence collocated with the edge of the tropical rain-belt is crucial in setting the location of the southern edge of the rain-belt in spring and early summer. Although the findings of Nicholson (2018) and Howard and Washington (2019) are crucial, additional research is required to better understand the link between the surface wind convergence and rainfall maxima.

The Botswana High (**Figure 2.1**), well expressed at mid-levels, i.e., at 500 mb (it is not well understood why this system appears at the mid-levels, not at the high-levels), typically forms in August to the southwest of the Congo Basin, thermally induced in response to heat released by high rainfall over this Congo Basin (Reason, 2016; Driver and Reason, 2017). It then shifts poleward over southern Africa and at the same time strengthening during the spring and early summer (Reason, 2016; Driver and Reason, 2017). In late summer, it retreats northward. On average, its centre during summer is located over central Namibia/western Botswana (**Figure 2.1**), which includes the southern ORB (**Figure 1.1b**). This important high-pressure system is linked with subsidence, and its weakening (strengthening) is typically linked with above (below) average rainfall over subtropical southern Africa. Although its relationship with patterns in dry spells over southern Africa has been considered previously (Driver and Reason, 2017), not much attention has been paid to this relationship over the ORB region.

Further south of the ITCZ but over the surrounding southern Atlantic and southern Indian Oceans, there are two other important high-pressure systems, namely, the South Atlantic High (also known as the St. Helena High) and the South Indian High (also known as the Mascarene High), respectively (Tyson and Preston-Whyte, 2000, 2015) (**Figure 2.1**). These semi-permanent near-surface anticyclonic systems are linked with the Southern Hemisphere subtropical belt around 30°S. The St. Helena High, on average has seasonal shifts of ~13º zonally and ~6º meridionally between summer and winter (Reason et al., 2006). These seasonal shifts drive changes in surface winds such that they are only upwelling favourable along the west coast of South Africa in summer, but are such all year round along the Namibian coast. During summer, the zonal movement and intensification of the St. Helena High near southwestern southern Africa, is linked with the development of a coastal low-level jet along the Namibian coast (Nicholson, 2009; Lima et al., 2018).

On average, the Mascarene High has a zonal shift of 24º between summer and winter (Tyson and Preston-Whyte, 2000). A stronger (weaker) Mascarene High is associated with increased (decreased) moisture transport from the Indian Ocean towards southeastern Africa, resulting in increased (decreased) rainfall over the latter region (Reason and Mulenga, 1999; Behera and Yamagata, 2001; Cook et al., 2004; Reason and Jagadheesha, 2005; Reason et al., 2006; Manhique et al., 2011; Munday and Washington, 2017; Blamey et al., 2018).

Ridging of the Mascarene High in the northwest direction together with the Mozambique Channel Trough (MCT) (**Figure 2.1**), which is a low-pressure area over the central/southern Mozambique Channel, can produce an easterly flow into Mozambique and eastern South Africa (Cook et al., 2004; Hart et al., 2010; Ratna et al., 2013; Munday and Washington, 2017; Barimalala et al., 2018, 2020). This regional circulation feature is prominent in austral summer. Barimalala et al. (2018, 2020) noted that formation of the MCT is related to the dynamical adjustment of the easterlies flowing over the Madagascan high topography and that this system can be sustained by local air-sea interaction of relatively warm SST over the Mozambique Channel. A strong (weak) MCT tends to be associated with decreased (increased) moisture penetrating into the southern African mainland from the southwest Indian and the tropical western Indian Oceans, which can lead to rainfall decrease (increase) during austral summer (Barimalala et al., 2018, 2020). Further south, anticyclonic ridging along the south and east coasts of South Africa is an important contributor to summer rainfall over the Eastern Cape and KwaZulu Natal (Weldon and Reason, 2014; Dyson, 2015; Engelbrecht et al., 2015; Ndarana et al., 2020).

Another important regional circulation system is the Angola Low (**Figure 2.1**) mentioned earlier. This near-surface cyclonic feature develops over southern Angola/northern Namibia

(Mulenga et al., 2003; Reason et al., 2006; Ratna et al., 2013; Munday and Washington, 2017; Howard and Washington, 2018; Cretat et al., 2019; Pascale et al., 2019), and is defined as a heat low during its development stage in October-November and a tropical low during January-February when it strengthens considerably (Munday and Washington, 2017; Howard and Washington, 2018). The development of the Angola Low in October-November is associated with dry convection driven by intense surface heating (e.g., Rácz and Smith, 1999), and then in December, it develops a vertical structure dominated by moist convection (Munday and Washington 2017; Howard and Washington 2018) typical of a tropical low. Variations in the strength and location of the Angola low affect moisture transport from the southeast Atlantic and western tropical Indian Oceans into the interior (Cook et al. 2004; Reason et al., 2006; Lyon and Mason, 2007; Fauchereau et al. 2009; Crétat et al., 2018). A stronger (weaker) Angola Low is associated with increased (decreased) moisture advection which result in increases (decreases) in seasonal rainfall in the region.

The Angola Low also acts as a tropical source region for the tropical-extratropical cloud bands (**Figure 2.1**) which bring most of the rainfall over subtropical southern Africa during summer and are sometimes associated with heavy rainfall events (Harrison, 1984; Todd and Washington, 1999; Fauchereau et al., 2009; Hart et al., 2010, 2013, 2018; Ratna et al., 2013; Macron et al., 2014). These cloud bands, which typically extend in a northwest-southeast direction from southern Angola to the southwest Indian Ocean, develop from the interaction of tropical and extratropical systems (typically a cold front). They also help export moisture and heat from the tropics to the midlatitudes (Hart et al., 2010). The preferred axis of the tropical-extratropical cloud bands constitutes the SIOCZ (Cook, 2000; Lazenby et al., 2016; Blamey et al., 2018).

Other weather systems known to make important contributions to rainfall over subtropical southern Africa include tropical lows (Munday and Washington, 2017; Howard et al., 2019; Howard and Washington, 2020; Rapolaki et al., 2019, 2020) and random air mass thunderstorms or organised MCSs (Blamey and Reason, 2009, 2012, 2013; Morake et al., 2021). However, the importance of MCSs, tropical lows as well as tropical-extratropical cloud bands to some aspects of the rainfall season such as extreme rainfall events over the ORB region have not been given much attention. MCSs tend to be more frequent during November-February(Blamey and Reason, 2012; Morake et al., 2021). Typically, the organisation of MCSs is characterised by different processes, namely, available moisture sources (e.g., warm ocean), strong heating of sufficiently moist and unstable air masses over land, a lifting mechanism such as high topography, and favourable wind shear (Laing et al., 2008; Rehbein et al., 2018). Tropical lows are more frequent during the late summer (Rapolaki et al., 2019). Tropical lows that occur over oceans may intensify into tropical cyclones when conditions are conducive (e.g., large and continuous supply of warm and moist air, high sea temperatures ≥ 27°C, low wind shear, converging winds near the ocean surface, an upper level outflow of air), but those that occur over land and do not intensify are much less disastrous than tropical cyclones, as well as more frequent (Malan et al., 2013; Hunt and Fletcher, 2019; Howard et al., 2019).

Tropical cyclones, developing from tropical lows as already mentioned, are known to cause intense rainfall mainly during the late summer (Tyson and Preston-Whyte, 2000; Dyson and van Heerden, 2001; Reason and Keibel, 2004; Reason, 2007; Mavume et al., 2009; Malherbe et al., 2012; Fitchett and Grab, 2014; Mawren et al., 2020). It is estimated that on average, nine tropical cyclones or eleven if tropical storms are included, develop in the southwest Indian Ocean on an annual basis, of which only 5% make landfall over the southern African mainland (Reason, 2007; Mavume et al., 2009). Often, tropical cyclones cause widespread flooding over the eastern coastal areas, and occasionally, also over the eastern interior of the subcontinent, which may be related to the strength of the convective cells. Easterly disturbances may also occasionally penetrate further west across subtropical southern Africa from the southern Indian Ocean and cause flooding there (Dyson and van Heerden, 2001; Reason and Keibel, 2004).

Cut-off lows make large contributions to rainfall often over a short period of time, hence may lead to flash-flooding (Singleton and Reason, 2006, 2007; Favre et al., 2012, 2013). These weather systems occur in all seasons, but with an annual frequency maximum in autumn and a secondary maximum in spring (Singleton and Reason, 2007; Pinheiro et al., 2017). It is not well understood why frequency maximum and secondary maximum of cut-off lows occur in autumn and spring, respectively. Cold fronts contribute to rainfall mainly over the extreme southern parts of southern Africa. The southwestern Cape region of South Africa, which is mainly a winter rainfall region, receives its rainfall mainly from cold fronts (Harrison, 1984; Reason et al., 2006). These weather systems also contribute to rainfall received over the south coast of South Africa, an all-season rainfall region. During summer, cold fronts also play an important role in the development of tropical-extratropical cloud bands as already alluded to (Hart et al., 2010).

2.2 Adjacent Oceans and interannual variability of southern Africa rainfall

The tropical southeast Atlantic Ocean, western tropical Indian Ocean and the southwest Indian Ocean are the primary oceanic sources of atmospheric moisture transported into subtropical southern Africa during austral summer (Walker, 1990; D'Abreton and Tyson, 1995; Mason, 1995; Reason and Mulenga, 1999; Rouault et al., 2003a; Cook et al., 2004; Reason et al., 2006; Hansingo and Reason, 2009; Vigaud et al., 2009; Manhique et al., 2015; Reason and Smart, 2015), and, the Congo Basin is an important continental source through evaporation (D'Abreton and Tyson, 1995; Rapolaki et al., 2020). While most climate studies in the region have often considered tropical southeast Atlantic influences to be not as important as those emanating from the tropical western Indian Ocean (Reason et al., 2006), it can make important contributions during some summer seasons (Rouault et al., 2003; Cook et al., 2004; Hansingo and Reason, 2009; Vigaud et al., 2009; Reason and Smart, 2015; Rapolaki et al., 2020). North of ~15°S, tropical South Atlantic influences during summer are important via westerly moisture flux linked with the Angola low (Rouault et al., 2003a; Reason et al., 2006). Moisture transported from the adjacent oceans into the subcontinent may be affected by the strength of this Angola Low, which increases (decreases) when the Low is stronger (weaker) than usual (e.g., Cook et al., 2004; Lyon and Mason, 2007; Hart et al., 2010; Blamey et al., 2018).

Latent heat released from another important moisture source, the warm Agulhas Current (**Figure 2.1**) region off the south coast of southern Africa, may have significant influence on the regional atmospheric circulation, rainfall received over large parts of neighbouring southern Africa, and may strengthen cold fronts passing there which may aid the development of the midlatitude component of the tropical-extratropical cloud bands (Walker and Mey, 1988; Walker 1990; Jury et al., 1993; Mason, 1995; Crimp et al., 1998; Reason, 1998; Reason and Mulenga, 1999; Reason, 2001b; Rouault et al., 2002; Rouault et al., 2003b). A shift of the Mascarene High further eastward from the southeast coast of South Africa creates favourable conditions for these cold fronts to track closer to the south coast of southern Africa, increasing the prospect for cloud band formation (Harrison, 1984; Hart et al., 2010; 2013). Latent heat fluxes from the Agulhas Current region also play a role in the development of cut-off lows (Singleton and Reason, 2006), MCSs (Blamey and Reason, 2009) and may also play a role on the storm track activity that might affect the rainfall variability in southern Africa (Nakamura, 2012).

Significant relationships between SST anomalies in the adjacent oceans and rainfall variability over southern Africa have been found often through the expression of regional climate modes such as the subtropical Indian Ocean Dipole (SIOD) and the Benguela Niño. The SIOD, defined as the normalised difference in SST anomalies between two poles, one over the southwestern Indian Ocean south of Madagascar and the other one over the southeastern Indian Ocean near western Australia (Behera and Yamagata, 2001), may affect southern Africa on interannual scales. Warmer than usual SST over the former pole and cooler than usual SST over the latter pole, a condition referred to as the positive phase of the SIOD, is associated with rainfall increase over subtropical southern Africa landmass during summer, whereas the reverse polarity is associated with rainfall decrease (Behera and Yamagata, 2001; Reason, 2001a, 2002). Often, this climate mode develops in December-January and peaks in February (Behera and Yamagata, 2001). It is thought that the evolution of SIOD events is influenced by the Mascarene High (Behera and Yamagata, 2001; Hermes and Reason, 2005).

Benguela Niños occur in the southeast Atlantic Ocean typically in late summer (Shannon et al., 1986; Reason et al., 2006; Rouault et al., 2018; Koungue et al., 2019). These Benguela Niños are sporadic, strong warm events close to the frontal area between the southward-flowing Angola Current and the Benguela upwelling system off southwestern Africa (Shannon et al., 1986; Reason et al., 2006). They have been associated with above average rainfall particularly in Angola and Namibia, and in some cases in other parts of southern Africa (Hirst and Hastenrath, 1983; Rouault et al., 2003a; Hansingo and Reason, 2009; Reason and Smart, 2015). The strong warmth associated with Benguela Niño events may imply more evaporation, which may contribute to the regional rainfall increase associated with these events.

Other climate modes in the Atlantic that have potentials in affecting the southern African rainfall include the South Atlantic Subtropical Dipole (SASD; Venegas et al., 1997) and the Atlantic Meridional Mode (AMM; Chiang and Vimont, 2004). The AMM is the dominant source of coupled ocean-atmosphere variability in the Atlantic, and it has a significant influence on the interannual-to-decadal variability in the interhemispheric SST gradient within the tropical Atlantic (Chiang and Vimont, 2004; Amaya et al., 2016). The SASD, which is the dominant mode of variability of SST in the South Atlantic, has been found to display seasonal variability similar to that of the SIOD (discussed above), with their peaks in austral summer (Morioka et al., 2012). Boschat et al. (2013) linked the interannual variability of these two modes to ENSO. Like the SIOD, the SASD exerts a great influence on precipitation in the region (Reason, 2001a; 2002; Vigaud et al., 2009; Morioka et al., 2012).

2.3 ENSO, Southern Annular Mode and interannual variability of southern Africa rainfall

In addition to influences from the surrounding oceans, the regional circulation of southern Africa is also influenced by the Southern Annular Mode (SAM) and ENSO. The SAM is the major interannual mode in the mid- to high-latitude Southern Hemispheric atmospheric circulation (Hall and Visbeck, 2001; Marshall, 2003; Gillet et al, 2006). It consists of an oscillation in the atmospheric pressure between the Southern Hemispheric midlatitudes near 40°S and the Antarctic region near 65°S, with this mode being positive when the pressure is unusually low over the latter region and unusually high over the former region (Gong and Wang, 1999; Thompson and Wallace, 2000). It is the reverse for the negative SAM. A positive SAM generates anomalous easterly flow over east and southeast of South Africa, which weakens approaching cold fronts and prevents moisture advection into the southwestern coastal region of the country, which often cause a decrease in winter rainfall there (Reason and Rouault, 2005, Mahlalela et al., 2019). Gillett et al. (2006) found the SAM to have a positive relationship with summer rainfall over southeastern southern Africa while Reason and Rouault (2005) found a negative relationship over the western Cape region of South Africa with winter rainfall, but the influence of this climate mode over other parts of southern Africa is not well understood.

ENSO in the tropical Pacific Ocean is a major driver of interannual climate variability over tropical southern Africa during the summer (Lindesay, 1988; Nicholson and Kim, 1997; Rocha and Simmonds, 1997; Reason et al., 2000; Cook, 2001; Reason and Jagadheesha, 2005; Lyon and Mason, 2007; Blamey et al., 2018; Crétat et al., 2018; Hart et al., 2018; Driver et al., 2019). Warm (El Niño) and cool (La Niña) ENSO events tend to suppress and enhance rainfall, respectively. Whether a particular ENSO event modulates the Angola Low significantly or not, may influence the level of the impact. For example, the expected drought conditions during the 1997/98 and 2009/10 El Niño events did not happen because the Angola Low, which, as highlighted earlier, acts as the source for the tropical-extratropical cloud bands did not weaken as it usually does during a typical El Niño event (Reason and Jagadheesha, 2005; Lyon and Mason, 2007; Blamey et al., 2018; Driver et al., 2019). However, the mechanism by which ENSO modulates the Angola Low is not well understood. The fact that during 1997/98 and 2009/10 the Angola Low did not weaken as it usually does during a typical El Niño event indicates that it may modulate the influence of ENSO somehow and regulate the regional rainfall variability over southern Africa. Note that in this thesis, ENSO was found to correlate significantly with the Angola Low at the 95% significance level, during October-November (0.38), May-April (0.31) and December-February (0.72), over the period 1981-2021.

During El Niño events, the tropical-extratropical cloud bands tend to shift further eastwards from southern Africa interior to the western Indian Ocean, resulting in dry conditions over the interior and enhanced rainfall offshore (Lindesay et al., 1986; Mason and Jury, 1997; Cook, 2000, 2001; Mulenga et al., 2003; Reason and Jagadheesha, 2005; Fauchereau et al., 2009; Ratnam et al., 2014; Hart et al., 2018). On the other hand, during La Niña events, these cloud bands are often located over the interior, resulting in above average rainfall. It is thought that such variations in the position of the cloud bands during ENSO events occur through modification of the Indian Ocean Walker cell, whose ascending limb shifts further eastwards from southern Africa interior to the western Indian Ocean during El Niño events, whereas during La Niña events, it is located over the interior resulting in strong convection there (e.g., Harrison, 1986; Lindesay, 1988; Cook, 2001). Hart et al. (2018) found that during La Niña, eddy-driven subtropical jets are common over mainland southern Africa thereby favouring tropical-extratropical cloud band development, whereas during El Niño, the likelihood of these jets is reduced and hence the likelihood of cloud band development is also reduced. ENSO events may also modulate regional atmospheric systems such as the Botswana High, which tends to be stronger (weaker) during El Niño (La Niña), which may help suppress (enhance) rainfall over southern Africa (Reason, 2016; Driver and Reason, 2017). As in the case for the Angola Low, the mechanism by which ENSO modulates the Botswana High is not well understood. This may be through changes in the local rainfall over the Congo Basin or large-scale atmospheric circulation changes such as Walker/Hadley cell in the tropics and Rossby wave propagation from midlatitudes.

The link between El Niño events and droughts is complicated because droughts can also occur during non-El Niño years and those that are El Niño related may not always be severe or widespread. Also, it is not completely understood how the dry and wet conditions are generated during ENSO events or as highlighted above, the mechanisms by which regional atmospheric circulations are modulated. Furthermore, ENSO impacts may be complicated by SST patterns in the Indian and Atlantic Oceans surrounding southern Africa, which may influence the circulation and rainfall patterns over southern Africa either independent of ENSO (Reason, 2001a; Washington and Preston, 2006) or both partially dependent on ENSO (Goddard and Graham, 1999; Hoell et al., 2015), and which may also reinforce or oppose ENSO impacts (Reason and Smart, 2015; Hoell et al., 2017).

The response of southern African rainfall to El Niño impacts, investigated more recently, has been found to vary depending on how the anomalous warming in the tropical Pacific is distributed (Ratnam et al., 2014; Preethi et al., 2015). During atypical El Niño, SST anomalies are warmer in the central Pacific and cooler in the eastern and western Pacific whereas during a typical El Niño, SST anomalies are warmer in the eastern Pacific (Ashok et al., 2007; Kao and Yu, 2009). The former type of El Niño is referred to as El Niño Modoki, central Pacific El Niño or warm pool El Niño (Kao and Yu, 2009; Kug et al., 2009; Yeh et al., 2009). Impacts of El Niño Modoki and typical El Niño events may vary around the globe due to differences in the Walker circulation and the teleconnection patterns generated by these events (Ashok et al., 2007; Weng et al., 2009; Ashok and Yamagata, 2009; Feng et al., 2010; Taschetto et al., 2010; Ratnam et al., 2011, 2014; Tadeschi et al., 2013; Hoell et al., 2015; Preethi et al., 2015). Although southern Africa generally experiences below normal rainfall during both El Niño Modoki and typical El Niño events, the anomalies tend to be larger during the latter (Ratnam et al., 2014).

2.4 General climate trends over southern Africa

This section discusses trends in temperatures and rainfall previously found over southern Africa. For temperatures, Jury (2013) found significant increasing historical temperature trends of up to 0.3°C/decade in the 20th century over southern Africa, based on various datasets that included gridded datasets of the National Climate Data Centre (NCDC; Smith et al., 2008). Engelbrecht et al. (2015) found significant warming historical trends in the observed annual average time series over subtropical southern Africa during the period of 1961-2010, based on the Climatic Research Unit (CRU) homogenised time series data for 5° longitude x 5° latitude grid boxes (Jones et al., 2012). Meque et al. (2022), using 2m temperature data from ERA5 reanalyses (Copernicus Climate Change Service, 2017), found significant positive trend in heat wave numbers over the northern part of southern Africa during the entire November-March season, over the period 1981-2018.

Jury (2013) found a temperature increase of 2°C in the future (by the end of the 21st century) over southern Africa, based on global circulation models such as the Institut Pierre Simon Laplace (IPSL; Hourdin et al., 2006). Engelbrecht et al. (2015), using the conformal-cubic atmospheric model (CCAM; McGregor and Dix., 2008) of the Commonwealth Scientific and Industrial Research Organisation (CSIRO), projected plausible temperature increases of 4-6°C over this region in the future, i.e., by the end of the 21st century (relative to 1961-2010). Using regional climate model simulations from the Coordinated Regional Downscaling Experiment Africa domain (CORDEX-Africa; Giorgi et al., 2009), Maúre et al. (2018) found temperature increases of 0.5-1.5°C and 1.5-2.5°C over southern Africa for the global warming levels of 1.5°C and 2.0°C, respectively, by the end of the 21st century (relative to 1971-2000). They found the largest warming trends over South Africa, Namibia and Botswana particularly during September-November. The high amplitude of warming over southern Africa predicted by the CCAM model compared to the warming predicted by the CORDEX-Africa project could be related to differences in the reference period, model resolution and physics. Note that the future warming trend is larger than the historical warming trend, which may be related to the anticipated increase in concentrations of greenhouse gases in the atmosphere (e.g., IPCC, 2013, 2021).

For rainfall, Karypidou et al. (2021) found a good agreement in rainfall historical trends in terms of the signal and the magnitude of the trend, calculated using satellite and gauge-based observations [included CPC Merged Analysis of Precipitation (CMAP) at 2.5° resolution, and Global Precipitation Climatology Centre (GPCC) at 0.5° resolution] over southern Africa, on monthly basis (October-March) during the period 1986-2005. Generally, these authors found decreasing (increasing) rainfall trends during October and February (November, December, January and March) over the bulk of southern Africa. Also, they found the CORDEX-Africa and CMIP5 ensembles to underestimate the trends when compared to satellite and gauge-based trends during their period of study. In addition, these authors found persistent drying in CMIP6 ensemble over most of southern Africa, in contrast to the satellite and gauge-based trends.

A spatially more limited study conducted by MacKellar et al. (2014) using station data, found no significant trends generally, in mean rainfall over South Africa during December-February and June-August, 1960-2010, but during March-May and September-November, these authors found significant decreasing trends over some parts of the eastern half of the country. For most seasons, they also found significant increasing trends in the observed mean temperatures over South Africa except for the central interior. Comparing the observed trends with statistically downscaled global climate models, MacKellar et al. (2014) found that the models tended to show an opposite rainfall trend to that in the observations, whereas for temperature trends, the observations and the models were consistent.

Thoithi et al. (2021) found two sharp horizontal gradients in dry spell frequency during December-February (1982-2019), one extending southeast from southern Angola to the south coast of South Africa (termed diagonal gradient), and the other one extending west from the Limpopo River Valley along 22°-24°S (termed meridional gradient). They found the former dry spell gradient to be weakening whereas for the latter dry spell gradient, a part of it (over northern Botswana/western Zimbabwe and northeastern South Africa) also showed a weakening trend. These authors also found increasing trends in December-February moderate (10-30 mm/day) wet days over parts of southern Africa such as central Angola, Zambian/Democratic Republic of Congo border, western Zimbabwe/eastern Botswana, and the northern tip of Madagascar. The increasing trends in the wet days are consistent with the weakening trends in dry spell gradients.

For future rainfall trends, Maúre et al. (2018), using regional climate model simulations from the CORDEX-Africa, found a decrease of up to ~20% (during September-November) of the climatological values over parts of South Africa and Zambia under the 1.5°C global warming level by the end of the 21st century. They also found a slight increase of up to 0.1 mm/day over a few areas such as southern Namibia during the same period. Under the 2.0°C global warming level, these authors found rainfall to decrease by 10-20% over most of central southern Africa. However, these authors noted large model uncertainty on rainfall change as less than 80% of the models agree on the sign of change. Munday and Washington (2019), using Coupled Model Intercomparison Project Phase 5 (CMIP5; Taylor et al. 2012) models, found drying trends in 95% of the models in the early summer (October-December) over subtropical southern Africa by the end of the 21st century. However, they found an order of magnitude difference in the scale of rainfall decline between models, which ranged from 10 to 100 mm/season, and they also found that the models systematically overestimate present-day early summer rainfall. Due to the large spread between the models and overestimates of present-day early summer rainfall, Munday and Washington (2019) noted that an agreement between models in the sign of the projected change is not necessarily a strong argument for confidence in the projection.

Wainwright et al. (2021), using an ensemble of Coupled Model Intercomparison Project Phase 6 (CMIP6; Eyring et al. 2016) and CMIP5 models, found delays of up to two weeks in the onset of the wet seasons by 2070-2099 over southern Africa. They also found an increase in both mean and maximum dry spell length during the dry season over this region. These authors used an objective methodology to determine the timing of the wet and dry season at each location, which enabled investigation of changes in these seasons using a location-specific, not month-based, seasonal definition.

The warming and drying trends found by previous studies may have unfavourable impacts on rain-fed subsistence farming, water availability and ecosystems. Therefore, there is need to assess these trends over particular regions in southern Africa such as the ORB.

2.5 Climate, vegetation and river discharge over the ORB region

This section discusses previous research that examined relationships in the variability of climatic variables, vegetation and hydrological patterns over the ORB region. Such relationships are an indication of climate influences on vegetation and hydrological patterns.

Before discussing such relationships, it is useful to discuss key features of the ORB. The ORB extends from a high rainfall zone in the Angolan Highlands to a low rainfall zone in northwestern Botswana (**Figures 1.1** and **1.2**). The Angolan Highlands are the highest section of this basin, with an elevation of up to 1800 m above sea level (**Figure 1.1a**). Sections of the ORB that lie over Botswana and Namibian are relatively flat, with the highest elevation of about 1300 m above sea level. This basin comprises of two main rivers, the Cubango and Cuito, which originate from the Angolan Highlands and merge in southeastern Angola to form the Okavango River which then feeds into the Okavango Delta in northwestern Botswana (**Figure 1.1** and **1.2**). The discharge of this river into the Delta is measured at Mohembo (**Figure 1.1b**). Thus, flooding in the Delta results mainly from the annual flood wave originating from the Angolan section of the ORB (Andersson et al., 2003; Wolski et al., 2006; Wolski and Murray-Hudson, 2008). Although rains that fall over the Delta contribute to the interannual variability of flood magnitude mainly by way of "wetting" the system before the arrival of the Okavango River flood wave rather than by inducing flooding itself, in well above average rainfall years, local rain induced floods do occur (Wolski et al., 2006). Wetting the system by local rains means the soil is made wet making it easy for saturation to be reached when the Okavango River flood wave arrives. Rainfall that occurs over the Delta and over the ORB generally as well as over the adjoining areas is also important for agricultural activities. However, extreme rainfall events as well as other climate extremes such as droughts and temperature extremes have not been well studied over the ORB.

Vegetation cover in the Angolan section of the ORB predominantly forms part of the Miombo woodlands, which become increasingly less dense with distance towards the southern border of Angola (Frost, 1996; Revermann et al., 2016). In portions of this ORB section, other species such as dense evergreen Brachystegia woodland (e.g., Julbernadia paniculate) do occur, as well as geoxylic grasslands in the mid and bottom slopes of the valleys (Mendelson and el Obeid, 2004; Revermann et al., 2016). Further south, in relatively dry southern Angola extending into Namibia, the species composition changes to more open Baikiaea-Burkea woodlands (Kgathi et al., 2006; Revermann et al., 2016). Shrubs and grasslands are also prominent in this area stretching south-southeastwards towards northwestern Botswana, where the proportion of woody species decreases further due to a drier climate. More vegetation has been cleared in portions of the mid Okavango in Namibia for agricultural purposes than in the Angolan part of the ORB (Kgathi et al., 2006). However, subsistence farming is practiced across the ORB in general, with maize and millet being commonly used (Kgathi et al., 2006; Weinzierl and Schilling, 2013).

In the Delta in northwestern Botswana, typically, tall reeds and Cyperus papyrus occur in deeper water, whereas channel fringe and floodplain vegetation are dominated by emergent graminoid macrophytes (sedges and grasses) which have varying tolerance for flooding, depending on whether they are seasonal swamp or perennial swamp communities (SMEC, 1986; Ringrose et al., 1988; Smith, 1976; Ellery et al., 2003; Murray-Hudson et al., 2006). In areas adjoining the Delta, Mopane (Colophospermum mopane) woodlands do occur mainly on the east/northeast, and Acacia woodlands (Acacia erioloba, Acacia tortilis) occur mainly to the southwest/west (Kgathi et al., 2006). In a nutshell, the high rainfall zone in the Angolan Highlands has a greater proportion of thicker woodland than elsewhere in the ORB, with more grassland in the low rainfall zone in northwestern Botswana. The ORB vegetation as well as its streamflow supports highly biodiverse and sensitive wildlife species in the area, which are important for tourism, a major source of income (Mbaiwa, 2004, 2015, 2017; Kgathi et al., 2006; Weinzierl and Schilling, 2013).

Studies that examined relationships in the variability of climatic variables and vegetation patterns are now discussed. In semi-arid regions of Africa, rainfall variability is regarded as the most important issue for agricultural activities, vegetation growth and ecosystems (Camberlin et al., 2007; Martiny et al., 2010). On a continental scale, over Africa, Camberlin et al. (2007) examined the response of photosynthetic vegetation activity (represented by NDVI) to rainfall variations during the period 1981-2000. These authors found significant relationships between the two variables. Rainfall data used were the CRU (New et al., 2000) and Climate Prediction Centre Merged Analysis of Precipitation (CMAP; Xie and Arkin, 1997), both at coarse resolutions (0.5° and 2.5°, respectively). On a subcontinental scale, over southern Africa, Gondwe and Jury (1997) found significant relationships between rainfall and the NDVI during the period 1982-1993. Rainfall data used were from the CRU, at a coarse resolution of 2.5° x 3.7° available then. Similarly, Richard and Poccard (1998) also found significant relationships between the two variables over southern Africa during a shorter period, i.e., 6 years (1983-1988).

Spatially more limited studies have also been conducted over southern Africa. Over Botswana, Nicholson and Farrar (1994) found significant NDVI-rainfall relationships during the period 1982-1987, with significant differences in these relationships for various soil types over the country. Farrar et al. (1994) extended that study by examining the extent to which differences in the rate of soil moisture generation (as a function of soil type or locality) can account for the NDVI-rainfall relationships, to find that they cannot. Over Namibia, in addition to NDVI-rainfall relationships, Wingate et al. (2019a) found significant NDVI trends over about 23% of the country, during the period 2001-2017. Over parts of South Africa, Richard et al. (2012) examined interannual memory effects on vegetation dynamics using NDVI and precipitation data, during the period 1981-1999. Memory effects refer to persistence effects in vegetation dynamics, and these memory effects can last for one year (Camberlin et al., 2007; Richard et al., 2012). Richard et al. (2012) concluded that of the 20-30% NDVI variance that is not explained by the concurrent rainfall, one third is explained by memory effects.

Examination of NDVI-rainfall relationships in the above-mentioned studies included computing linear correlations as well as the slope and intercept of the linear regression between the two variables. Those studies also considered possible lags between the two variables to account for the delayed adjustment of soil moisture content (Camberlin et al., 2007). For the linear regression, the slope can be considered as the response of vegetation activity per unit increase in rainfall, and the intercept as a descriptor of interannual variation in rain-use efficiency (Camberlin et al., 2007). Although the above-mentioned spatially more limited NDVI-rainfall studies over Botswana, Namibia and South Africa found significant relationships between the two variables, they did not cover the entire ORB region. For the studies over southern Africa and over the African continent, although they included the ORB region, for rainfall, they used coarser resolution datasets. In addition, the studies over southern Africa focused on shorter periods (12 years or shorter). Camberlin et al. (2007) suggested that to analyse relationships of NDVI with climatic variables, relatively long interannual time series are required. A global scale study (Yang et al., 2019) found NDVI to also correlate significantly with temperature over southern Africa. No studies were found that discuss relationships between the NDVI and temperature in the ORB region. There is a need to better understand relationships of climatic variables with NDVI over the ORB, as well as NDVI-climate mode relationships over this region, which have not been given much attention previously.

Having discussed studies that considered NDVI-rainfall relationships, the focus of the discussion is now switched to studies that examined climate-hydrological patterns. Murray-Hudson et al. (2006) used a mathematical model to assess impacts of changing hydrological inputs (e.g., local rainfall, extractions, river inflow) on flooding in the Delta. They found that changes resulting from existing climatic variability and possible effects of future climate change were larger than changes related to extractions or damming. Andersson et al. (2006) also found that simulations of increased water extractions for domestic use, livestock, and informal irrigation had very limited impact on modelled river discharge. Using outputs of three different global climate models to drive a suite of hydrological models, Wolski and Murray-Hudson (2008) found future conditions for the Delta to vary from much drier to much wetter than those recorded in the past. Hughes et al. (2011) assessed hydrological responses to scenarios of climate change in the ORB. Although these authors found a substantial change in mean flow associated with a global warming level of 2°C, they noted a considerable uncertainty in the sign and magnitude of the projected changes between different climate models.

Wolski and Murray-Hudson (2006a) found that water levels and river discharge in the Delta are influenced by a complex interplay of flood wave and local rainfall inputs. Jury (2010) found SST to show a warm-north/cool-south Atlantic dipole condition as the Okavango River rises. This SST dipole pattern is related to the Atlantic Meridional Mode (Chiang and Vimont, 2004; Amaya et al., 2016) discussed above. Jury (2010) also found a statistically significant relationship between the North Atlantic Oscillation (NAO) and river discharge. Wolski et al. (2012) found that multi-decadal wet and dry phases in the ORB result from multi-decadal oscillations in rainfall. All of these findings are important for water management in the ORB. However, very few of these studies have investigated potential influences of climate modes on river discharge, particularly ENSO which is known to be the main interannual climate mode affecting southern Africa (Lindesay, 1988; Reason et al., 2000; Reason and Jagadheesha, 2005; Blamey et al., 2018; Hart et al., 2018).

2.6 Summary

Regional atmospheric circulation and weather systems influencing the weather and climate of the ORB and southern Africa as a whole, as well as factors contributing to variability have been reviewed in this chapter. The climate of the region is complex, responding to several factors that interact with each other, hence it is not well understood. The region experiences high climate variability both spatially and temporally, with climate extremes such as droughts, temperature extremes, and extreme rainfall events being common. However, not much attention has been paid to climate extremes over the ORB region. Climate variability impacts agricultural activities, vegetation and hydrological patterns in this region. However, relationships in the variability of climate, vegetation and hydrological patterns are not well understood over the ORB, as well as potential influences of climate modes. Warming and drying trends over southern Africa found by other studies provides a motivation to assess these trends over particular regions like the ORB.

This thesis attempts to make a key contribution to the body of knowledge about potential relationships between climate, NDVI and river discharge over the ORB region, as well as about climate extremes (droughts, temperature extremes, extreme rainfall events). It also attempts to better understand the potential links of these variables with climate modes such as ENSO and regional circulation systems such as the Botswana High over the ORB. In addition, the study considers whether any of the variables show significant trends over the ORB.

Chapter 3: Data and Methods

This chapter mainly provides a description of how the Cumulative Drought Intensity (CDI) metric, introduced in the thesis, was derived. This metric has been used in **Chapter 6**. Various standard methods including time series analysis, linear correlations, composite analysis and trend analysis have also been used in each of the results chapters (**Chapters 4** to **6**), and in **Chapter 4**, linear regressions also. Trends in the time series have been computed and tested for statistical significance at the 95% confidence level, using mainly the Hamed and Rao (1998) and Yue and Wang (2002) tests, both modified from the nonparametric Mann-Kendall test (MKT) (Mann, 1945; Kendall, 1975). The MKT is widely used because it is robust against outlier effects, and it does not make assumptions about the distribution of the data. However, unlike the modified trend tests used in the thesis, the original MKT does not take data autocorrelation into consideration. Possible relationships, for example, between climate extremes (droughts, hot days, extreme rainfall events) and climate modes such as ENSO and regional circulation systems such as the Botswana High have been investigated using the Pearson's product-moment correlations with significance reported at the 95% level.

Given the size of the domain, for climate influences on NDVI in **Chapter 4**, the study area has been divided into north (11°-18.9°S, 13°-31.5°E) and south (18.9°-28°S, 13°-31.5°E) zones based on the mean rainfall patterns. The dividing latitude between these north and south zones (high and low rainfall zones, respectively) is 18.9°S (hereafter, L18), which is discussed further in **Chapter 4**. In **Chapter 5**, because many rainfall events extend over a much larger region than the ORB, the analysis has been performed within a larger region than the ORB catchment area, referred to as the WCSA in **Chapters 1** and **5**. Detailed descriptions about how the study area has been divided, and about how various standard methods have been used as well as descriptions of datasets used are provided in each of the three results chapters (**Chapters 4** to **6**). A detailed description of the CDI metric is provided below.

3.1 The CDI metric

Drought tends to involve both a lack of rain as well as high temperatures, and it is the compounded effect of large anomalies in these variables which negatively impacts on agriculture, ecosystems and people, hence a Cumulative Drought Intensity (CDI) metric was derived. Such a metric then provides another measure of the relative severity of a particular season (focusing on the months October-April) with anomalous dry conditions, analogous to cumulative intensity often used to determine the severity of marine heat waves (Hobday et al., 2016). The CDI metric was derived as shown in **Equations 3.1** to **3.4** below.

$$CDI = n \times anomTmax \tag{3.1}$$

$$anomTmax = Tmax_{ds} - climTmax \tag{3.2}$$

$$Tmax_{ds} = \frac{1}{n}\sum_{i=1}^{n} Tmax_i \tag{3.3}$$

$$climTmax = \frac{1}{n \times m}\sum_{j=1}^{m}\sum_{i=1}^{n} Tmax_{ij} \tag{3.4}$$

This metric was computed by multiplying the maximum dry spell duration (n) in days, in a particular season by the corresponding maximum temperature anomaly (anomTmax) (**Equation 3.1**). Maximum dry spell duration is the largest number of consecutive days receiving < 1 mm each in a particular season [based on the Expert Team on Climate Change Detection and Indices (ETCCDI; Zhang et al., 2011; Sillmann et al., 2013)]. The temperature anomaly is the maximum temperature averaged over the duration of the dry spell ($Tmax_{ds}$) minus the climatological maximum temperature (climTmax) (**Equation 3.2**) for that time of year. $Tmax_{ds}$ in **Equation 3.2** was computed using **Equation 3.3**, where $Tmax_i$ is the ith maximum temperature value over a particular dry spell event, and n is ≥ 3, which means each dry spell had to last at least 3 days. $climTmax$ in **Equation 3.2** was computed using **Equation 3.4**, where the index (ij) in $Tmax_{ij}$ means the ith maximum temperature value over a particular dry spell event in a particular year j, and m = 41 (in years). This m in **Equation 3.4** is the length of the study period 1981-2021. Note that based on **Equation 3.1**, the CDI metric has the units °C days.

3.2 Datasets

3.2.1 CHIRPS

Due to lack of high-resolution in-situ rainfall stations in the ORB region, the Climate Hazards Group Infrared Precipitation with Station data (CHIRPS; Funk et al., 2015) version 2, were used in the thesis. CHIRPS data have high spatial (0.05°) and temporal (daily) resolutions and are available from 1981 to near real time. These data were used to compute the CDI metric in **Chapter 6** and to identify dry spells and monthly evolution of the tropical rain-belt in the same chapter. They were also used to identify extreme rainfall events in **Chapter 5** and to examine mean rainfall patterns in **Chapter 4**.

CHIRPS data have been used successfully in southern Africa by past studies, who found them to agree well with rain gauge data (e.g., Rapolaki et al., 2019; Mahlalela et al., 2020; Thoithi et al., 2021). In this thesis, over the ORB region, CHIRPS data were found to perform reasonably well when compared with station data available in northern Botswana and Namibia, provided by national meteorological services of these two countries, with some station data provided by the Southern African Science Service Centre for Climate Change and Adaptive Land Management (SASCCAL). Only stations (shown in **Figure 1.1**) with sufficient quality data were used in the validation of CHIRPS in the thesis. As an additional check, rainfall characteristics over the study area were compared with the Tropical Rainfall Measuring Mission (TRMM; Huffman et al., 2007) and Precipitation Estimation from Remotely Sensed Information using Artificial Neural Networks-Climate Data Record (PERSIANN-CDR; Nguyen et al., 2019) datasets, both at a coarser resolution of 0.25°, to find very similar results to those for CHIRPS.

3.2.2 ERA5 reanalyses

Two-meter air temperature from ERA5 reanalyses at a resolution of 0.25° (Copernicus Climate Change Service, 2017; Hersbach et al., 2020) were used together with CHIRPS data to compute the CDI metric in **Chapter 6**. Note that the ERA5 temperature resolution was deemed sufficient since the dataset showed little spatial variation in temperature within small boxes with sides of lengths 28 km (~0.25°) by 28 km. The ERA5 temperature data also compared well (not shown) with other datasets such as the few available stations (Shakawe and Maun shown in **Figure 1.1a**, data provided by the Botswana Meteorological Services) with quality data. In addition, the 2m air temperature data from ERA5 were also used to identify hot days in **Chapter 6**, defined as the number of days with a maximum temperature greater than the 90th percentile per season, over the observational record. A percentile-based method was used to derive hot days based on the Expert Team on Climate Change Detection and Indices (ETCCDI; Zhang et al., 2011; Sillmann et al., 2013) and on other pertinent studies (e.g., Lyon, 2009; Mueller and Seneviratne, 2012).

ERA5 reanalyses were also used for other purposes, including the following. They were used to identify the dominant weather systems associated with extreme rainfall events in **Chapter 5** as explained in detail there. ERA5 reanalyses fields including specific humidity, omega, winds, 500 hPa and 850 hPa geopotential heights, along with National Oceanic and Atmospheric Administration (NOAA) Optimally Interpolated SST data (0.25° resolution) (Huang et al., 2021), were used to analyse circulation patterns in **Chapters 5** and **6**. Reanalysis data from the National Centres for Environmental Prediction-Department of Energy (NCEP/DOE2) at 2.5° resolution (Kalnay et al., 1996; Kanamitsu et al., 2002) were also used to analyse circulation patterns. Previous studies found NCEP/DOE2 reanalyses to perform reasonably well over southern Africa (e.g., Zhang et al., 2013; Moalafhi et al., 2016). Consistent with those studies, in this thesis, ERA5 and NCEP/DOE2 reanalyses gave very similar results on circulation patterns in **Chapters 5** and **6**, hence only ERA5 circulation results are reported in these chapters. When the work was done in **Chapter 4**, there were not adequate computing facilities to download and process the higher resolution ERA5 data, hence NCEP/DOE2 reanalyses were used.

3.2.3 NDVI

NDVI data provided by the third generation Global Inventory Monitoring and Modelling System (GIMMS; Tucker et al., 1991; Tucker et al., 2005) were used to assess photosynthetic vegetation activity (greenness or brownness) in **Chapter 4**, and to assess NDVI trends in the case study conducted in **Chapter 6**. This data is defined as the difference between near-infrared and red reflectance divided by their sum (Curran, 1983). It has a bi-monthly temporal and 1/12° spatial resolution, and it is available over the period of 1982-20215 (years with full data coverage). Its high spatial resolution makes it suitable in this thesis. NDVI data accounts for different undesired effects such as calibration loss. It has been extensively used to study regional and global land vegetation processes (e.g., Nicholson and Farrar, 1994; Richard and Poccard, 1998; Camberlin et al., 2007; Martiny et al., 2010; Richard et al., 2012; Pinzon and Tucker, 2014; Chu et al., 2019; Luo et al., 2020). Other similar products such as the Moderate Resolution Imaging Spectroradiometer (MODIS)-NDVI, i.e., MODIS-NDVI, were considered in the thesis. MODIS-NDVI is only available from the year 2000, hence it could not be used due to its shorter temporal time scale. Note that NDVI data provided by GIMMs and MODIS-NDVI were very similar (not shown) during the recent period after 2000. The compositing process of this dataset is provided in the National Aeronautics and Space Administration (NASA)'s MODIS web site (MODIS, 1999).

As mentioned above, detailed descriptions on how various standard methods were used as well as descriptions of datasets used, including those not highlighted in the present chapter, are provided in **Chapters 4** to **6**, presented next. Website links for data download are given in the acknowledgments.

Chapter 4: Relationships between NDVI, river discharge and climate in the Okavango River Basin region

This chapter is presented as the paper published in International Journal of Climatology. It addresses the questions below:

Moses, O., Blamey, R.C., Reason, C.J.C., 2022. Relationships between NDVI, river discharge and climate in the Okavango River Basin region. International Journal of Climatology 42(2), 691-713.

- How are the NDVI and river discharge influenced by rainfall and temperature variability in the ORB region?
- Are relationships between the NDVI and rainfall/temperature in the high rainfall zone statistically different from those on the low rainfall zone?
- Do large-scale climate modes, such as ENSO, impact strongly on NDVI, river discharge, temperature and rainfall in the ORB region?

Abstract

The Okavango River Basin (ORB) is a highly sensitive and biodiverse region in southern Africa where climate, vegetation and river discharge characteristics are not well understood. This study investigated relationships between rainfall, temperature, Normalized Difference Vegetation Index (NDVI) and river discharge over the region as well as their trends and interannual variability. It is found that spatial patterns of NDVI are closely related to those of rainfall, but less so with temperature at monthly and seasonal time scales. The relationships between the NDVI and rainfall/temperature differ north of 18.9°S where rainfall is higher than to its south. Typically, there are lags of 1-2-months between NDVI and rainfall. Also, there are large areas across the region that show significant warming trends in all seasons as well as wetting (mainly in the north). This increasing trend in surface temperature may act to worsen the impacts of extreme events such as severe drought and fire in the region. There is also pronounced interannual variability of rainfall, temperature and NDVI, with significant correlations found with El Niño-Southern Oscillation (ENSO), the subtropical Indian Ocean Dipole (SIOD) and the Botswana High for rainfall and temperature, and for NDVI with ENSO. The correlations for rainfall (temperature) with ENSO and the Botswana were negative (positive), with the SIOD they were positive (negative), and the NDVI-ENSO correlations were negative. For the Southern Annular Mode, significant correlations were found with rainfall (positive) and temperature (negative) only in December and April. On longer time scales, focus was also placed on the wet 2006-2013 period relative to much drier 1999-2005 epoch for October-December. The wetter conditions during 2006-2013 appear related to La Niña Modoki conditions and warmer sea surface temperature near Angola as well as regional circulation differences.

4.1 Introduction

Like most of southern Africa, the Okavango River Basin (ORB; **Figure 1.1**) and the adjoining areas are affected by climate variability which is likely to be aggravated by anthropogenic climate change (Andersson et al., 2003; Wolski and Murray-Hudson, 2008). Climate variability impacts are reflected in, for example, changes in hydrological conditions which impact vegetation distribution (Murray-Hudson et al., 2006). Different vegetation types are present (**Figure 4.1**) and are summarized here based on Smith (1976), White (1984), SMEC (1986), Ellery et al. (2003), Murray-Hudson et al. (2006), Revermann et al. (2016) and Bouvet et al. (2018). In the Angolan Central Plateau, Miombo forests are predominant, with geoxylic grasslands being prominent in the mid and bottom slopes of the valleys. In the Angola/Namibia border area, the Miombo woodlands are less widespread than the more open Baikiaea-Burkea woodlands. Shrubs and grasslands are also prominent in this area stretching south of 18.9°S where the proportion of woody species decreases due to a drier climate. In the Okavango Delta, channel fringe and floodplain vegetation are dominated by emergent graminoid macrophytes (sedges and grasses) which have varying tolerance for flooding, depending on whether they are seasonal swamp or perennial swamp communities.

Farmers use seasonal swamp floodplains in the outskirts of the Delta for flood recession farming, with maize being one of the commonly produced crops. It is thought that vegetation patterns reflect those in rainfall and the prevalent hydrological conditions (Murray-Hudson et al., 2006; Revermann et al., 2016). However, there is limited amount of knowledge about whether climate influences on vegetation in the higher rainfall regions in the north of the ORB are different from those in the drier regions in the south. Vegetation is sensitive to severe drought or floods, resulting from the impacts of ENSO for example, and can be compounded by climate change. Such change together with human activity such as clearing of vegetation for farming or settlement has implications for wildlife distribution and tourism, which is a major contributor to the Botswana economy. The Okavango Delta, which is a world heritage and Ramsar site, has extremely high biodiversity supporting economically vital ecotourism (Mbaiwa, 2004, 2015). Climate variability and change also impact water security and flood recession farming on the outskirts of the Delta (Murray-Hudson et al., 2006; Mbaiwa, 2015; Moses and Hambira, 2018).

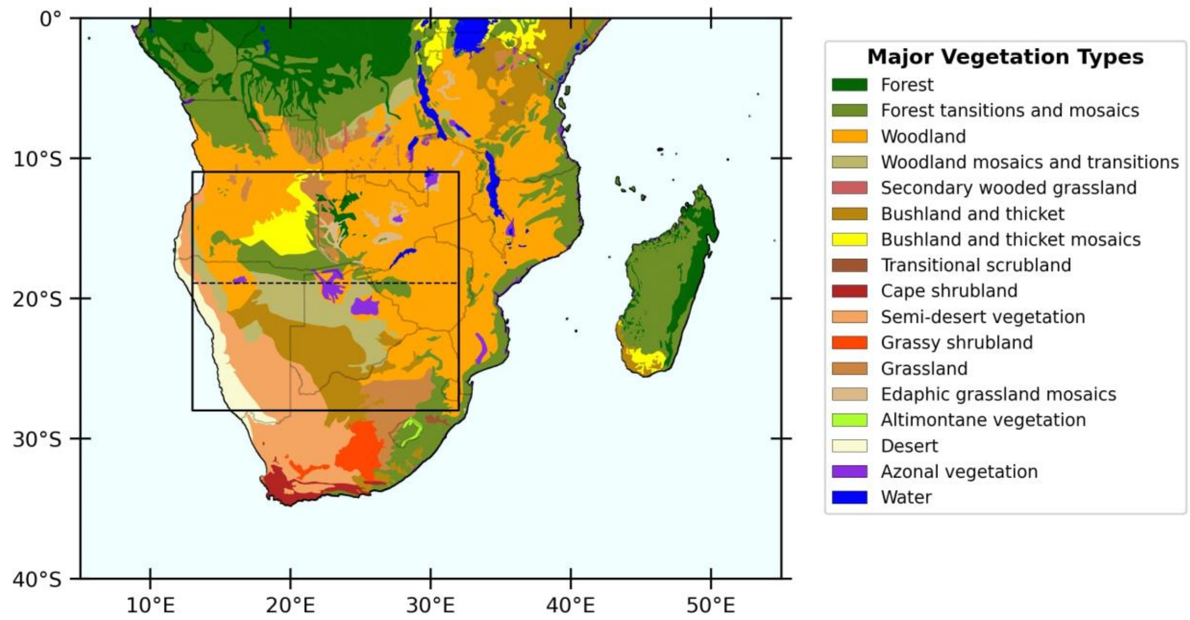

Figure 4.1 The spatial distribution of the main vegetation classes in southern Africa (source: UNESCO/AETFAT/UNSO and White, 1984). The black square depicts the study area, while the dotted line is the location of the L18 described in the text. The *Azonal vegetation* class consists mostly of herbaceous swamp and aquatic vegetation in the Delta, as well as halophytic vegetation which occurs in the salt pans to the west (northern Namibia) and southeast of the Delta.

Rainfall in the ORB region is highly variable, occurring mainly during October to March, although April can also sometimes receive considerable rainfall. Totals range from about 1000 mm/year in the Angolan Highlands (high rainfall zone where most of the streamflow is generated) to about 450 mm/year in the Delta (low rainfall zone). Temperatures are generally high particularly over Botswana where daily maximums can exceed 42°C (Moses and Gondwe, 2019). Such extreme temperatures may exacerbate the impacts of severe drought, heat waves and fire in the region (Barros and Field, 2014; Engelbrecht et al., 2015; Maúre et al., 2018). Both rainfall and temperature over the ORB are influenced in summer by the near-surface Angola Low (Mulenga et al., 2003; Cook et al., 2004; Crétat et al., 2018) and the Botswana High. The latter is a midlevel feature whose weakening (strengthening) typically enhances (suppresses) rainfall (Reason, 2016; Driver and Reason, 2017). A deeper Angola Low is associated with more tropical convection and hence more tropical-extratropical cloud bands (or tropical-temperate troughs). These cloud bands typically extend from southern Angola diagonally in a southeastwards direction to the southwest Indian Ocean and are the most important rain-producing synoptic system over subtropical southern Africa (Hart et al., 2013). The Angola Low, which is typically a heat low in early summer and a tropical low in late summer (Munday and Washington, 2017), together with orographic uplift, are the main contributors to high rainfall in the Angolan Highlands. Moisture feeds into the Angola Low region from both the western tropical Indian Ocean and the tropical southeast Atlantic (Rouault et al., 2003a; Cook et al., 2004; Reason et al., 2006; Vigaud et al., 2009; Manhique et al., 2015; Reason and Smart, 2015) with the Congo Basin also sometimes making important contributions (Rapolaki et al., 2019, 2020).

Climate variability in the ORB and more generally, southern Africa, may be related to sea surface temperature (SST) anomalies in the neighbouring oceans or the tropical Pacific. The El Niño-Southern Oscillation (ENSO) is the main interannual climate mode affecting southern Africa (Lindesay, 1988; Reason et al., 2000; Reason and Jagadheesha, 2005; Blamey et al., 2018; Crétat et al., 2018), but its impacts may differ across the region. Typically, El Niño (La Niña) events are associated with droughts (floods) over large parts of southern Africa, but this is not always the case such as during the 1997/1998 and 2009/2010 El Niño austral summers (Reason and Jagadheesha, 2005; Lyon and Mason, 2007; Driver et al., 2019). Other climate modes which may affect the region on interannual scales include the subtropical Indian Ocean Dipole (SIOD; Behera and Yamagata, 2001; Reason, 2001a, 2002), the Southern Annular Mode (SAM; Gillett et al., 2006) and the Benguela Niño (Rouault et al., 2003a; Hansingo and Reason, 2009). However, the latter mode was found not to correlate significantly with rainfall, Normalized Difference Vegetation Index (NDVI) or river discharge (correlations = 0.17, 0.19 and 0.03, respectively, $p > 0.05$ in all cases) in the ORB during January-April, and hence is not considered further. Drier (wetter) than average summers over some parts of southern Africa are expected during negative (positive) SIOD events. For the SAM, Gillett et al. (2006) found a positive relationship with summer rainfall over some parts of southern Africa while Reason and Rouault (2005) found a negative relationship over western South Africa with winter rainfall. Quasi-decadal to decadal wet and dry spells are a well-known aspect of subtropical southern Africa climate (e.g., Tyson et al., 1975; Tyson, 1986; Wolski et al., 2012; Malherbe et al., 2014; Reason, 2016) and may be linked to decadal-scale variability in ENSO and SAM impacts (Reason and Rouault, 2002, 2005; Allan et al., 2003).

Although climate influences on vegetation in southern Africa have been considered (e.g., Farrar et al., 1994; Nicholson and Farrar, 1994; Richard and Poccard, 1998; Wingate et al., 2019a) very few studies (except Richard and Poccard, 1998) cover the entire ORB and its adjoining areas or the potential influences of climate modes on vegetation. While numerous studies considered the hydrology of the basin (Andersson et al., 2003; McCarthy et al., 2003; Gumbricht et al., 2004; Andersson et al., 2006; Wilk et al., 2006; Murray-Hudson et al., 2006; Wolski et al., 2006; Jury, 2010; Wolski and Murray-Hudson, 2006b, 2008; Hughes et al., 2011; Wolski et al., 2012; Wolski et al., 2014), very few have investigated potential influences of climate modes on river discharge. Most of those studies found that climate variability is pronounced over the basin, and some like Murray-Hudson et al. (2006) and Hughes et al. (2011), found that upstream development related changes are relatively small compared to changes resulting from climatic factors.

A better understanding of rainfall variability over the basin and its links with river discharge and vegetation is needed for appropriate management of the water resources and ecosystems of the biodiverse and unique ORB region as well as for assessing how the region may respond to a globally warming climate. Specifically, the following three questions are posed: (a) How are the NDVI (representing photosynthetic activity of vegetation) and river discharge influenced by rainfall and temperature variability in the ORB region? (b) Are relationships between the NDVI and rainfall/temperature in the high rainfall zone statistically different from those on the low rainfall zone? (c) Do large-scale climate modes, such as ENSO and SIOD, impact strongly on NDVI, river discharge, temperature and rainfall in the ORB region?

4.2 Data and Methods

Figure 1.1 shows the study area, the ORB region (11°-28°S, 13°-31.5°E), as well as its surface elevation. Over Botswana, the land surface is relatively flat, with an elevation that ranges from about 700 to 1300 m above sea level. **Figure 1.1b** shows the two main rivers, the Cubango and Cuito, which originate from the southern Angolan Highlands and merge in southeastern Angola to form the Okavango River which then feeds into the Okavango Delta in northwestern Botswana. The location of the Mohembo hydrological station, which measures the Okavango River discharge into the Delta, is also shown. Discharge data from this station, available from 1934 to near present, were provided by the University of Botswana. The Delta lies more than 600 km away from the Okavango River headwaters; hence there is a substantial time lag between rainfall received upstream over southern

Angola, and water levels in the Delta apex. This time lag is approximately two months (Andersson et al., 2003).

Given the size of the domain, for climate influences on NDVI or vegetation (vegetation types described earlier), the study area has been divided into north (11°-18.9°S, 13°-31.5°E) and south (18.9°-28°S, 13°-31.5°E) zones based on the mean rainfall maps (**Figure 4.2**). Based on the said rainfall maps, the dividing latitude between these high (north) and low rainfall (south) zones is 18.9°S, denoted by "L18." To consider climate influences on river discharge, a "Cor_Box" is used which is defined as 11.7°-18.9°S, 14.8°-23°E (to represent the northern part of the catchment, found to give better correlations than a larger region by trial and error; **Figure 1.1b**).

Since the ORB has few in-situ rainfall stations particularly in Angola where most of the streamflow is generated, Climate Hazards Group Infrared Precipitation with Station data (CHIRPS) version 2 data were used. CHIRPS data has high spatial (0.05°) and temporal (daily) resolution and is available from 1981 to near real time (Funk et al., 2015). The CHIRPS rainfall estimate is derived from merging rain gauges with satellite data. Previous studies have found CHIRPS data to agree well with rain gauge data for stations in the Eastern Cape, South Africa (Mahlalela et al., 2020) as well as those near the South African/eastern Botswana border (Thoithi et al., 2021). Over the study area, CHIRPS was validated using rainfall observations obtained from national meteorological services and from the Southern African Science Service Centre for Climate Change and Adaptive Land Management (SASCCAL). For the ORB, only stations in parts of Botswana and Namibia had sufficient quality data during the 1981-2019 period (**Figure 1.1a**). CHIRPS data were also compared with the Precipitation Estimation from Remotely Sensed Information using Artificial Neural Networks-Climate Data Record (PERSIANN-CDR), which is available daily from 1983 to near-present at a spatial resolution of 0.25° (Nguyen et al., 2019). The common time span of station and PERSIANN-CDR data overlap was 1983-2012, hence this period was selected for comparison with CHIRPS data.

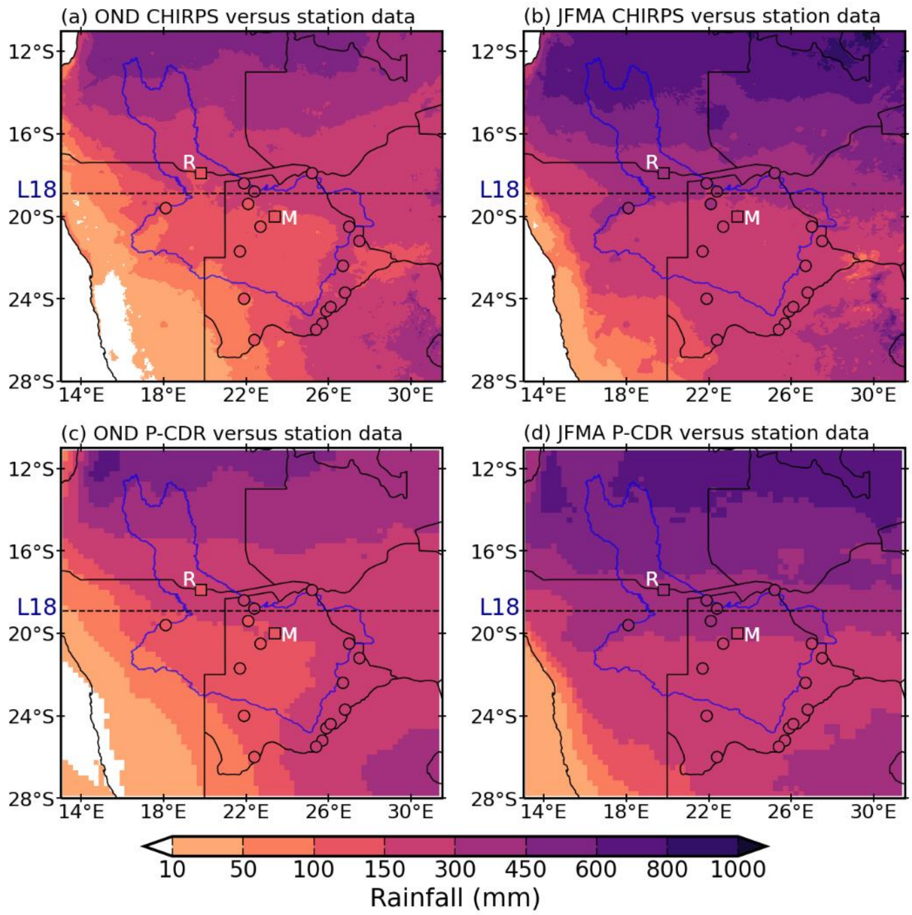

Figure 4.2 (a) and (b) show CHIRPS mean rainfall versus station data (denoted by circles and squares, with station data plotted in them) for OND and JFMA, respectively, over the ORB region (1983-2012). The location of the two stations used for the comparison in Figure 4.3 are denoted by a square symbol ("R" and "M" in the square symbol denote Rundu and Maun, respectively). (c) and (d) are as in (a) and (b) but for PERSIANN-CDR (P-CDR). The blue polygon is the outline of the Okavango River catchment. "L18" is the 18.9°S latitude dividing the study area into high and low rainfall zones.

For temperature analysis, gridded 2m air temperature of the combined Global Historical Climatology Network (GHCN) and Climate Anomaly Monitoring System (CAMS) for the period 1982-2015 was used (Fan and Van den Dool, 2008). This 0.5° spatial resolution temperature dataset is regularly updated with available station observations. NDVI data provided by the third generation Global Inventory Monitoring and Modelling System (GIMMS; Tucker et al., 1991; Tucker et al., 2005) was used to assess photosynthetic activity of vegetation (greenness or brownness). This bi-monthly temporal and 1/12° spatial resolution NDVI dataset accounts for various undesired effects including calibration loss. It has been widely used to study regional and global land vegetation processes (e.g., Pinzon and Tucker, 2014; Luo et al., 2020). For the analysis, only years with full data coverage (1982-2015) were considered. It is important to note that the rainfall and temperature datasets described above were linearly re-gridded to the same resolution of 1/12° as the NDVI dataset.

Long-term means (1982-2015) of NDVI, river discharge, temperature and rainfall were computed for the different seasons of October-December (OND; early summer), January-April (JFMA; late summer) and May-September (MJJAS; winter). December-March (DJFM) was also considered. Note that the vegetation growing period in the ORB is from November to May (Revermann et al., 2016). Trends in the time series of each variable were analysed and tested at a significance level (α) = 0.05 using the nonparametric Mann-Kendall test (MK; Luo et al., 2020). Before applying the MK test, three methods were used (for comparison) to remove the trend and pre-whiten the time series (to minimize the influence of autocorrelation on the MK test), namely, the Hamed and Rao (1998) test (MMKHR), the Yue and Wang (2002) pre-whitening test (MMKYW) and the Yue et al. (2002) test (MMKYPPC). Unlike the original MK test, the three modified MK tests take into consideration data autocorrelation.

Circulation patterns were investigated using reanalysis data (including precipitable water, geopotential height, and zonal, meridional and vertical winds at 850 and 500 hPa levels) from the National Centres for Environmental Prediction (NCEP/DOE2; Kalnay et al., 1996; Kanamitsu et al., 2002), together with outgoing longwave radiation (OLR). The NCEP/DOE2 data has a spatial resolution of 2.5° and available from 1979 to 2020. Correlations of some of the main climate modes, including ENSO, SIOD and SAM, versus NDVI, river discharge, rainfall and temperature were computed. For ENSO, the Niño 3.4 index was used which is defined as the monthly average of the SST anomalies in the Central Pacific (5°N-5°S; 120°-170°W). Data for this index was obtained from the National Oceanic and Atmospheric Administration (NOAA)'s Climate Prediction Centre (Huang et al., 2017). NOAA Optimally Interpolated SST (Huang et al., 2021) was used to compute the SIOD index, defined as the normalized difference in SST anomalies averaged over the western (37°-27°S, 55°-65°E) and eastern (28°-18°S, 90°-100°E) poles in the southern Indian Ocean (Behera and Yamagata, 2001). For the SAM, the Marshall (2003) index is used, which is based on the zonal pressure difference between 40°S and 65°S. Correlations of NDVI, river discharge, rainfall and temperature with indices of the Angola Low and the Botswana High were also performed.

The Angola Low index was computed as the 850 hPa geopotential height averaged over 16°-20°S, 18°-22°E (based on Munday and Washington, 2017) and the Botswana High index was computed as the 500 hPa geopotential height averaged over 19°-23°S, 16°-21°E (based on Driver and Reason, 2017) using the NCEP/DOE2 reanalysis data.

Monthly and seasonal lag correlations (detrended) of NDVI and river discharge with rainfall/temperature, and with the indices described above were computed at time lags of 0-2 months or seasons using the Pearson correlation method and tested for significance at $\alpha = 0.05$. For NDVI correlations with rainfall/temperature over north and south of L18, time series of these variables for each region were generated by spatially averaging their datasets accordingly over those regions, and similarly for river discharge versus rainfall/temperature correlations over the Cor_Box. Information on the websites for data download is given in the acknowledgments.

4.3 Results and Discussion

4.3.1 Seasonality

Figure 4.2 plots early and late summer mean CHIRPS and PERSIANN-CDR rainfall over the region together with the available 19 in-situ stations shown in **Figure 1.1a**. The datasets are consistent in their mean rainfall distribution both within and outside the ORB. In general, the rainfall totals are greater during the late summer than the early summer. Furthermore, the annual cycle of rainfall for all the stations were compared with those from the nearest grid-points in CHIRPS and PERSIANN-CDR. The results were similar for all the stations, but for convenience, only those for Maun and Rundu (south and north of L18, respectively) are shown (**Figure 4.3**). A very dry May-September is followed by a steady increase in rainfall through early summer to January, the wettest month on average, and then a sharp decrease through the rest of the summer. While all three datasets show the same annual cycle, there are some differences in magnitude. PERSIANN-CDR consistently overestimates the mean values relative to CHIRPS and the station data, with the latter two datasets agreeing more closely with each other at Maun than at Rundu. Overestimation of rainfall by the PERSSIANN-CDR could be related to its lower resolution or its data processing procedure. In terms of interannual variability, **Figures 4.3c,d** show that the datasets agree on anomalous wet and dry years, but that PERSIANN-CDR again tends to give larger values than either CHIRPS or station data. The datasets are also consistent in each showing a slightly increasing trend, but these are not statistically significant using the MMKHR, MMKYW and MMKYPPC tests. Based on **Figures 4.2** and **4.3a-d**, CHIRPS has been used as the main rainfall dataset in the study.

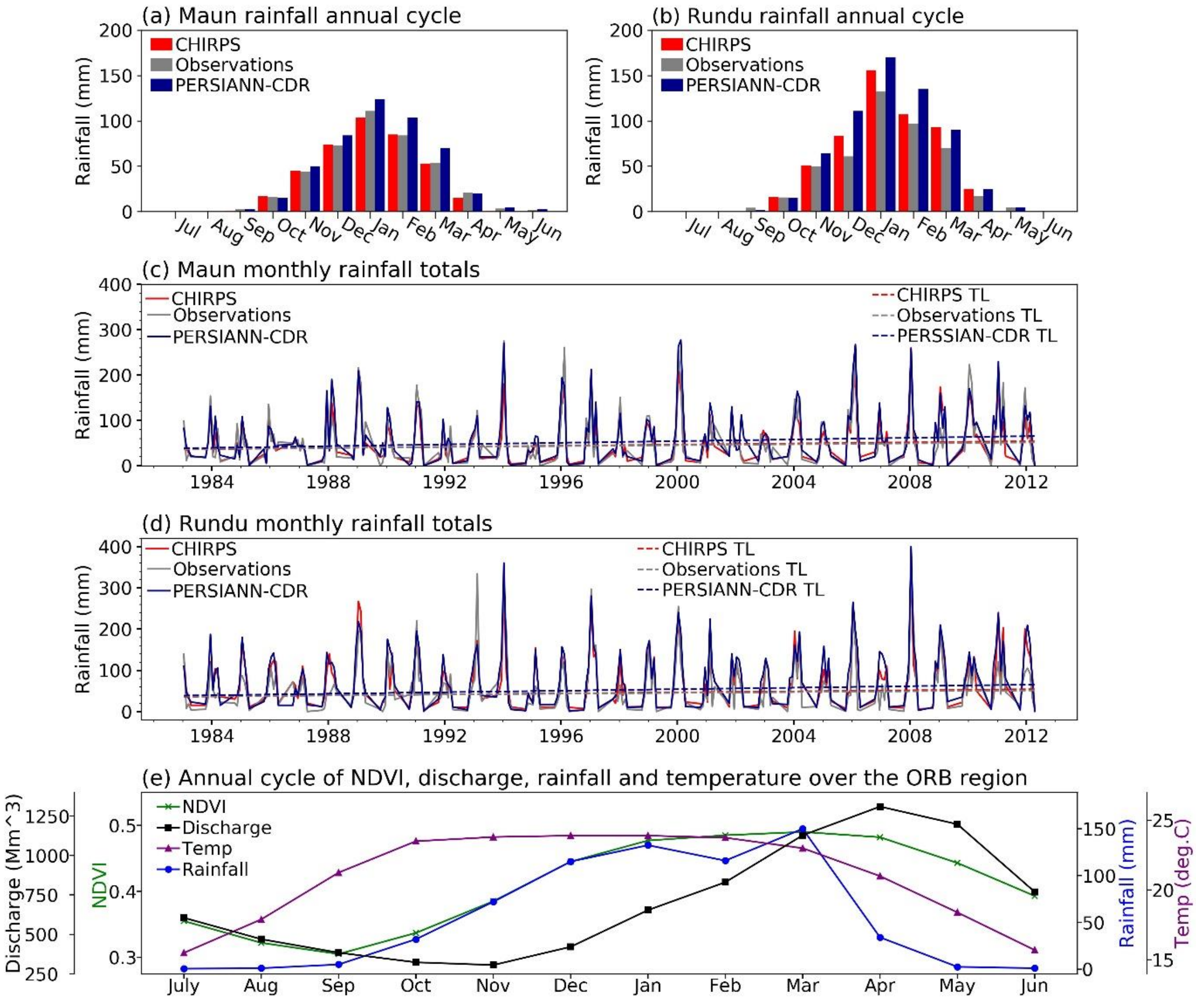

Figure 4.3 (a) monthly mean rainfall in CHIRPS, PERSIANN-CDR and Maun station (station 6 in Figure 1.1) data for the period 1983-2012. (b) as in (a) but for the Rundu station (station 2 in Figure 1.1). (c) CHIRPS versus observed and PERSIANN-CDR monthly rainfall for Maun. (d) is as in (c) but for Rundu, with “TL” denoting trend line. None of the trends were statistically significant at $\alpha = 0.05$. (e) Monthly mean NDVI, temperature and rainfall spatially averaged over the ORB region (11°-28°S, 13°-31.5°E), and of river discharge at Mohembo (1982-2015).

Figure 4.4 shows that mean NDVI and rainfall distributions are closely linked for the early and late summer but less so during the very dry MJJAS months. Overall, throughout the year, the wetter area north of L18 has higher NDVI values (greener vegetation) than the drier area south of L18. This area has a greater proportion of thicker woodland than that south of L18 where there is more grassland. Although MJJAS is very dry compared to the other months, its NDVI pattern within the ORB is like that of OND, suggesting that it responds to rainfall of the previous summer. For temperature, the largest area of high values (mean > 25°C) occurs during OND (**Figures 4.4g-i**) and there is no obvious relationship between these patterns and NDVI. However, since previous studies indicate that variability of vegetation over southern Africa is mainly due to rainfall of the current wet season (Camberlin et al., 2007; Richard et al., 2008, 2012; Martiny et al., 2010; Good and Caylor, 2011), partial correlation analysis was performed to remove the effects of rainfall on NDVI and test for any possible temperature-NDVI relationship. Spatially averaged over the region, the NDVI correlations with temperature were -0.34, -0.41 and -0.50 for OND, JFMA and MJJAS, respectively, whereas after the effects of rainfall are removed, the resulting partial correlations of NDVI with temperature were -0.34, -0.12 and -0.53. Thus, only in JFMA is there any difference implying that the temperature-NDVI relationship is partly explained by rainfall influences in this season only. Partial correlations for data averaged over the area north (south) of L18 were stronger (weaker) than those for the ORB region, but differences in these partial correlations were small, so the fact that they were stronger in the area north of L18 is not surprising. In both cases, the correlation results as well as spatial patterns (**Figure 4.4**) using DJFM are very similar to JFMA.

Spatially averaged over the ORB region, **Figure 4.3e** shows that NDVI reaches its maximum in March and April before sharply dropping in May and June to a minimum in September, while rainfall drops sharply from March (maximum) to April and then to virtually no rain from May to September. Thus, a 1-2-month lag between rainfall and NDVI may exist from April until September after which the two variables appear in phase until at least January. The annual cycle of temperature shows near-constant warm temperatures during the summer half of the year and sharp changes either side of the broad peak to the cool mid-winter months of June and July. For river discharge at Mohembo, with a minimum in November and a peak in April, **Figure 4.3e** suggests a 1-2-month lag with monthly rainfall in late summer but a longer lag in early summer. On a seasonal basis, highest discharge occurs in JFMA with mean and standard deviation of 3920 Mm^3 (“M” denotes mega) and 1190 Mm^3, respectively, followed by MJJAS with a mean and standard deviation of 3430 and 840 Mm^3, respectively, whereas lowest discharge occurs in OND with a mean and standard deviation of 1050 and 210 Mm3, respectively.

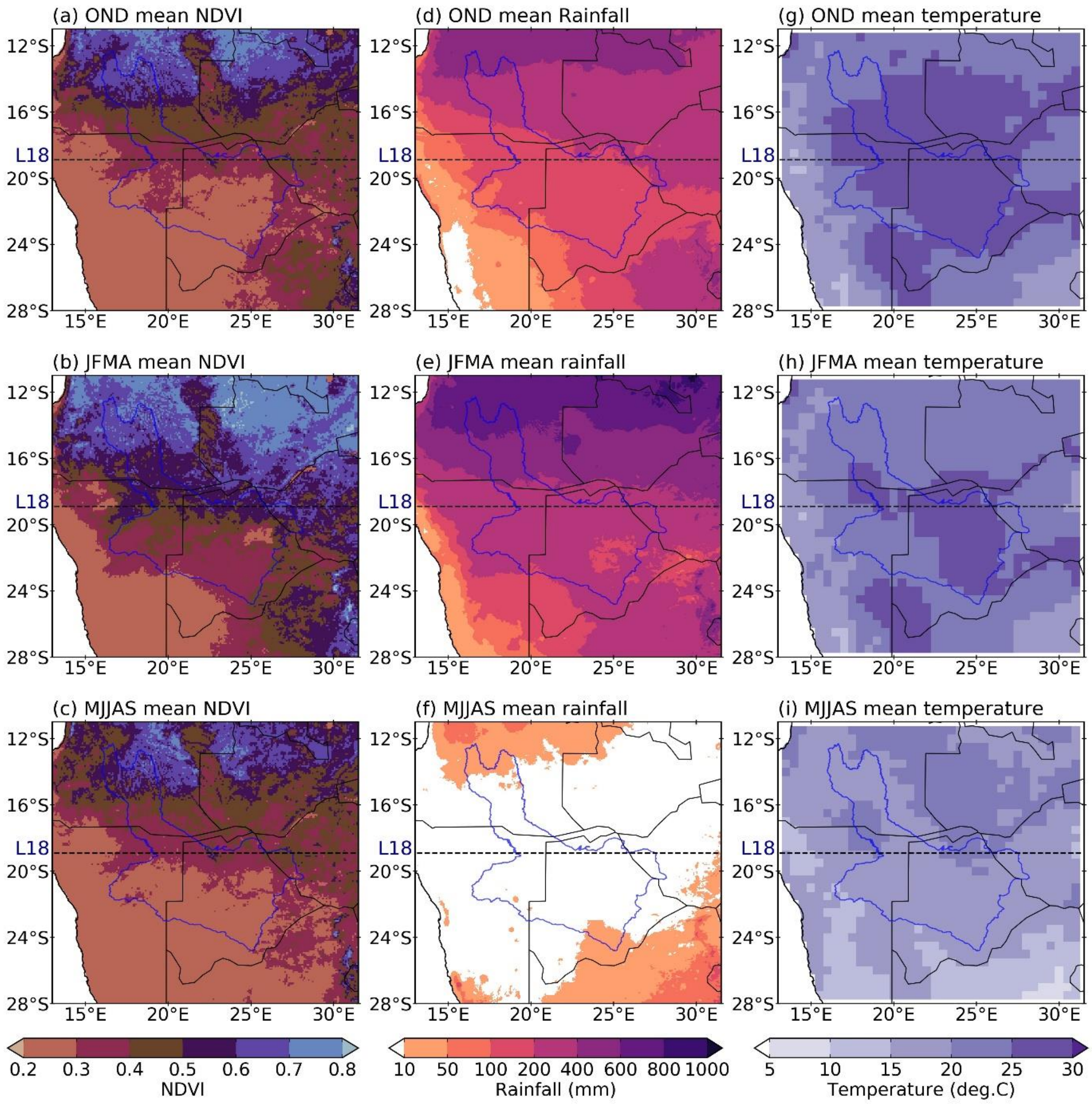

Figure 4.4 Long-term mean (1982-2015) NDVI, temperature and rainfall over the ORB region. (a)-(c) show NDVI over OND, JFMA and MJJAS, respectively. (d)-(f) are as in (a)-(c) but for rainfall. (g)-(i) are as in (a)-(c) but for temperature. The blue polygon is the outline of the Okavango River catchment. “L18” is the 18.9°S latitude dividing the study area into high and low rainfall zones.

4.3.2 Lag correlations

Table 4.1 shows monthly lag correlations between NDVI and rainfall over the ORB region, and north and south of L18 for December to April (October and November are not shown as the correlations are weak). At 1-month lag, over the ORB, there are significant correlations for each month (highest r = 0.83 in April) except January which shows a weaker but still significant zero lag correlation. March and April also show strong 2-month lag correlations. South of L18, the 1-2-month lag correlations are generally stronger than those computed for the area north of L18, which suggests that rainfall is more important to grassy species which are more dominant in the former region than in the latter region (e.g., Smith, 1976; Murray-Hudson et al., 2006; Bouvet et al., 2018).

This 1-2-month lag of the NDVI response to rainfall over each region is consistent with the results of Nicholson and Farrar et al. (1994) obtained over Botswana. For temperature, **Table 4.1** shows that the area south of L18 typically has stronger lag correlations with NDVI than does the whole ORB region and there are no significant correlations for the area north of L18 except in April. As the rainy season comes to an end in April, vegetation over the ORB may start to become more sensitive to temperature as suggested by their in-phase cycle during April-June (**Figure 4.3e**).

Table 4.1 also shows seasonal correlations of NDVI with rainfall and temperature. At zero lag, the only significant NDVI-rainfall correlations are those for JFMA over the ORB and more strongly for the area south of L18. The high correlations of MJJAS NDVI at 1-season lag suggest that JFMA rainfall strongly influences winter vegetation. There is also a significant but weaker 1-season lag correlation between OND rainfall and JFMA NDVI but only for the area north of L18. For temperature, the stronger 1-month lag than zero lag NDVI correlations in MJJAS are consistent with the annual cycle in **Figure 4.3e** which shows temperature starting to fall in March whereas NDVI only starts decreasing in April and then more obviously in May.

Table 4.1 Monthly lag detrended correlations (0-2 months) of NDVI with rainfall (RN) and temperature (TE) over the ORB region (upper panel) (1982-2015). Lower panel is as in the upper panel but for seasonal lag (0-1) correlations. Only correlations significant at α = 0.05 are shown

Monthly correlations

		ORB			North of L18			South of L18		
		0	1	2	0	1	2	0	1	2
Dec	RN		0.76			0.59			0.69	
	TE									
Jan	RN	0.43						0.53		
	TE	-0.56		-0.42				-0.75		-0.45
Feb	RN		0.77			0.48	0.37	0.43	0.78	
	TE	-0.54	-0.66					-0.71	-0.74	
Mar	RN	0.47	0.62	0.76			0.35	0.46	0.81	0.78
	TE	-0.64	-0.71	-0.65				-0.74	-0.81	-0.69
Apr	RN		0.83	0.63		0.40			0.80	0.65
	TE	-0.77	-0.70	-0.64	-0.47	-0.51	-0.41	-0.82	-0.72	-0.59

Seasonal correlations

		ORB		North of L18		South of L18	
		0	1	0	1	0	1
OND	RN						
	TE	-0.34	-0.50	-0.36	-0.50		-0.36
JFMA	RN	0.42			0.50	0.89	
	TE	-0.41	-0.41			-0.85	
MJJAS	RN		0.86		0.84		0.77
	TE	-0.50	-0.69	-0.55	-0.66	-0.42	-0.62

Monthly lag correlations of rainfall with river discharge (not shown) are less coherent than those computed in **Table 4.1** for NDVI. Only April shows a significant rainfall-discharge correlation (r = 0.55 at 1-month lag). For temperature, there are significant inverse correlations at 0 and 1-month lags with discharge in October, November and December. However, on seasonal scales there are significant rainfall-discharge correlations for OND (r = 0.51 at zero lag) and at 0.55 for JFMA rainfall versus MJJAS discharge consistent with **Figure 4.3e**. OND rainfall versus MJJAS discharge correlations were weak. DJFM-MJJAS and OND-DJFM correlations were significant (not shown) but weaker than those for JFMA-MJJAS. The lag correlations suggest that although MJJAS experiences very little rainfall, its relatively high river discharge values are still responding to the previous summer's rainfall. Discharge-temperature seasonal correlations were weak. Also, there were no significant relationships found between discharge and any of the climate modes or Angola Low/Botswana High.

Table 4.2 shows monthly lag detrended correlations of ENSO with NDVI, rainfall and temperature, over the ORB region, and north and south of L18. Only the summer months are shown because this is when ENSO tends to have strongest impacts on southern African rainfall, temperature and atmospheric circulation (Lindesay, 1988; Reason et al., 2000). For rainfall, there are significant correlations in January-February at zero lag over all three regions which also exist at 1-month lag in February. March shows significant 1-month lag correlations (but weaker than in February) for the ORB and north of L18, the latter also at zero lag. For NDVI, there are significant ENSO relationships in February and March over the ORB and south of L18 (at both zero and 1-month lag) and in all three regions in April at both zero and 1-2-month lags. In February and March, there appears to be a significant ENSO-NDVI relationship south of L18 but not north of L18. This result might be related to differences in vegetation type between the two regions since the open woodlands with shrubs and grasslands south of L18 are more sensitive to ENSO events than the mainly woody cover north of L18 (Erasmi et al., 2009). Over southern Africa, ENSO is the main interannual climate mode affecting rainfall as already mentioned, and this rainfall is more important to grassy species, which, unlike the woodier species, do not have long roots that can draw water from deeper layers of the soil (Guilpart et 2828 al., 2017). For rainfall, its nonsignificant correlations with ENSO in March are not that much smaller than the significant ones, so the fact that they are only significant north of L18 is not that surprising. Temperature shows an even stronger ENSO connection than rainfall over all regions, mainly at 0 and 1-month lags, and unlike rainfall, also for December and April.

Table 4.2 Monthly lag detrended correlations (0-2 months) of ENSO with NDVI, rainfall (RN) and temperature (TE) over the ORB region, and north and south of L18 (1982-2015). Only correlations significant at $\alpha = 0.05$ are shown

ENSO		ORB			North of L18			South of L18		
		0	1	2	0	1	2	0	1	2
Dec	NDVI									
	RN				-0.39	-0.38	-0.38			
	TE	0.73	0.74	0.77	0.73	0.75	0.78	0.69	0.71	0.73
Jan	NDVI							-0.37		
	RN	-0.51			-0.53			-045		
	TE	0.58	-0.38	-0.37					-0.37	-0.36
Feb	NDVI	-0.41	-0.37					-0.47	-0.45	
	RN	-0.54	-0.54		-0.47	-0.47		-0.45	-0.45	
	TE	0.76	0.75		0.77	0.77		0.69	0.69	
Mar	NDVI	-0.53	-0.54	-0.52				-0.54	-0.54	-0.52
	RN		-0.35		-0.35	-0.36				
	TE	0.69	0.72	0.72	0.73	0.76	0.75	0.58	0.62	0.62
Apr	NDVI	-0.36	-0.44	-0.44	-0.34	-0.35	-0.36		-0.42	-0.42
	RN									
	TE	0.65	0.76	0.77	0.67	0.78	0.78	0.56	0.68	0.68

For SIOD, **Table 4.3** shows significant zero lag correlations with rainfall in January-April north of L18, and only in April over the ORB. Since the area of strongest SIOD rainfall impacts in southern Africa only partly overlaps the ORB region (Behera and Yamagata, 2001), the relatively less coherent signal than found for ENSO is not unexpected. The SIOD correlations with temperature mainly occur in February-April (over all three regions) and are in the opposite sense (a positive SIOD may be associated with wetter and cooler conditions). NDVI shows significant correlations with the SIOD at 0-1-month lags in March and April over the ORB and north of L18. For the SAM (not shown), only December rainfall over the ORB region and over the area south of L18 were significantly positively correlated (both at zero lag). December and April showed 0 and 1-month negative lag correlations with temperature. No significant NDVI correlations were found.

Table 4.3 Monthly lag detrended correlations (0-2 months) of SIOD with NDVI, rainfall (RN) and temperature (TE) over the ORB region, and north and south of L18 (1982-2015). Only correlations significant at α = 0.05 are shown

SIOD		ORB region			North of L18			South of L18		
		0	1	2	0	1	2	0	1	2
Dec	NDVI	0.40						0.37		
	RN									
	TE									
Jan	NDVI									
	RN				0.47					
	TE				-0.39					
Feb	NDVI							0.36		
	RN				0.45	0.38				
	TE	-0.45			-0.47	-0.36		-0.40		
Mar	NDVI	0.36	0.37		0.35	0.35	0.34			
	RN									
	TE	-0.51	-0.51		-0.52	-0.54	-0.45	-0.44	-0.41	
Apr	NDVI				0.35	0.36	0.40			
	RN	0.36			0.38					
	TE	-0.45	-0.48	-0.39	-0.46	-0.52	-0.41	-0.39	-0.38	

Table 4.4 shows a relatively strong inverse correlation between the Angola Low and rainfall in January, February and April mainly at zero lag over each region. A deeper low implies more tropical convection and hence more cloud bands over the region, consistent with increased rain and cooler temperatures (Mulenga et al., 2003; Cook et al., 2004; Munday and Washington, 2017; Crétat et al., 2018). The latter is apparent in the strong temperature correlations in January at zero lag across the regions and in February at both zero and 1-month lags. NDVI shows significant correlations at 1 and 2-month lags in February and March, respectively over the ORB and south of L18, and in December at zero lag for the latter area. The Botswana High tends to show stronger relationships with rainfall and temperature (**Table 4.5**) than does the Angola Low. The strongest relationships with rainfall and temperature are in January and February at zero lag over all three regions. For NDVI, there are significant zero lag correlations in January, February and April in the ORB and south of L18 (stronger over the latter). One-month lag correlations exist in February and March over the ORB and south of L18 and 2-months over these two regions in April. As for

the climate modes, the temperature relationships with the Botswana High are generally stronger than for rainfall and exist in all months over each region.

Table 4.4 Monthly lag detrended correlations (0-2 months) of Angola Low (AL) with NDVI, rainfall (RN) and temperature (TE) over the ORB region, and north and south of L18 (1982-2015). Only correlations significant at $\alpha = 0.05$ are shown

AL		ORB region			North of L18			South of L18		
		0	1	2	0	1	2	0	1	2
Dec	NDVI							-0.45		
	RN									
	TE			0.44			0.46			0.40
Jan	NDVI	-0.41						-0.52		
	RN	-0.59			-0.55			-0.55		
	TE	0.75			0.76			0.66		
Feb	NDVI		-0.43						-0.51	
	RN	-0.61	-0.52		-0.59			-0.48	-0.48	
	TE	0.45	0.70		0.47	0.68		0.39	0.68	
Mar	NDVI			-0.59						-0.60
	RN					-0.40				
	TE		0.41	0.59		0.45	0.58			0.55
Apr	NDVI									
	RN	-0.43			-0.43			-0.38		
	TE			0.41			0.38			0.41

Seasonal correlations between the variables are given in **Table 4.6** for two different definitions of summer; namely JFMA (left column) and DJFM (right column) since there are variations in the December and April correlations in **Tables 4.2-4.5**. Note that OND is not shown as none were significant. ENSO has a stronger relationship with rainfall over all three regions in JFMA than does the SIOD but in DJFM the reverse is true. For NDVI and temperature, ENSO is more strongly correlated than is SIOD in both JFMA and DJFM. As was the case for the monthly correlations, the Botswana High has stronger relationships with rainfall, NDVI or temperature than does the Angola Low. The not so strong relationships with the Angola Low could be due to differences in the peak seasons for the development of this Angola Low, which is strongest in January-February (Munday and Washington, 2017; Howard and Washington, 2018). In general, relationships for temperature with any of the indices are stronger than those with either rainfall or NDVI. No significant correlations were found for the SAM (not shown). Overall, **Table 4.6** shows stronger correlations north of L18 than south of L18 in both JFMA and DJFM.

Table 4.5 Monthly lag detrended correlations (0-2 months) of Botswana High (BH) with NDVI, rainfall (RN) and temperature (TE) over the ORB region, and north and south of L18 (1982-2015). Only correlations significant at α = 0.05 are shown

BH		ORB region			North of L18			South of L18		
		0	1	2	0	1	2	0	1	2
Dec	NDVI									
	RN				-0.36					
	TE	0.76			0.78			0.71		
Jan	NDVI	-0.48						-0.58		
	RN	-0.71			-0.63			-0.67		
	TE	0.80			0.78			0.75		
Feb	NDVI	-0.42	-0.56					-0.50	-0.64	
	RN	-0.75	-0.55		-0.62			-0.64	-0.55	
	TE	0.85	0.75		0.84	0.69		0.80	0.77	
Mar	NDVI		-0.58	-0.63				-0.35	-0.66	-0.67
	RN		-0.40		-0.39	-0.52				
	TE	0.69	0.78	0.62	0.67	0.77	0.58	0.64	0.71	0.63
Apr	NDVI	-0.43		-0.51				-0.43		-0.54
	RN				-0.40		-0.36			
	TE	0.64	0.65	0.72	0.55	0.68	0.68	0.70	0.56	0.69

Partial correlation analyses were performed to understand how the relationships of the Botswana High with the NDVI, rainfall and temperature change if the influence of ENSO on the Botswana High is removed, to find that such relationships got weaker but generally still remained significant at the 95% significance level. For example, in JFMA, over the ORB region as a whole, correlations (partial correlations) of the Botswana High with the NDVI, rainfall and temperature were -0.48 (-0.04), -0.70 (-0.47) and 0.83 (0.52), respectively. Note that the stated correlations are the ones shown in **Table 4.6**, and that except for the stated Botswana High – NDVI partial correlation, the other two are significant. Relationships of the Angola Low and the SIOD with the NDVI, rainfall and temperature similarly got weaker when the influence of ENSO was removed. The results of partial correlation analysis were similar when DJFM and the monthly data were used.

Table 4.6 JFMA zero lag detrended correlations of ENSO, SIOD, Angola Low (AL) and Botswana High (BH) versus NDVI, rainfall (RN) and temperature (TE) over the ORB region, and north and south of L18 (1982-2015) (left panel). Right panel is as in the left panel but for DJFM zero lags of the same variables. Only significant correlations at α = 0.05 are shown

	ORB	L18: North	L18: South	ORB	L18: North	L18: South
ENSO-NDVI	-0.39		-0.56	-0.44		-0.55
ENSO-RN	-0.59	-0.51	-0.49	-0.63	-0.57	-0.52
ENSO-TE	0.76	0.81	0.69	0.83	0.87	0.75
SIOD-NDVI				0.42		0.53
SIOD-RN	0.45	0.51		0.67	0.58	0.58
SIOD-TE	-0.44	-0.50	-0.36	-0.80	-0.77	-0.80
BH-NDVI	-0.48		-0.64	-0.41		-0.57
BH-RN	-0.70	-0.60	-0.60	-0.72	-0.63	-0.61
BH-TE	0.83	0.84	0.83	0.90	0.90	0.86
AL-NDVI			-0.38			-0.44
AL-RN	-0.45	-0.41	-0.38	-0.57	-0.53	-0.45
AL-TE	0.52	0.56	0.52	0.73	0.76	0.66

4.3.3 Trends

Scatter plots and best-fit linear regression lines between the variables are shown in **Figure 4.5** for cases where the slopes are significant. Rainfall amounts for the high rainfall zone (north of L18) in OND, JFMA and DJFM are more than double those for the low rainfall area to its south but only the latter shows significant slopes with NDVI (**Figures 4.5c,d,e**). For temperature, there is a negative relationship with NDVI in OND and MJJAS for north of L18 (**Figures 4.5a,b**) but only in summer (either JFMA or DJFM) south of L18 (**Figures 4.5f,g**). Overall, **Figure 4.5** suggest that NDVI in the two regions has different relationships with temperature and rainfall which may relate to the fact that south of L18, grassy species are more dominant and the reverse to the north. The sensitivity of NDVI to rainfall south of L18 is in line with other studies for semi-arid African regions where water availability is a constraint for vegetation growth (Malo and Nicholson, 1990; Farrar et al., 1994; Camberlin et al., 2007; Richard et al., 2008, 2012).

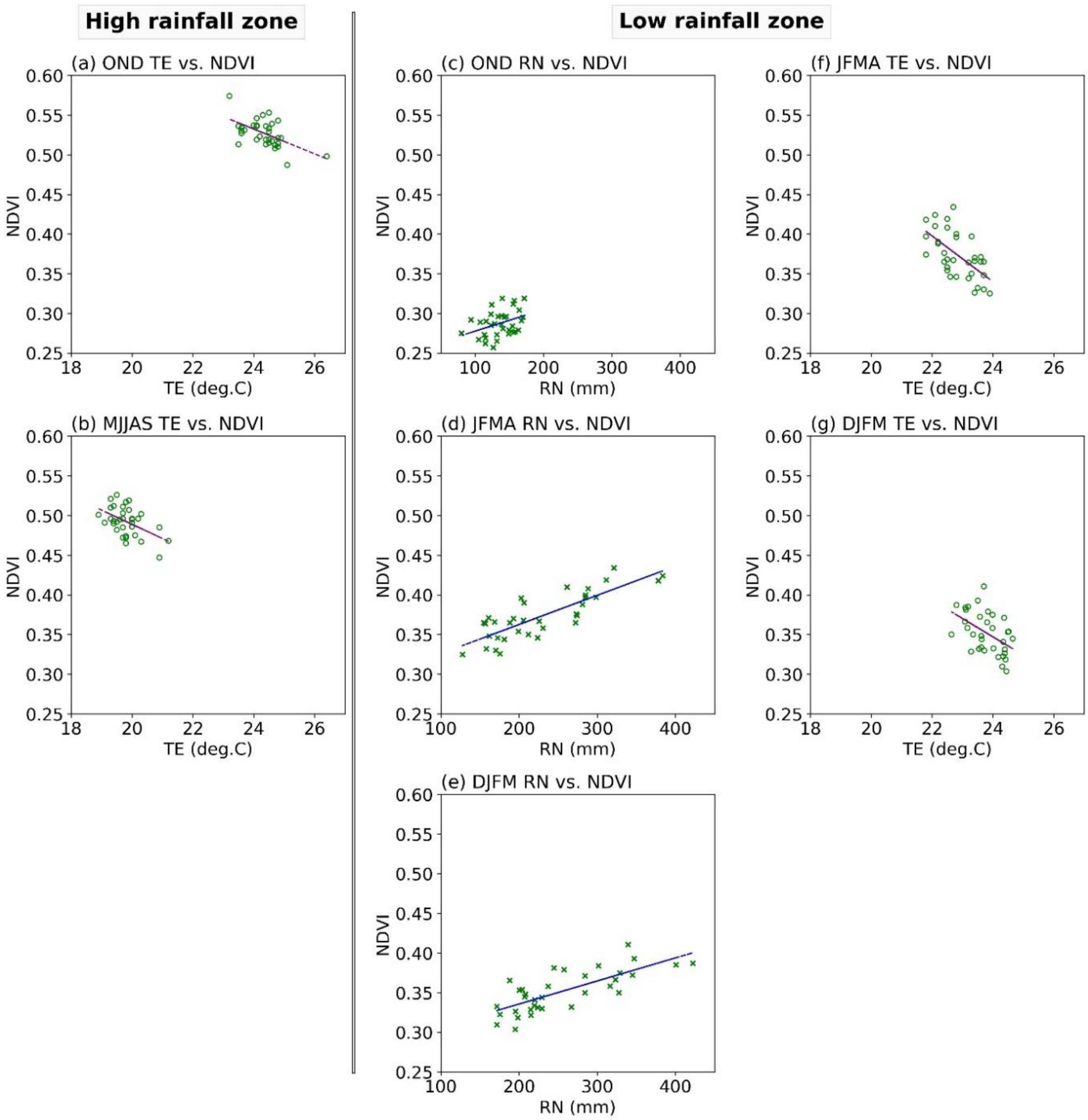

Figure 4.5 Scatter plots and best-fit linear regression lines showing the relationships between temperature (TE) and NDVI north of L18 [(a) and (b), left column] and between rainfall (RN) or temperature and NDVI south of L18 [(c)-(g)], for the period 1982-2015. All slopes are significant at $\alpha = 0.05$. x and y axis limits in TE-NDVI panels are the same. Also, x and y axis limits in RN-NDVI panels are the same.

Trends in the time series of NDVI, rainfall, temperature and river discharge are now considered. For temperature, the strongest warming trend occurs in OND for the area north of L18 (0.35°C/decade). Weaker but still significant warming trends in OND exist over the area south of L18 and the ORB (0.27°C/decade and 0.28°C/decade, respectively). Significant MJJAS warming exists over the ORB (0.22°C/decade) and north of L18 (0.25°C/decade), but the warming trend south of L18 is not significant. JFMA and DJFM temperature trends were not significant. The strongest NDVI trends occur in JFMA (0.37/decade) over the area south of L18 (**Figure 4.6d**), followed by that for the overall ORB region (0.22/decade; not shown), whereas that for the area north of L18 was not significant (**Figure 4.6b**). Using DJFM instead of JFMA gives very similar results. For OND, NDVI trends are significant over both the area north (-0.15/decade; **Figure 4.6a**) and south (0.18/decade; **Figure 4.6c**) of L18, whereas those for the overall ORB region were not significant. None of the regions had significant MJJAS NDVI trends.

For rainfall, OND north of L18 shows a significant trend (wetting, 12.43 mm/decade; **Figure 4.6a**) but not for the other two regions. The significant browning trend in this region may seem counter-intuitive; however, there is a very strong warming trend which may imply more evaporation and desiccation, suggesting that vegetation may be more vulnerable to the temperature increase than the rainfall increase. In addition, the negative NDVI trend may be biased by large negative anomalies in 2005 and 2012-2015 and a very large positive anomaly in 1986. Neither the 1986 nor the 2005 NDVI extremes are matched by corresponding extremes in rainfall. The wetting trends in JFMA in both regions are not significant (**Figures 4.6a,c**) nor are there any trends in DJFM and in the dry MJJAS season. Although the wetting trend in JFMA in the area south of L18 is not significant, it is increasing (1.22 mm/decade), which is consistent with the greening trend there. For river discharge trends over the Cor_Box, there is a significant increasing trend in MJJAS (259.76 Mm^3/decade).

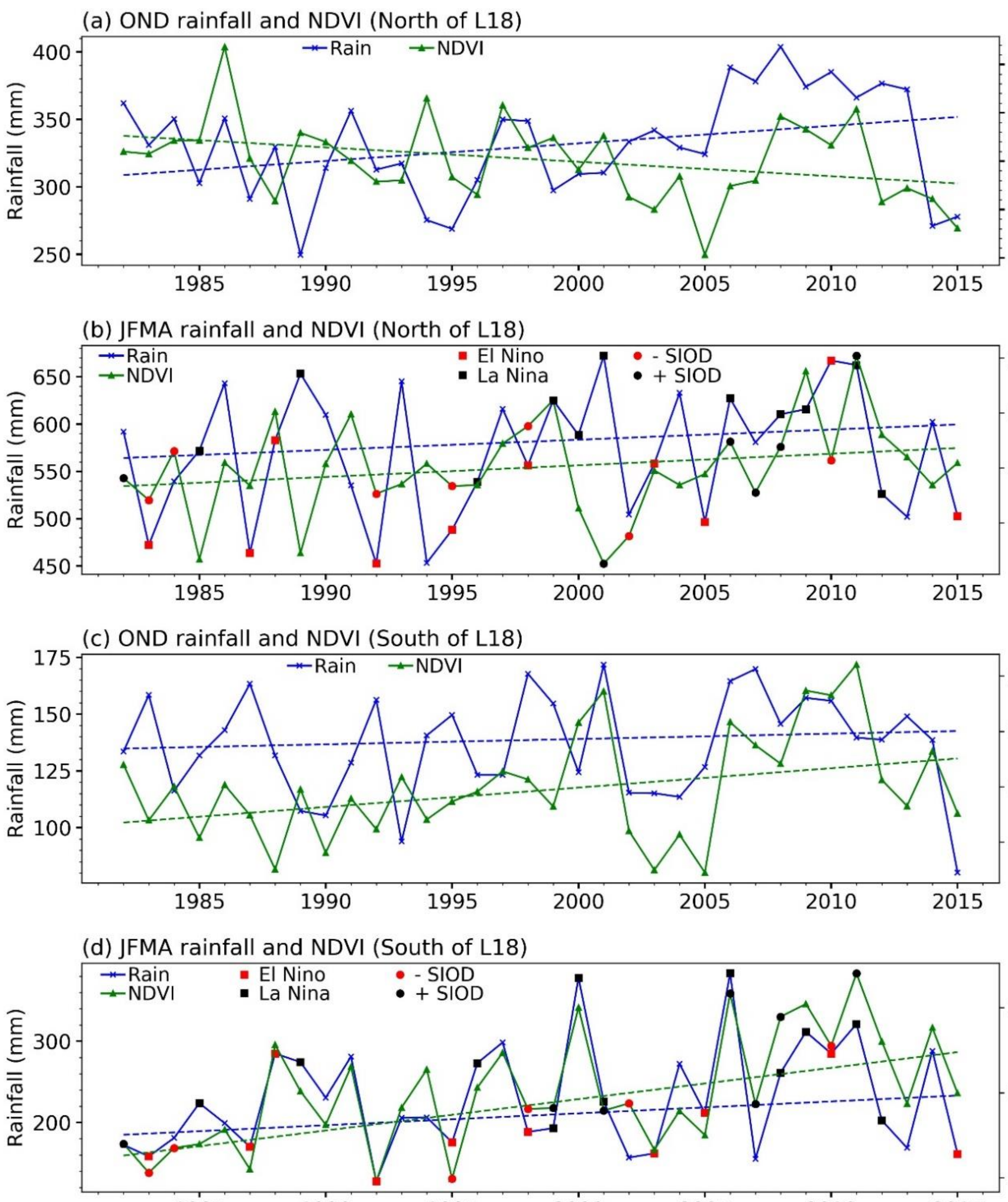

Figure 4.6 (a) Time series of OND rainfall and standardised NDVI anomalies north of L18 (11°-18.9°S, 13°-31.5°E) (1982-2015). (b) is as in (a) but for JFMA. (c) Time series of OND rainfall and standardised NDVI anomalies south of L18 (18.9°-28°S, 13°-31.5°E). (d) is as in (c) but for JFMA. El Niño, La Niña, -SIOD and +SIOD events are labelled in (b) and (d). Dashed lines are trend slopes. Significant slopes at $\alpha = 0.05$ in: (a) 12.43 mm/decade (rainfall), -0.15/decade (NDVI); (c) 0.18/decade (NDVI); (d) 0.37/decade (NDVI).

Figure 4.7 shows spatial trends in the variables. South of L18, there is a generally positive trend in NDVI over the Okavango catchment area as well as the neighbouring region to the southeast, which is more widespread in the summer than in OND or MJJAS (**Figures 4.7a-d**). These results are consistent with Wingate et al. (2019b) who found greening trends across largescale agriculture on communal land in Namibia and with Thoithi et al. (2021) who found significant greening over parts of northern Namibia and northern Botswana in their analyses for December-February. North of L18, there are some significant browning areas in OND and MJJAS whereas the summer shows a mixture of browning and greening. For rainfall (**Figures 4.7e-h**), north of L18 shows mostly significantly increasing OND rainfall as does a small part south of L18 in the catchment area. In JFMA, much of the area south of L18 shows significant wetting as well as a few areas just to the north of this latitude. DJFM rainfall trends are similar but with smaller areas of significance while MJJAS shows no significant trend except drying in the far east. For temperature, **Figures 4.7i-l** show significant warming over most of the region in OND but only over the west and far north in the other seasons. The strong OND warming in the north and west may weaken the NDVI-rainfall pattern similarity in those regions. In summer, the areas of greening are more closely aligned with those showing wetting but there is not complete correspondence since NDVI also depends on other factors such as human activities and fire. Much of the browning NDVI trend in the north or far northwest of the domain seems to match up with large increasing temperature trends there in all seasons.

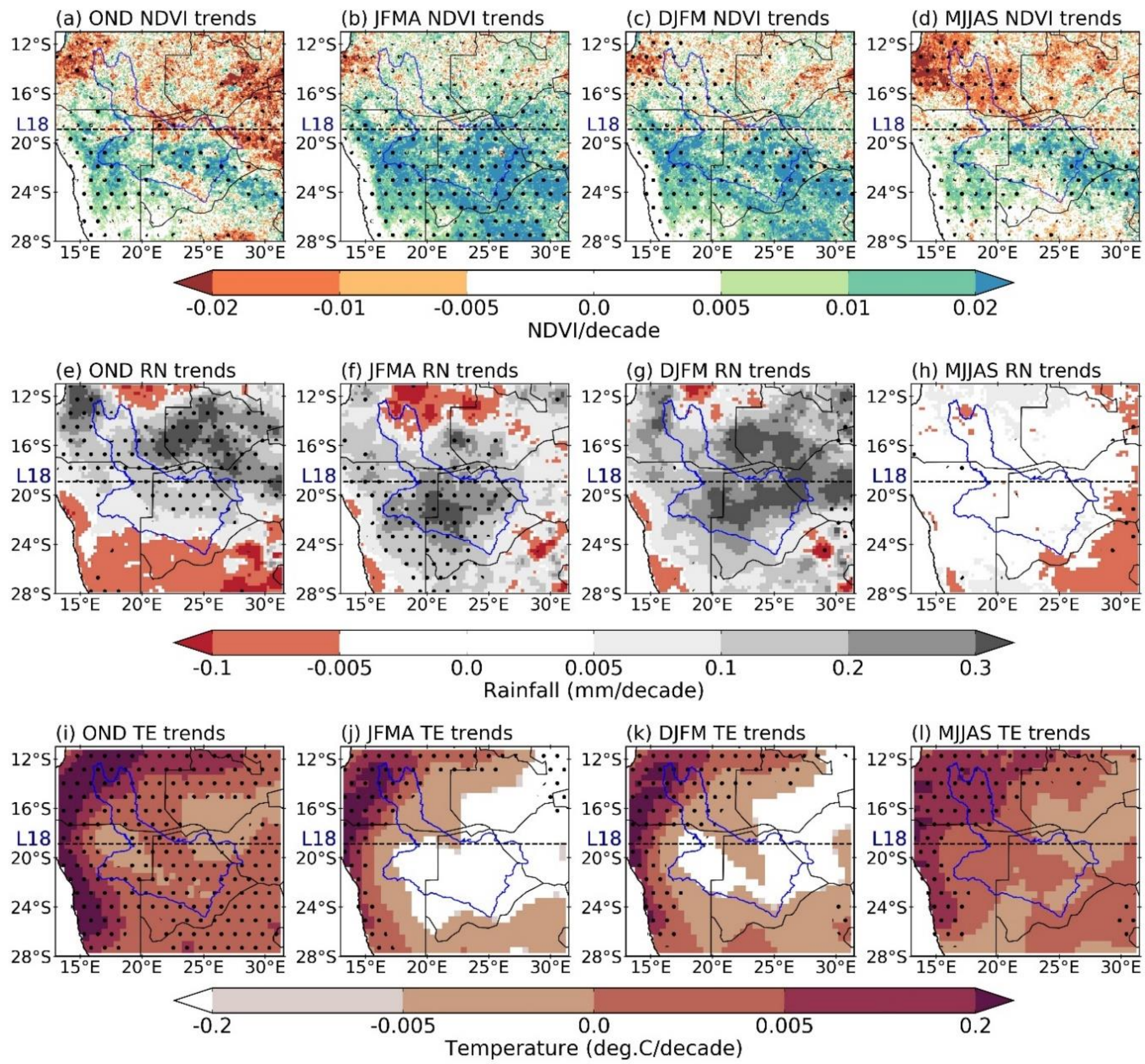

Figure 4.7 (a)-(d) Spatial distribution of trends (represented as per decade) for NDVI in OND, JFMA, DJFM and MJJAS, respectively, over the ORB region (1982-2015). (e)-(h) is as in (a)-(d) but for rainfall (RN). (i)-(j) is as in (a)-(d) but for temperature (TE). Areas with significant trends at α = 0.05 are denoted with stippling. The blue polygon is the outline of the ORB. "L18" is the 18.9°S latitude dividing the study area into high and low rainfall zones.

4.3.4 Interannual variability

In addition to trends, **Figure 4.6** shows that the region is characterized by considerable interannual variability in rainfall and NDVI (as well as temperature and river discharge, not shown). The lowest values of rainfall and NDVI tend to coincide with El Niño/negative SIOD (hereafter, -SIOD) events, whereas their highest values tend to coincide with La

Niña/positive SIOD (hereafter, +SIOD) events. As already shown (*Section 4.3.2*), ENSO and SIOD correlate significantly with rainfall, NDVI and temperature in JFMA but not in OND. **Figures 4.6a,c** also show relatively long wet/dry periods such as wet 2006-2013 and dry 1999-2005, which are reflected in NDVI and river discharge. In general, there is a relatively consistent influence of ENSO on NDVI and temperature, consistent with that previously found for rainfall (Nicholson and Entekhabi, 1987; Reason et al., 2000).

While El Niño (La Niña) and negative (positive) SIOD events are known to generally be associated with droughts (floods) over large areas of southern Africa, there are exceptions. **Figure 4.6** shows that the expected droughts during the El Niño events of 1987/1988, 1997/1998 and 2009/2010 did not occur and NDVI values and river discharge (not shown) were not as low as for other El Niño events. The last two cases have been previously analysed in detail (Reason and Jagadheesha, 2005; Lyon and Mason, 2007; Driver et al., 2019) to find that the Angola Low, which acts as the source for the tropical-extratropical cloud bands and much of the convective activity over the region, did not weaken as expected during an El Niño event. The reason why the Angola Low did not weaken during the 1997/98 and 2009/10 El Niño events could be related to the fact that ENSO impacts may be complicated by SST patterns in the adjacent Indian and Atlantic Oceans, which may influence the circulation and rainfall patterns over southern Africa either both partially dependent on ENSO (Goddard and Graham, 1999; Hoell et al., 2015), or independent of ENSO (Reason, 2001a; Washington and Preston, 2006), and which may also reinforce or oppose ENSO impacts (Reason and Smart, 2015; Hoell et al., 2017).

Although the expected rainfall response of a drought during an El Niño did not happen during the 1987/1988 event, its regional impacts and circulation have not been given much attention. It is important to better understand these non-conforming events; 1987/1988 is also of interest as it was part of the protracted 1986-1988 El Niño. Although protracted El Niño events are often associated with drought over the region (Allan et al., 2003), only JFMA 1987 experienced dry conditions when SST anomalies showed a more eastern equatorial Pacific El Niño than the more central Pacific or Modoki type pattern in summer 1987/1988.

It was anomalously wet in both regions in JFMA 1988 (**Figures 4.6b,d**) but less obviously wet in OND 1987 north of L18 (**Figure 4.6a**) compared to south of L18 (**Figure 4.6c**), hence only JFMA circulation anomalies are shown (**Figure 4.8**). For JFMA, 1988 was the second wettest El Niño summer during the record after 2010 and NDVI values were correspondingly high (**Figures 4.6b,d**). **Figure 4.8a** shows that it was also anomalously wet over many areas in southern Africa. There were positive low-level moisture flux convergence anomalies over most of the subcontinent particularly over Angola, northern Namibia and western Zambia (**Figure 4.8b**), and positive precipitable water anomalies (**Figure 4.8c**) indicating more moisture over the region. Easterly anomalies in the northern Mozambique Channel region suggest less export of moisture away from tropical southeast Africa towards northern Madagascar by the northwesterly monsoon and hence more moisture available over the mainland. The anticyclonic anomaly over and east of Madagascar also helped advect more moisture inland. The lack of an obvious strengthening of the mid-level Botswana High in JFMA 1988 and reduced subsidence (not shown), unlike the strengthening of this system which occurs in most other El Niño events (Driver and Reason, 2017), may also help explain the relatively wet conditions. Interpolated OLR anomalies were negative over most of the region (**Figure 4.8d**) suggesting enhanced convective cloud, consistent with the wetter conditions. SST anomalies in the tropical southeast Atlantic Ocean were positive (**Figure 4.8e**) which has previously been associated with wetter summers over subtropical southern Africa (Cook et al., 2004; Reason et al., 2006). Thus, regional circulation anomalies during summer 1987/1988 were more favourable for wetter conditions over subtropical southern Africa than are typically expected during El Niño events.

Given more frequent occurrences of ENSO Modoki events in recent decades (Ashok and Yamagata, 2009; Yeh et al., 2009), it was also of interest to calculate correlations of the ENSO Modoki index (Ashok et al., 2007) with NDVI, rainfall and temperature over the ORB region. Except for the correlation between the ENSO Modoki index and NDVI ($r = -0.22$, $p > 0.05$) which was not significant, those between the ENSO Modoki index and the other two variables [rainfall ($r = -0.33$, $P < 0.05$), temperature ($r = 0.36$, $p < 0.05$)] were significant during JFMA 1982-2015. All these three correlations are relatively weaker than those between the Niño 3.4 index (discussed above) representing ENSO and the three variables (NDVI, rainfall, temperature) shown in **Table 4.6**.

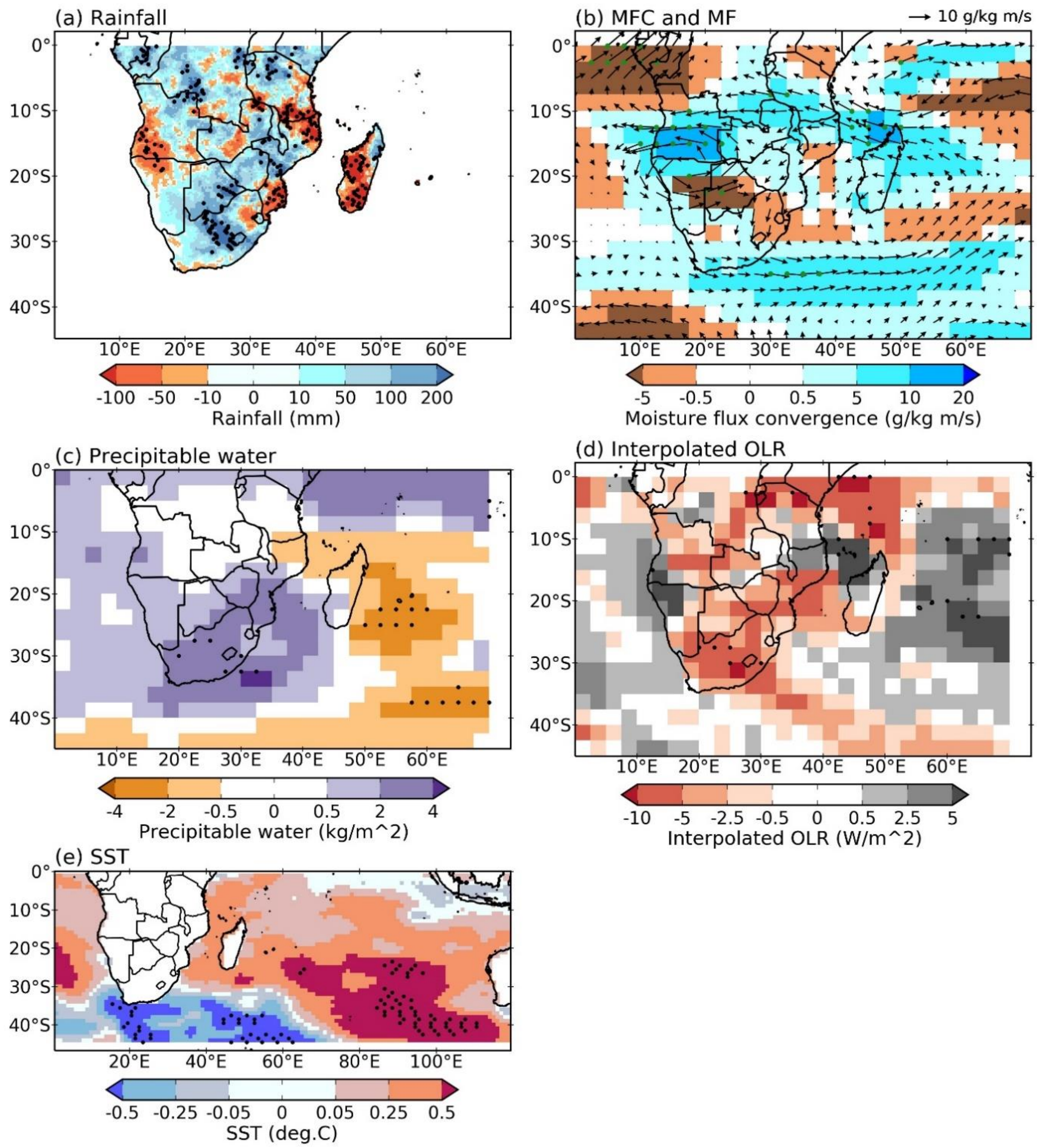

Figure 4.8 JFMA 1988 circulation anomalies with respect to 1981-2010 climatology. (a), (b), (c), (d) show anomalies of rainfall, 700 hPa moisture flux convergence (MFC) (shading) and moisture flux (MF) (vectors), precipitable water and interpolated OLR, respectively, over the region 45°S-0°N, 0°-70°E. (e) shows anomalies of SST (45°S-0°N, 0°-120°E). Areas with statistically significant anomalies based on bootstrap 95% confidence level are denoted with stippling.

As already mentioned, summer 1987/1988 showed a central Pacific type of El Niño SST anomaly. Ratnam et al. (2014) investigated the impacts on December-February southern

African rainfall of central Pacific (CP) versus eastern Pacific (EP) type of events to find that El Niño related dry conditions over southern Africa tend to be more severe for the latter type. Although both types of El Niño generally suppress precipitation over southern Africa, the impacts on moisture fluxes into the region are stronger for the former than for the latter type of events, such as 1987/1988. Yeh et al. (2009) found that the frequency of CP El Niño events has increased compared to the EP type particularly from the 1990s, which they associated with a change in the thermocline structure in the equatorial Pacific as a result of anthropogenic global warming. Ashok and Yamagata (2009) suggested that the CP El Niño events would become more frequent in the future than the EP type. If that happens, then the relationships of ENSO with rainfall, temperature and NDVI over the ORB (**Tables 4.2** and **4.6**) may change in the future.

4.3.5 The 2006-2013 wet epoch

The substantially wet and greener (2006-2013) period compared to the dry (1999-2005) period (**Figure 4.6**) mentioned in the preceding section is now considered. These wet and dry periods are clearer in the area north of L18 than in the area south of this latitude. Most attention on these well-known quasi-decadal to decadal wet and dry spells of subtropical southern Africa climate (e.g., Tyson et al., 1975; Tyson, 1986; Wolski et al., 2012; Malherbe et al., 2014; Reason, 2016) has focused on the mid or late summer rather than on OND. Here the wet (2006-2013) and dry (1999-2005) signal is stronger in OND, hence it is of interest to investigate the potential mechanisms associated with it. In addition, it has been shown above that OND rainfall may influence JFMA vegetation and river discharge. These longer-term wet anomalies are important since they have positive effects on NDVI and water resources.

Composite difference anomalies between the wet 2006-2013 and 1999-2005 dry epoch are shown in **Figure 4.9**. Although many parts of southern Africa were wetter in OND 2006-2013 relative to 1999-2005, the signal was particularly strong over the lower lying area of southeastern Angola/western Zambia/northern Botswana. This area of particularly wet OND seasons matches up well with that in low-level moisture flux convergence (**Figure 4.9b**) which arises from stronger than average low-level westerly anomalies from the tropical southeast Atlantic into northern Angola/Congo and southerly anomalies over western Zambia. **Figure 4.9c** indicates that there were large positive anomalies in precipitable water over Angola and the neighbouring ocean, which may be related to the warmer SST conditions in the tropical southeast Atlantic (**Figure 4.9f**) and westerly anomalies there (**Figure 4.9b**). In the Pacific, La Niña Modoki type SST anomalies were present. Almost all of Angola and the western half of Zambia show relative uplift (**Figure 4.9d**) consistent with the rainfall composite differences.

Furthermore, the OLR differences (**Figure 4.9e**) suggest that the increased rainfall over the eastern Angola/western Zambia/northern Botswana may have resulted from increased local tropical convection and associated cloud band activity stretching southeast towards northeastern South Africa and the neighbouring northern Agulhas Current region. Differences in low to mid-level specific humidity (not shown) suggest that the Congo Air Boundary, which separates moist equatorial unstable air from drier subtropical air further south over southern Africa (Howard and Washington, 2019, 2020) shifted slightly further south during 2006-2013 relative to 1999-2005, favourable for more moisture over the region. Taken together **Figures 1.1** and **4.9a-d** suggest that low-level moisture converging over southeastern Angola/western Zambia border region was confined there to some extent by the surrounding topography which together with the enhanced uplift led to larger positive rainfall anomalies there than elsewhere in southern Africa.

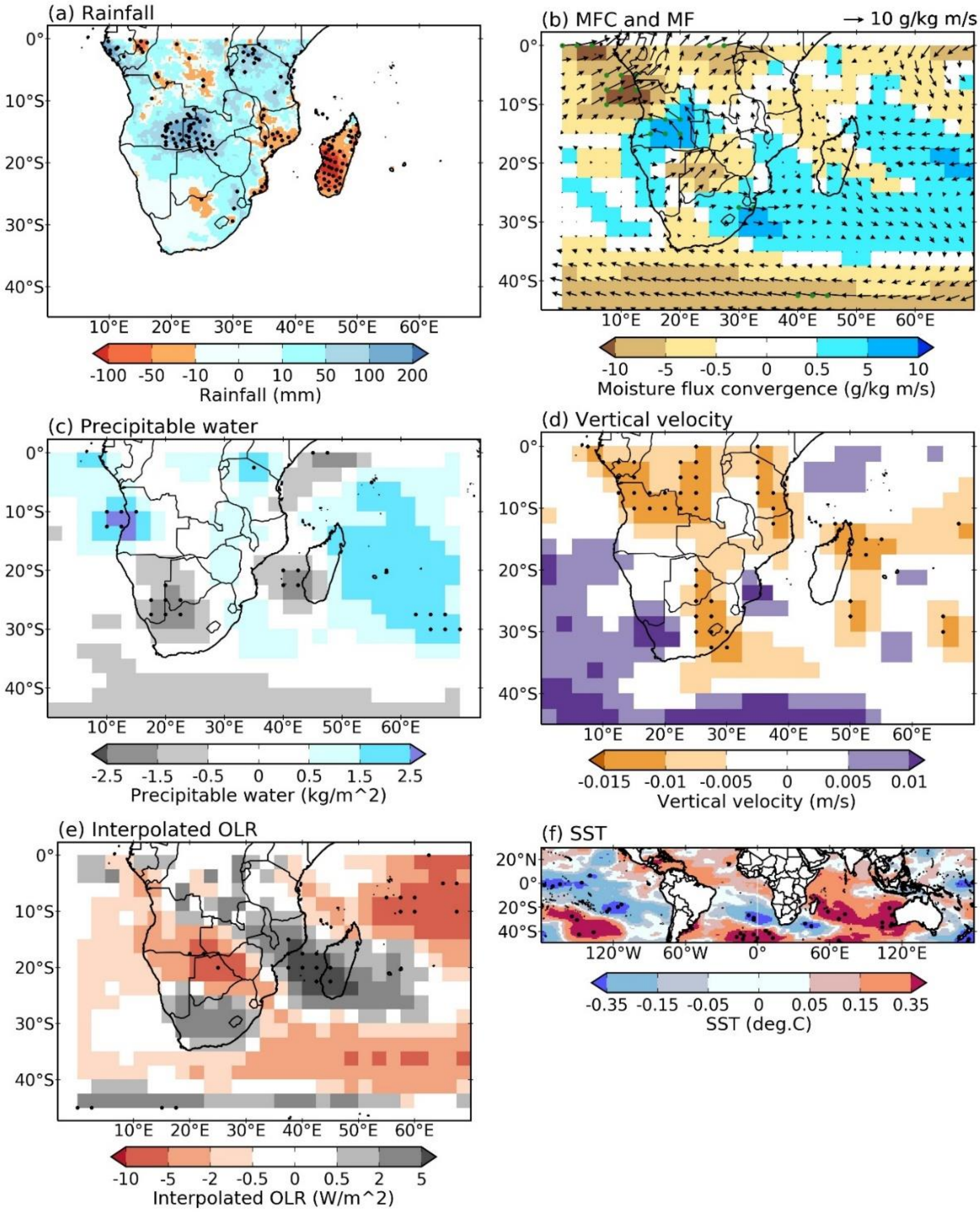

Figure 4.9 OND composites of wet (2006-2013) minus dry (1999-2005) period. (a), (b), (c), (d) and (e) show composite anomalies of rainfall, 700 hPa moisture flux convergence (MFC) (shading) and moisture flux (MF) (vectors), precipitable water, 700 hPa vertical velocity and interpolated OLR, respectively, over the region 45°S-0°N, 0°-70°E. (f) shows composite anomalies of SST (50°S-30°N, 180°W-180°E). Areas with statistically significant anomalies based on bootstrap 95% confidence level are denoted with stippling.

4.4 Conclusions

Rainfall, temperature and their relationships with NDVI and river discharge over the Okavango River Basin, a highly biodiverse and sensitive region in southern Africa, have been studied on various time scales. A pronounced annual cycle is present over the basin with 1-2-month lags between NDVI and rainfall. Consistent with other studies (e.g., Murray-Hudson et al., 2006; Hughes et al., 2011), rainfall and temperature show pronounced interannual variability which is reflected in river discharge and NDVI. Monthly lag correlations for river discharge are less coherent than those for NDVI, but both discharge-rainfall and discharge-temperature correlations are significant [positive (negative) for the former (latter) correlation] at 1-month lags. Both river discharge and NDVI are more strongly correlated with rainfall than with temperature at monthly and seasonal time scales. MJJAS river discharge essentially responds to the previous season's rainfall (MJJAS rainfall is minimal).

Rainfall-NDVI regression slopes are significant over the area south but not north of L18, suggesting that vegetation is more sensitive to rainfall over the former region. Overall, NDVI-rainfall and NDVI-temperature relationships are statistically different north and south of L18. Relationships between rainfall and the various climate mode or circulation indices tend to be stronger for the region north of L18 than for the area south of L18. The correlations are stronger in the summer than in OND. These relationships with rainfall, are consistent with other studies over southern Africa (Lindesay, 1988; Reason et al., 2000; Behera and Yamagata, 2001; Driver and Reason, 2017). On monthly scales during the summer, there are significant relationships at both 0 and 1-month lags between rainfall or temperature (and to lesser extent NDVI) and the climate modes [El Niño-Southern Oscillation (ENSO), subtropical Indian Ocean Dipole (SIOD)] or the Botswana High, which are generally strongest in February and March. The rainfall (temperature) correlations with the Botswana High and ENSO were negative (positive), with the SIOD they were positive (negative), and the NDVI correlations (negative) were significant mainly with ENSO.

The 1987/1988 El Niño has been found to be one of the few El Niño events during which drought conditions (typical for these events [Reason and Jagadheesha, 2005; Lyon and Mason, 2007; Driver et al., 2019]) did not occur. Such El Niño events imply higher vegetative activity and water availability than during typical El Niño events; hence this 1987/1988 case has been investigated. Increased low-level moisture flux convergence and warm SST anomalies in the tropical southeast Atlantic Ocean favoured wetter conditions over the ORB region in this summer rather than the expected El Niño drought. Similarly, the wetter and greener OND 2006-2013 epoch was related to warmer SST in the tropical southeast Atlantic (as well as La Niña Modoki conditions), increased low-level moisture flux convergence and uplift over Angola and western Zambia relative to the preceding dry and browner 1999-2005 dry epoch.

Finally, significant greening trends were found south of L18, particularly in summer, while north of L18, there was a strong browning trend in MJJAS but not in the other seasons (except in the far west). Rainfall trend maps show significant increasing trends over most of the area north of L18 in OND as well as central Botswana while JFMA shows significant wetting over most of the area south of L18 as well as northwestern Namibia. River discharge over the Cor_Box are significant and positive only in MJJAS. Note that the river discharge and NDVI trends could, to some extent, be masked by human activity such as land clearing for agriculture and settlement (VanderPost et al., 2005; Weinzierl and Schilling, 2013). Almost the entire region shows significant warming in OND while in the other seasons, such warming mainly occurs in the far west and north of the ORB region. The warming in temperature is consistent with other studies over southern Africa and more broadly over Africa (Barros and Field, 2014; Engelbrecht et al., 2015; Maúre et al., 2018). The strong warming trend may worsen water losses from the region with adverse impacts on vegetation growth, water availability, floodplain farming on the periphery of the Okavango Delta, and tourism while compounding the effects of extreme events such as heat waves, droughts and fires in the region.

The next chapter considers extreme rainfall events over the ORB region.

Chapter 5: Extreme rainfall events over the Okavango River basin, southern Africa

This chapter is presented as the paper submitted to Weather and Climate Extremes. It addresses the questions below:

Moses, O., Blamey, R.C., Reason, C.J.C., 2022. Extreme rainfall events over the Okavango River basin, southern Africa. Submitted to Weather and Climate Extremes.

- What are the characteristics of extreme rainfall events over the western central southern Africa (WCSA)?
- What are the most important weather systems driving these events?
- What proportion of these extreme events contribute to summer rainfall totals?
- What are the factors that might have contributed to the severe floods that occurred over Ngamiland during the summer of 2017?

Abstract

Characteristics of extreme rainfall events in the highly biodiverse Okavango River Basin (ORB) in western central southern Africa are analysed for the main rainy season, January-April (JFMA). These characteristics include frequencies, intensities, spatial distributions, variability and trends of extreme rainfall events accumulated over 1-day (DP1) and 3-days (DP3). On average, DP1 (DP3) events contribute ~10% (~17%) rainfall totals but in some years they both contribute more than 30%. Tropical-extratropical cloud bands are responsible for most of the events with tropical lows also important. The considerable interannual variability in extreme events appears related to El Niño-Southern Oscillation (ENSO) and the Botswana High variability. Although ENSO influences the extreme events as well as rainfall totals more generally over southern Africa, by far the wettest season over the iconic Okavango Delta region, in Ngamiland, Botswana, occurred during neutral JFMA 2017. These heavy rains resulted from a deeper Angola Low, weaker mid-level Botswana High which favoured convection in the region together with anomalous westerly moisture fluxes from the tropical southeast Atlantic and enhanced low-level moisture convergence over most of the region during January-early March. A dry period from mid-March was broken by the second most intense rainfall event on April 22nd, resulting from a cut-off low. Significant increasing trends were found in DP1 frequencies, as well as in rain-days and rain totals over many areas. These trends have important implications for water and agricultural management, and wildlife conservation in the highly biodiverse ORB.

5.1 Introduction

Although drought is often considered to be the most damaging climate event in southern Africa in terms of socio-economic impact, devastating floods resulting from severe weather can sometimes cause significant loss of life and devastation to infrastructure. For example, about 1000 people died as a result of Tropical Cyclone Eline making landfall near Beira, Mozambique in February 2000 (Reason and Keibel, 2004). Other well-known tropical cyclone induced floods in southeastern Africa which caused huge loss of life, displaced tens of thousands of people and resulted in much damage are Favio in 2007, Idai and Kenneth in 2019 (Mawren et al., 2020). In addition to tropical cyclones, the region has sometimes experienced devastating floods resulting from mesoscale convective systems (Blamey and Reason, 2013; Morake et al., 2021), tropical lows and tropical-extratropical cloud bands (Rapolaki et al., 2019; Mpungose et al., 2022). For example, the January 2013 event in northern South Africa/southern Mozambique which involved both a cloud band and a tropical low caused 113 deaths and temporal displacement of over 185 000 people (Manhique et al., 2015).

More recently in April 2022, severe flooding along the east coast of South Africa associated with a cut-off low resulted in over 400 deaths and displacement of over 40000 people (UNICEF, 2022). These and other examples highlight the vulnerability of the population in many parts of southern Africa to extreme rainfall events. Such vulnerability is an ongoing problem since the Intergovernmental Panel on Climate Change (IPCC) fifth (IPCC, 2013) and sixth (IPCC, 2021) reports show that the frequency and intensity of extreme rainfall events are likely to increase in a warming climate, and thus there is need to better understand these events over the region.

While extreme rainfall events have been relatively well studied over some parts of southern Africa such as South Africa (e.g., Dyson et al., 2015), Namibia (e.g., Muller et al., 2008) and Mozambique (e.g., Manhique et al., 2015; Rapolaki and Reason, 2018), relatively little research has been done on these events in the Okavango River Basin (ORB). The little research on extreme rainfall events in the ORB include that done by Wolski et al. (2014), who analysed results from an attribution modelling system designed to examine how anthropogenic greenhouse gas emissions contributed to the floods that occurred in this ORB in 2009-2011. They found that the probability of occurrence of these floods in the current climate is likely lower than it would have been in a climate free of anthropogenic greenhouse gases. The ORB region (blue polygon in **Figure 5.1a**), located in central southern Africa, is of particular interest since it has high biodiversity, contains unique ecosystems as well as the Okavango Delta, where the streamflow originating largely in the Angolan Highlands terminates. The Delta is a United Nations Educational, Scientific and Cultural Organization (UNESCO) world heritage and Ramsar site (UNESCO, 2014).

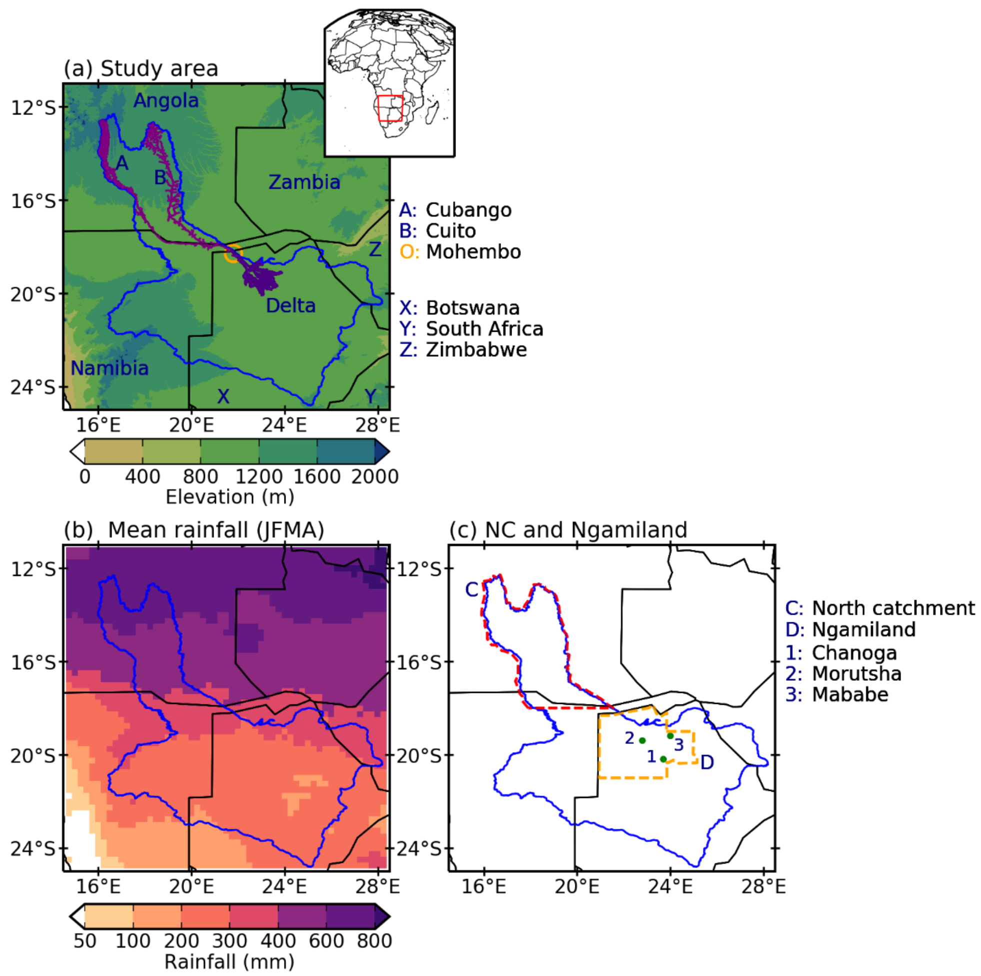

Figure 5.1 (a) The study area, i.e., the WCSA (11°-25°S, 14.5°-28.5°E) and its elevation (highest elevation of 1600-1800 m above sea level is in central Angola). Location of the study area in southern Africa is shown in the insert of this panel. The Okavango Delta, the two main rivers (Cubango and Cuito), and country names are indicated and labelled on the right of the figure. (b) JFMA mean rainfall (1981-2021). (c) Location of the north catchment (NC) and Ngamiland within the ORB (blue polygon in all 3 panels). Villages in Ngamiland that reported floods during JFMA 2017 include those denoted by "1", "2" and "3", labelled on the right of the figure.

Over the ORB and typically elsewhere in Africa south of 10°S, seasonal rains typically start sometime after the beginning of October and end in March or April, except in the far southwest and the south coast of South Africa. This rainfall has mostly convective origins, either brought about by random air mass thunderstorms or organised mesoscale convective systems (MCSs; Blamey and Reason, 2012, 2013), tropical lows (Munday and Washington, 2017; Howard et al., 2019; Howard and Washington, 2020; Rapolaki et al., 2019, 2020) or tropical-extratropical cloud bands (or tropical-temperate troughs) (Harrison, 1984). The latter are synoptic scale features typically extending from southern Angola diagonally in a southeastwards direction to the southwest Indian Ocean and producing widespread rainfall (Hart et al., 2010, 2013; Ratna et al., 2013; Manhique et al., 2011, 2015; Macron et al., 2014). In anomalously dry summers over subtropical southern Africa, the cloud bands tend to be located much further east and mainly over the southwest Indian Ocean.

There is relatively strong rainfall gradient within the ORB with the Angolan Highlands receiving much higher rainfall totals compared to the Okavango Delta (**Figure 5.1b**). The Angolan Highlands are typically wetter than elsewhere in the ORB due to the presence of the Angola Low (Mulenga et al., 2003; Cook et al., 2004; Munday and Washington, 2017; Crétat et al., 2018; Howard and Washington, 2018) as well as orographic uplift and convection. This low-level convergence results from moisture sources in the western Indian Ocean (main source), the tropical southeast Atlantic Ocean north of about 16°S and the Congo Basin (D'Abreton and Tyson, 1995; Rouault et al., 2003a; Cook et al., 2004; Reason et al., 2006; Vigaud et al., 2009; Manhique et al., 2015; Reason and Smart, 2015; Rapolaki et al., 2019, 2020).

As with other parts of southern Africa, the summer rains over the ORB are influenced by the El Niño-Southern Oscillation (ENSO; Lindesay, 1988; Reason et al., 2000; Reason and Jagadheesha, 2005; Blamey et al., 2018; Moses et al., 2022). Other modes of variability affecting subtropical southern African summer rainfall [Subtropical Indian Ocean Dipole (Behera and Yamagata, 2001), Southern Annular Mode (Thompson and Wallace, 2000)] do not seem to strongly impact on the ORB however (Moses et al., 2022). Although much work has been done in connection with ENSO and its relationship with seasonal rainfall totals over southern Africa, not much attention has been paid to its impact on extreme rainfall events over the ORB. Further work is also needed to better understand the role of ENSO on impacting regional circulation features. For example, the mid-level Botswana High tends to suppress rainfall when it is strong since a strong Botswana High is associated with increased subsidence over the region, and the opposite tends to occur when it is weak (Reason, 2016; Driver and Reason, 2017).

While it can be argued that extreme rainfall events make an important contribution to the ORB streamflow and maintain the much-needed water levels to support the unique biodiversity in this region, they can also cause local flash flooding leading to loss of life and widespread damage to crops and settlements. For example, severe flooding in 2004 damaged crops on flood recessed land in the periphery of the Delta (Magole and Thapelo, 2004). Also, over Ngamiland, which is the administrative district in northwestern Botswana within which the iconic Okavango Delta lies (see **Figure 5.1c** for locations), records from the Botswana Disaster Management Office reveal that severe floods occurred in 2009, 2010, 2011, and 2017 with all causing substantial damage.

This Delta region has the most biodiverse and sensitive ecosystems in the ORB and has been termed a global biodiversity hotspot (Francis et al., 2021), attracting tourists from all around the world (Mbaiwa, 2017). The ecosystems of this iconic Delta crucially depend on the highly seasonal streamflow which originates from rainfall in the Angolan Highlands (McCarthy et al., 2003; Andersson et al., 2003, 2006; Gumbricht et al., 2004; Murray-Hudson et al., 2006; Wilk et al., 2006; Hughes et al., 2011; Wolski and Murray-Hudson, 2006b, 2008; Wolski et al., 2006; Wolski et al., 2012; Wolski et al., 2014), further highlighting the importance of the ORB. In addition, the streamflow reaching the Delta region is the major source of freshwater for the rural population there, most of whom are impoverished and rely on subsistence farming (mainly maize) or basic livestocking for survival (Kgathi et al., 2006; Weinzierl and Schilling, 2013).

However, since many rainfall events typically extend beyond river basin boundaries, here a larger region is chosen within which to perform the analysis; namely a box in western central southern Africa (hereafter referred to as WCSA) (**Figure 5.1a**). This box was chosen such that the position of its boundaries did not exceed a distance of 2° from the western-, northern-, eastern- and southern-most point of the Okavango River catchment spatial extent (blue polygon), to ensure that extreme events that covered a substantial part of this catchment were captured. Specifically, this study (i) examines variability in the distribution of extreme rainfall events and their trends over the WCSA, (ii) identifies the most important weather systems driving these events, (iii) examines the contribution of these events to the summer rainfall totals and (iv) examines factors that might have contributed to the severe floods that occurred over Ngamiland during the summer of 2017. A better understanding of these extreme rainfall characteristics as well as the weather patterns associated with them is important for improving weather and seasonal forecasts in the region. Such understanding is also crucial for resource management purposes, given that the water and food security of the ORB as well as its unique ecosystems depend crucially on rainfall distribution during the summer rainy season.

5.2 Data and Methods

5.2.1 Datasets

The study area is the WCSA box (11°-25°S, 14.5°-28.5°E) (**Figure 5.1a**) within which the ORB (blue polygon) lies. Due to a shortage of rainfall observations in this region, particularly in Angola, the Climate Hazards Infrared Precipitation with Station dataset (CHIRPS) version 2 (Funk et al., 2015) is used. This dataset has daily data available from 1981 to near-present and a spatial resolution of 0.05°. Moses et al. (2022) found that CHIRPS data performed reasonably well when compared with monthly rain gauge data for stations in northern Botswana and Namibia. Similarly, Rapolaki et al. (2019) and Thoithi et al. (2021) found good agreement between CHIRPS and station data in northern South Africa. As a further check, rainfall characteristics over the WCSA were also evaluated using the Tropical Rainfall Measuring Mission (TRMM; Huffman et al., 2007) and Precipitation Estimation from Remotely Sensed Information using Artificial Neural Networks-Climate Data Record (PERSIANN-CDR; Nguyen et al., 2019) datasets (both at a coarser resolution of 0.25°), to find very similar results to those for CHIRPS; hence only the latter are shown.

ERA5 reanalyses (0.25° resolution) from the Copernicus (Copernicus Climate Change Service, 2017) were used to investigate circulation patterns and weather systems associated with extreme rainfall events. Atmospheric variables used included 500 and 850 hPa geopotential heights, wind fields, specific humidity and omega. National Oceanic and Atmospheric Administration (NOAA) interpolated outgoing longwave radiation (OLR) and South African Weather Service (SAWS) synoptic charts were also used. ERA5 reanalysis and

OLR datasets are available from 1979 to near real time. In addition, 3-hourly Gridded Satellite (GridSat-B1) data (0.07° spatial resolution) (Knapp et al., 2011) were used for weather system identification.

The Niño 3.4 index, defined as the monthly average of the Sea Surface Temperature (SST) anomalies in the Central Pacific (5°N-5°S; 120°-170°W), from NOAA Climate Prediction Centre (CPC) (Huang et al., 2021), was used for ENSO. For an index of the Botswana High, 500 hPa geopotential height averaged over 19°-23°S, 16°-21°E (based on Driver and Reason, 2017) was used. Positive (negative) anomalies of this index indicate a strong (weak) Botswana High. A stronger Botswana High implies more regional subsidence over much of southern Africa, and hence less convective rainfall (Reason, 2016). NOAA Optimally Interpolated SST data (Huang et al., 2021) (0.25° resolution) were used to assess SST patterns during the summer.

Data related to the impacts of the floods that occurred over Ngamiland during January-April (JFMA) 2017 were provided by the Botswana Disaster Management Office. Data download links are provided in the acknowledgments.

5.2.2 Methods

Extreme rainfall events were identified considering all grid-points with positive rainfall anomalies over the WCSA. A thorough method used to identify these events, which accounts for both event intensity and spatial extent, is discussed from the fourth paragraph of this section. While extreme rainfall events can often cover large areas such as the WCSA, attention was also paid to their spatial characteristics over two sections of the ORB. One is the Ngamiland district already mentioned and the other, referred to as north catchment, is that part of the ORB upstream of the Delta apex at Mohembo (18°S) (**Figure 5.1c**), where most of the ORB streamflow is generated (Andersson et al., 2003; Wolski and Murray-Hudson, 2008; Moses et al., 2022). Downstream after Mohembo, the Okavango River feeds into the Okavango Delta located in Ngamiland. While the largest rainfall contributions to the streamflow occur over the north catchment, contributions over the Delta itself can be considerable, inducing flooding in well above average rainfall years (Andersson et al., 2003; Wolski et al., 2006; M. Murray-Hudson, personal communication, 2022). Hence, extreme rainfall events that cover either the north catchment or Ngamiland or both are examined below.

Two types of extreme rainfall events were considered; those accumulated over a 1-day (DP1) and those over a 3-day period (DP3). Note that extreme events accumulated over a 2-day period were very similar to the DP3 events, whereas those accumulated over 4-days or longer were rare and hence were not considered. It was of interest to consider extreme events that are common in the ORB since they are likely to contribute more to the streamflow and are also likely to be associated with most of the disasters.

Previous work over southern Africa (New et al., 2006) has used indices developed by the Expert Team on Climate Change Detection and Indices (ETCCDI; Zhang et al., 2011; Sillmann et al., 2013) based on the 95th percentile of precipitation, to assess extreme events. Indeed percentile-based indices are suitable for spatial comparisons of extremes (Zhang et al., 2011). While high-intensity rainfall events that are restricted to one or two grid-points can have impacts there, those with a larger spatial extent can affect a much greater area, hence accounting for both event intensity and spatial extent over large areas like the WCSA is important. For this reason, this study makes use of the method developed by Hart and Grumm (2001) and further adopted by Ramos et al. (2014, 2017, 2018) to rank extreme events based on both their intensity and their spatial extent. This method has been used successfully to study extreme rainfall events elsewhere in southern Africa such as the Limpopo region (Rapolaki et al., 2019) as well as in the Iberian Peninsula (Ramos et al., 2014, 2017, 2018).

Using this method of Ramos et al. (2014, 2017, 2018), DP1 and DP3 events were identified and ranked in three steps. The first step involved computation of the 95th percentile for each grid-point. To smooth the highly variable 95th percentile series, a 7-day running mean was applied. Then, extreme precipitation anomaly (N) for each grid-point was computed by subtracting the smoothed 95th percentile (μ) from daily precipitation totals (precip) using the equation

$$N_{d,i,j} = precip_{d,i,j} - \mu_{d,i,j} \qquad (5.1)$$

where subscripts d, i, j denote day d and grid point (i,j). A day was taken to be an extreme day if at least one grid-point had a positive extreme rainfall anomaly.

The second step involved accumulation of rainfall anomalies for the DP3 events over each 3-day period. For example, the 3-day accumulated rainfall anomaly for 8 February 1981 was obtained by summing up the anomalies for 6-8 February 1981 (with event date being that of the last day of the 3-day period). To be considered as a single event, the associated rainfall anomaly for each day of the 3-day period had to be greater than zero.

The third step involved computation of anomalous magnitudes of both DP1 and DP3 events used to rank both events. The anomalous magnitude (R) of an extreme event was given by an index that was computed using the equation

$$R = A \times M \tag{5.2}$$

where A is the area (in percentage) of grid-points with positive standardised rainfall anomalies and M is the average value of these positive anomalies. The DP1 event with the largest R was ranked number 1, and similarly for the DP3 events.

The dominant weather systems responsible for the top 200 DP1 and DP3 events were then identified. Rapolaki et al. (2019) similarly derived the top 200 daily extreme rainfall events over the Limpopo River basin, focusing only on DP1 events. Cloud bands were identified from reanalyses, satellite images and synoptic charts using the definition provided by Harrison (1986) and Kuhnel (1989), where these systems had to have their origin near the equator, and a northwest-southeast direction extending to the midlatitude southern Indian Ocean. Following Blamey and Reason (2012) and Morake et al. (2021) who used an adapted version of Maddox (1980) criteria for identifying Mesoscale Convective Complexes (MCCs, one of the most well-known type of MCSs), which, for example, identifies MCCs as systems that contain a cloud top temperature less than -52 °C, in this thesis MCSs were identified as follows. Cloud top temperature (brightness temperature) of the system had to be colder than -52°C, the system had to last for more than three hours, and the rainfall produced by the system had to cover at least 100 km in a linear or quasi-circular pattern. Tropical lows were identified using the International Best Track Archive for Climate Stewardship (IBTrACS) dataset (Knapp et al., 2010).

Possible relationships between extreme rainfall events and climate modes (ENSO, Botswana High) were investigated using Pearson's product-moment correlation coefficient (r) at the 5% significance level ($\alpha = 0.05$). Other climate modes like the Southern Annular Mode, Benguela Niño and Angola Low were found to not have strong relationships with rainfall totals over the WCSA (Moses et al., 2022) or with the extreme rainfall events considered here. The not strong link with the Angola Low could be related to the fact that this circulation feature is strongest in January-February (Munday and Washington, 2017; Howard and Washington, 2018) but here the correlations were computed for JFMA, which also contains March and April.

Frequency and intensity analysis of DP1 and DP3 events was performed, and trends in these extreme event characteristics were computed and tested for statistical significance at $\alpha = 0.05$, using the Hamed and Rao (1998) and Yue and Wang (2002) tests, which are both modified from the nonparametric Mann-Kendall test (MKT) (Mann, 1945; Kendall, 1975). The MKT is widely used because it does not make assumptions about the distribution of the data. However, the original MKT does not account for data autocorrelation, unlike the modified trend tests used here.

Focus here is placed on the late summer, i.e., JFMA, which is the peak of the rainfall season over this part of southern Africa. Note that the early summer, i.e., October-December (OND) had a small number of DP1 and DP3 (14 and 19, respectively) events making it into the top 200 events when the entire October-April (ONDJFMA) season is used, hence results are only presented for JFMA 1981-2021. This concentration of extreme events in JFMA may result from the circulation over subtropical southern Africa being much more tropically influenced than in OND when midlatitude influences can still be significant (Walker, 1990; D'Abreton and Tyson, 1995, Cook et al., 2004; Dyson et al., 2015; Blamey et al., 2017). For context, in addition to the DP1 and DP3 events, the spatial distributions of rain-days receiving >1mm and >10 mm as well as their trends are also considered.

5.3 Results

5.3.1 Extreme events spatial distribution and weather types

Figure 5.2 shows spatial distributions of the 9 out of the top 20 DP1 events that had their large rainfall values covering the north catchment and/or Ngamiland. In some cases, heavy rainfall is mainly restricted to the north catchment (e.g., plots a and b), in others it is more over Ngamiland (e.g., plots c and i) or else more patchily distributed. Four of the nine plots (**Figure 5.2a,b,g,h**) show that the heavy rainfall in the north catchment occurred in February, which, climatologically, is the month for the heavy rainfall in the north catchment. **Figure 5.3** shows the same information but for the DP3 events with again similar variations in relative distributions between the north catchment and Ngamiland. Very similar results are obtained if the extreme events are determined from PERSIANN-CDR or TRMM data (not shown) instead of CHIRPS, thereby giving some confidence in the results.

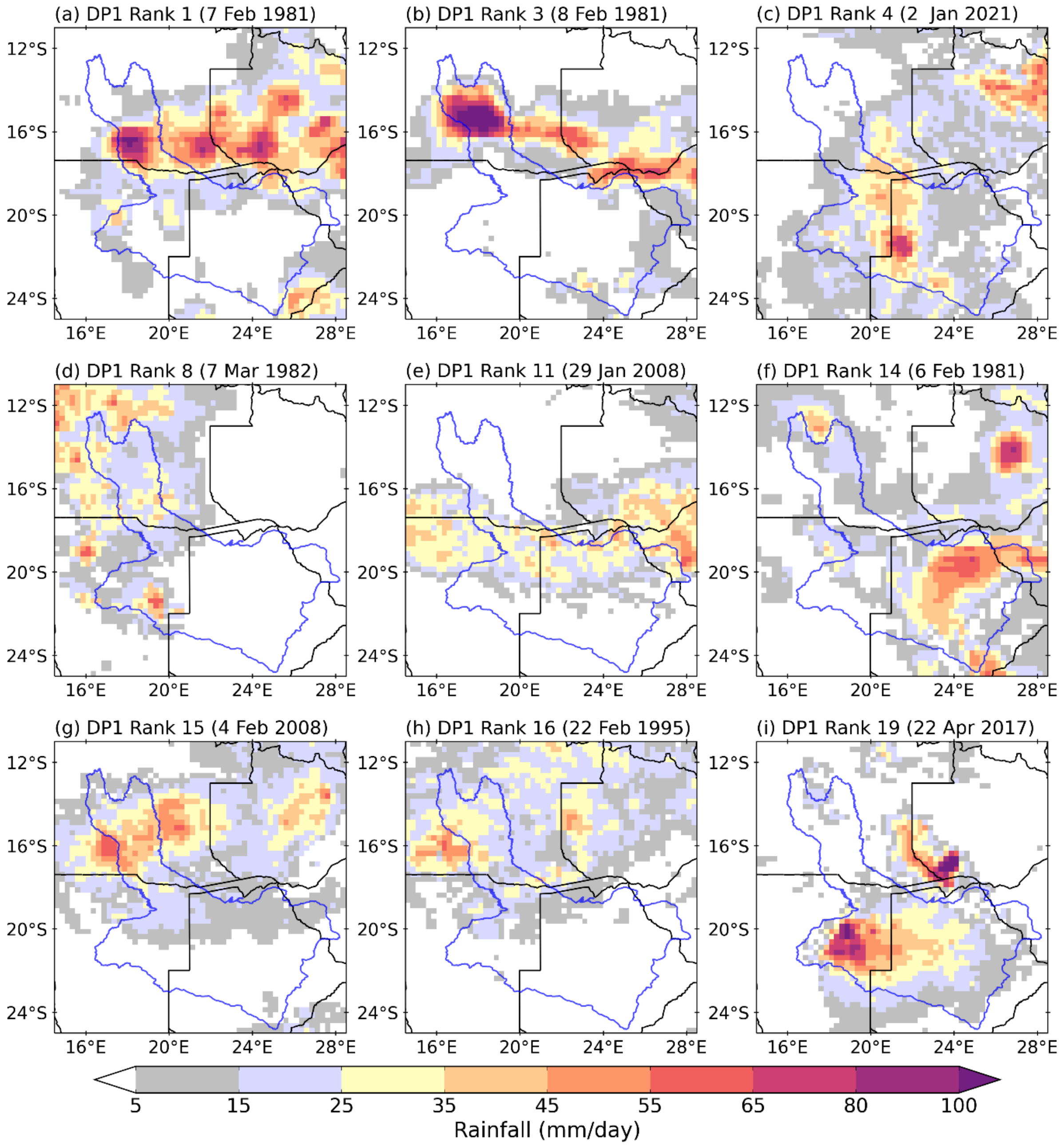

Figure 5.2 Spatial distribution of the 9 out of the top 20 DP1 events that had their large rainfall values covering the north catchment and/or Ngamiland during JFMA 1981-2021. The events are arranged in descending order of magnitude (defined in Equation 5.2) from (a) to (i). Dates of the events are shown at the top of the panels. The blue polygon is as in Figure 5.1.

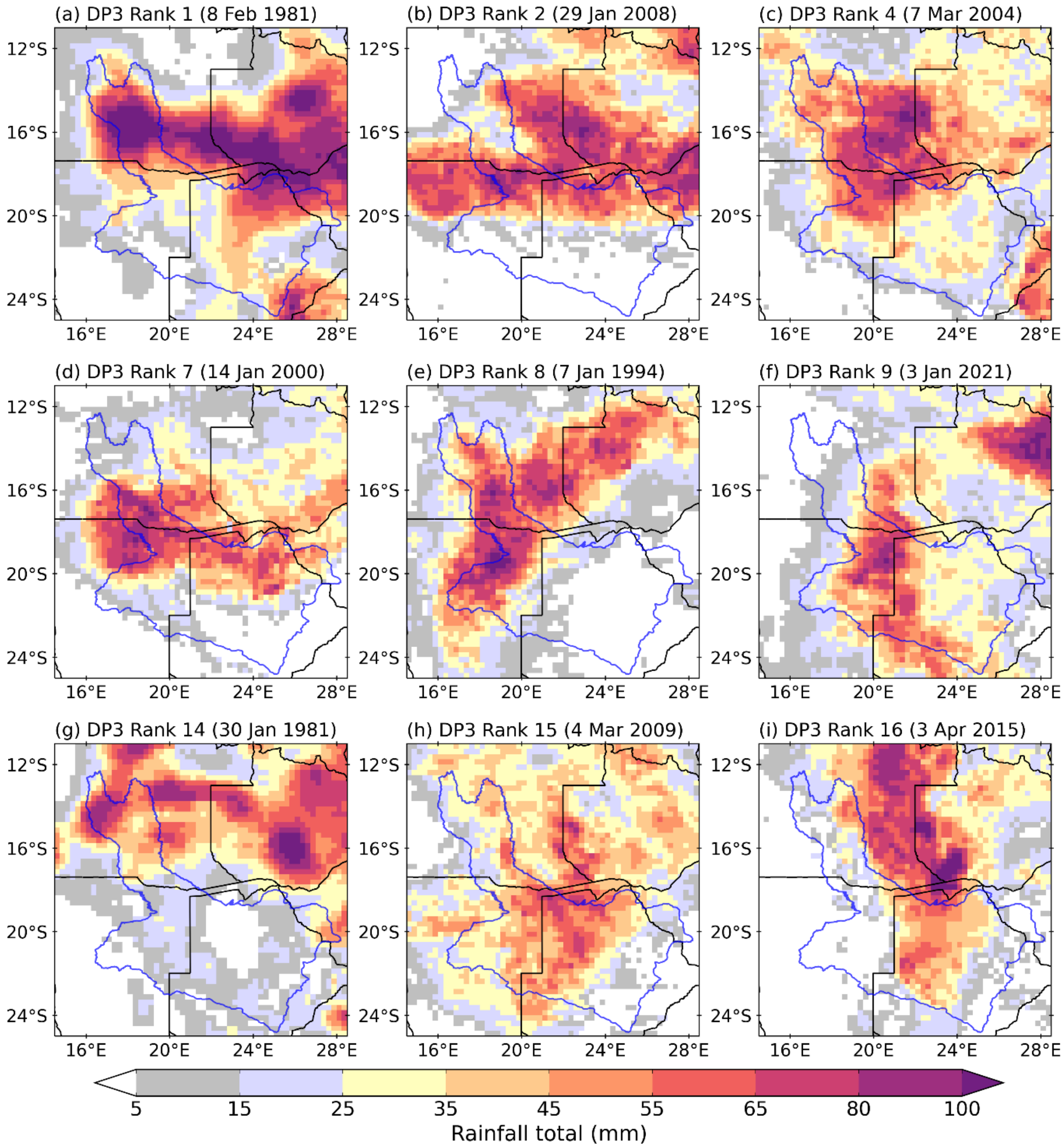

Figure 5.3 As in Figure 5.2, but for DP3 events.

Figure 5.4 shows the proportion (denoted by bars) of grid-points over the WCSA with positive standardised rainfall anomalies and the average values of these rainfall anomalies for each of the DP1 events, with the top ranked plotted in the upper panel on the left through to rank 200 on the bottom right of the lowest panel. The figure also shows the distribution of the heavy rain of these events over the study domain using coloured squares, i.e., blue, red and green squares on each bar in the figure are used to indicate whether the heavy rain of these events fell over the north catchment, over Ngamiland, or over both areas, respectively. Note that the dates in magenta colour are for the DP1 events that occurred during JFMA 2017, which are discussed further in *Section 5.4*. Out of the top 200, 94 had their heavy rain falling over the north catchment, 46 over Ngamiland, 45 over both regions, whereas the remaining 15 events had their heavy rain falling mainly elsewhere in the WCSA. For the DP3 events, **Figure 5.5** shows the same information where it is found that 103 out of 200 cases had their heavy rain falling over the north catchment, 38 over Ngamiland, 55 over both regions, and only 4 mainly elsewhere in the WCSA box.

Since the north catchment is lower latitude than Ngamiland as well as closer to the Angola Low and the Congo Air Boundary, it receives more rainfall on average (**Figures 5.1b** and **5.6a**); hence the greater numbers of DP1 and DP3 events falling over the north catchment are not unexpected. On average, the north catchment also experiences a greater number of rain-days receiving >1 mm, or >10 mm (**Figures 5.6c,e**). Like almost the entire subcontinent north of ~18°S, the north catchment experiences at least 40 rain-days (> 1 mm) during JFMA on average out of a maximum possible of 120. Similarly, most areas north of 18°S show at least 15 days of heavy rain (>10 mm) on average.

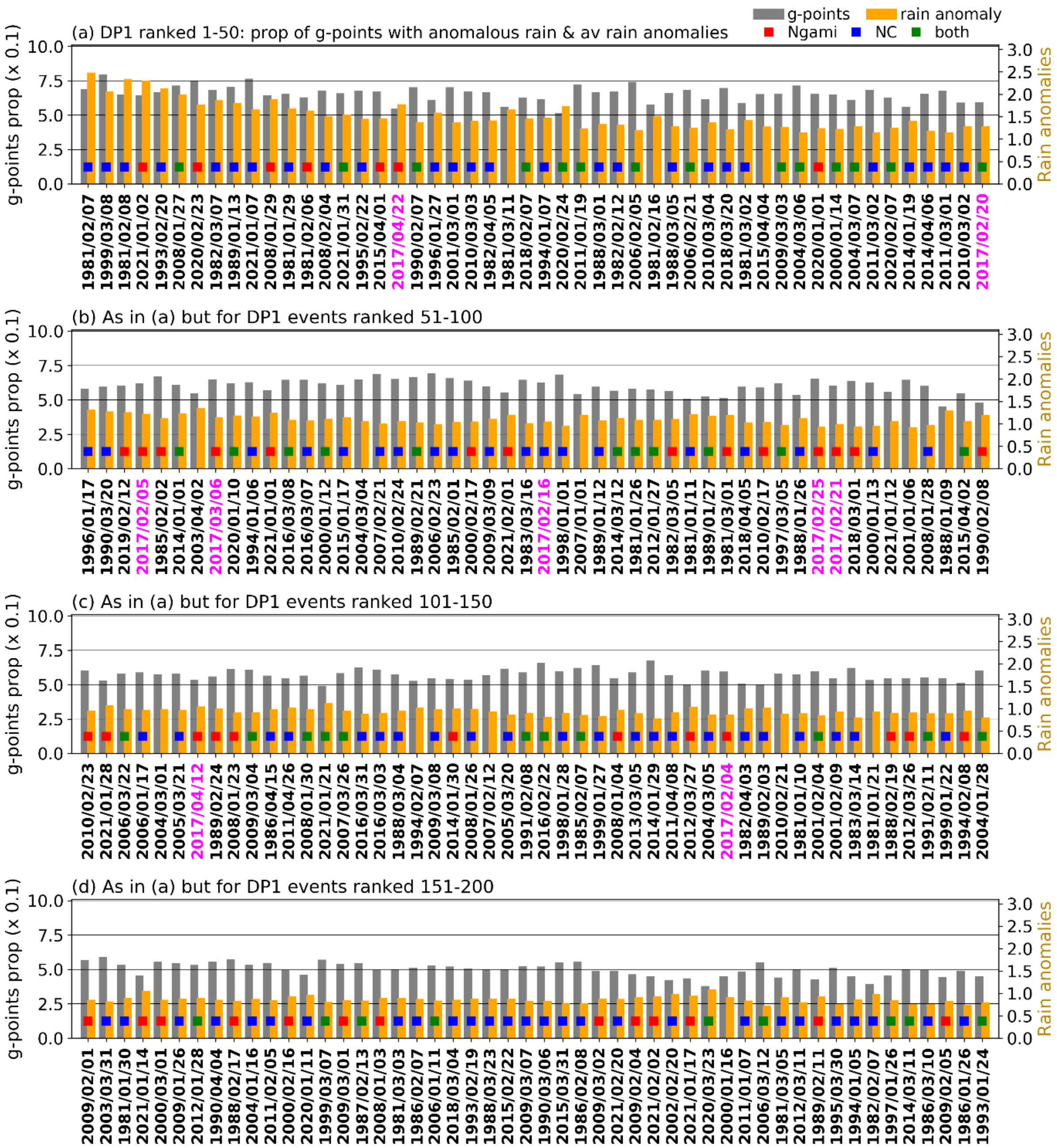

Figure 5.4 (a)-(d) Proportion (prop; denoted by bars) of grid-points (g-points) over the WCSA with positive standardised rainfall anomalies and the average (av) values of these rainfall anomalies, for the top 200 DP1 events during JFMA 1981-2021. The top ranked event is plotted in the upper panel on the left through to rank 200 on the bottom right of the lowest panel. Blue, red and green squares on each bar are used to indicate whether the heavy rain of these events fell over the north catchment (NC), Ngamiland (Ngami) or over both areas, respectively, whereas the bars with no squares on are used for the events whose heavy rain did not fall on either of these 2 areas. Dates in magenta colour are for the events that occurred during JFMA 2017.

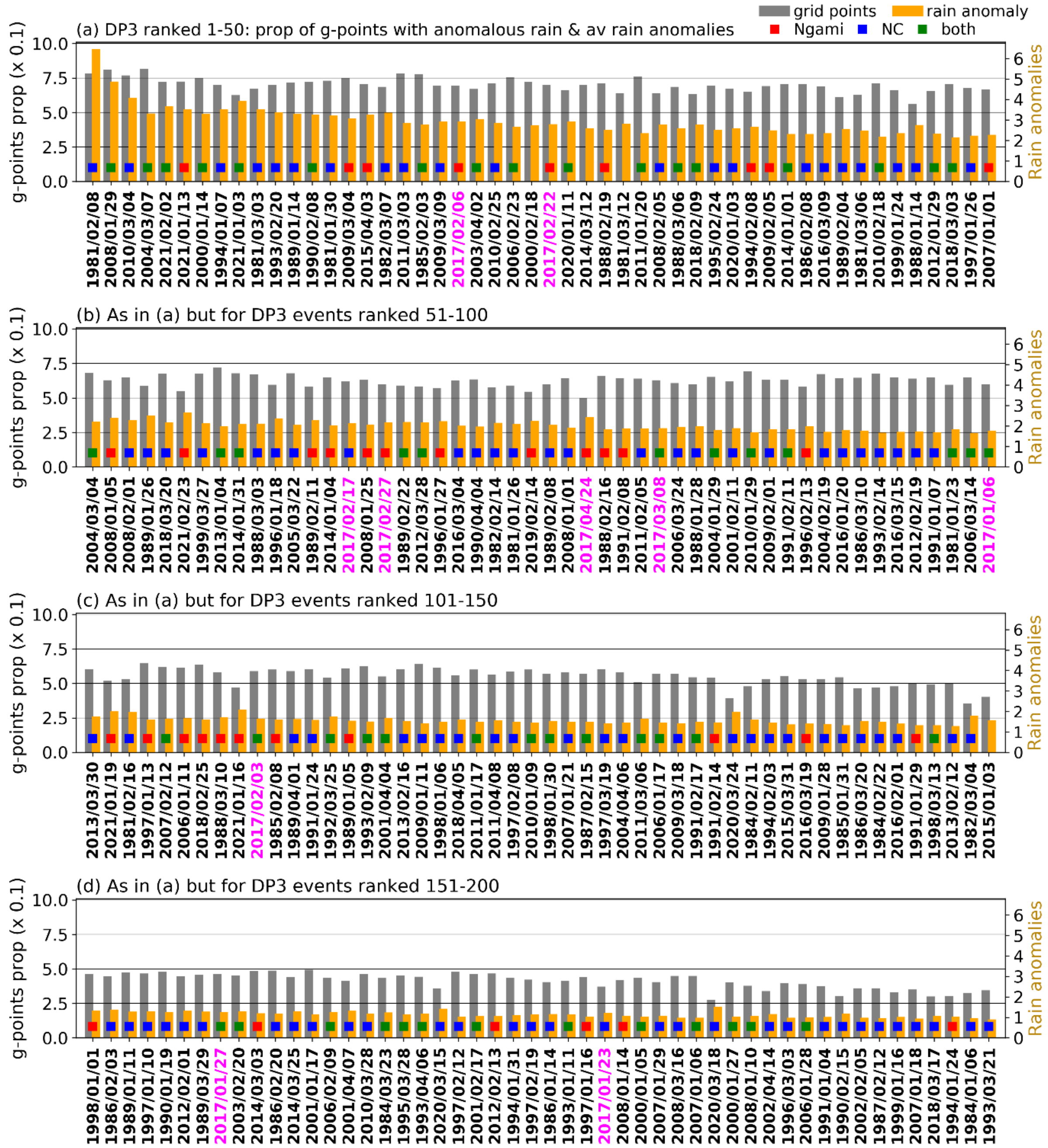

Figure 5.5 As in Figure 5.4 but for DP3 events.

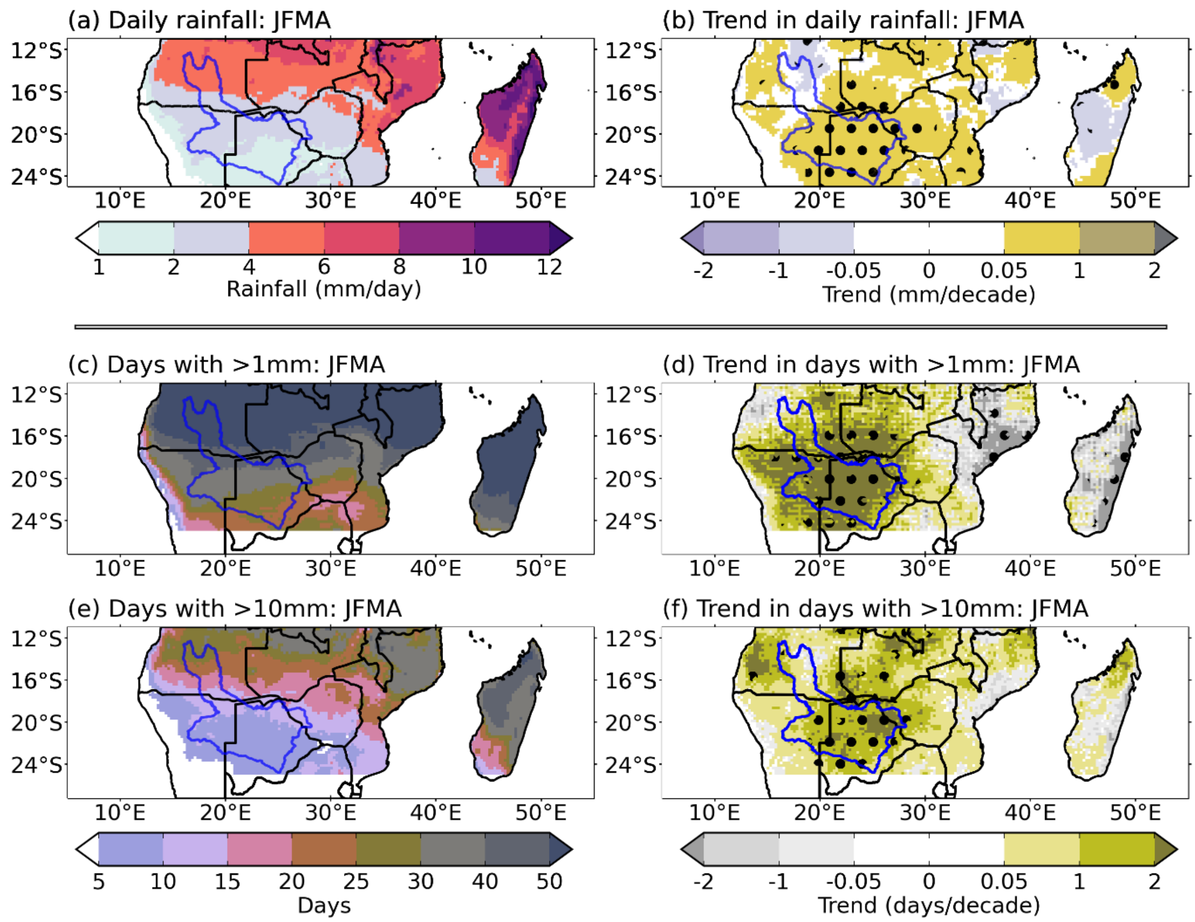

Figure 5.6 (a) and (b) Mean daily rainfall and its spatial trends, respectively, in JFMA (1981-2021), over tropical southern Africa. (c) and (e) Mean number of rain-days receiving >1 mm and >10 mm, respectively. (d) and (f) Spatial trends for (c) and (e), respectively. Stippling in (b), (d) and (f) denotes areas with significant trends at α = 0.05. The blue polygon is as in Figure 5.1.

This 18°S latitude roughly marks the centre of the Angola Low in southern Angola/northern Namibia and the poleward edge of the tropical rain belt extending east across the subcontinent to the Mozambique Channel Trough (Barimalala et al., 2018, 2020). This latitude also lies near the centre of the tropical edge over southern Africa, defined by Howard et al. (2019) as the region spanning 12°-22°S, from the west to the east coast of the subcontinent, which they found to be one of the regions of highest rainfall variability. Almost all of Botswana (except the far south east) and a few adjacent areas in neighbouring Zimbabwe and Namibia show significant trends in JFMA daily rainfall totals as well as in the number of rain-days receiving >1 mm and >10 mm (**Figures 5.6b**,**d**,**f**). Thus, almost the entire southern half of the WCSA shows a significant wetting trend in the second half of summer. It seems the Angola Low does not contribute much to the wetting trend since it shows a significant weakening trend (0.34 m/decade based on the 850 hPa geopotential height) at the 95% significance level. If the wetting trends persist into the future, then they imply a weakening of the meridional rainfall gradient from Botswana to Zambia and a blurring of the edge of the tropical rain-belt over northern Botswana at least. Similar trends in wet days of 10-30 mm/day were found for December-February by Thoithi et al. (2021).

Based on the identification methods described in *Section 5.2.2*, the dominant weather systems that resulted in the top 200 DP1 events (**Figure 5.4**) were tropical-extratropical cloud bands, which were associated with 112 events, followed by tropical lows (86), whereas 1 event was associated with a cut-off low and 1 with an MCS. Cloud band cases (not shown) tend to show more diagonally-oriented rainfall than the tropical low cases. However, MCSs can be embedded within other systems like cloud bands, hence their contribution to extreme rainfall events may be underestimated as noted by other studies (Blamey and Reason, 2013; Rapolaki et al., 2019). Furthermore, MCSs tend to be shorter-lived than cloud bands or tropical lows which may also lead to an underestimate of their relative contribution. For the top 200 DP3 events (**Figure 5.5**), in cases where a single weather system was dominant on each day of the 3-day period, 121 were associated with cloud bands and 74 with tropical lows. However, there are some DP3 cases where two weather systems were involved. Such cases include combinations of MCS-tropical low (1), MCS-cloud band (1) and tropical low-cloud band (3).

The importance of cloud bands for extreme rainfall events found here is consistent with other studies highlighting their large contribution to summer rainfall over subtropical southern Africa (Washington and Todd, 1999; Cook et al., 2004; Hart et al., 2010, 2013; Ratna et al., 2013; Manhique et al., 2011; Macron et al., 2014). That tropical lows also make a substantial contribution to WCSA extreme events is consistent with previous work for lower latitude southern Africa (Howard et al., 2019).

Some of the tropical lows identified here were associated with ex-tropical cyclones such as DP1 events ranked 72 (17 February 2000) due to ex-tropical cyclone Eline and DP3 event ranked 65 (15-17 February 2017) associated with ex-tropical cyclone (Dineo). The evolution and impacts of these ex-tropical cyclones over inland southern Africa have been previously studied (Reason and Keibel, 2004; Moses and Ramotonto, 2018).

5.3.2 Extreme events interannual variability and trends

The top 200 DP1 and DP3 events show high interannual variability in their frequencies (**Figure 5.7a**) and percentage contribution to JFMA seasonal rainfall totals (**Figure 5.7b**) over the WCSA. Overall, DP3 events show larger contributions than DP1 events since their rainfall is accumulated over a longer (3 days) timespan than the latter (1 day). The largest DP3 contribution to seasonal rainfall totals occurred in 1991 (38.5%) whereas that for DP1 events occurred in 1981 (36.5%). Throughout the 1981-2021 period, DP1 events made an average contribution of almost 10% and DP3 events 17% to JFMA rainfall totals, highlighting their importance for the climate of the region. However, the combined average contribution (27%) of these DP1 and DP3 events is less compared with other regions of the tropics/subtropics such as West Africa (3°N-16°N, 18°W-16°E), where the contribution of extreme rainfall events can reach ~50-90% in the northern part and ~30-50% in the south (Ta et al., 2016).

Out of these 41 seasons, **Figure 5.7a** shows that, 22 experienced above average frequencies in DP1 and 23 seasons experienced above average DP3 frequencies. Above average occurrences in DP1 and DP3 events mostly translate into above average rainfall since about 80% of the seasons that experienced above average number of DP1 or DP3 events over the WCSA also received above average rainfall totals (**Figure 5.8a**). Over Ngamiland (**Figure 5.8b**) and the north catchment (**Figure 5.8c**), the corresponding percentages are even lower at around 70% and 65% respectively. The higher percentage over Ngamiland than that over the north catchment suggests that extreme rainfall events make a somewhat larger contribution to rainfall totals over the former region.

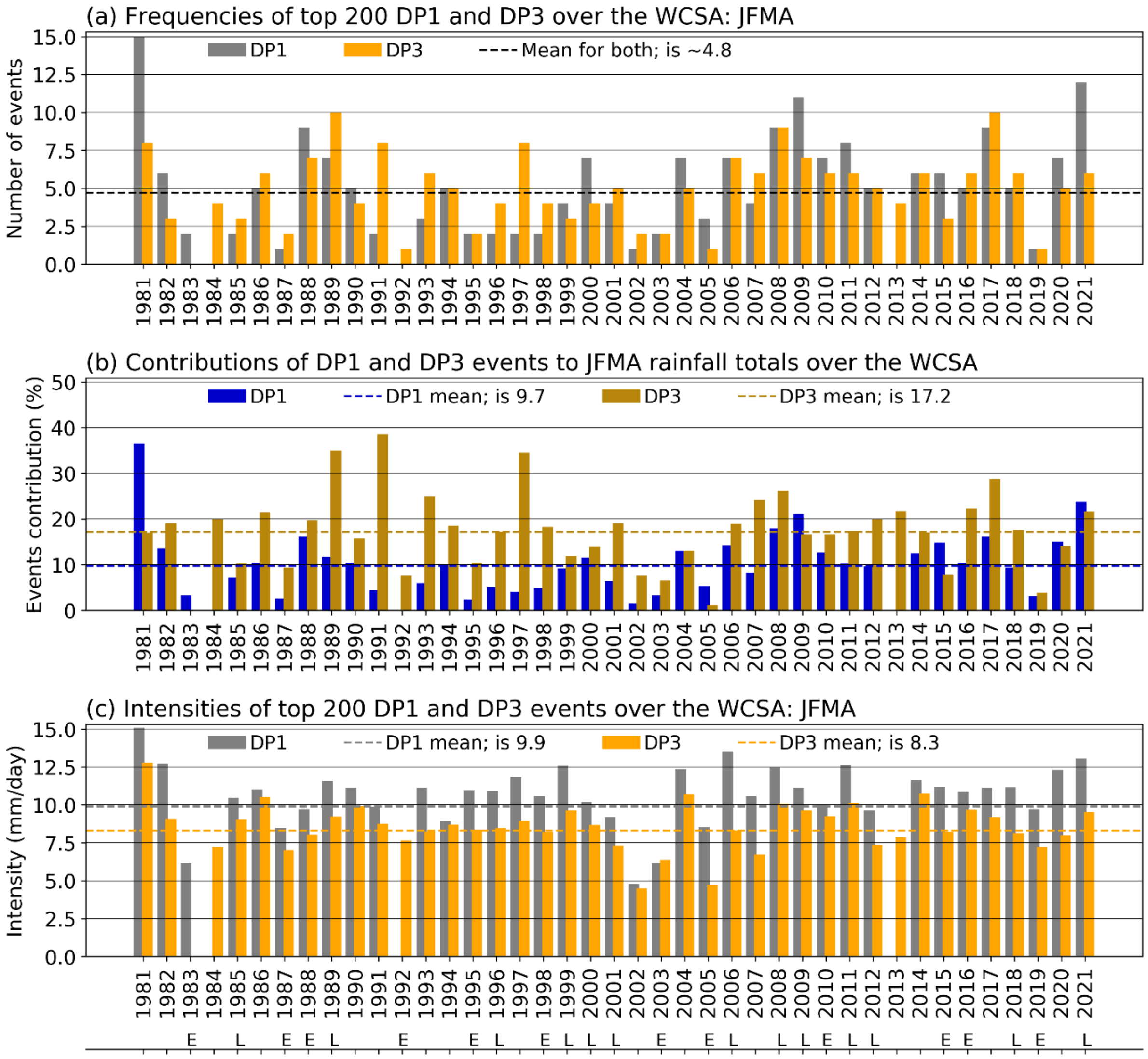

Figure 5.7 (a) Frequencies of the top 200 DP1 and DP3 events over the WCSA, for JFMA 1981-2021. (b) Percentage contribution of the top 200 DP1 and DP3 events to JFMA rainfall totals over the WCSA. (c) As in (a) but for Intensity-Max (as described in the text). Dashed lines are the means of the shown variables. Notation below the x axis in (c): E, El Niño; L, La Niña.

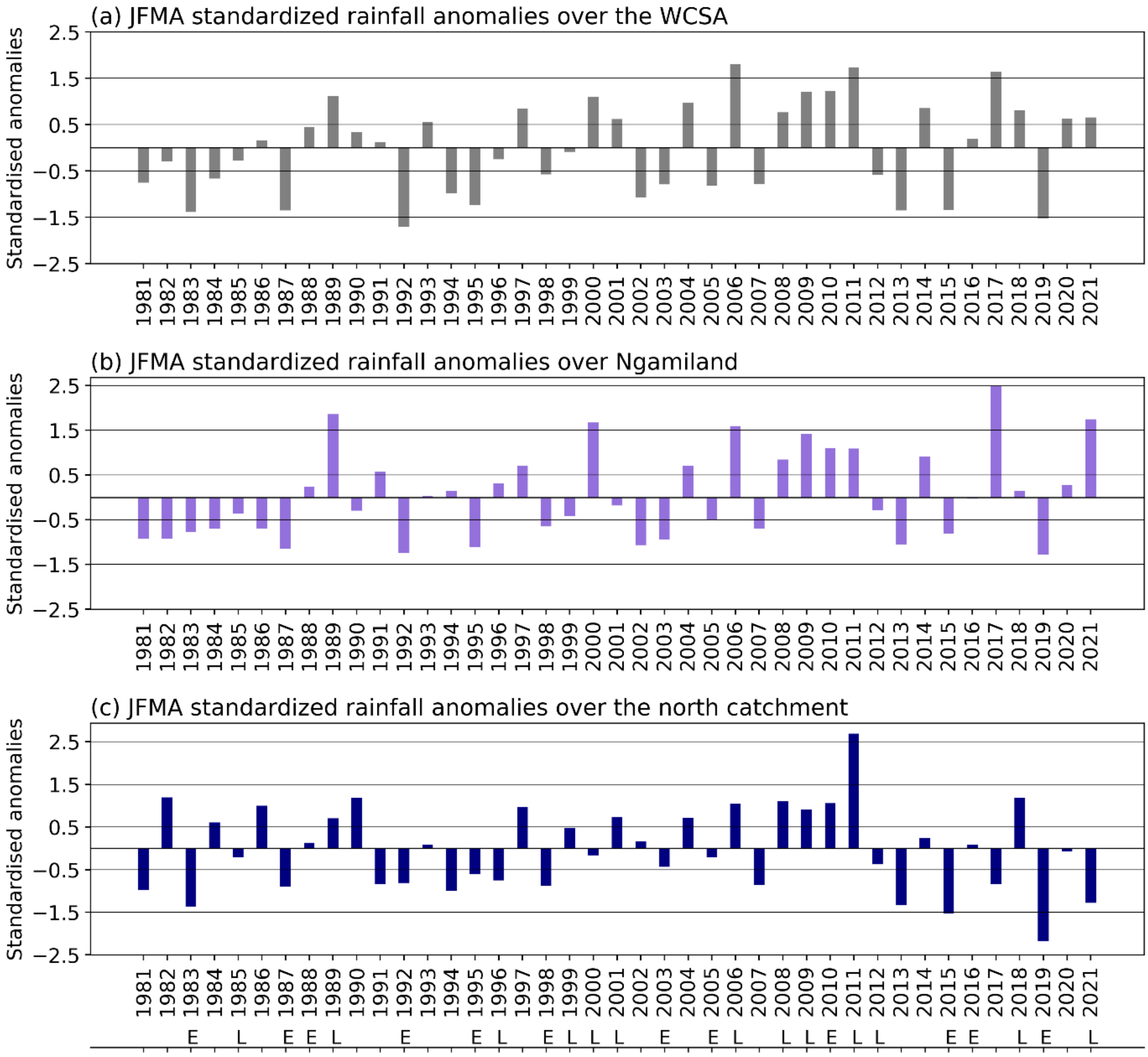

Figure 5.8 (a) Standardised rainfall anomalies over the WCSA for JFMA 1981-2021. (b) As in (a) but for Ngamiland. (c) As in (a) but for the north catchment. Notation below the x axis in (c) is as in Figure 5.7c.

Both DP1 and DP3 frequencies correlated significantly with WCSA rainfall totals ($r = 0.58$ and 0.73, respectively, $p < 0.05$) and with Ngamiland rainfall totals ($r = 0.59$ and 0.72, respectively, $p < 0.05$), whereas for the north catchment, only DP3 frequencies showed a significant correlation with rainfall totals there ($r = 0.36$, $p < 0.05$) (**Table 5.1**). Note that calculating these correlations using either rainfall totals or standardised rainfall anomalies shown in **Figure 5.8** gave the same results. Rainfall totals over Ngamiland and the north catchment are moderately but significantly correlated with each other ($r = 0.36$, $p < 0.05$) although there are some obvious cases when they are out of phase such as in JFMA 2017, the wettest season by far in Ngamiland but somewhat dry over the north catchment (**Figures**

5.8b,c). Also, all of JFMA 1981-1987 was dry over Ngamiland whereas three of these seasons showed well above average rainfall over the north catchment. Stronger correlations exist between Ngamiland and WCSA rainfall totals (r = 0.88, p <0.05), or between north catchment and WCSA rainfall totals (r = 0.68, p <0.05).

Table 5.1 Correlations of DP1 and DP3 characteristics (frequencies and Intensity-Max) with rainfall totals (for the WCSA, Ngamiland and north catchment), ENSO and the Botswana High, over the period JFMA 1981-2021. Only significant correlations at α = 0.05 are shown

	DP1 frequency	DP3 frequency
WCSA rainfall totals	0.58	0.73
Ngamiland rainfall totals	0.59	0.72
north catchment rainfall totals		0.36
ENSO	-0.38	-0.44
Botswana High	-0.39	-0.46

	DP1 Intensity-Max	DP3 Intensity-Max
WCSA rainfall totals	0.55	0.48
Ngamiland rainfall totals	0.45	0.37
north catchment rainfall totals	0.34	
ENSO		-0.41
Botswana High	-0.33	-0.43

Events with the highest spatially averaged rainfall intensity (hereafter, Intensity-Max) over the WCSA box in a particular season were derived for DP1 and DP3 (**Figure 5.7c)**. This parameter tends to be higher for DP1 (mean = 9.9 mm/day) than for DP3 (mean = 8.3 mm/day) events. This tendency suggests that there is a possibility for a DP1 event to have a greater impact than a DP3 event in a particular location within the WCSA. As with frequency, Intensity-Max of both DP1 and DP3 events correlated significantly with WCSA rainfall totals (r = 0.55 and 0.48, respectively, p <0.05) and with Ngamiland rainfall totals (r = 0.45 and 0.37, respectively), but for the north catchment, only DP1 Intensity-Max correlated significantly (r = 0.34, p <0.05) (**Table 5.1**). Overall, correlations of both frequency and Intensity-Max of DP1 and DP3 events with rainfall totals suggest that these events are more important to seasonal rainfall totals over Ngamiland which receives smaller rainfall totals than the north catchment.

Calculated for 1981-2021, a significant increasing trend was found in the DP1 frequency (0.9 events/decade, $p < 0.05$), but none was found for the DP3 frequency, nor in the Intensity-Max of either type of event (**Figure 5.7c**). The significant increasing trend in DP1 frequency is consistent with the IPCC (2013) and (2021) reports which indicate that the frequency and intensity of extreme rainfall events is likely to increase due to global warming. If this DP1 trend persists over the region, then there may be an increasing tendency for JFMA flooding with associated crop and livestock losses.

Since Moses et al. (2022) found that JFMA rainfall totals over the WCSA were significantly related to ENSO, it is worth considering potential ENSO relationships with DP1 and DP3 events. **Figure 5.7** shows that 8 (9) out of 12 El Niño summers received below average DP1 (DP3) frequencies. For La Niña, the corresponding numbers for average or above average are both 9 out of 13. Both DP1 and DP3 make their smallest (largest) contributions to seasonal rainfall totals mainly during El Niño (La Niña) summers (**Figure 5.7b**).

ENSO correlated significantly with frequencies of both DP1 and DP3 events ($r = -0.38$ and -0.44, respectively, $p < 0.05$), whereas for Intensity-Max, only DP3 events correlated significantly ($r = -0.41$, $p < 0.05$) (**Table 5.1**). The significant correlation between ENSO and extreme event characteristics is consistent with JFMA being the season when this climate mode is generally fully developed and has its strongest impact over southern Africa (Lindesay, 1988; Reason et al., 2000; Reason and Jagadheesha, 2005; Blamey et al., 2018). Both DP1 and DP3 frequencies correlated significantly with the Botswana High ($r = -0.39$ and -0.46, respectively, $p < 0.05$) (**Table 5.1**). Similarly, the Botswana High was significantly correlated with Intensity-Max of both types of events ($r = -0.33$ and -0.43, respectively, $p < 0.05$) (**Table 5.1**). Note that this mid-level Botswana High typically develops over southern Angola/northern Namibia in spring and then moves south and strengthens over central Namibia and western Botswana during summer (Reason, 2016; Driver and Reason, 2017) leading to anomalous subsidence and reduced rainfall when it is stronger than average. Hence, the negative significant correlations between these extreme event characteristics and the Botswana High are consistent. Note also that when the ENSO influence was removed by partial correlation analysis, the correlation between DP1 (DP3) frequency and the Botswana High was -0.14 (-0.18), and that between DP1 (DP3) intensity and the Botswana High was -0.16 (-0.17), which are all nonsignificant.

5.4 JFMA 2017 floods over Ngamiland

As mentioned in the introduction, the Ngamiland district which contains the world-famous Okavango Delta experienced severe flooding in 2004, 2009, 2010, 2011 and 2017. **Figure 5.8b** shows that JFMA 2017 was by far the wettest season (2.5 standard deviations) over Ngamiland during 1981-2021 as well as third wettest over the WCSA box as a whole (**Figure 5.8a**). It is also of interest because it is neutral with respect to ENSO unlike 2009 and 2011 which were La Niña when subtropical southern Africa is expected to be wet (Lindesay, 1988; Reason et al., 2000; Reason and Jagadheesha, 2005). Other JFMA seasons with well above average rainfall over Ngamiland (1989, 2000, 2006 and 2021) are also all La Niña summers, but there were no records of local floods over this region. In addition, JFMA 2017 is a season which experienced well below average JFMA rainfall over the north catchment (**Figure 5.8c**), implying that the Ngamiland floods then were mainly due to rainfall over the district itself, with little contribution from upstream river flow during JFMA. Most of the river flow that feeds into the Okavango Delta is generated over the north catchment. Indeed, examination of river discharge data from Mohembo (not shown) on the northern border of Ngamiland shows that the river flow there only noticeably increased after mid-January 2017 since the rainfall anomalies for OND 2016 (not shown) were only slightly above average over the north catchment. Thus, the importance of local rainfall in causing the JFMA 2017 floods over Ngamiland is evident.

Before analysing the circulation patterns associated with the JFMA floods, it is useful to consider the timing of the rains during this anomalously wet season over Ngamiland. Anomalously wet summer rainy seasons in other parts of southern Africa often result from one or two intense spells of rain rather than frequent but less intense rain events. For example, this was the case in 2006 in Tanzania (Kijazi and Reason, 2009) and western Namibia (Muller et al., 2008), 2011 in southern Mozambique/northeastern South Africa (Manhique et al., 2015; Rapolaki et al., 2021), and most recently (April 2022) in Kwa-Zulu Natal, South Africa. These, and other cases, highlight the need to better understand the contributions of extreme rainfall events to anomalously wet summers.

Figure 5.7a shows that JFMA 2017 experienced the highest number (10) of DP3 events over the WCSA box as well as the fourth highest number of DP1 events during 1981-2021. For Ngamiland, **Figures 4** and **5** indicate that there were 8 (8) DP1 (DP3) events, which is well above average (**Figure 5.7a**). On the other hand, Intensity-Max values of these events during JFMA 2017 were only slightly above average over the whole of the WCSA (**Figure 5.7c**), whereas over Ngamiland itself, Intensity-Max values were 2.6 and 2.3 for DP1 and DP3, respectively (figure not shown) times higher than those shown in **Figure 5.7c**. Also, the spatially averaged intensities for the events that occurred during this season were considerably higher over Ngamiland (13.1 and 9.0 mm/day for DP1 and DP3 events, respectively) than over the north catchment (4.7 and 5.8 mm/day, for DP1 and DP3 events, respectively) where most of the ORB streamflow is generated as mentioned. Taken together, **Figures 5.4**, **5.5** and **5.8b** indicate that the joint percentage contribution of DP1 and DP3 events to the JFMA 2017 rainfall total over the WCSA was ~45%, whereas over Ngamiland itself, this contribution was 21% and 27% for DP1 and DP3 events, respectively (figure not shown), or 48% jointly. These percentage contributions imply that the remaining rain-days of the season must also have had some other substantial rainfall events over Ngamiland.

Daily rainfall and their anomalies from 1981-2021 climatology averaged over Ngamiland and the north catchment are shown in **Figure 5.9**. This figure shows that just over the first two months of the season were extremely wet over Ngamiland followed by a long dry period before the second most intense wet spell of the season on 22 April which experienced an average value of 29 mm (6 February also received 29 mm and the preceding day 21 mm). On the other hand, the north catchment experienced more regular but less intense wet spells during JFMA 2017 as well as numerous rather dry periods, leading to below average summer totals for this area. It experienced only 11 days receiving at least 10 mm which is well below average (**Figure 5.6e**). By contrast, Ngamiland whose daily average summer rainfall is about half of that in the north catchment (red dashed lines in **Figures 5.9a**,**c**) experienced 21 rain-days >10 mm which is about double the average (**Figure 5.6e**). Almost all of these heavy rain-days over Ngamiland occurred in January (8) and February (11). Since there were very few no-rain days in Ngamiland before the second week of March, these initial two months of heavy rainfall saturated the soils thereby causing the flooding. It is worth noting that records related to the impacts of the floods that occurred over Ngamiland during the season of interest do not specify the exact month in which those floods occurred, but they are reported just as JFMA 2017 floods.

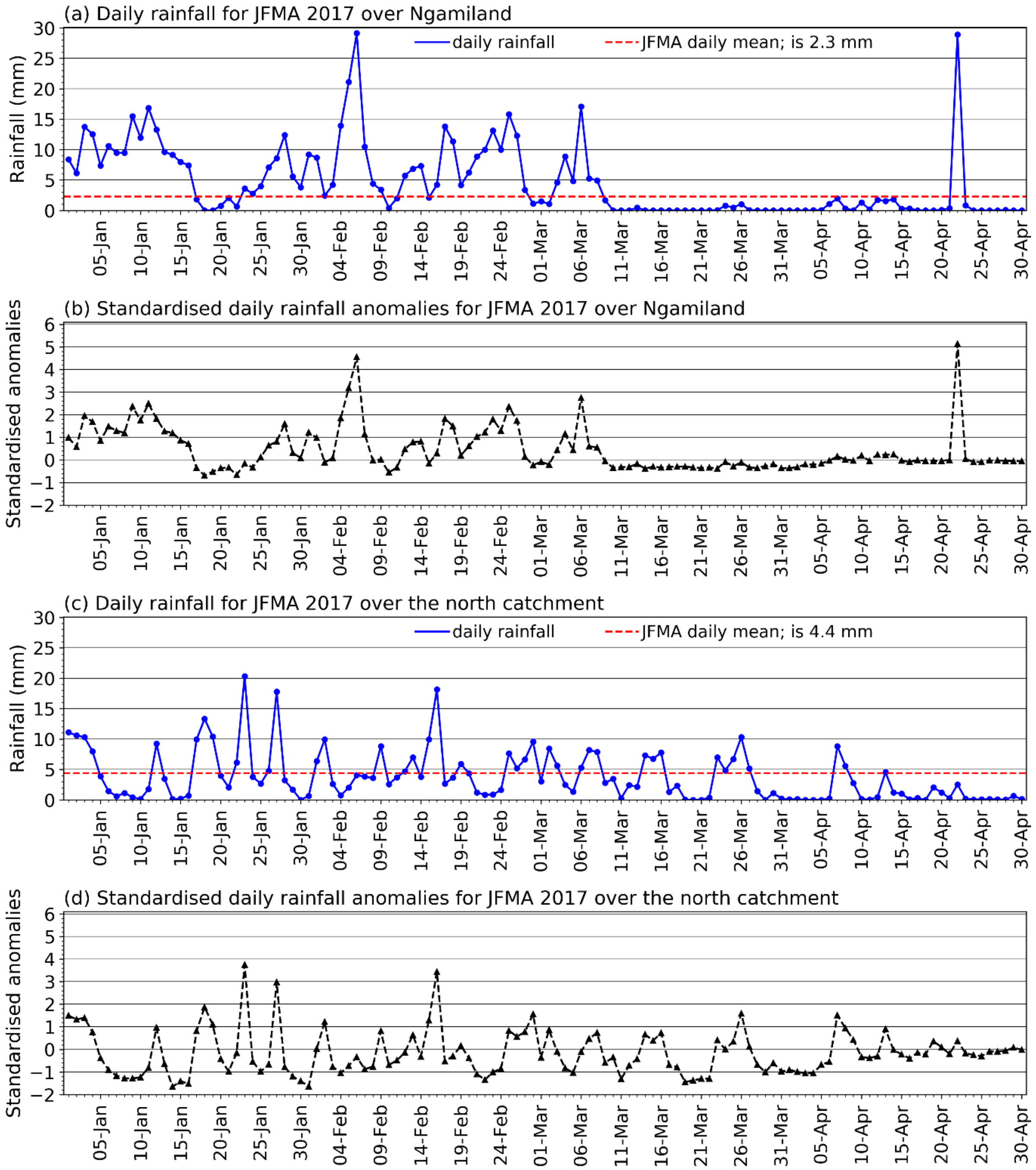

Figure 5.9 (a) Daily rainfall totals for JFMA 2017 averaged over Ngamiland. The red dashed line is the mean (1981-2021) daily rainfall averaged over JFMA, for Ngamiland. (b) Standardised daily rainfall anomalies for the series in (a), computed by subtracting long-term mean rainfall (1981-2021) of JFMA days from the corresponding JFMA 2017 daily rainfall totals. (c) and (d) are as in (a) and (b), respectively, but for the north catchment.

Although the period after March 10 was characterised by relatively few rain-days of which all but one were of low intensity, the exceptionally wet day of 22 April (~5 standard deviations) may have exacerbated and prolonged the floods. Occurring so late in the season, this case is a reminder that many studies as well as seasonal forecasting practices which often consider April to be outside the core rainy season, can quite often miss very significant rainfall in some years, and hence such practice should be viewed with caution.

Given the daily distribution of rainfall during the JFMA 2017 floods over Ngamiland shown in **Figure 5.9a**, the associated circulation anomalies are separately analysed for the long-wet period of 1 January – 8 March, and then the synoptic scale period 21-23 April. The second most intense wet day of 22 April corresponds to DP1 ranked 18 in the top 200 events in the WCSA box (**Figure 5.4a**) and, unusually, was a cut-off low. Most of the other 9 DP1 events in the top 200 over the WCSA during JFMA 2017 resulted from cloud bands with 3 due to tropical lows. The DP3 events during this season were equally induced by cloud bands and tropical lows.

5.4.1 January-early March 2017 wet period

Figures 5.10 and **5.11** show large-scale circulation anomalies over the southern African region for the 1 January – 8 March 2017 period. In addition to Ngamiland, most of Botswana, southern Zambia, Zimbabwe and central Mozambique experienced a very wet JFMA 2017 while most of Angola (including the northern half of the north catchment), the Democratic Republic of Congo, northern Mozambique and Tanzania were very dry (**Figure 5.10a**). OLR anomalies suggest that most of Botswana as well as northeastern Namibia experienced anomalous convective cloud conditions during this period (**Figure 5.10b**), consistent with the heavy rainfall and few non-rain days over Ngamiland (**Figure 5.9a**). This OLR anomaly pattern together with the strong cyclonic anomaly centred over the Angola/Namibia eastern border region (**Figure 5.10d**) indicate that the Angola Low was anomalously strong during JFMA 2017. The Angola Low acts as the tropical source for the cloud bands that bring most of the summer rainfall over subtropical southern Africa (Cook et al., 2004; Hart et al., 2010, 2013) and indeed many of the DP1 and DP3 events during this season resulted from cloud bands. This anomalously strong Angola Low was associated with enhanced westerly moisture transport from the tropical southeast Atlantic (**Figure 5.10c**), one of the important moisture sources for southern Africa (Cook et al., 2004; Rapolaki et al., 2020). Summers with increased moisture transport from this source are typically also very wet over northern and central South Africa, as is also seen in JFMA 2017 (**Figure 5.10a**).

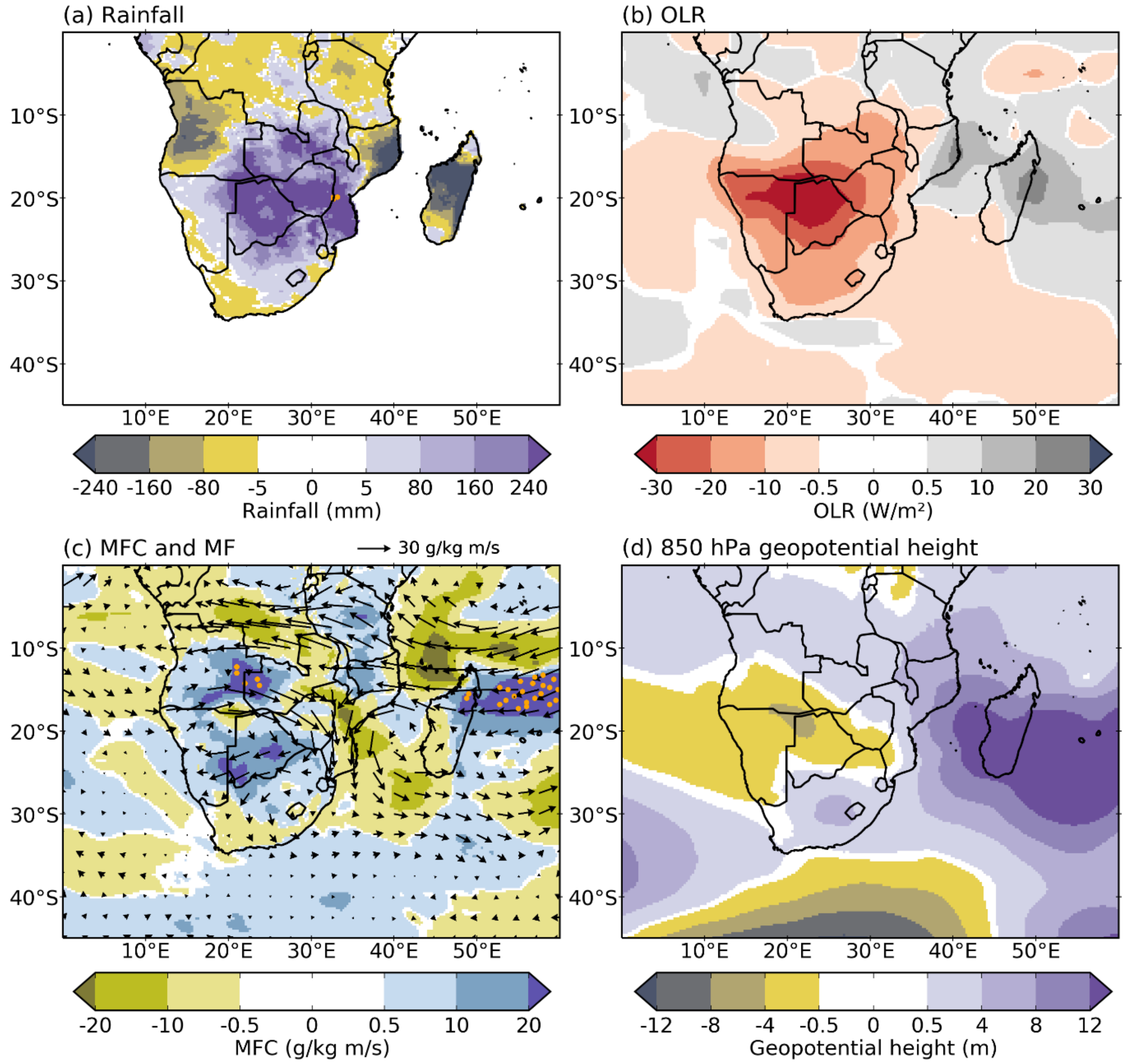

Figure 5.10 Circulation anomalies for 1 January - 8 March 2017 with respect to 1981-2021 climatology, over southern Africa. (a), (b), (c) and (d) show anomalies of rainfall, OLR, 850 hPa moisture flux convergence (MFC; shading) and moisture flux (MF; vectors), and 850 hPa geopotential height, respectively. Areas with statistically significant anomalies based on bootstrap 95% confidence level are denoted with stippling.

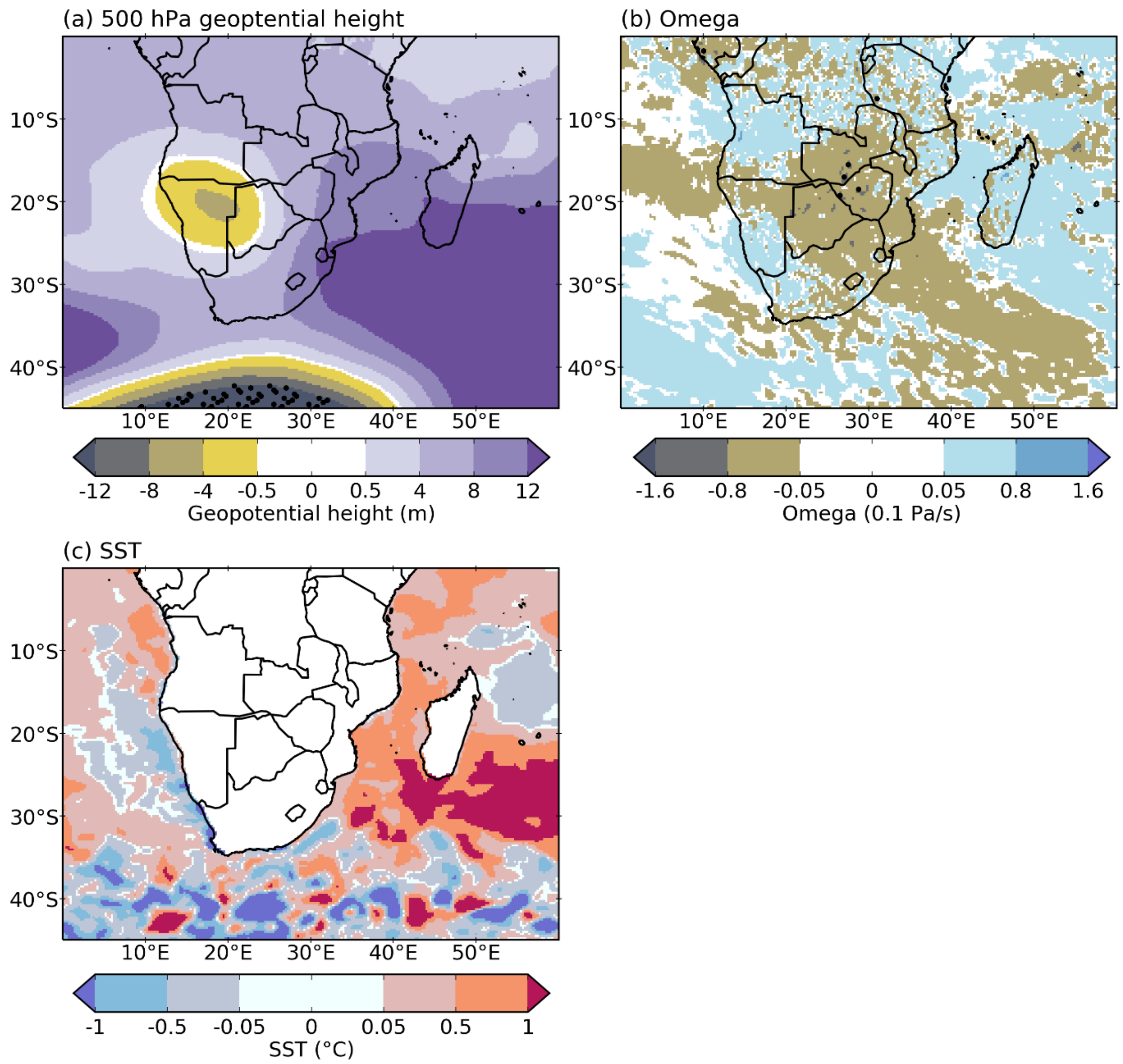

Figure 5.11 As in Figure 5.10 but for (a) 500 hPa geopotential height, (b) 500 hPa omega and (c) SST.

Over Ngamiland itself as well as Botswana, Zimbabwe and southern Mozambique, the strong cyclonic moisture flux anomalies (**Figure 5.10c**), together with the easterly export of moisture across southern Africa from the western Indian Ocean, leading to strong low-level moisture flux convergence over most of Botswana, favoured the very wet conditions. Over the Mozambique Channel, anticyclonic moisture flux anomalies occurred, suggesting that the Mozambique Channel Trough was weaker than normal, hence more moisture was transported from the southwest Indian Ocean into the southern Africa landmass mainly through Eswatini (**Figures 2.1 and 5.10c**) and the surrounding areas rather than circulating in the Channel itself (Barimalala et al., 2018, 2020). This low-level moisture then converged over Botswana leading to the floods over Ngamiland. Low-level moisture flux convergence anomalies appear to have been relatively lower over Ngamiland itself (vertical integration of the anomalies from 850 hPa to 200 hPa did not substantially improve the lower anomaly values) over the period as a whole. However, daily values of these fluxes at 850 hPa were very high (not shown) over this area during the heavy wet spells (such as 6 February in **Figure 5.9a**).

Another very favourable feature for the very wet period over Botswana was the weaker mid-level Botswana High (**Figure 5.11a**). This feature, together with the northwest-southeast band of increased uplift stretching from northeastern Namibia/southern Angola across Botswana to the southwest Indian Ocean as well as the enhanced troughing south of South Africa (**Figure 5.11b**), implies favourable conditions for deep convection and strong cloud bands leading to the wet conditions over Botswana, Zimbabwe and most of South Africa shown in **Figure 5.10a.** SST anomalies in the southwest Indian Ocean were strongly positive in many areas (**Figure 5.11c**) but negative near western Australia in a subtropical Indian Ocean Dipole-like pattern which has previously been associated with above average summer rainfall in eastern South Africa, Botswana and Zimbabwe (Reason and Mulenga, 1999; Behera and Yamagata, 2001; Reason, 2001a) since they increase the moisture content of the easterly flow towards the subcontinent.

5.4.2 Synoptic wet spell 21-23 April 2017

Examination of South African Weather Service synoptic charts together with ERA5 500 hPa geopotential height and 250 hPa winds for 17-23 April 2017 (not shown) indicate that during this period a cut-off low situated rather far north over the ocean west of Namibia became centred over the central Namibian coast on the very wet day (22 April) while near the surface there was a surface trough over Botswana and a strong midlatitude cyclone east of South Africa. The latter can be clearly seen in the low-level moisture flux anomalies for 21-23 April 2017 (**Figure 5.12c**), which also shows strong easterly/northeasterly fluxes into Ngamiland and most of Botswana together with strong moisture convergence.

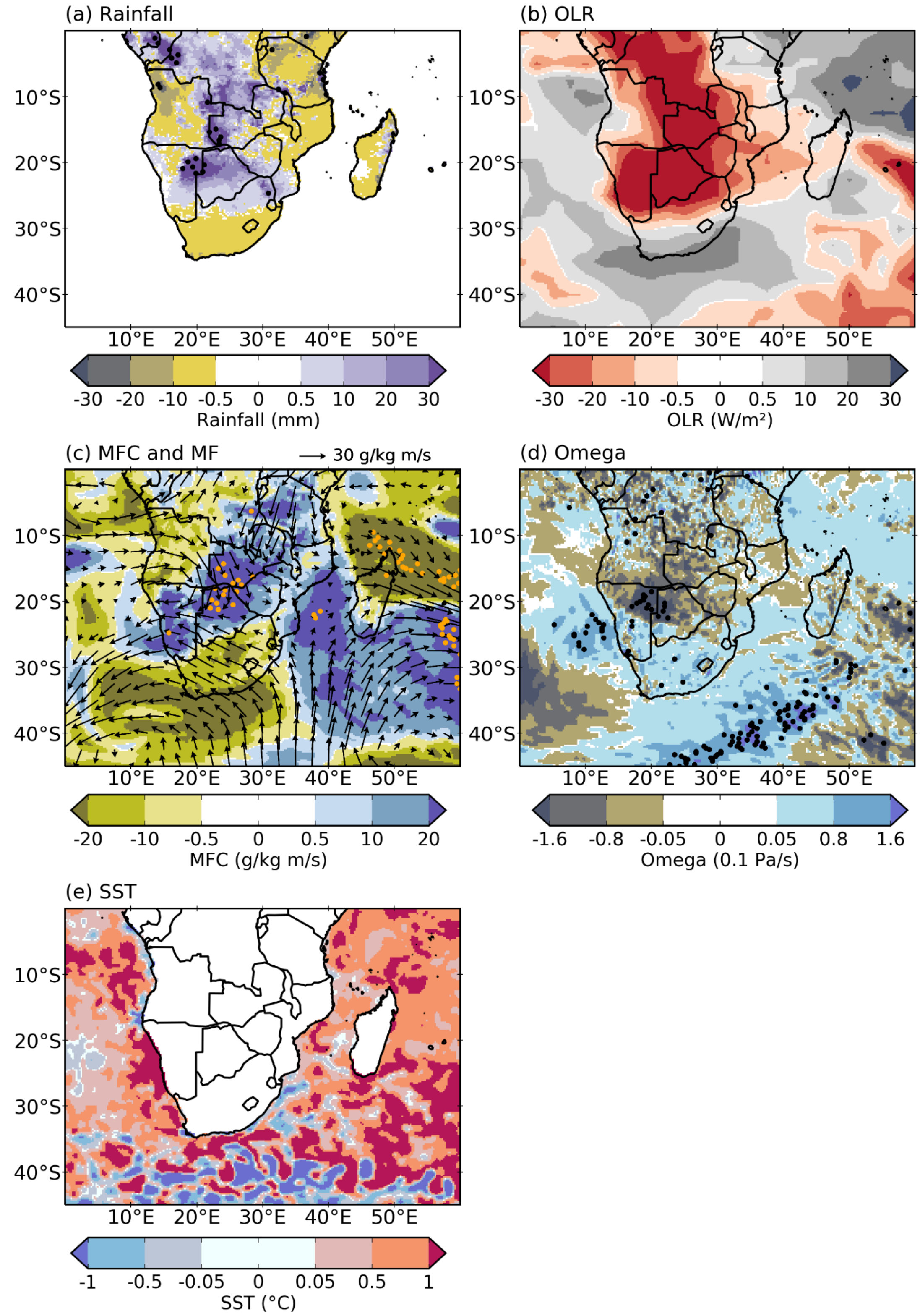

Figure 5.12 Circulation anomalies for 21-23 April 2017, with respect to 1981-2021 climatology, over southern Africa. The fields and stippling are as described in Figures 5.10 and 5.11, with the variables in (c) and (d) measured at 850 hPa and 500 hPa, respectively.

As in the case for the 1 January – 8 March 2017 period, highest positive rainfall anomalies during 21-23 April 2017 also occurred over Ngamiland and northern Botswana/eastern Namibia, but during the latter they extended northward along Angola/Zambia border (**Figure 5.12a**), consistent with the lowest negative OLR anomalies (**Figure 5.12b**). Off the coast of Namibia, westerly moisture fluxes are apparent (**Figure 5.12c**), which together with anomalously warm water there (**Figure 5.12e**) suggest that they were favourable for increased moisture convergence over the Ngamiland region. Warm SST anomalies persisted over the southwest Indian Ocean (**Figure 5.12e)** in an ongoing subtropical dipole-like pattern, favourable for wet conditions. **Figure 5.12d** shows strong uplift centred over northeastern Namibia/northwestern Botswana during 21-23 April consistent with the very heavy rainfall on the 22^{nd} of this month. As with the 1 January-March 8 period, westerly moisture fluxes over the tropical southeast Atlantic played an important role in the very heavy rainfall on 22 April. However, the latter period was characterised by a cut-off low located rather far north whereas the heavy rain earlier in the summer resulted from cloud bands and tropical lows.

Note that *Sections 5.4.1* (January-early March 2017 wet period) and *5.4.2* (synoptic wet spell 21-23 April 2017) show that physical processes (stronger Angola Low, weaker Botswana High, weaker Mozambique Channel Trough) underlie the 2017 floods over Ngamiland which are not associated with ENSO. These atmospheric variability without ENSO forcing could be related to the fact that SST patterns in the surrounding Indian and Atlantic Oceans may influence the circulation and rainfall patterns over southern Africa either both partially dependent on ENSO (Goddard and Graham, 1999; Hoell et al., 2015), or independent of ENSO (Reason, 2001a; Washington and Preston, 2006), and may also reinforce or oppose ENSO impacts (Reason and Smart, 2015; Hoell et al., 2017).

5.5 Discussion and conclusions

This study has analysed characteristics of extreme rainfall events accumulated over 1-day (DP1) and 3-day (DP3) periods in the Okavango River Basin (ORB) in Western Central Southern Africa (WCSA), for January-April (JFMA), 1981-2021. These characteristics include frequencies, intensities [highest spatially averaged rainfall intensity (here, referred to as Intensity-Max) in a particular season], spatial distributions, variability and trends. The most important weather systems driving these events have been identified, contributions of these events to JFMA rainfall totals have been examined, as well as factors that might have contributed to the severe floods that occurred over Ngamiland during the ENSO-neutral JFMA 2017.

Consistent with the IPCC (2013) and (2021) assessments that the frequency and intensity of extreme rainfall events is likely to increase due to global warming, a significant increasing trend was found in the DP1 frequency over the period 1981-2021. This trend, if it persists, may increase the tendency for JFMA flooding with associated crop and livestock losses. Positive significant trends were also found in JFMA daily rainfall totals and in rain-days receiving >1 mm and >10 mm, over the southern half of the WCSA as well as adjacent areas in Namibia, South Africa, Zimbabwe and Zambia. The implication of these trends if they persist into the future is that there may be a weakening of the meridional rainfall gradient from Botswana to Zambia and fading of the edge of the tropical rain-belt over northern Botswana. These trends compare well with trends in wet days of 10-30 mm/day found for December-February by Thoithi et al. (2021), and with an increase in average daily rainfall found by New et al. (2006).

DP1 and DP3 events show large interannual variability in their frequencies and percentage contributions to JFMA seasonal rainfall totals. While on average DP1 (DP3) events contribute ~10% (17%) to JFMA rainfall totals, in some years their contributions reach above 30% over the WCSA. The size of these contributions to seasonal rainfall totals shows that they play an important role in the regional climate. However, although these extreme rainfall events make substantial contributions to water resources, they also have the potential to cause local flooding and significant damage to crops and human settlements.

Consistent with the fact that most of the ORB streamflow is generated over the north catchment (Andersson et al., 2003; Wolski and Murray-Hudson, 2008; Moses et al., 2022), it has been found here that DP1 and DP3 events over the WCSA drop more of their heavy rainfall over the north catchment than Ngamiland. This result is also consistent with the spatial distributions of JFMA daily rainfall totals and rain-days receiving >1 mm and >10 mm, which are higher over the north catchment than Ngamiland. Correlation analysis showed stronger significantly positive correlations of Ngamiland JFMA rainfall totals with DP1 and DP3 frequencies ($r = 0.59$ and 0.72, respectively, $p < 0.05$) whereas for the north catchment, rainfall totals are only correlated significantly positive (and less strongly) with DP3 events (r

= 0.36, p <0.05). These correlations, and the spatial maps of rain-days and heavy rain-days, suggest that extreme rainfall events are more important to rainfall totals over Ngamiland than over the north catchment.

El Niño-Southern Oscillation (ENSO) impacts strongly on frequencies/intensities of both DP1 and DP3 events in JFMA, consistent with when this climate mode generally has its strongest impact over southern Africa (Lindesay, 1988; Reason et al., 2000; Reason and Jagadheesha, 2005; Blamey et al., 2018). El Niño (La Niña) events typically lead to less (more) intense DP1/3 events, and they also lead to low (high) frequency of these DP1/3 events. The Botswana High which typically moves south and strengthens during the summer also impacts on extreme event characteristics (Reason, 2016; Driver and Reason, 2017) since it leads to less regional subsidence when it is weaker than average and allows more favourable conditions for convection (Reason, 2016; Driver and Reason, 2017).

Cloud bands were found to be the dominant synoptic weather type associated with most of the top 200 DP1 and DP3 events, consistent with other studies for rainfall in general over southern Africa (e.g., Washington and Todd, 1999; Hart et al., 2010, 2013), with tropical lows (Howard et al., 2019) also making a large contribution. Mesoscale Convective Systems (MCSs) make a small contribution to the top 200 events, although their contribution may be underestimated since they tend to be embedded within other systems like cloud bands, and they tend to be shorter-lived than cloud bands or tropical lows (Blamey and Reason, 2013; Rapolaki et al., 2019).

Finally, a case study of the floods that occurred over Ngamiland during the ENSO-neutral JFMA 2017 indicated that these floods were caused by several factors. These included the fact that JFMA 2017 experienced the largest number of DP3 events in the WCSA box, i.e., 10 in total, over the 1981-2021 study period. Heavy rain of 8 of these 10 DP3 events fell over Ngamiland. Similarly, 8 of the 9 WCSA DP1 events that occurred during this season had their heavy rain falling over Ngamiland. The number of rain-days receiving >10 mm was also more than double the average number during JFMA 2017.

Based on the daily distribution of rainfall during the JFMA 2017 floods over Ngamiland, the associated circulation anomalies were separately analysed for 1 January – 8 March and 21-23 April. During the 1 January – 8 March period, the Angola Low, which acts as the tropical source for the cloud bands that bring most of the summer rainfall over subtropical southern Africa (Cook et al., 2004; Hart et al., 2010, 2013), was anomalously strong. Indeed, many of the DP1 and DP3 events during this season resulted from cloud bands.

Other circulation anomalies that contributed to these floods include a weaker than usual Mozambique Channel Trough, which resulted in more moisture advection from the southwest Indian Ocean into the southern Africa landmass (Barimalala et al., 2018, 2020), where it converged over Botswana leading to the floods over Ngamiland. The Botswana High was weaker than normal, and there was increased uplift over most of the WCSA, implying that conditions were favourable for deep convection and cloud band development. SST anomalies in the southwest Indian Ocean were strongly positive, which has previously been associated with above average summer rainfall (Reason and Mulenga, 1999; Behera and Yamagata, 2001; Reason, 2001a). Overall, the heavy rain during the 1 January – 8 March period resulted from cloud bands and tropical lows. After a relatively long dry period (March 10 - 20 April), the second most intense wet spell of the summer occurred on 22 April due to a cut-off low centred over the central Namibian coast and surface trough over Botswana. This is a caution that April is not necessarily out of the core rainy season, possibly for most of southern Africa.

The fact that TRMM and PERSIANN-CDR rainfall show the same interannual variability and seasonal totals as CHIRPS, as well as compare favourably with the few stations available in the ORB (Moses et al., 2022), provides confidence in the robustness of the extreme rainfall event results presented here. These results may be useful for forecasting, and may help with the management of water resources, agricultural activities and the highly biodiverse ecosystems in the ORB region. Furthermore, they highlight the importance of better understanding the characteristics of extreme rainfall events over different parts of southern Africa.

The following chapter focusses on drought metrics and temperature extremes (hot days) over the ORB, and their links with regional circulation systems such as the Botswana High.

Chapter 6: Analysis of drought metrics and temperature extremes over the Okavango River basin, southern Africa, and links with the Botswana High

This chapter is presented as the paper submitted to International Journal of Climatology. It addresses the questions below:

Moses, O., Blamey, R.C., Reason, C.J.C., 2022. Analysis of Drought metrics and temperature extremes over the Okavango River basin, southern Africa, and links with the Botswana High. Submitted to International Journal of Climatology.

- How do spatial mean patterns in dry spell frequencies and in 90th percentiles of maximum temperature vary seasonally, and are there relationships with the African tropical rain-belt, Congo Air Boundary and the Botswana High?
- How do drought metrics and hot day frequencies vary interannually, and do they show significant trends?
- Do these variables have relationships with climate modes such as ENSO?

Abstract

The Okavango River Basin (ORB), including the World Heritage site Okavango Delta, is a region of high biodiversity projected to suffer increased early summer drying under climate change. Little work has been done on drought over this sensitive region. Here, various drought metrics are analysed over the ORB. These include a Cumulative Drought Intensity (CDI) index, based on the product of maximum temperature anomaly and maximum duration of a dry spell, and the Standardised Precipitation-Evapotranspiration Index (SPEI). Strong gradients in dry spell and hot day frequencies shift south over the ORB from August to November as the tropical rain-belt moves south of the equator, the Congo Air Boundary declines and the Botswana High strengthens and moves southwestwards. By December, the tropical gradient in dry spell frequencies has vanished while that across the Limpopo River and southern ORB region, where the Botswana High is centred, is prominent. Seasonal analyses highlight October-November 2013-2021 as particularly dry and hot over the Okavango Delta region (Ngamiland district). This dry/hot epoch is shown to be related to a stronger and southward shifted Botswana High and reduced low-level moisture convergence. For December-February, this period was also anomalously dry and hot over Ngamiland and the north catchment of the ORB. On interannual scales, strong relationships were found with the Botswana High, and to a lesser extent El Niño-Southern Oscillation (ENSO). El Niño (La Niña) events were generally associated with high (low) dry spell and hot day frequencies. The early summer shows a strong drying-warming trend, related to a significant strengthening of the Botswana High. These trends, together with the Coupled Model Intercomparison Project Phase 6 (CMIP6) projected early summer drying over southern Africa found in the literature, may impact severely on the sensitive ecosystems of the ORB and on subsistence agriculture in the region.

6.1 Introduction

Southern Africa is a region with high climate variability whose rural population and the urban poor depend on rainfed agriculture (Tyson, 1986; Reason et al., 2006; Conway et al., 2015). The region is prone to droughts which are threats to agriculture, hence to food security. For example, droughts that had severe impacts in southern Africa include those that occurred in 1982/83, 1991/92 and 2015/16 (Reason and Jagadheesha, 2005; Blamey et al., 2018). Impacts included widespread crop losses, livestock mortality and severe water shortages.

Drought impacts during the rainy season can be worsened by co-occurrence of other extremes such as hot days and heat waves (Lyon, 2009; Ye et al., 2019). The Intergovernmental Panel on Climate Change (IPCC) fifth (IPCC, 2013) and sixth (IPCC, 2021) reports based on the Coupled Model Intercomparison Project Phase 5 (CMIP5) and 6 (CMIP6), respectively, show that the frequency of co-occurrence of droughts and hot extremes has increased on the global scale, motivating us to assess these over particular regions in southern Africa. These reports also show that intensity and frequency of these and other climate extremes are likely to increase over the subcontinent because of global warming. Like hot extremes, dry spells are also a crucial aspect of the rainy season that are related to drought impacts. Too many dry spells during the rainy season lead to the drying out of soils which may cause rainfed crop failure, hence posing a threat to food security (Rockström and Falkenmark, 2000; Guilpart et al., 2017). Since drought impacts during the rainy season can be aggravated by co-occurrence of hot extremes and too many dry spells, it is therefore important to better understand how these variables evolve during the rainy season.

Co-occurrences of these extremes during the summer rainy season have not been given much attention over southern Africa. Lyon (2009) investigated characteristics of heat waves, drought, and their joint occurrence during December-February while Meque et al. (2022) investigated heat wave characteristics during November-March. Driver and Reason (2017) examined interannual variability in dry spell frequency and maximum air temperatures. Dry spell frequencies during December-February were examined by Usman and Reason (2004) who found evidence of a drought corridor existing across the sub-continent in the 20°-24°S zone. This drought corridor was further refined by Thoithi et al. (2021) who found a second such corridor over the Zambezi River region in early summer as well as significant decreasing trends in dry spells over parts of Namibia and Botswana in mid-summer. These regions include parts of the southern half of the Okavango River Basin (ORB), located in central southern Africa (blue polygon in **Figure 6.1a**), which is focussed on in this study. The ORB region is of particular interest and importance since it has high biodiversity, contains unique ecosystems as well as the worldwide-known Okavango Delta, which is a United Nations Educational, Scientific and Cultural Organization (UNESCO) world heritage and Ramsar site (UNESCO, 2014). To date, there has been little work on drought, dry spells and hot extremes and their evolution over the ORB.

The ORB and most of Africa south of 10°S (except the far southwest and the south coast of South Africa) experience highly variable seasonal rains from October to March or April. While El Niño-Southern Oscillation (ENSO) is known to be the main interannual climate mode affecting southern Africa (Lindesay, 1988; Reason et al., 2000; Reason and Jagadheesha, 2005; Blamey et al., 2018), its impact on drought over the ORB has not been given much attention. Also, its role on impacting regional circulation features like the mid-level Botswana High is not well understood. This Botswana High tends to suppress (enhance) rainfall when it is strong (weak) due to increased (reduced) subsidence over the region (Reason, 2016; Driver and Reason, 2017). These authors noted that while the Botswana High is typically weaker (stronger) during La Niña (El Niño), large anomalies in this high-pressure system can also occur during neutral ENSO summers.

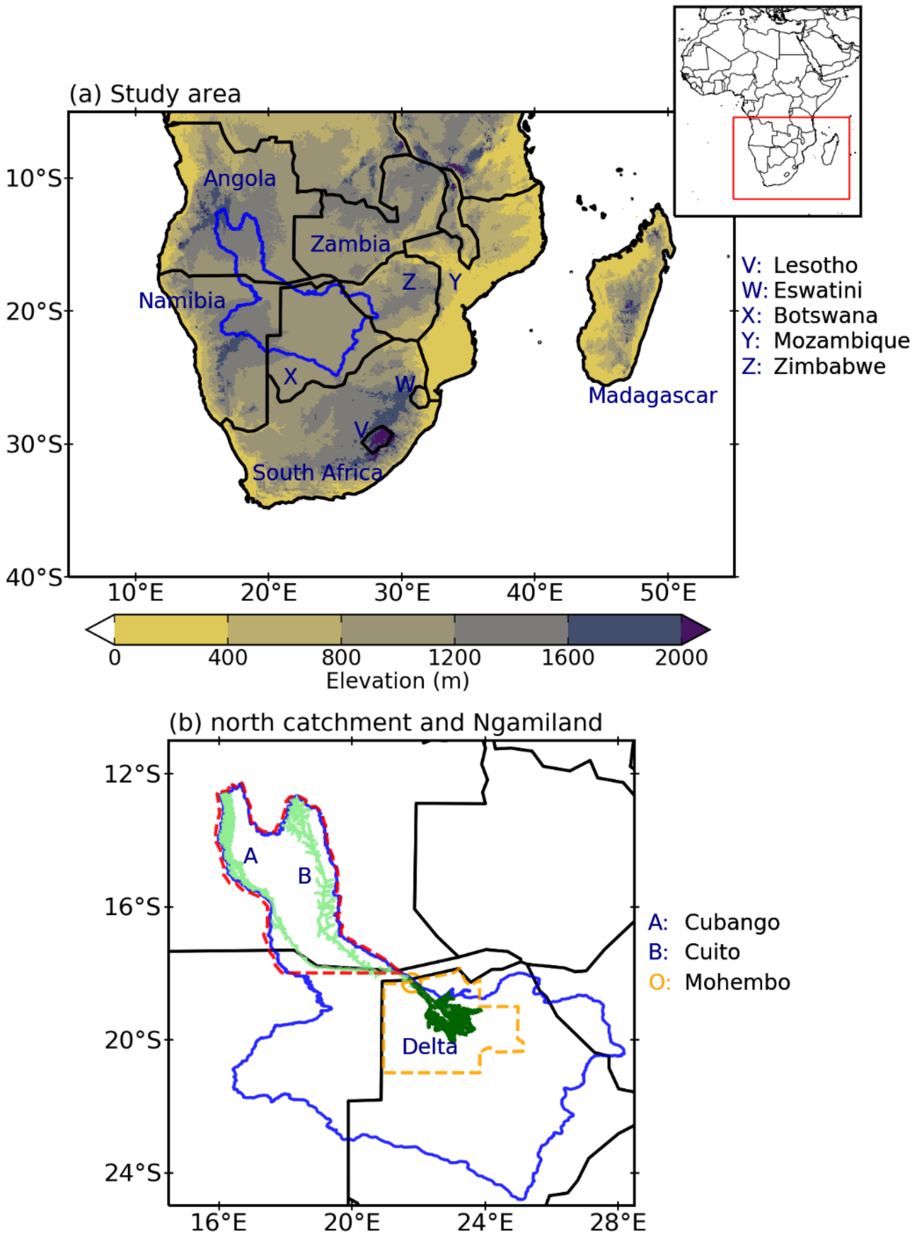

Figure 6.1 (a) The study area, i.e., southern Africa (5°-40°S, 5°-55°E), with its surface elevation shown. It's location in Africa is shown in the insert of the panel. The blue polygon is the extent of the Okavango River Basin (ORB). Country names denoted by letters are spelt out on the right of the panel. (b) Subdivision of the ORB into the north catchment (red dashed polygon) and Ngamiland (orange dashed polygon). The two main rivers, i.e., Cubango and Cuito, denoted by "A" and "B", respectively, which originate from the southern Angolan Highlands and merge in southeastern Angola to form the Okavango River, and Mohembo hydrological station (orange circle) at the apex of the Okavango Delta are shown.

The Congo Air Boundary is also an important feature associated with rainfall variability over southern Africa. This feature is a band of surface humidity gradient and/or near-surface wind convergence located at the northern edge of the easterly Indian Ocean trade winds and the southern edge of the low-level westerlies (Howard and Washington, 2019, 2020). This means that both the convergence of surface winds and the horizontal distribution of surface humidity are important for establishing the Congo Air Boundary. This boundary typically extends from central Angola to western Zambia, and it marks the location of the southern edge of the African tropical rain-belt. Until the Congo Air Boundary disintegrates in November/December, it inhibits penetration of moist and unstable Congo air from the tropics further into the southern African subtropics, resulting in less rain over the latter. The Congo Basin is an important continental source of moisture during summer for subtropical southern Africa (D'Abreton and Tyson, 1995; Rapolaki et al., 2020) while major oceanic sources are the tropical southeast Atlantic Ocean, western tropical Indian Ocean and the southwest Indian Ocean (Rouault et al., 2003a; Cook et al., 2004; Reason et al., 2006; Vigaud et al., 2009; Manhique et al., 2015).

Given the vulnerability of the unique ORB ecosystems to drought and the reliance of the local population on rain-fed agriculture, the objectives here are to (i) assess seasonal spatial mean patterns in dry spell frequencies and in hot days, as well as relationships with the African tropical rain-belt, Congo Air Boundary and the Botswana High, (ii) examine interannual variability and trends in drought metrics and hot day frequencies, and (iii) determine possible relationships of these variables with climate modes such as ENSO.

6.2 Data and Methods

First, spatial distributions of mean dry spell frequencies and 90th percentiles of maximum temperature were considered over southern Africa south of 5°S. Note that **Chapters 4** and **5** consider southern Africa south of 10°S whereas the present chapter considers a bigger region, i.e., southern Africa south of 5°S, to capture regions of high dry spell frequencies better. After considering the spatial distributions, time series of dry spell frequencies and hot days with maximum temperature greater than 90th percentiles, as well as Standardised Precipitation-Evapotranspiration Index (SPEI; Vicente-Serrano et al., 2010, 2015) were examined for the particular region of interest and importance, the ORB. Over the ORB, the focus was placed on the north catchment and on the Ngamiland district which contains the world-famous Okavango Delta (**Figure 6.1b**). The north catchment is the part of the ORB upstream of the Okavango Delta apex at Mohembo (18°S) (**Figure 6.1b**), where most of the ORB streamflow is generated (Andersson et al., 2003; Wolski and Murray-Hudson, 2008).

Based on previous analyses for rainfall over the ORB (Moses et al., 2022) and for dry spells over southern Africa (Thoithi et al., 2021), the analyses were done for October-November (ON), December-February (DJF) and March-April (MA), over the period 1981-2021. Very little rain falls in the ORB during May-September. December to February are typically the wettest months, hence the main growing season, but some years also have significant falls in ON (onset of the rainy season) or March-April (end of the rainy season).

Various indices have been developed to quantify drought. Here, droughts are identified using a multi-scalar index, SPEI, from the Spanish National Research Council (CSIC) (Vicente-Serrano et al., 2010, 2015). Formulation of this index is based on precipitation as well as temperature-based potential evapotranspiration component, and its multi-scalar characteristics enable identification of droughts in the context of global warming (IPCC 2013, 2021). Available precipitation and temperature-based data can be used for its calculation. SPEI has a spatial resolution of 0.5° and can be calculated on various time scales from monthly to several years. It has been used successfully in the southern African region, for example, to study drought in Botswana (Byakatonda et al., 2020) and in South Africa (Edossa et al., 2014). Like in Yu et al. (2014), SPEI values $\leq$ -1 are considered to be a drought on the corresponding time scale used to calculate this parameter which in this study were 2-month (SPEI-2) (for ON and MA) and 3-month (SPEI-3) (for DJF).

Following Usman and Reason (2004) and Thoithi et al. (2021), a dry spell is defined as a 5-day period (pentad) receiving less than 5 mm. Due to shortage of rainfall observations in the study area, the Climate Hazards Infrared Precipitation with Station data (CHIRPS; Funk et al., 2015) version 2, with a 0.05° (spatial) and daily (temporal) resolution, was used for identification of dry spells and monthly evolution of the tropical rain-belt. Previous studies found that CHIRPS data performed reasonably well when compared with monthly station data in northern Botswana and Namibia (Moses et al., 2022), and with station data in northern South Africa (Rapolaki et al., 2019; Thoithi et al., 2021). This could be related to the fact that CHIRPS is based on the interpolation of station data.

Hot days were defined as the number of days with a maximum temperature greater than the 90th percentile per season, over the observational record (1981-2021), using 2m air temperature from 0.25° resolution ERA5 reanalyses (Copernicus Climate Change Service, 2017; Hersbach et al., 2020). The choice of the percentile-based index was based on the Expert Team on Climate Change Detection and Indices (ETCCDI; Zhang et al., 2011; Sillmann et al., 2013) and on other relevant studies (Lyon, 2009; Mueller and Seneviratne, 2012). Unlike threshold-based indices, percentile-based indices are more suitable for spatial comparisons of extremes (Zhang et al., 2011). ERA5 reanalyses along with NOAA Optimally Interpolated SST data (0.25° resolution, Huang et al., 2021) were used to analyse potential mechanisms associated with an extended dry period during 2013-2021.

Since drought tends to involve both a lack of rain as well as high temperatures, and it is the compounded effect of large anomalies in these variables which negatively impacts on agriculture, ecosystems and people, a Cumulative Drought Intensity (CDI) metric was derived. This metric was computed by multiplying the maximum dry spell duration (n) in a particular season by the corresponding maximum temperature anomaly (anomTmax) such that each dry spell had to last at least 3 days. This temperature anomaly is the average maximum daily temperature over that dry spell event ($Tmax_{ds}$) minus the climatological maximum temperature (climTmax) for that time of year. Maximum dry spell duration is the largest number of consecutive days receiving < 1 mm each in a particular season (based on the ETCCDI above). Such a metric then provides another measure of the relative severity of an extremely dry summer rainy season, analogous to cumulative intensity often used to determine the severity of marine heat waves (Hobday et al., 2016). The equations below (**Equations 6.1** to **6.4**) show how the CDI metric was derived.

$$CDI = n \times anomTmax \qquad 6.1$$

$$anomTmax = Tmax_{ds} - climTmax \qquad 6.2$$

$$Tmax_{ds} = \frac{1}{n}\sum_{i=1}^{n} Tmax_i \qquad 6.3$$

$$climTmax = \frac{1}{n \times m}\sum_{j=1}^{m}\sum_{i=1}^{n} Tmax_{ij} \qquad 6.4$$

where n, anomTmax, $Tmax_{ds}$ and climTmax are as described in the paragraph preceding the equations. In **Equation 6.3**, $Tmax_i$ is the ith maximum temperature value over a particular dry spell event. In **Equation 6.4**, the index (ij) in $Tmax_{ij}$ means the ith maximum temperature value over a particular dry spell event in a particular year j, and in the same equation, m = 41 (in years), which is the length of the study period 1981-2021. The units of the CDI metric are °C days, based on **Equation 6.1**.

Possible relationships of the above-mentioned variables with ENSO or indices for regional circulation systems (Botswana High, Angola Low) were examined using the Pearson's product-moment correlations with significance reported at the 95% level. Correlations with the Southern Annular Mode, the subtropical Indian Ocean Dipole and the Benguela Niño were weak (not shown). For ENSO, the Niño 3.4 index is used. This index, defined as the monthly average of the SST anomalies in the Central Pacific (5°N-5°S; 120°-170°W), was obtained from NOAA Climate Prediction Centre (CPC) (Huang et al., 2021). To compute the Angola Low index, the 850 hPa geopotential height from ERA5, averaged over 16°-20°S, 18°-22°E (based on Munday and Washington, 2017) was used, whereas for the Botswana High index, the 500 hPa geopotential height averaged over 19°-23°S, 16°-21°E (based on Driver and Reason, 2017) was used.

Trends in the variables were computed and tested for statistical significance at $\alpha = 0.05$, using the Hamed and Rao (1998) and Yue and Wang (2002) tests, which are both modified from the nonparametric Mann-Kendall test (MKT) (Mann, 1945; Kendall, 1975). The MKT is widely used because it is not affected by the actual distribution of the data and is less sensitive to outliers. However, the original MKT does not take into consideration data autocorrelation, unlike the modified trend tests used here.

6.3 Results

6.3.1 Annual cycle

This section discusses the monthly evolution of dry spell frequencies during the austral summer half of the year, and how they may align with key features of the southern African climate like the African tropical rain-belt, the Congo Air Boundary (CAB), and the Botswana High.

Figure 6.2 plots monthly dry spell frequencies over southern Africa. October shows high dry spell frequencies over most of southern Africa with two prominent gradients (here dry spell gradient refers to diagonally or zonally elongated regions with high dry spell frequencies) standing out, which are obvious in November (**Figures 6.2a-b**). The stronger of the two is the diagonal gradient noted by Thoithi et al. (2021) which extends in northwest-southeast direction from southern Angola across the western Kalahari Desert into the southern part of the Karoo Desert on the leeward side of the south coast mountains in South Africa. The second gradient extends from southern Angola northeastwards across Zambia towards Tanzania and more or less follows the CAB in October (Howard and Washington, 2019). As previously found by Thoithi et al. (2021), this second gradient shifts poleward in November with the core of highest dry spells along the Zambezi River valley near 15°-17°S (**Figure 6.2b**). Further south, there is a strong gradient from November onwards in the subtropics extending from central Namibia and Botswana along the Limpopo River valley into southern Mozambique, termed the meridional gradient (Thoithi et al., 2021). By December, only this meridional gradient is clearly evident (**Figure 6.2c**) and remains very prominent through the rest of the summer (**Figures 6.2d-f**) until April when the tropical gradient re-establishes itself (**Figure 6.2g**) as the summer rains come to an end.

The above monthly evolution of dry spell frequencies is compared with the monthly climatology of firstly surface specific humidity and surface winds for the CAB (**Figure 6.3**), and secondly, the African tropical rain-belt (**Figure 6.4**) averaged over longitudes corresponding to the ORB's north catchment and Ngamiland (**Figure 6.1b**). Howard and Washington (2019) showed that the CAB marks the position of the southern edge of the African tropical rain-belt whose seasonal shift is associated with rainfall onset over the continent (Dunning et al., 2016). In August and September (**Figures 6.3a-b**), the presence of the CAB is evidenced by a strong humidity gradient with low-level wind convergence across northern Angola and southern Democratic Republic of Congo. During these months, the maximum in tropical rainfall occurs north of the equator near 8°N (**Figure 6.4**). South of the equator, the CAB is evident in **Figure 6.4** in the rainfall gradient near 5°-8°S in September whereas polewards of the CAB, the air is dry, with very little rainfall in the 11°-21°S latitude band which corresponds to the north catchment and Ngamiland. By October, as the CAB shifts polewards to the northern ORB (12°-15°S) and northwestern Zambia (**Figure 6.3c**), so does the maximum in tropical rainfall to lie near 2°-3°S. In this month, low dry spell frequencies are now evident over the far north of the ORB as well as most of Angola and the DR Congo (**Figure 6.2a**).

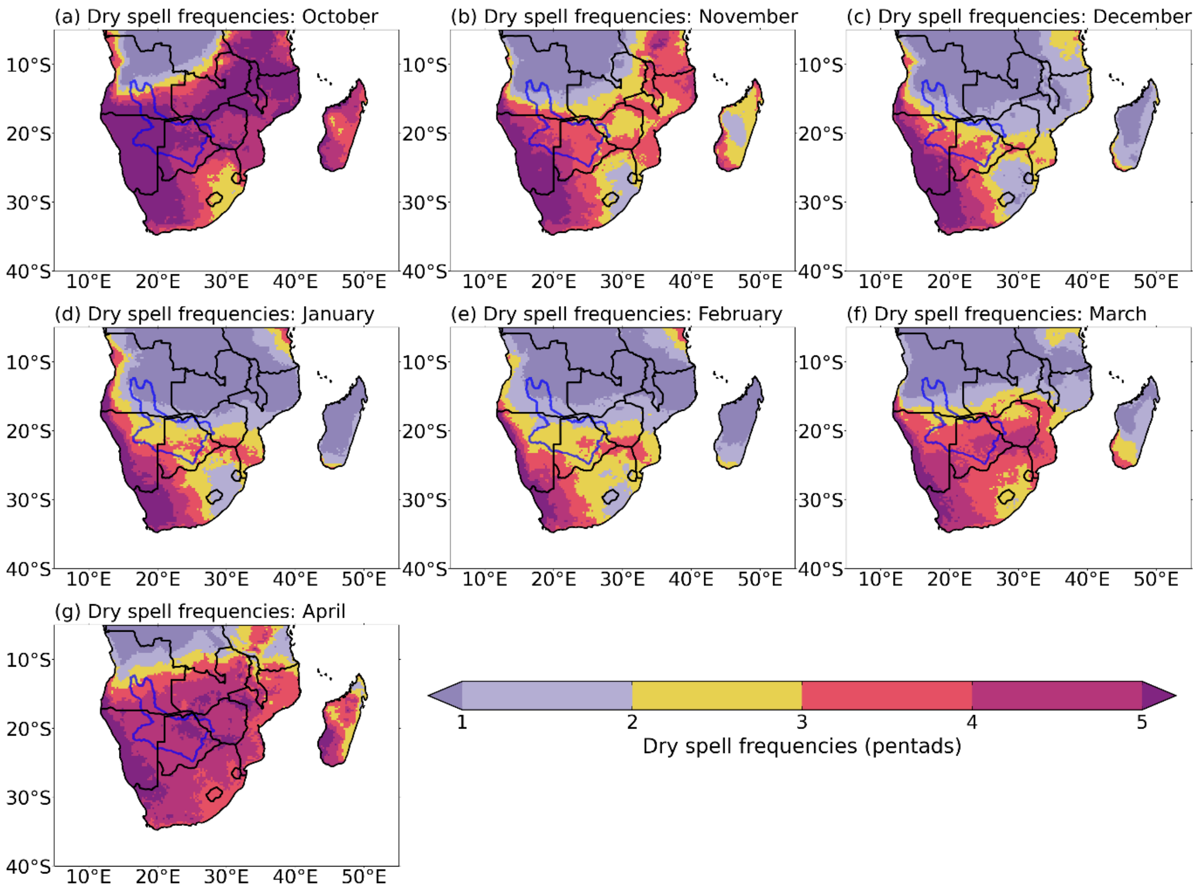

Figure 6.2 (a)-(g) Monthly mean of dry spell frequencies for October to April, respectively, over southern Africa for the period 1981-2021. The blue polygon is as in Figure 6.1.

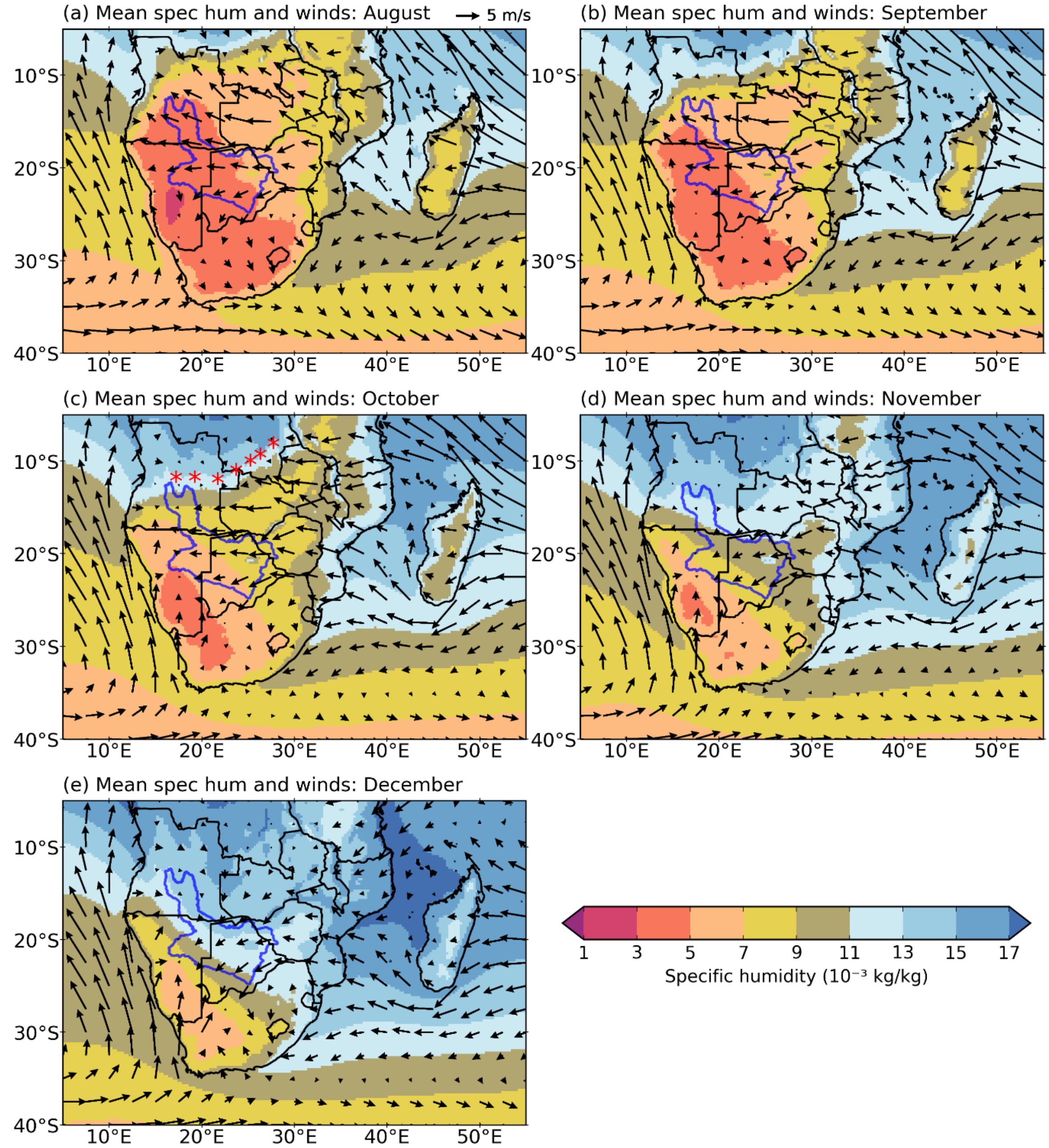

Figure 6.3 (a)-(e) Monthly mean of 2 m specific humidity (spec hum; shading) overlaid with 10 m winds (vectors), for August to December over southern Africa for the period 1981-2021. The humidity gradient and wind convergence in these plots are used to identify the Congo Air Boundary described in the text. The approximate position of this boundary is marked with red stars in (c) as an example. The blue polygon is as in Figure 6.1.

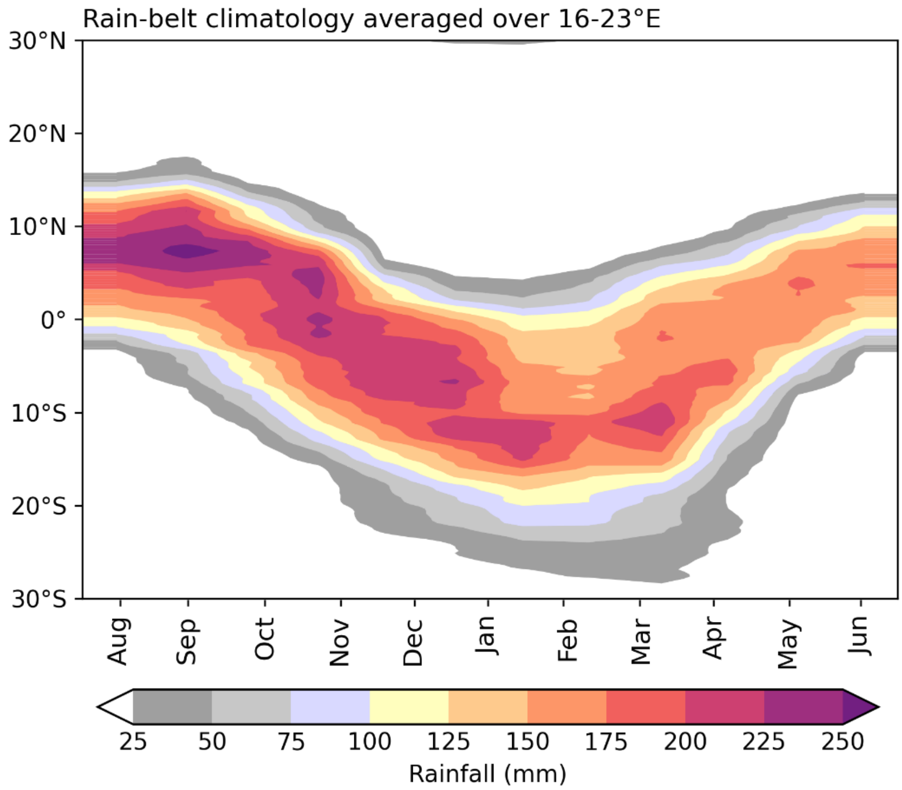

Figure 6.4 Monthly climatology of the African tropical rain-belt averaged over longitudes 16°-23°E, for the period 1981-2021.

As the summer rainy season sets in over southern Africa during October/November, the CAB shifts further polewards (**Figures 6.3c-d**) with the maximum in tropical rainfall following along just to its north (**Figure 6.4**), resulting in poleward shift in the region of lower frequencies of dry spells (**Figures 6.2a-b**). As described by Howard and Washington (2019), the CAB collapses typically in November/December (consistent with **Figures 6.3d-e** of this thesis) and the tropical gradient in dry spell frequency over the Zambezi River Valley disappears (**Figure 6.2c**). As the CAB collapses, the maximum in tropical rainfall shifts poleward to near 7°-10°S (**Figure 6.4**), just north of the ORB, since the moist Congo air is able to move farther poleward after the collapse of this CAB. Also, during December, there is a poleward expansion of the area of relatively low frequencies of dry spells to cover the north catchment and most of southern Africa north of ~18°S (**Figure 6.2c**).

During the mid-summer, the maximum rainfall continues to shift polewards to reach about 12°-14°S, the northernmost part of the ORB, by February (**Figure 6.4**). The tropical dry spell gradient is not evident during December-February, whereas the meridional dry spell gradient along the Limpopo River valley near 20°-23°S as well as the diagonal gradient extending southeastwards from northwestern Namibia to the south coast of South Africa are prominent (**Figures 6.2c-e**). Usman and Reason (2004) termed the 20°-24°S zone the drought corridor because although on average the maximum dry spell frequencies are only about 7-10 out of a maximum possible of 18 pentads, the interannual variability is such that many summers show considerably higher dry spell frequencies and hence experience severe drought. In March, dry spell frequencies begin to increase over the ORB, Zimbabwe and southern Zambia (**Figure 6.2f**) as the maximum rainfall in the tropical rain-belt moves slightly equatorward (**Figure 6.4**). April shows a more obvious withdrawal of the rainfall maximum back towards the equator (**Figure 6.4**), and the re-establishment of the tropical dry spell gradient (**Figure 6.2g**) as the summer rainy season ends over most of southern Africa.

It is worth noting that in **Figure 6.4**, the rainfall belt appears to migrate poleward more slowly than it retreats equatorward, and that clearly the latitude of the maximum rainfall belt during austral summer (January-March) is south of 10°S while that during boreal summer is south of 10°N. The fact that this rainfall belt reaches at higher latitudes over southern Africa may be due to the existence of the two oceans that surround southern Africa and provide ample moisture related to persistence of the tropical rain-belt and hence the long dry spells south of the belt.

Figure 6.5 shows monthly climatologies of 500 hPa geopotential height used to identify the location of the Botswana High. The exact location of this Botswana High, denoted by BH in the figure, was taken to be the central point of the highest closed contour (darkest red contour). The figure shows that the location of the mid-level Botswana High, like that of the maximum rainfall in the tropical rain-belt, also influences the distributions of dry spell frequencies (**Figure 6.2**). The Botswana High tends to suppress rainfall when it is strong due to increased subsidence over the region, whereas when it is weak, rainfall conditions are more favourable (Reason, 2016; Driver and Reason, 2017). August is the first month in which the Botswana High starts to appear (not shown), when it is centred mainly over southern Angola. As the maximum in tropical rainfall moves polewards in spring (**Figure 6.4**) so does the Botswana High so that by October, it is centred over the northern half of the ORB and adjoining areas in southern Angola/northern Namibia/northwestern Botswana (**Figure 6.5a**). At the same time, the diagonal gradient of dry spells is strong and located furthest east with highest dry spell frequencies of 4-5 pentads per month occurring on average over most of the ORB (**Figure 6.2a**).

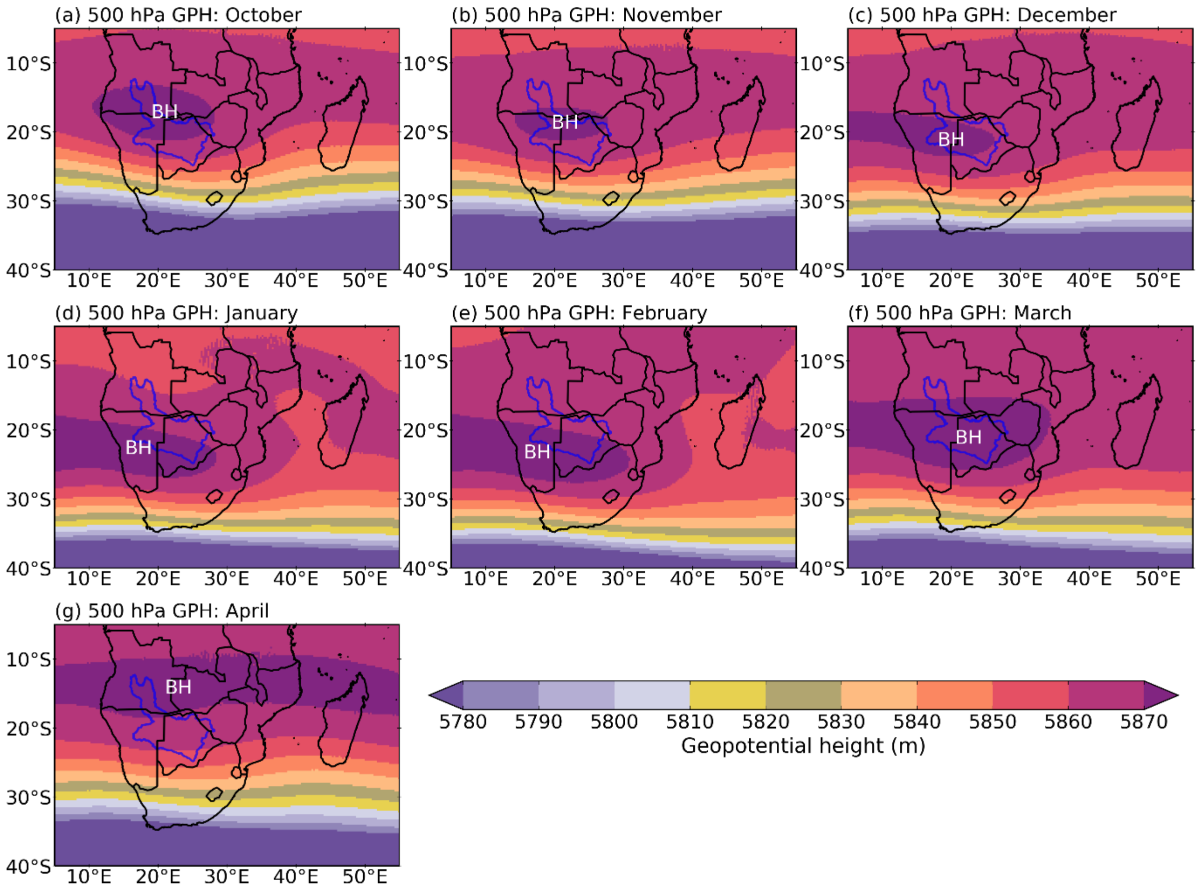

Figure 6.5 (a)-(g) Monthly mean of 500 hPa geopotential height (GPH; shaded) for October to April over southern Africa, showing the mean position of the Botswana High (BH) (position determined as described in the text) for the period 1981-2021. The blue polygon is as in Figure 6.1.

The Botswana High continues to move poleward through until January/February as well as extending zonally (**Figures 6.5c-e**), while at the same time the meridional gradient of dry spell frequencies in the Limpopo River valley becomes more and more prominent (**Figures 6.2c-e**). The zonally elongated structure of the Botswana High over southern Africa with westward extension over the South Atlantic which is obvious after December (**Figure 6.5a-g**) is consistent with Reason (2016) who, during January-March, found a ridge of high pressure extending across the subtropical landmasses in the Southern Hemisphere at 500 hPa, with closed anticyclones located over Botswana/Namibia (where "BH" is in **Figures 6.5d-f**, hence confirming the location of the Botswana High in these figures), the South Atlantic, Bolivia and western Australia. From March, the Botswana High retreats northward so that by April, its centre is over the far north of the ORB (**Figure 6.5g**) while the tropical dry spell gradient becomes re-established over northern Zambia (**Figure 6.2g**). High dry spell frequencies are now present over most of southern Africa roughly like in October/November (**Figure 6.2**). Taken together, **Figures 6.2-6.5** show how regions of high dry spell frequencies evolve through the summer half of the year in relation to the positions of the African tropical rain-belt and the Botswana High.

6.3.2 Seasonal climatological patterns

In this section, mean spatial patterns in dry spell frequencies and in 90th percentiles of maximum temperature for ON, DJF and MA are considered (**Figure 6.6**). In early summer (ON), largest values of the 90th percentiles of maximum temperature occur over most of the ORB through the Limpopo and Zambezi River valleys into the southern half of Mozambique (**Figure 6.6a**). This area roughly corresponds to those with high dry spell frequencies (**Figure 6.6d**). In DJF (**Figure 6.6b**), the pattern is similar to that for ON, but the values are now lower over the northern ORB and Zambezi River valley, as cloud cover and the tropical rain-belt shift south (**Figure 6.4**), and dry spell frequencies over these regions are much reduced compared to ON (**Figure 6.6e**). In MA (**Figure 6.6c**), the 90th percentiles of maximum temperature show patterns that are similar to those for DJF, but with values that are lower than those for both DJF and ON, as maximum insolation has now shifted north to lie near the equator. Dry spell frequencies in MA (**Figure 6.6f**) show a similar pattern to ON but reduced in magnitude over the southern half of the ORB as well as most of subtropical southern Africa.

In ON and MA, the tropical gradient in dry spell frequencies is evident from southern Angola/northern ORB/east to northeastern Zambia and is not present in DJF. The meridional gradient in the Limpopo River valley, and southern part of the ORB, is particularly strong in DJF but less so in ON or MA (**Figures 6.6d-f**). The latter two seasons also show a more eastward extended diagonal gradient in South Africa than is the case for DJF. This change in the diagonal gradient may reflect the greater contribution of ridging anticyclones to summer rainfall over southeastern South Africa relative to ON and MA (Weldon and Reason, 2014; Engelbrecht et al., 2015; Ndarana et al., 2020). Note that ridging anticyclones refers to the eastward extension of the South Atlantic High (St. Helena High) around the South African landmass (Ndarana et al., 2021), thereby drawing moisture from the South Atlantic and Southwest Indian Oceans (Rapolaki et al., 2020). While southeastern South Africa only shows low dry spell frequencies in DJF, the Congo Basin experiences low numbers throughout the entire summer half of the year.

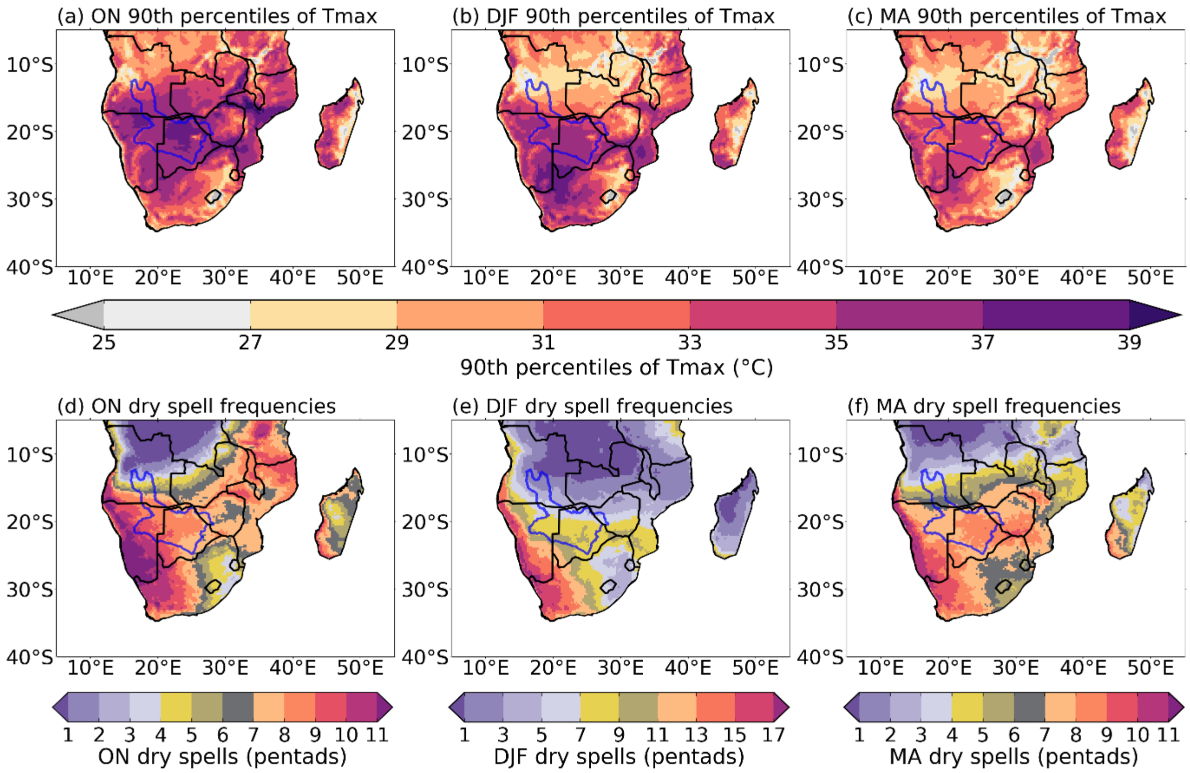

Figure 6.6 (a)-(c) show 90th percentiles of maximum temperatures (Tmax) for ON, DJF and MA, respectively, over southern Africa for the period 1981-2021. (d)-(f) show dry spell frequencies for ON, DJF and MA, respectively. The blue polygon is as in Figure 6.1.

6.3.3 Interannual variability

Focus is now placed on interannual variability in drought-related parameters over the ORB. These data are analysed for two key regions, namely, the north catchment which is the source region for the Okavango River flow measured at Mohembo, upstream of the Okavango Delta (**Figure 6.1b**), and Ngamiland which is the district within which the Delta is found. As apparent in **Figure 6.6**, the north catchment displays far fewer dry spells and has cooler 90th percentile temperatures than Ngamiland, so it is appropriate to analyse them separately.

Figure 6.7 shows ON longitude-time Hovmoller plots of SPEI-2 values, frequencies of dry spells, hot days with maximum temperatures greater than 90th percentiles and anomalies of 500 hPa geopotential height. These data are presented in two columns, with the left column averaged over latitudes corresponding to the north catchment (11°-17°S) and the right over Ngamiland (18°-21°S). While there is considerable interannual variability throughout, an obvious contrast exists between a multi-year period of negative SPEI, more dry spells, more hot days and a stronger Botswana High from 2013 onwards and the opposite during 1982-1988. This multi-year contrasting pattern is more obvious over Ngamiland (**Figures 6.7e-h**) than over the north catchment (**Figures 6.7a-d**). On these multi-year scales, a clear linkage exists between a stronger (weaker) Botswana High with more (less) mid-tropospheric subsidence and hotter, drier (cooler, wetter) ON seasons. However, for some of the years in between these two multi-year periods, the relationship is less clear. For example, 1992-1995 shows a weaker Botswana High (**Figures 6.7d**,**h**) but much of this period had negative SPEI (**Figures 6.7a**,**e**) and relatively large number of dry spells (**Figures 6.7b**,**f**) over most longitudes. The reasons as to why dry spell frequencies are so different between the north catchment and Ngamiland are not clear since there are small differences in the SPEI, the number of hot days and the geopotential height anomalies. The period 1992-1995 included a protracted El Niño when southern African rainfall impacts tend to differ from shorter ENSO events (Allan et al., 2003). Protracted El Niño events are often associated with more severe droughts than canonical El Niño events (Allan et al., 2003). Nevertheless, the multi-year 2013-2021 period stands out in **Figure 6.7** and is analysed as a case study in the next section.

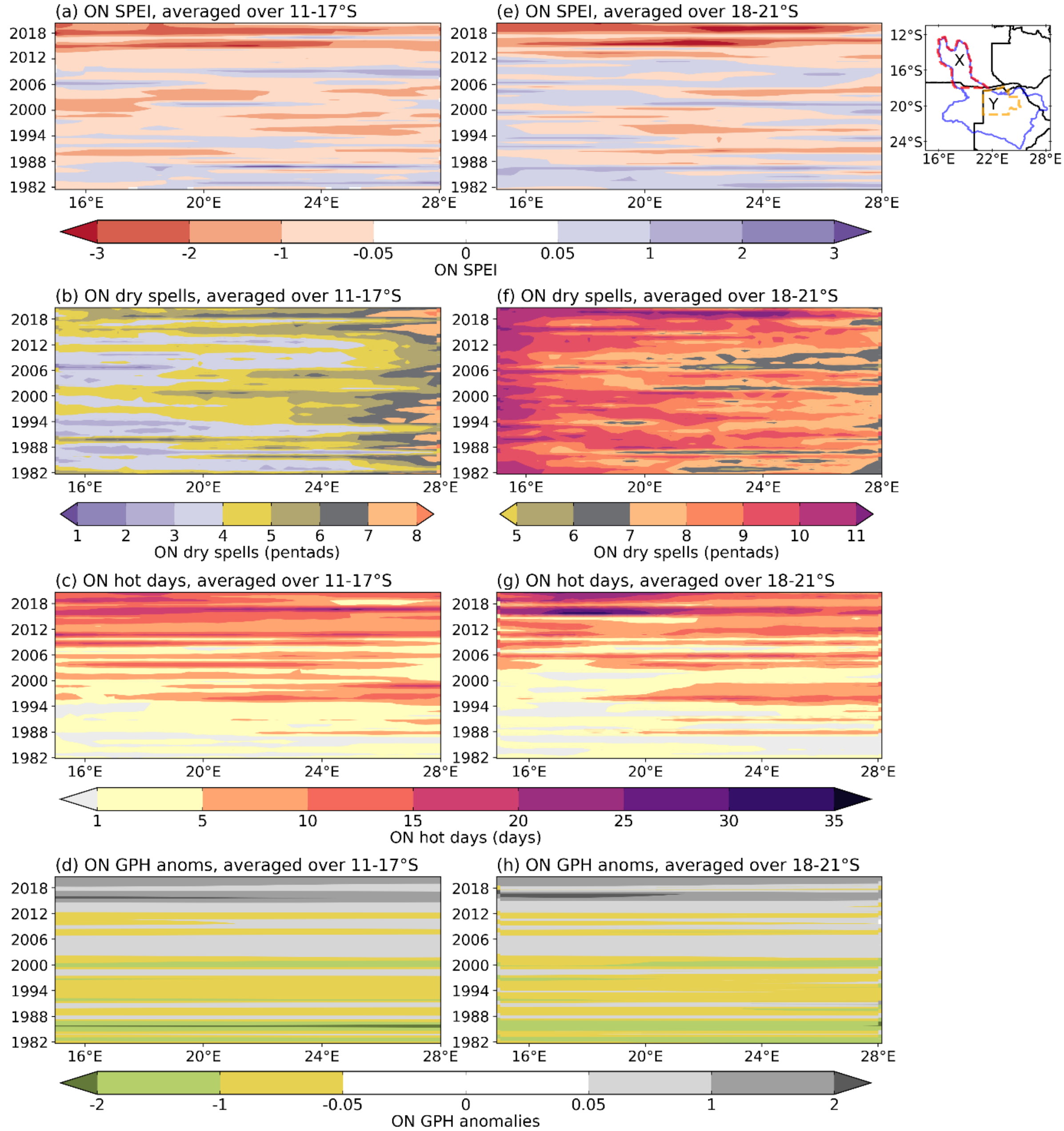

Figure 6.7 First column: (a) Evolution of SPEI-2 values for ON (ON SPEI) averaged over latitudes 11°-17°S; (b)-(d) Dry spell frequencies, hot day frequencies and 500 hPa geopotential height (GPH) anomalies (anoms), respectively, for ON, averaged over the same latitudes as in (a). Second column: (d)-(h) are as in (a)-(d), respectively, but averaged over latitudes 18°-21°S. Latitudes in the first and second columns correspond with the north catchment and Ngamiland, respectively, i.e., red (orange) dashed polygon marked X (Y) to the right of panel (e).

In DJF, the post-2013 period also tends to show mainly negative SPEI, more dry spells and hot days (particularly in the western longitudes) and a stronger Botswana High (**Figure 6.8**) but the signal is not as strong as it is for ON. A period of positive (relatively moist) SPEI (**Figures 6.8a**,**e**) is evident over much of the region during 2006-2012, which corresponds to a weaker Botswana High (**Figures 6.8d**,**h**). Such quasi-decadal periods of weaker and stronger Botswana High are consistent with earlier work (Reason, 2019). **Figure 6.8** also shows co-occurrence of hotter, drier, stronger than average Botswana High and large negative SPEI during strong El Niño events like 1982/83, 2002/03, 2015/16, and co-occurrence of cooler, wetter, weaker than average Botswana High and large positive SPEI during La Niña events such as 1988/89, 1999/00, 2011/12, particularly for Ngamiland but to a lesser extent the north catchment. Note that there are some prominent exceptions to this general pattern of drier (wetter) conditions during El Niño (La Niña) (Lindesay, 1988; Nicholson and Kim, 1997; Reason et al., 2000) such as the very strong 1997/98 El Niño and the moderately strong 2009/10 El Niño when the expected droughts did not occur over subtropical southern Africa (Reason and Jagadheesha, 2005; Lyon and Mason, 2007; Blamey et al., 2018; Driver et al., 2019). During the 1997/98 and 2009/10 El Niño events, the Angola Low which acts as the source for the tropical-extratropical cloud bands did not weaken as expected during a typical El Niño event (Reason and Jagadheesha, 2005; Lyon and Mason, 2007; Blamey et al., 2018; Driver et al., 2019).

For MA (not shown), the negative SPEI epoch after 2013 that is evident in ON and DJF is not as clear. Also, the ENSO relationship is less obvious in MA which is not surprising since ENSO events often weaken or reverse sign in April and the teleconnection patterns to southern Africa break down.

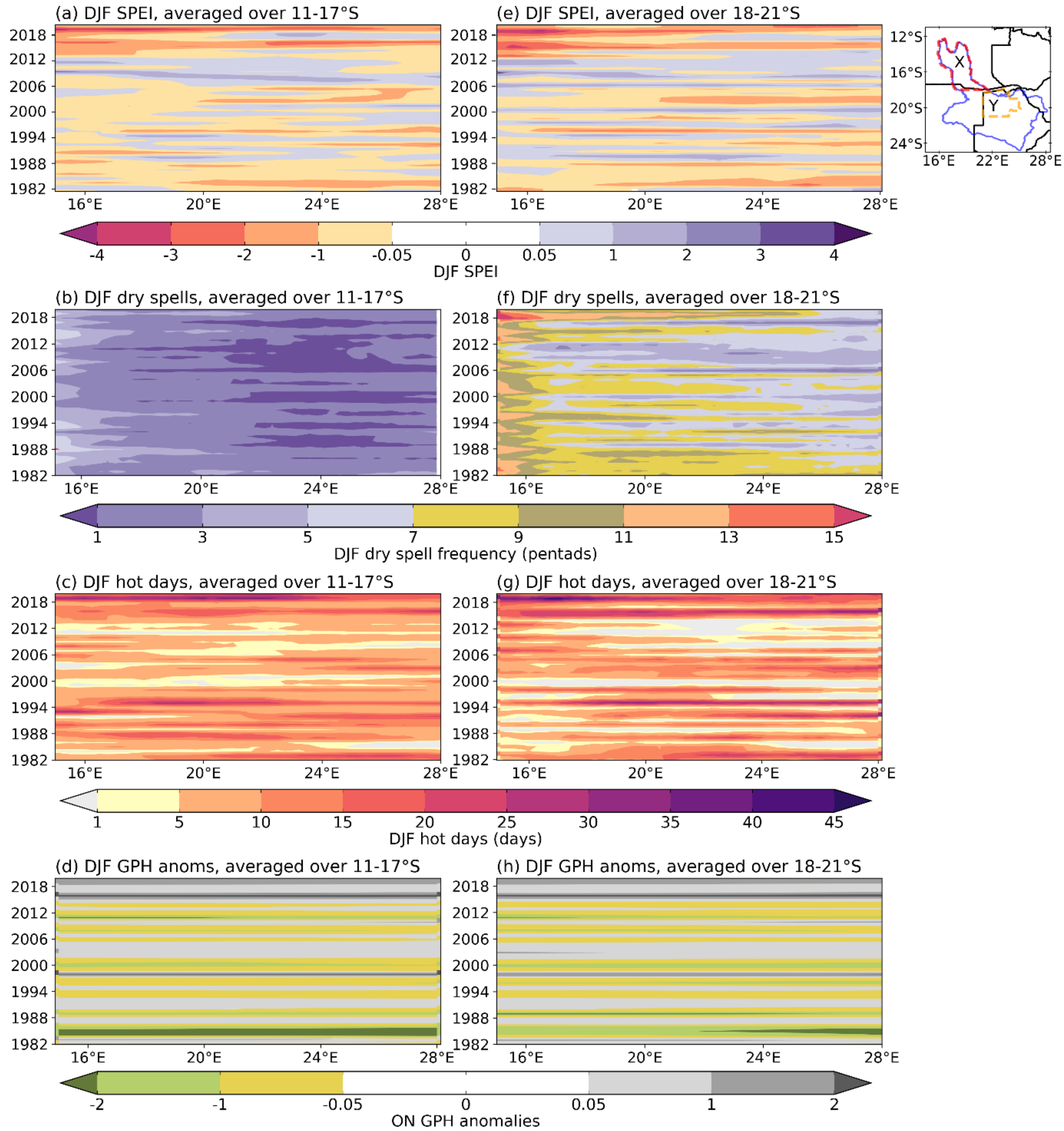

Figure 6.8 First column: (a) Evolution of SPEI-3 values for DJF (DJF SPEI) averaged over latitudes 11°-17°S; (b)-(d) Dry spell frequencies, hot day frequencies and 500 hPa geopotential height (GPH) anomalies (anoms), respectively, for DJF, averaged over the same latitudes as in (a). Second column: (d)-(h) are as in (a)-(d), respectively, but averaged over latitudes 18°-21°S. Latitudes in the first and second columns correspond with the north catchment and Ngamiland, respectively, i.e., red (orange) dashed polygon marked X (Y) to the right of panel (e). The year 1981 means December 1981 to February 1982, and so on.

To further highlight the multi-year post-2013 period, **Figures 6.9a-b** plot time series of SPEI and the Cumulative Drought Intensity (CDI) metric for ON, averaged over the north catchment and over Ngamiland. The CDI metric derived in this study as the product of the maximum dry spell duration with the anomaly in maximum temperature (*Section 6.2*), gives another measure of the severity of a dry-hot spell. While there are some exceptions, ON seasons with negative SPEI (drought) generally correspond to ones of positive CDI. As suggested by **Figure 6.7**, the period from 2013 onwards experienced mostly large negative SPEI values ≤ -1 (reflecting drought conditions) in both regions (**Figure 6.9a**). Almost all of these seasons received well below average rainfall totals (shown in the next section). Similarly, the post-2013 period shows large positive values in the CDI metric over both regions, which is consistent with the hot conditions that are accompanied by many dry spells (**Figures 6.9a-b**). However, for this parameter, the positive anomalies in fact began a few years before 2013. While there are other multi-year runs of the same signed anomaly in both records, the negative SPEI/positive CDI period after 2013 stands out with large magnitudes (severe drought) particularly for Ngamiland. In particular, very large negative SPEI values of at least -2.5 occurred in 4 (2) ON seasons over Ngamiland (north catchment) during 2013-2021. For CDI, almost all the large positive values over the north catchment occurred after 2010 while for Ngamiland, 5 of the 7 largest values are found then. Hence the common 2013-2021 period is analysed further in the next section.

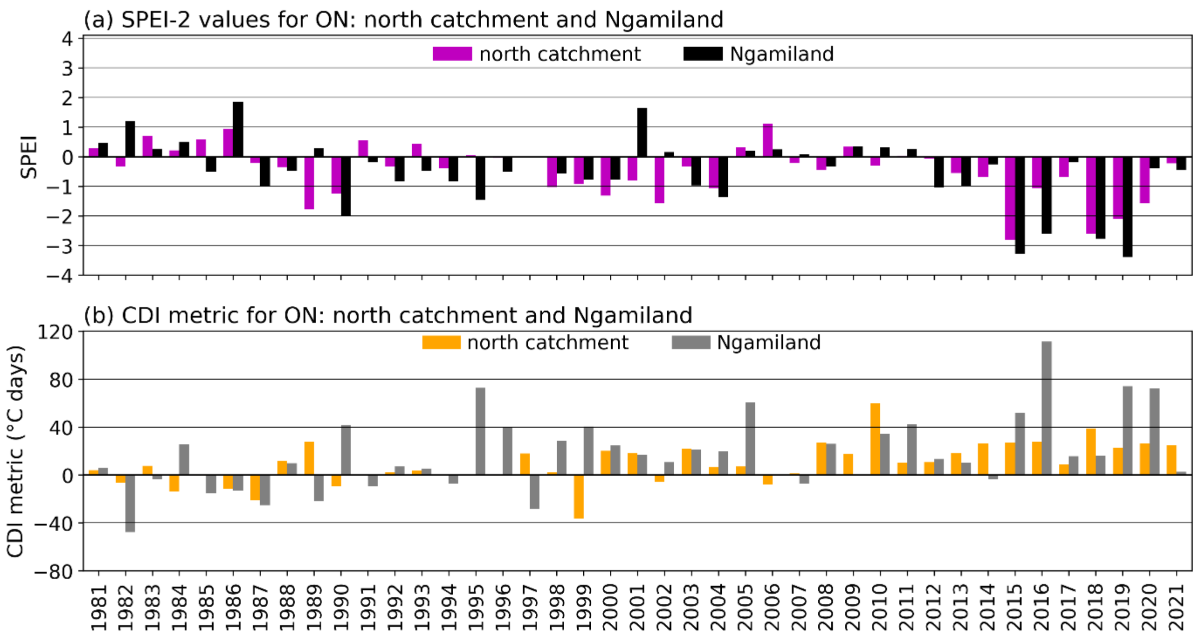

Figure 6.9 (a) SPEI-2 values for ON for the period 1981-2021, averaged over the north catchment and Ngamiland. (b) Cumulative Drought Intensity (CDI) metric for ON.

Table 6.1 shows that SPEI is not significantly correlated with ENSO over either region in ON. Since ENSO tends to impact rainfall strongly over southern Africa from December to March (Lindesay, 1988; Reason et al., 2000), the lack of a significant correlation is not surprising. Nevertheless, three ON El Niño seasons after 2013 (2015, 2016, 2019) experienced very negative SPEI values as well as large positive values of the CDI metric. **Table 6.1** does however show a significant correlation of both the SPEI and the CDI metric with the Botswana High for both regions. This regional circulation system is centred over the north catchment and Ngamiland during October and November (**Figures 6.5a-b**) implying severe dry-hot spells and more negative SPEI conditions for seasons when the high is stronger than average.

Table 6.1 Correlations of SPEI and the Cumulative Drought Intensity (CDI) metric, averaged over the north catchment and Ngamiland, with ENSO, Botswana High (BH) and Angola Low (AL), for ON, DJF and MA (1981-2021). Only significant correlations at α = 0.05 are shown

		north catchment			Ngamiland		
		ENSO	BH	AL	ENSO	BH	AL
ON	SPEI		-0.54			-0.66	
	CDI metric		0.48			0.56	
DJF	SPEI	-0.41	-0.52	-0.36	-0.63	-0.71	-0.55
	CDI metric				0.50	0.59	0.47
MA	SPEI	-0.38	-0.65		-0.41	-0.36	
	CDI metric		0.39		0.50	0.37	

In the other seasons, **Table 6.1** shows that Ngamiland shows significant correlations of both SPEI and CDI with the Botswana High, the Angola Low and ENSO. As already mentioned, a stronger Botswana High implies more regional subsidence and hence hotter, drier conditions. On the other hand, a weaker Angola Low implies less convection in the tropical source region of the cloud bands (Hart et al., 2010) and thus clearer skies as well as hotter, drier conditions. For the north catchment, SPEI is correlated significantly with all three indices but not CDI. In MA, there are no longer any significant correlations for the Angola Low in either region while those with ENSO and with the Botswana High are mostly weaker than those found for DJF. The significant correlations of the Angola Low with the SPEI that occur in DJF but not in MA could be related to the fact that this Angola Low is strongest in January and February

(Munday and 688 Washington, 2017; Howard and Washington, 2018). Based on **Table 6.1**, it appears that the Botswana High-drought relationship over both regions is stronger than the ENSO-drought relationship in all three seasons.

For completeness, **Figures 6.10-6.11** plot time series of SPEI and CDI over both regions for DJF and MA. In DJF, the post-2013 period of negative SPEI/positive CDI (severe drought) is largely present, but it is not as clear as in the ON season (**Figure 6.9**). For MA, this pattern is even less coherent. Since both regions experienced at least two DJF and MA seasons post-2013 which received well above average rainfall amounts (not shown), whereas this did not happen in ON, the post-2013 drought period is less well expressed in the mid- and late summer months. To confirm that the CDI metric may help evaluate the contribution of the temperature anomaly to the drought events, additional plots were made (not shown), i.e., plots of maximum temperature anomalies together with the SPEI. Temporal distribution patterns of maximum temperature anomalies were found to be very similar to those for the CDI metric, with the post-2013 period also standing out particularly in ON. Thus, the temporal distribution patterns of maximum temperature anomalies were in support of the use of the CDI metric to evaluate the contribution of the temperature anomaly to the drought events.

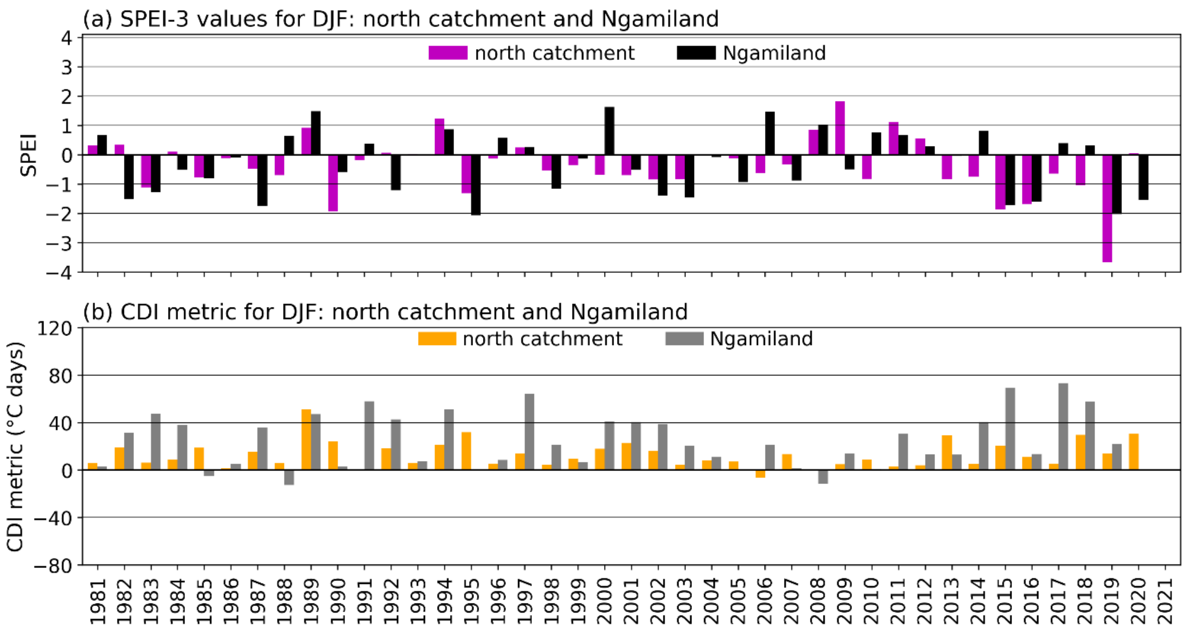

Figure 6.10 SPEI-3 values for DJF for the period 1981-2021, averaged over the north catchment and Ngamiland. (b) Cumulative Drought Intensity (CDI) metric for DJF. The year 1981 means December 1981 to February 1982, and so on.

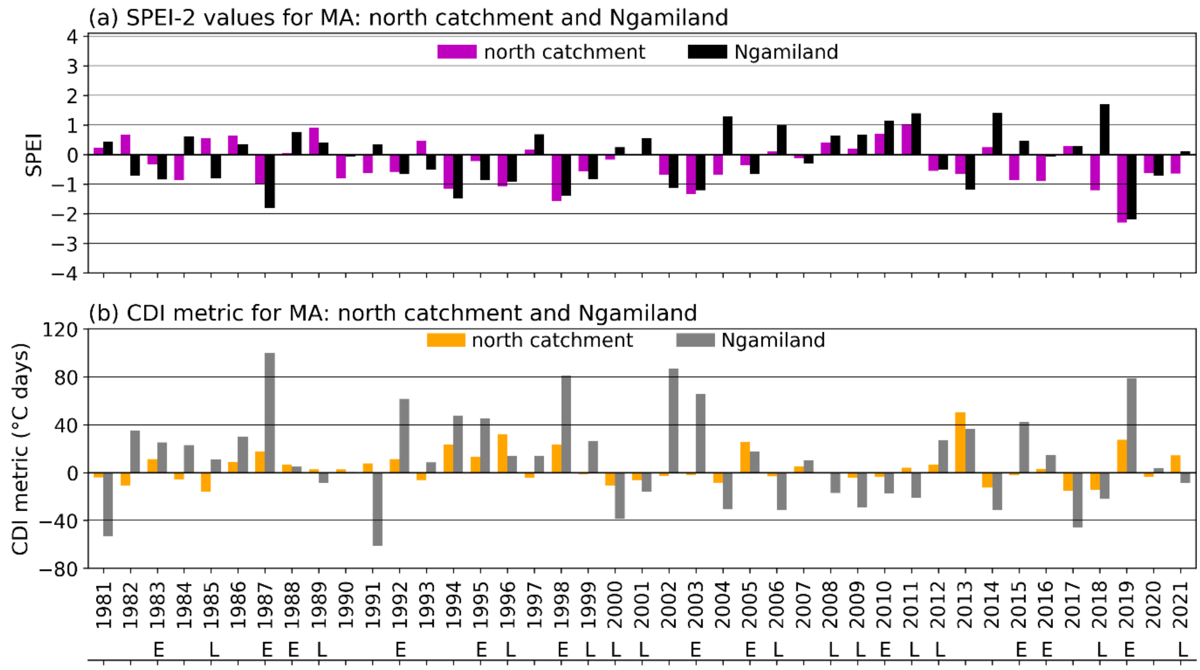

Figure 6.11 SPEI-2 values for MA for the period 1981-2021, averaged over the north catchment and Ngamiland. (b) Cumulative Drought Intensity (CDI) metric for MA. Notation below the x axis in (b): E, El Niño; L, La Niña.

6.3.4 Circulation anomaly patterns associated with the 2013-2021 epoch during ON

To help explain the 2013-2021 period of very large negative SPEI/positive CDI values and hence severe drought during this epoch in ON, anomaly patterns in rainfall, SST and various circulation fields are examined (**Figure 6.12**). **Figure 6.12a** plots ON standardised rainfall anomalies over the north catchment and Ngamiland which highlight the low rainfall amounts received during the epoch. Comparison of **Figure 6.12b** with **Figures 6.5a-b** indicates that the Botswana High was anomalously strong as well as shifted southwestwards during ON 2013-2021 relative to climatology. This stronger and southwestward shifted Botswana High during the period suggests unfavourable conditions for the source region of the tropical-extratropical cloud bands, implying less cloudy and hotter/drier conditions. Furthermore, there are positive anomalies at 850 hPa over Angola/Namibia (**Figure 6.12e**) indicating a weaker Angola Low, also unfavourable for tropical convection and cloud band development (Mulenga et al., 2003; Cook et al., 2004; Crétat et al., 2018), and hence drought. Unfavourable conditions also existed for the midlatitude input into these cloud bands (Hart et al., 2010) due to the presence of anticyclonic anomalies southwest of South Africa which would act to weaken and steer cold fronts further south than average. **Figure 6.12c** shows increased mid-level subsidence over almost all of subtropical southern Africa, again favourable for drier and hotter conditions during ON 2013-2021.

Much of southern Africa, including Ngamiland and the southern two-thirds of the ORB experienced low-level moisture flux divergence during 2013-2021 relative to climatology (**Figure 6.12d**), again suggesting hotter and drier conditions. The northwest-southeast diagonal band of increased divergence across Botswana and South Africa is consistent with reduced cloud band activity over the mainland and favourable for drought. Over the southwest Indian Ocean, there are westerly anomalies implying less moisture advected towards the mainland and drier, hotter conditions. Over Angola, there are easterly anomalies consistent with the weaker Angola Low and less moisture advected from the tropical southeast Atlantic towards the source region of the cloud bands, again implying hotter and drier conditions.

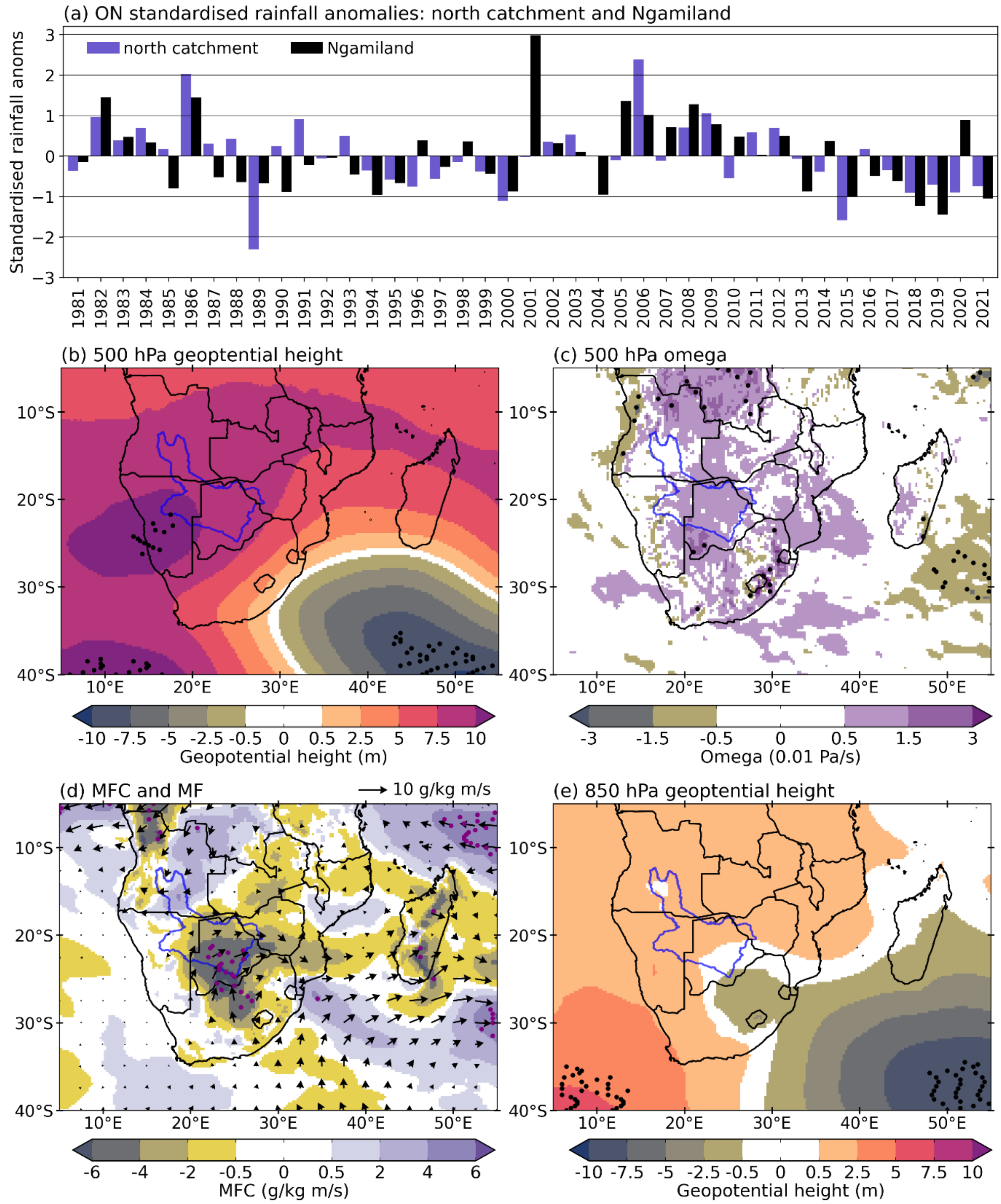

Figure 6.12 (a) Standardised rainfall anomalies (anoms) averaged over the north catchment and Ngamiland, for ON 1981-2021. (b) Anomalies of 500 hPa geopotential height for ON 2013-2021 with respect to 1981-2021 climatology, over southern Africa. (c) As in (b) but for omega. (d) As in (b) but for 850 hPa moisture flux convergence (MFC; shading) and moisture flux (MF; vectors). (e) As in (b) but for 850 hPa geopotential height. The blue polygon in (b)-(d) is as in Figure 6.1, and areas with statistically significant anomalies based on bootstrap 95% confidence level are denoted with stippling.

Figure 6.13 shows anomalies in the annual cycle of the tropical rain-belt for 2013-2021 relative to the climatology plotted in **Figure 6.4**. It is clear that over the ORB latitudes of 11°-24°S in October-November the rain-belt remained equatorwards of its mean position during 2013-2021 leading to wetter conditions in the 5°-9°S band and considerably drier over the ORB region, including the Ngamiland latitudes of ~18°-21°S. The drier conditions are also clearly apparent in this latitude band in January and February but not in March and April. Overall, **Figure 6.13** implies a drier early and mid-summer in the 2013-2021 period, with some evidence of wetter conditions at the end of the summer rainy season south of the equator relative to the mean. Taken together with **Figure 6.12c**, **Figure 6.13** implies a stronger CAB with a wetter near-equatorial region north of the CAB and, further south, drier/hotter conditions over the ORB.

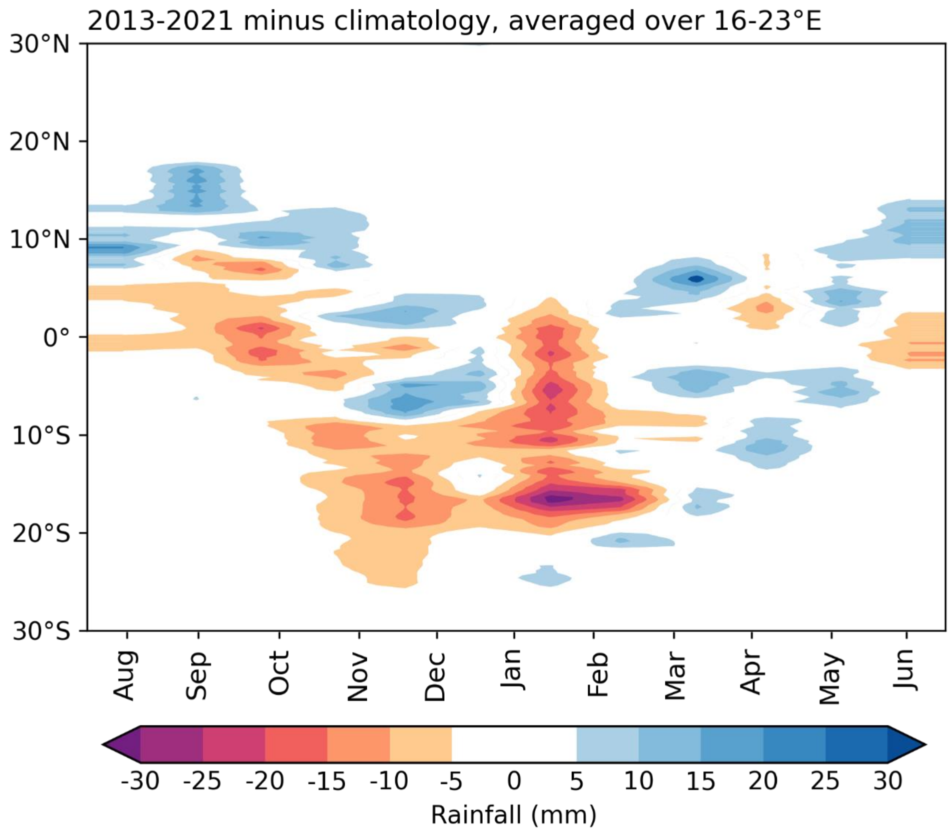

Figure 6.13 Monthly average of the African tropical rain-belt for the period 2013-2021 minus the climatology (1981-2021) shown in Figure 6.4.

SST anomalies during 2013-2021 relative to climatology (not shown) indicate significant cool anomalies in the southwest Indian Ocean which have previously been associated with reduced summer rainfall over southern Africa (Reason and Mulenga, 1999). Significant cool anomalies are also present in the subtropical South Atlantic, also previously associated with drier summers over southern Africa (Vigaud et al., 2009). Over the tropical Pacific and tropical Indian Oceans, relatively weak El Niño-like conditions are present in 2013-2021 relative to climatology. Typically, El Niño summers are dry over most of southern Africa (Lindesay, 1988; Nicholson and Kim, 1997; Reason et al. 2000; Reason and Jagadheesha, 2005; Blamey et al., 2018), hence are consistent with the drier and hotter conditions during the epoch. It is also known that decadal modulation of ENSO is important for decadal rainfall variability over southern Africa through atmospheric variability, but the decadal SST variability in the southwest Indian and southeast Atlantic Oceans also contributes to the rainfall variability by modulating the overlying atmosphere on a decadal timescale (Morioka et al., 2015; Dieppois et al., 2016, 2019).

6.4 Discussion and conclusions

This study has examined spatial mean patterns in dry spell frequencies and in 90th percentiles of maximum temperature, as well as relationships with the Botswana High and the African tropical rain-belt whose southern edge position is marked by the Congo Air Boundary (CAB; Howard and Washington, 2019). Howard and Washington (2019) found that as the CAB collapses in November/December, the moist Congo air is then able to penetrate farther poleward, resulting in the poleward shift of the maximum in tropical rainfall from the tropics into southern African subtropics. Consistent with this finding, the monthly progression of high dry spell frequencies has also been found to shift in a poleward direction, from October through until February/March. Additionally, the poleward shift in the monthly progression of high dry spell frequencies has been found to align with the Botswana High (Reason, 2016; Driver and Reason, 2017). This mid-level anticyclone, like the maximum in tropical rainfall, shifts poleward in spring so that by October, while it is centred over the northern half of the Okavango River Basin (ORB) and adjoining areas, the diagonal gradient of dry spells (Thoithi et al., 2021) is strong and located furthest east.

As the Botswana High continues with its poleward movement through until January/February, the meridional gradient of dry spells (Thoithi et al., 2021) in the Limpopo River valley becomes more and more prominent. At the same time, the area of greatest numbers of hot days over southern Africa shifts south from northern Namibia/northern

Botswana in October-November to the southern parts of these countries and the Northern Cape province (South Africa) in December-February, and thus in both seasons is located beneath the southern margins of the Botswana High. When the Botswana High retreats northward in March/April, high dry spell frequencies occur over most of southern Africa and are distributed roughly like in October/November, with again the area of greatest hot day numbers shifting back northwards. The alignment of the monthly evolution of dry spell frequencies with the African tropical rain-belt and Botswana High helps give insight into the evolution of rainfall through the summer half of the year over subtropical southern Africa. The alignment of regions of high numbers in hot days and dry spell gradients identifies areas that are prone to severe desiccation during the summer half of the year such as Ngamiland and the southern half of the ORB as well as the Limpopo River Basin. Staple crop farming (e.g., maize) in these parts of subtropical southern Africa is therefore more risky here than in most other areas.

Latitude-time plots over the longitudes of southern Africa bounding the north catchment and Ngamiland regions of the ORB show substantial interannual variability in the SPEI, Botswana High strength, and in frequencies of dry spells and hot days. The period during 2013-2021 stands out as one of particularly large negative anomalies in the SPEI, increased dry spell and hot day numbers and a stronger Botswana High, and hence drought conditions during the ON season, and to lesser extent in DJF. Such quasi-decadal variability has previously been noted in the Botswana High (Reason, 2019). A Cumulative Drought Intensity (CDI) metric, which combines the duration of the season's longest dry spell together with the anomaly in maximum temperature during that dry spell, also highlights the post-2013 period as being unusually severe. Thus, the ON 2013-2021 period was chosen as a case study for which it was found that the regional circulation anomalies were unfavourable for convection and cloud band development and instead conducive for hotter and drier conditions. These anomalies included a stronger and southward shifted Botswana High, a weaker Angola Low, and low-level divergence over most of subtropical southern Africa.

Correlations of the Botswana High or the Niño3.4 index with the SPEI and with the CDI derived for the north catchment and Ngamiland regions of the ORB indicate stronger relationships with the former variable than with ENSO. This result suggests that seasonal forecasting efforts over southern Africa may need to pay more attention to regional circulation features in addition to ENSO. Climate models should realistically simulate parameters such as geopotential heights to better predict regional circulation features such as the Botswana High and Angola Low. The ENSO-rainfall relationship over subtropical southern Africa is nonlinear with some strong El Niño events (e.g., 1997/98, 2009/10) not producing the expected summer drought. Evidence has been provided that these anomalous ENSO cases tend to be associated with regional circulation features (the Angola Low, the Botswana High) not being impacted to the same extent as during other ENSO events and thus the expected rainfall response is muted (Reason and Jagadheesha, 2005; Blamey et al., 2018; Driver et al., 2019). As already mentioned, the reason why these regional circulation features did not weaken during the 1997/98 and 2009/10 El Niño events could be related to the fact that ENSO impacts may be complicated by SST patterns in the neighbouring Indian and Atlantic Oceans, which may influence the circulation and rainfall patterns over southern Africa either independent of ENSO (Reason, 2001a; Washington and Preston, 2006), or both partially dependent on ENSO (Goddard and Graham, 1999; Hoell et al., 2015), and which may also oppose or reinforce ENSO impacts (Reason and Smart, 2015; Hoell et al., 2017).

On longer time scales, if the early summer drier and hotter conditions persist over the ORB, they are likely to adversely impact crops and livestock (Guilpart et al., 2017) as well as worsen surface water losses from sources like the ORB (Murray-Hudson et al., 2006). Thus, increased water shortages and dying out of sensitive ecosystems could occur. Climate models project a strong early summer drying over southern Africa (IPCC, 2021; Lazenby et al., 2018; Munday and Washington, 2019; Wainwright et al., 2021). Evident in the observational record are strong increasing trends in the number of hot days over almost all of southern Africa in ON as well in dry spell frequency although the latter are only significant over the southern part of the northern ORB region and parts of eastern South Africa (**Figure 6.14**). **Figure 6.15** suggests that these increasing trends in hot days may be related to the significant strengthening trend of the Botswana High during ON. There are also browning trends in NDVI over Ngamiland and parts of the northern ORB (not shown). These trends in hot day frequencies are consistent with the general warming trends found in other studies over southern Africa (Barros and Field, 2014; Engelbrecht et al., 2015; Maúre et al., 2018; Meque et al., 2022; Moses et al., 2022).

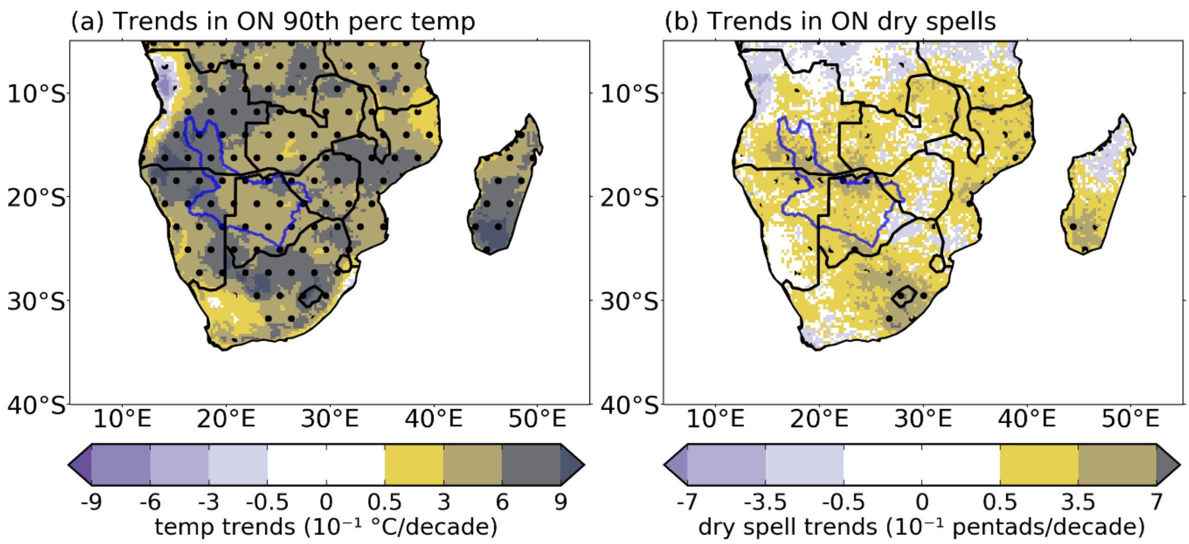

Figure 6.14 (a) Trends in 90th percentiles (perc) of maximum temperatures (temp) for ON, for the period 1981-2021 over southern Africa. (b) Trends in dry spell frequencies for ON. Stippling denotes areas with significant trends at $\alpha = 0.05$. The blue polygon is as in Figure 6.1.

Taken together with the climate model projections, these trends suggest that the early summer period may become increasingly challenging for agricultural and water management purposes over many parts of subtropical southern Africa. It may be suggested that seasonal forecasting efforts during the ON season, when the summer rains typically start, should also focus on regional circulation features such as the Botswana High since ENSO signals over southern Africa region are typically much weaker in early than in mid- or late summer.

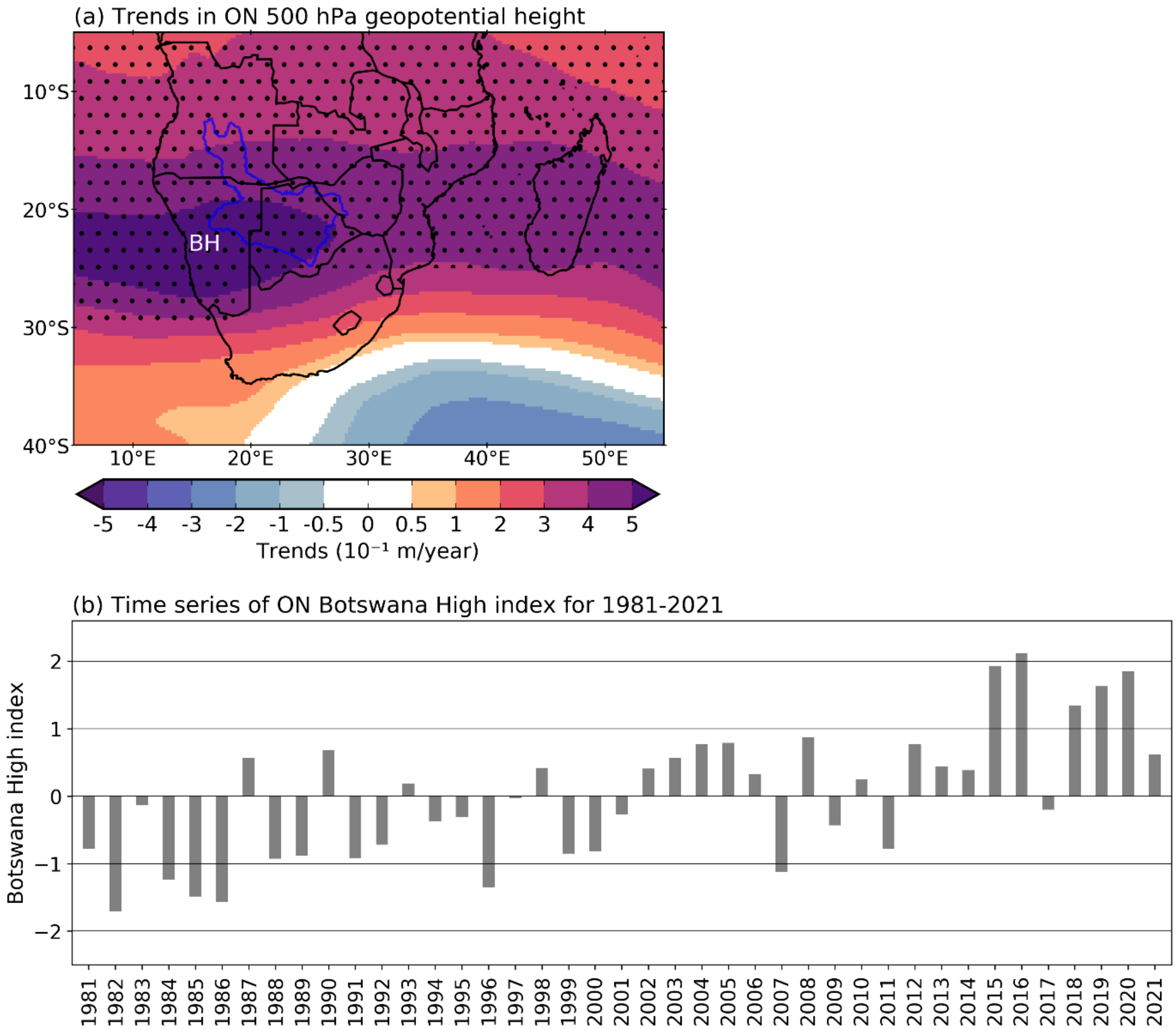

Figure 6.15 (a) Spatial trends in ON 500 hPa geopotential height for the period 1981-2021 showing trend in the Botswana High (BH). Stippling denotes areas with significant trends at $\alpha = 0.05$. The blue polygon is as in Figure 6.1. (b) ON time series of Botswana High index (defined in the text) for the period 1981-2021. Trend slope (trend line unshown) = 0.06 m/year, significant at $\alpha = 0.05$.

Chapter 7: Summary and conclusions

The main aim of the thesis has been firstly to better understand potential relationships among climate, Normalised Difference Vegetation Index (NDVI) and river discharge in the Okavango River Basin (ORB) region, their variability and trends (**Chapter 4**). Following that, the thesis has examined extreme rainfall events over the region (**Chapter 5**) and, at the other end of the spectrum, drought and extreme temperatures (**Chapter 6**). The thesis also aimed to better understand potential links of these variables with climate modes such as El Niño-Southern Oscillation (ENSO) and regional systems such as the Botswana High. Potential trends in the various rainfall and temperature metrics were also examined. The analysis focused on the extended summer (October-April), during which the region receives most of its rainfall.

The climate of the ORB and of subtropical southern Africa in general, is complex in the sense that it responds to several factors like ENSO in the tropical Pacific (e.g., Lindesay, 1988; Reason et al., 2000; Blamey et al., 2018; Hart et al., 2018) and regional systems like the Botswana High (Reason, 2016; Driver and Reason, 2017), hence it is not well understood. There is high spaciotemporal variability, with recurring climate extremes such as droughts, hot days and floods brought about by extreme rainfall events (e.g., Tyson, 1986; Reason et al., 2006; Meque et al., 2022). Influences of climate modes such as ENSO on these climate extremes have not been well studied over the ORB region, which may have been due to significant shortage of high-resolution observational data. The Botswana High has been found previously to have a relationship with dry spell frequencies over southern Africa (Driver and Reason, 2017), but this relationship has not been examined over the ORB region until now. Over this ORB region, it is thought that vegetation patterns are influenced by rainfall and hydrological conditions (Murray-Hudson et al., 2006; Revermann et al., 2016), but it is not well understood whether climate influences on vegetation in the wetter regions of the ORB in the north differ from those in the drier regions in the south. Warming trends (e.g., Maúre et al., 2018; Meque et al., 2022) and early summer drying (e.g., IPCC, 2021; Munday and Washington, 2019; Wainwright et al., 2021) found over southern Africa by previous studies may have adverse impacts on rain-fed subsistence farming, water availability and ecosystems, hence there was a need to assess these trends over particular regions of the subcontinent like the ORB.

To better understand relationships between climatic variables (rainfall, temperature), NDVI and river discharge over the ORB region, as well as relationships of these variables with climate modes and regional circulation systems, and trends in the variables, all these were examined in **Chapter 4** of the thesis. Given the size of the domain, for climate influences on NDVI, the study area was divided by 18.9°S latitude (L18) into a high rainfall zone north of L18 and a low rainfall zone south of L18, based on the mean rainfall maps.

Chapter 4 found pronounced interannual variability in rainfall and temperature, reflected in NDVI and river discharge. This variability compares well with other studies (e.g., Murray-Hudson et al., 2006; Hughes et al., 2011). Monthly lag correlations of rainfall with river discharge were incoherent, but for temperature-discharge, there were significant inverse correlations at 0 and 1-month lags. NDVI had significant positive 1-2-month lag correlations with rainfall over both south and north of L18, with generally stronger correlations over the former than over the latter region. Similarly, NDVI-temperature correlations were generally stronger over the area south than north of L18. The 1-2-month lag of the NDVI response to rainfall over the two regions compares well with the results of Nicholson and Farrar et al. (1994) obtained over Botswana. Stronger NDVI correlations south than north of L18 may be related to differences in vegetation type, with the latter region having a greater proportion of thicker woodland than that south of L18 where there is more grassland (e.g., Kgathi et al., 2006; Revermann et al., 2016). Grasslands are more sensitive to rainfall changes than woodlands (Erasmi et al., 2009), hence the stronger correlations south than north of L18. On seasonal scales, there were significant positive 1-season lag correlations between January-April (JFMA) rainfall and either May-September (MJJAS) NDVI or river discharge, reflecting that the latter two variables essentially respond to the previous season’s rainfall (MJJAS rainfall is minimal). Correlations of October-December (OND) rainfall with JFMA NDVI, and of OND rainfall and discharge, were also significant but weaker.

As found using correlation analysis, regression slopes between rainfall and NDVI were mainly significant over the area south but not north of L18, which is related to the more grasslands south of L18 being more sensitive to rainfall changes than the more woodlands north of L18. Overall, regression slopes showed that NDVI-rainfall and NDVI-temperature relationships are statistically different over the two regions. The sensitivity of NDVI to rainfall over the area south of L18 is consistent with other studies for semi-arid African regions where water availability is a constraint for vegetation growth (Malo and Nicholson, 1990; Farrar et al., 1994; Camberlin et al., 2007; Richard et al., 2008, 2012).

Significant correlations of climate modes [ENSO, subtropical Indian Ocean Dipole (SIOD)] and the Botswana High with NDVI, rainfall and temperature were found, but the Angola Low correlations were generally weak. The correlations of ENSO and the Botswana High with rainfall (temperature) were negative (positive), those for the SIOD were positive (negative), and the NDVI showed significant (negative) correlations mainly with ENSO. These correlations indicate the sensitivity of the ORB climate system to various climate modes which tend to be stronger in JFMA than in OND, reflecting the seasonal-phase locking of ENSO and the SIOD. Stronger ENSO-rainfall correlations in JFMA are consistent with other authors who found ENSO to impact strongly over southern Africa during the summer (Lindesay, 1988; Reason et al., 2000; Reason and Jagadsheesha, 2005). Correlations of the Southern Annular Mode (SAM) with NDVI, rainfall and temperature were found to be weak and no significant correlations were found between river discharge and the various climate modes.

Consistent with other studies over southern Africa that El Niño events do not always lead to severe droughts (Reason and Jagadheesha, 2005; Lyon and Mason, 2007; Blamey et al., 2018; Driver et al., 2019), it was found in **Chapter 4** that the 1987/1988 El Niño, not previously analysed, did not generate the expected drought conditions. Positive anomalies in low-level moisture flux convergence and SST in the tropical southeast Atlantic Ocean favoured wetter conditions over the ORB region in this summer rather than the expected El Niño drought. Other authors also found positive SST anomalies in the tropical southeast Atlantic to be associated with wetter conditions (e.g., Rouault et al., 2003; Reason and Smart, 2015).

The period 2006-2013 was found to be substantially wet and greener compared to the period 1999-2005 which was dry and browner. Unlike most studies focusing on these well-known quasi-decadal to decadal wet and dry spells of subtropical southern Africa climate (Tyson et al., 1975; Tyson, 1986; Wolski et al., 2012; Malherbe et al., 2014; Reason, 2016) during the mid or late summer rather than OND, in **Chapter 4**, the signal was stronger in OND, hence this season was chosen to analyse potential mechanisms associated with this signal. The wetter and greener OND 2006-2013 epoch was related to warmer SST in the tropical southeast Atlantic (as well as La Niña Modoki conditions), increased low-level moisture flux convergence and uplift over Angola and western Zambia relative to the preceding dry and browner 1999-2005 dry epoch.

Trend analysis in **Chapter 4** revealed significant greening trends in NDVI south of L18, particularly in summer, while north of L18, there was a strong browning trend in MJJAS. The greening trends are consistent with Wingate et al. (2019b) and Thoithi et al. (2021) who found significant greening trends over parts of Namibia and Botswana in December-February (DJF). Rainfall trends were significantly increasing over most of the area north of L18 in OND and over central Botswana while JFMA showed significant wetting over most of the area south of L18 and northwestern Namibia. These trends are consistent with New et al. (2006) who found an increase in average daily rainfall. Almost the entire region shows significant warming mainly in OND. This warming trend which is consistent with other studies over southern Africa and more broadly over Africa (Barros and Field, 2014; Engelbrecht et al., 2015; Maúre et al., 2018), may worsen water losses from the region with adverse impacts on vegetation growth including crops, water availability, ecosystems and tourism.

Chapter 5 analysed extreme rainfall events over the ORB. Since many rainfall events typically extend beyond river basin boundaries, a larger region was chosen to perform the analysis, i.e., a box in western central southern Africa (WCSA). Attention was also paid to extreme event spatial characteristics over two sections of the ORB. One was the north catchment, where most of the ORB streamflow is generated (e.g., Andersson et al., 2003; Wolski and Murray-Hudson, 2008), and the other was Ngamiland in northwestern Botswana which contains the world-famous Okavango Delta, where the streamflow terminates. Although the ORB streamflow is affected mainly by rainfall events that occur over the north catchment, contributions over the Delta itself can be substantial (Andersson et al., 2003; Wolski et al., 2006; M. Murray-Hudson, personal communication, 2022).

The analysis focused on extreme rainfall events accumulated over 1-day (DP1) and 3-day (DP3) periods. Extreme events accumulated over a 2-day period were very similar to the DP3 events, whereas those accumulated over 4-days or longer were rare and hence were not examined further. Focus was placed on JFMA since OND had a small number of DP1 and

DP3 (14 and 19, respectively) events within the top 200 events when the entire extended austral summer season was used, hence only results for JFMA are presented in **Chapter 5**.

It was found that the dominant synoptic weather type associated with most of the top 200 DP1 and DP3 (112 and 121, respectively) events in JFMA is the tropical-extratropical cloud band, consistent with other studies for summer rainfall over southern Africa (e.g., Washington and Todd, 1999; Hart et al., 2010, 2013, 2018). Tropical lows (Howard et al., 2019) also make a large contribution (86 and 74 for DP1 and DP3, respectively, out of the top 200). For DP3, there were a few cases (3) where cloud bands and tropical lows made a joint contribution. Mesoscale convective systems (MCSs) only make a small contribution to the top 200 events. Contribution of MCSs may be underestimated since often they are embedded within other systems like cloud bands, and they tend to be shorter-lived than cloud bands or tropical lows (Blamey and Reason, 2013; Rapolaki et al., 2019). One DP1 event out of the top 200 resulted from a cut-off low on 22 April, consistent with other authors that these weather systems can also lead to large rainfall amounts over a short period of time mainly in autumn and spring (Singleton and Reason, 2006, 2007).

DP1 frequency shows a significant upward trend consistent with the IPCC (2013) and (2021) assessments that the frequency and intensity of extreme rainfall events are likely to increase due to global warming. If this trend persists, it may increase the tendency for flooding with associated crop and livestock losses. Daily rainfall totals and rain-days receiving >1 mm and >10 mm also show significant increasing trends over the southern half of the WCSA and adjoining areas in Namibia, South Africa, Zimbabwe and Zambia. This implies that the meridional rainfall gradient from Botswana to Zambia may weaken and that the edge of the tropical rain-belt over northern Botswana may weaken. These trends are consistent with trends in wet days of 10-30 mm/day in DJF (Thoithi et al., 2021) and with an increase in average daily rainfall (New et al., 2006).

DP1 and DP3 events show large interannual variability in their frequencies as well as in their percentage contributions to JFMA seasonal rainfall totals. On average, their contributions are ~ 10% and ~17%, respectively, but in some seasons can be more than 30% over the WCSA, implying that they make considerable contributions to water resources. However, as mentioned above, these events may cause local flooding as well as significant damage to crops and human settlements. Correlations of rainfall totals with DP1 and DP3 events are significantly positive and stronger over Ngamiland than over the north catchment, suggesting that extreme rainfall events are more important to rainfall totals over the former region than over the latter region.

Consistent with **Chapter 4** and other studies over southern Africa (Lindesay, 1988; Reason et al., 2000; Driver and Reason, 2017) that ENSO impacts strongly on rainfall totals during summer, in **Chapter 5**, this climate mode was found to also impact strongly (significantly positive) on frequencies/intensities of DP1 and DP3 events during JFMA. El Niño (La Niña) events were found to typically lead to less (more) intense DP1/3 events, and to also lead to low (high) frequency of these DP1/3 events. Similarly, as found in **Chapter 4** that the Botswana High impacts strongly on summer rainfall totals, in **Chapter 5**, it was found to also impact strongly (significantly negative) on JFMA extreme event characteristics. This is because typically, this circulation system moves south and strengthens during the summer, leading to less regional subsidence when it is weaker than average and allows more favourable conditions for convection (Reason, 2016; Driver and Reason, 2017). Other climate modes (SIOD, SAM, Benguela Niño) as well as the Angola Low, were found to not have strong relationships with DP1 and DP3 characteristics.

A case study was conducted in **Chapter 5** to better understand contributions of DP1 and DP3 events as well as large-scale circulation anomalies, to the severe flooding that caused substantial damage to crops and settlements in JFMA 2017 over Ngamiland district which contains the world-famous Okavango Delta. JFMA 2017 was of interest because it was ENSO-neutral, and the flooding occurred over Ngamiland but not over the north catchment where most of the ORB streamflow is generated as mentioned above, which experienced well below average rainfall.

The case study indicated that JFMA 2017 experienced the largest number of DP3 events in the WCSA box, i.e., 10 in total in this season alone, of which 8 had their heavy rainfall over Ngamiland. During the same season, 8 of the 9 DP1 events had their heavy rainfall over Ngamiland as well. The number of rain-days receiving >10 mm was more than double the average. For circulation anomalies, during the period 1 January – 8 March 2017, the Angola Low was anomalously strong. Since this low acts as the tropical source for the tropical-extratropical cloud bands associated with most of the summer rainfall in the region (Cook et al., 2004; Hart et al., 2010, 2013, 2018), it is not surprising that these cloud bands caused many of the DP1 and DP3 events during JFMA 2017. Other circulation anomalies that contributed to these floods include a weaker than usual Botswana High, increased uplift over most of the WCSA, and strongly positive SST anomalies in the southwest Indian Ocean, which previously were linked with above average summer rainfall over many parts of southern Africa (e.g., Reason and Mulenga, 1999; Behera and Yamagata, 2001; Reason, 2001a).

Chapter 6 analysed drought metrics and temperature extremes over the ORB region as well as their links with regional systems such as the Botswana High, to better understand droughts in this region. The poleward shift in the monthly progression of high dry spell frequencies from October through until February/March was found to align with the poleward shift in the monthly progression of the Congo Air Boundary (CAB). The CAB shifts poleward from August and it eventually breaks down in November/December (Howard and Washington, 2019). These authors found that as long as the CAB has not broken down, it hinders the moist Congo air associated with the maximum in tropical rainfall from penetrating further poleward into the southern African subtropics. The poleward shift in the monthly progression of high dry spell frequencies was also found to align with the Botswana High (Reason, 2016; Driver and Reason, 2017). Like the maximum in tropical rainfall, the Botswana High shifts poleward in spring so that by October, while it is centred over the northern half of the ORB and adjoining areas, the diagonal gradient of dry spells (Thoithi et al., 2021) is strong and located furthest east. The Botswana High continues to shift poleward until January/February, as do the areas of greatest numbers of dry spells and hot days. When the Botswana High retreats northward in March/April, the area of greatest numbers of dry spells and hot days also retreats equatorwards.

The alignment of the monthly evolution of dry spell frequencies with the African tropical rain-belt and Botswana High in **Chapter 6**, not previously considered in the literature, helps provide insight into the evolution of rainfall through the extended summer over subtropical southern Africa. The alignment of regions of high numbers in hot days and dry spell gradients identifies areas that are susceptible to severe desiccation such as Ngamiland and the southern half of the ORB as well as the Limpopo River Basin. In these parts of subtropical southern Africa, commonly produced crops such as maize may perform more poorly than in most other areas.

Standardised Precipitation-Evapotranspiration Index (SPEI), Botswana High strength, dry spell and hot day frequencies exhibit substantial interannual variability over the ORB. The 2013-2021 period in **Chapter 6** (a sharp decrease in OND rainfall after 2013 is also evident in **Chapter 4**, **Figure 4.6a**) stands out as one of particularly large negative anomalies in SPEI, increased hot day and dry spell numbers and a stronger Botswana High, and hence drought conditions particularly during October-November (ON). The Cumulative Drought Intensity (CDI) metric, derived from maximum temperature anomaly and maximum dry spell duration, also highlights the post-2013 period as being unusually severe. NDVI shows browning trends during this period over Ngamiland and parts of the northern ORB, also reflecting the drought conditions. A case study of the ON 2013-2021 period revealed that regional circulation anomalies were conducive for hotter and drier conditions but not for convection and cloud band development. Some of these anomalies were a stronger and southward shifted Botswana High, low-level divergence over most of subtropical southern Africa, and a weaker Angola Low.

Correlations of the Botswana High or the Niño3.4 index with the SPEI (negative correlations) and with the CDI (positive correlations) over the ORB indicate stronger relationships with the former variable than with ENSO, suggesting that seasonal forecasting efforts over southern Africa should not only pay attention to ENSO but also to regional circulation features. Over this region, the ENSO-rainfall relationship is not linear with some strong El Niño events (e.g., 1997/98, 2009/10) not producing the anticipated summer drought (e.g., Reason and Jagadheesha, 2005; Lyon and Mason, 2007; Blamey et al., 2018; Driver et al., 2019). These papers as well as the results presented in this thesis point to the need to better understand the roles that regional circulation features like the Botswana High and the Angola Low play in influencing southern African rainfall during different ENSO events.

Regarding trends in the region, if the early summer drier and hotter conditions that have been found over the ORB persist, they are likely to negatively impact subsistence farming (Guilpart et al., 2017), increase water shortages and dying out of sensitive ecosystems (Murray-Hudson et al., 2006). The observational record also shows strong increasing trends in the number of hot days over most of southern Africa in ON, and in dry spell frequency although the latter are only significant over the southern part of the northern ORB region and parts of eastern South Africa. These trends suggest that the early summer period may become increasingly challenging for agricultural and water management purposes over many parts of subtropical southern Africa. **Chapter 6** provided evidence that upward trends in hot days may be related to the significant strengthening trend of the Botswana High during ON. These increasing trends in ON hot day frequencies are consistent with the general warming trend in OND over the ORB region found in **Chapter 4** and with the general warming trend found in other studies over southern Africa (Engelbrecht et al., 2015; Maúre et al., 2018; Meque et al., 2022). Similarly, the increasing trends in dry spell frequencies are consistent with climate model projections of a strong early summer drying over southern Africa (IPCC, 2021; Munday and Washington, 2019; Wainwright et al., 2021).

This thesis has helped improve understanding of the climate of the ORB region, its climate variability and trends. A particular focus has been placed on climate extremes over the region (droughts, hot days and extreme rainfall events) and their relationships with climate modes and regional circulation systems. Given the vulnerability of the region and the reliance of the local population on rain-fed agriculture, the results of the thesis may help with the management of water resources, agricultural activities and the highly biodiverse ecosystems, as well as for assessing how the region may respond to a globally warming climate. The results may also be useful for seasonal forecasting. For instance, seasonal forecasting efforts during the ON season, when the summer rains typically start, should also pay attention to regional circulation features such as the Botswana High since over southern Africa, ENSO signals are typically much weaker in early than in mid- or late summer. An important aspect not considered in this thesis, both from a seasonal forecasting perspective and for climate prediction, is the ability of climate models to adequately represent the climate of the ORB region. Although literature exists on the ability of CMIP models to capture important features such as the Angola Low (Munday and Washington, 2017) or cloud bands over southern Africa (James et al., 2020), these models do not have enough resolutions to simulate the local temperature and rainfall over the ORB region. There is need of the dynamical and statistical downscaling models in which the seasonal hindcast and prediction or future projection by CMIP models are used as boundary conditions and downscaled over the ORB region, in light of the trends in rainfall and temperature as well as in dry spell frequencies and the Botswana High found in this thesis. Except for a few studies such as Wolski (2009) who used a satellite rainfall product to downscale ten global circulation models, not much work has been done using downscaling techniques to study temperature and rainfall variations over the ORB region.

References

Allan, R.J., Reason, C.J.C., Lindesay, J.A., Ansell, T.J., 2003. Protracted'ENSO episodes and their impacts in the Indian Ocean region. *Deep Sea Res. Part II Top. Stud. Oceanogr., 50(12–13)*, 2331-2347.

Amaya, D.J., DeFlorio, M.J., Miller, A.J., Xie, S.P., 2017. WES feedback and the Atlantic meridional mode: Observations and CMIP5 comparisons. *Clim. Dyn., 49*, 1665-1679.

Andersson, L., Gumbricht, T., Hughes, D., Kniveton, D., Ringrose, S., Savenije, H., Todd, M, Wilk, J., Wolski, P., 2003. Water flow dynamics in the Okavango River Basin and Delta: a pre–requisite for the ecosystems of the Delta. *Phys. Chem. Earth., 28,* 1165-1172.

Andersson, L., Wilk, J., Todd, M.C., Hughes, D.A., Earle, A., Kniveton, D., Layberry, R., Savenije, H.H., 2006. Impact of climate change and development scenarios on flow patterns in the Okavango River. *J. Hydrol., 331(1-2)*, 43-57.

Ashok, K., Yamagata, T., 2009. The El Niño with a difference. *Nature, 461(7263)*, 481-484.

Ashok, K., Behera, S.K., Rao, S.A., Weng, H., Yamagata, T., 2007. El Niño Modoki and its possible teleconnection. *J. Geophys. Res., 112, C11007.* doi:10.1029/2006JC003798.

Barimalala, R., Desbiolles, F., Blamey, R.C., Reason, C.J.C., 2018. Madagascar influence on the South Indian Ocean convergence zone, the Mozambique Channel Trough and southern African rainfall. *Geophys. Res. Lett., 45(20)*, 11-380.

Barimalala, R., Blamey, R.C., Desbiolles, F., Reason, C.J.C., 2020. Variability in the Mozambique Channel Trough and impacts on southeast African rainfall. *J. Clim., 33(2)*, 749-765.

Barros, V.R., Field, C.B., 2014. Climate change 2014–Impacts, adaptation and vulnerability: Regional aspects. Cambridge University Press.

Behera, S.K., Yamagata, T., 2001. Subtropical SST dipole events in the Southern Indian Ocean. *Geophys. Res. Lett., 28(2),* 327-330.

Blamey, R.C., Reason, C.J.C., 2009. Numerical simulation of a mesoscale convective system over the east coast of South Africa. *Tellus A: Dyn. Meteorol. Oceanogr., 61(1),* 17-34.

Blamey, R.C., Reason, C.J.C., 2012. Mesoscale convective complexes over southern Africa. *J. Clim., 25(2),* 753-766.

Blamey, R.C., Reason, C.J.C., 2013. The role of mesoscale convective complexes in southern Africa summer rainfall. *J. Clim., 26(5),* 1654-1668.

Blamey, R.C., Middleton, C., Lennard, C., Reason, C.J.C., 2017. A climatology of potential severe convective environments across South Africa. *Clim. Dyn., 49(5),* 2161-2178.

Blamey, R.C., Kolusu, S.R., Mahlalela, P., Todd, M.C., Reason, C.J.C., 2018. The role of regional circulation features in regulating El Niño climate impacts over southern Africa: A comparison of the 2015/2016 drought with previous events. *Int. J. Climatol., 38(11),* 4276-4295.

Boschat, G., Terray, P., Masson, S., 2013. Extratropical forcing of ENSO. *Geophys. Res. Lett., 40(8),* 1605-1611.

Bouvet, A., Mermoz, S., Le Toan, T., Villard, L., Mathieu, R., Naidoo, L., Asner, G.P., 2018. An above-ground biomass map of African savannahs and woodlands at 25 m resolution derived from ALOS PALSAR. *Remote Sens. Environ., 206,* 156-173.

Byakatonda, J., Parida, B.P., Moalafhi, D.B., Kenabatho, P.K., Lesolle, D., 2020. Investigating relationship between drought severity in Botswana and ENSO. *Nat. Hazards, 100(1),* 255-278.

Camberlin, P., Martiny, N., Philippon, N. and Richard, Y., 2007. Determinants of the interannual relationships between remote sensed photosynthetic activity and rainfall in tropical Africa. *Remote Sens. Environ., 106(2),* 199-216.

Chiang JC, Vimont DJ (2004) Analogous Pacific and Atlantic meridional modes of tropical atmosphere-ocean variability. *J. Clim., 17*, 4143-4158.

Chu, H., Venevsky, S., Wu, C., Wang, M., 2019. NDVI-based vegetation dynamics and its response to climate changes at Amur-Heilongjiang River Basin from 1982 to 2015. *Sci. Total Environ., 650*, 2051-2062.

Conway, D., Van Garderen, E.A., Deryng, D., Dorling, S., Krueger, T., Landman, W., Lankford, B., Lebek, K., Osborn, T., Ringler, C., Thurlow, J., 2015. Climate and southern Africa's water–energy–food nexus. *Nat. Climate Change, 5(9)*, 837-846.

Cook, K.H., 1998, October. On the response of the Southern Hemisphere to ENSO. In Proc 23rd Climate Diagnostics and Prediction Workshop (323-326). Miami, FL: American Meteorological Society.

Cook, K., 2000. The South Indian convergence zone and interannual rainfall variability over southern Africa. *J. Clim. 13(21)*, 3789-3804.

Cook, K., 2001. A Southern Hemisphere wave response to ENSO with implications for southern Africa precipitation. *J. Atmos. Sci., 58(15)*, 2146-2162.

Cook, C., Reason, C.J.C., Hewitson, B.C., 2004. Wet and dry spells within particularly wet and dry summers in the South African summer rainfall region. *Clim. Res., 26(1)*, 17-31.

Copernicus Climate Change Service, 2017. ERA5: Fifth generation of ECMWF atmospheric reanalyses of the global climate. Copernicus Climate Change Service Climate Data Store (CDS). Available: https://cds.climate.copernicus.eu [2022, November 20).

Crétat, J., Pohl, B., Dieppois, B., Berthou, S., Pergaud, J., 2018. The Angola Low: relationship with southern African rainfall and ENSO. *Clim. Dyn., 52(3-4)*, 1783-1803.

Crimp, S.J., Lutjeharms, J.R.E., Mason, S.J., 1998. Sensitivity of a tropical-temperate trough to sea-surface temperature anomalies in the Agulhas retroflection region. *Water SA, 24,* 93-100.

Curran, P.J., 1983. Multispectral remote sensing for the estimation of green leaf area index. Philos. Trans. R. Soc. Lond. Ser. Math. Phys. Sci., 309(1508), 257-270.

D'Abreton, P.C., Tyson, P.D., 1995. Divergent and non-divergent water vapour transport over southern Africa during wet and dry conditions. *Meteorol. Atmos. Phys., 55(1)*, 47-59.

Davenport, M.L., Nicholson, S.E., 1993. On the relationship between rainfall and the Normalized Difference Vegetation Index for diverse vegetation types of East Africa. *Int. J. Remote Sens., 14*, 2369-2389.

Dieppois, B., Pohl, B., Rouault, M., New, M., Lawler, D., Keenlyside, N., 2016. Interannual to interdecadal variability of winter and summer southern African rainfall, and their teleconnections. *Geophys. Res. Atm., 121(11)*, 6215-6239.

Dieppois, B., Pohl, B., Crétat, J., Eden, J., Sidibe, M., New, M., Rouault, M., Lawler, D., 2019. Southern African summer-rainfall variability, and its teleconnections, on interannual to interdecadal timescales in CMIP5 models. *Clim. Dyn., 53*, 3505-3527.

Driver, P., Reason, C.J.C., 2017. Variability in the Botswana High and its relationships with rainfall and temperature characteristics over southern Africa. *Int. J. Climatol., 37,* 570-581.

Driver, P., Abiodun, B., Reason, C.J.C., 2019. Modelling the precipitation response over southern Africa to the 2009–2010 El Niño using a stretched grid global atmospheric model. *Clim. Dyn., 52(7-8),* 3929-3949.

Dunning, C.M., Black, E.C., Allan, R.P., 2016. The onset and cessation of seasonal rainfall over Africa. *J. Geophys. Res., 121*, 11405-11424.

Dyson, L., 2015. A heavy rainfall sounding climatology over Gauteng South Africa, using self-organising maps. *Clim. Dyn., 45*, 3051-3065.

Dyson, L.L., van Heerden, J., 2001. The heavy rainfall and floods over the northeastern interior of South Africa during February 2000. *S. Afr. J. Sci., 97*, 80-86.

Dyson, L.L., Van Heerden, J., Sumner, P.D., 2015. A baseline climatology of sounding-derived parameters associated with heavy rainfall over Gauteng, South Africa. *Int. J. Climatol., 35(1)*, 114-127.

Edossa, D.C., Woyessa, Y.E., Welderufael, W.A., 2014. Analysis of droughts in the central region of South Africa and their association with SST anomalies. *Int. J. Atmos. Sci.* http://dx.doi.org/10.1155/2014/508953.

Ellery, W.N., McCarthy, T.S., Smith, N.D., 2003. Vegetation, hydrology, and sedimentation patterns on the major distributary system of the Okavango Fan, Botswana. *Wetlands, 23(2)*, 357-375.

Engelbrecht, C.J., Landman, W.A., Engelbrecht F.A., Malherbe, J., 2015. A synoptic decomposition of rainfall over the Cape south coast of South Africa. *Clim. Dyn., 44*, 2589-2607.

Engelbrecht, F., Adegoke, J., Bopape, M.J., Naidoo, M., Garland, R., Thatcher, M., McGregor, J., Katzfey, J., Werner, M., Ichoku, C., Gatebe, C., 2015. Projections of rapidly rising surface temperatures over Africa under low mitigation. *Environ. Res. Lett., 10(8)*, 085004.

Erasmi, S., Propastin, P., Kappas, M., Panferov, O., 2009. Spatial patterns of NDVI variation over Indonesia and their relationship to ENSO warm events during the period 1982-2006. *J. Clim., 22(24)*, 6612-6623.

Eyring, V., Bony, S., Meehl, G.A., Senior, C.A., Stevens, B., Stouffer, R.J., Taylor, K.E., 2016. Overview of the Coupled Model Intercomparison Project Phase 6 (CMIP6) experimental design and organization. *Geosci. Model Dev., 9(5)*, 1937-1958.

Fan, Y., Van den Dool, H., 2008. A global monthly land surface air temperature analysis for 1948–present. *J. Geophys. Res. Atmos.*, *113(D1).* doi:10.1029/2007JD008470.

Farrar, T.J., Nicholson, S.E., Lare, A.R., 1994. The influence of soil type on the relationships between NDVI, rainfall, and soil moisture in semiarid Botswana. II. NDVI response to soil moisture. *Remote Sens. Environ.*, *50(2)*, 121-133.

Fauchereau, N., Pohl, B., Reason, C.J.C., Rouault, M., Richard, Y., 2009. Recurrent daily OLR patterns in the Southern Africa/Southwest Indian Ocean region, implications for South African rainfall and teleconnections. *Clim. Dyn.*, *32*, 575-591.

Favre, A., Hewitson, B., Tadross, M., Lennard, C., Cerezo-Mota, R., 2012. Relationships between cut-off lows and the semiannual and southern oscillations. *Clim. Dyn.*, *38*, 1473-1487.

Favre, A., Hewitson, B., Lennard, C., Cerezo-Mota, R., Tadross, M., 2013. Cut-off Lows in the South Africa region and their contribution to precipitation. *Clim. Dyn.*, *41*, 2331-2351.

Feng, J., Chen, W., Tam, C.-Y., Zhou, W., 2010. Difference impacts of El Niño and El Niño Modoki on China rainfall in the decaying phases. *Int. J. Climatol.*, *31*, 2091-2101.

Fitchett, J.M., Grab, S.W., 2014. A 66-year tropical cyclone record for south-east Africa: temporal trends in a global context. *Int. J. Climatol.*, *34*, 3604-3615.

Florenchie, P., Reason. C.J.C., Lutjeharms, J.R.E., Rouault, M., Roy, C., Masson, S., 2004. Evolution of interannual warm and cold events in the southeast Atlantic Ocean. *J. Clim.*, *17*, 2318-2334.

Francis, R., Bino, G., Inman, V., Brandis, K., Kingsford, R.T., 2021. The Okavango Delta's waterbirds–Trends and threatening processes. *Glob. Ecol. Conserv.*, *30*, e01763.

Frost, P., 1996. The ecology of miombo woodlands. The miombo in transition: woodlands and welfare in Africa. Bogor: CFIOR.

Funk, C., Peterson, P., Landsfeld, M., Pedreros, D., Verdin, J., Shukla, S., Husak, G, Rowland, J., Harisson, L., Hoell, A., Michaelson, J., 2015. The climate hazards infrared precipitation with stations a new environmental record for monitoring extremes. *Sci. Data, 2(1),* 1-21.

Gillett, N.P., Kell, T.D., Jones, P.D., 2006. Regional climate impacts of the Southern Annular Mode. *Geophys Res Lett, 33(23).*

Giorgi, F., Jones, C., Asrar, G.R., 2009. Addressing climate information needs at the regional level: The CORDEX framework. *WMO Bull., 58*, 175-183.

Goddard, L., Graham, N.E., 1999. Importance of the Indian Ocean for simulating rainfall anomalies over eastern and southern Africa. *J. Geophys. Res., 104*, 19099-19116.

Gondwe, M.P., Jury, M.R., 1997. Sensitivity of vegetation (NDVI) to climate over southern Africa: Relationships with summer rainfall and OLR. *South Afr. Geogr. J., 79(1)*, 52-60.

Gong, D., Wang, S., 1999. Definition of Antarctic oscillation index. *Geophys. Res. Lett., 26(4)*, 459-462.

Good, S.P., Caylor, K.K., 2011. Climatological determinants of woody cover in Africa. *PNAS, 108(12)*, 4902-4907.

Guilpart, N., Grassini, P., Van Wart, J., Yang, H., Van Ittersum, M.K., Van Bussel, L.G., Wolf, J., Claessens, L., Leenaars, J.G., Cassman, K.G., 2017. Rooting for food security in Sub-Saharan Africa. Environ. *Res. Lett., 12(11),* https://doi.org/10.1088/1748-9326/aa9003.

Gumbricht, T., Wolski, P., Frost, P., McCarthy, T.S., 2004. Forecasting the spatial extent of the annual flood in the Okavango Delta, Botswana. *J. Hydrol., 290(3-4),* 178-191.

Hall, A., Visbeck, M., 2001. Ocean and Sea Ice response to the Southern Hemisphere Annular Mode: Results from a coupled climate model. *Clivar Exchanges, 22*, 4-6.

Hamed, K.H., Rao, A.R., 1998. A modified Mann–Kendall trend test for autocorrelated data. *J. Hydrol., 204(1-4)*, 182-196.

Hammond, J.L., 2011. The resource curse and oil revenues in Angola and Venezuela. *Sci. Soc., 75*, 348–378.

Hansingo, K., Reason, C.J.C., 2009. Modelling the atmospheric response over southern Africa to SST forcing in the southeast tropical Atlantic and southwest subtropical Indian Oceans. *Int. J. Climatol., 29(7)*, 1001-1012.

Harrison, M.S.J., 1984. A generalized classification of South African summer rain-bearing synoptic systems. *J. Climatol., 4(5)*, 547-560.

Harrison, M.S.J., 1986. A synoptic climatology of South African rainfall variations. Ph.D. Thesis. University of the Witwatersrand.

Hart, R.E., Grumm, R.H., 2001. Using normalized climatological anomalies to rank synoptic-scale events objectively. *Mon. Weather Rev., 129*, 2426-2442.

Hart, N.C.G., Reason, C.J.C., Fauchereau, N., 2010. Tropical–extra tropical interactions over southern Africa: three cases of heavy summer season rainfall. *Mon. Weather Rev., 138*, 2608-2623.

Hart, N.C.G., Reason, C.J.C., Fauchereau, N., 2012. Building a Tropical-Extratropical Cloud Band Metbot. *Mon. Wea. Rev., 140*, 4005-4016.

Hart, N.C., Reason, C.J.C., Fauchereau, N., 2013. Cloud bands over southern Africa: Seasonality, contribution to rainfall variability and modulation by the MJO. *Clim. Dyn., 41(5)*, 1199-1212.

Hart, N.C., Washington, R., Reason, C.J.C, 2018. On the likelihood of tropical-extratropical cloud bands in the south Indian convergence zone during ENSO events. *J. Clim., 31(7)*, 2797-2817.

Heerden, J.V., Taljaard, J.J., 1998. Africa and surrounding waters. In Meteorology of the southern hemisphere (141-174). Boston: Amer. Meteor. Soc.

Hermes, J.C., Reason, C.J.C., 2005. Ocean model diagnosis of interannual coevolving SST variability in the South Indian and South Atlantic Oceans. *J. Clim., 18(15)*, 2864-2882.

Hersbach, H., Bell, B., Berrisford, P., Hirahara, S., Horányi, A., Muñoz-Sabater, J., Nicolas, J., Peubey, C., Radu, R., Schepers, D., Simmons, A., 2020. The ERA5 global reanalysis. *Q. J. R. Meteorol. Soc., 146(730)*, 1999-2049.

Hirst, A. C., Hastenrath, S., 1983. Atmosphere ocean mechanisms of climate anomalies in the Angola-tropical Atlantic sector. *J. Rhys. Oceanogr., 13*, 1146-1157.

Hobday, A.J., Alexander, L.V., Perkins, S.E., Smale, D.A., Straub, S.C., Oliver, E.C., Benthuysen, J.A., Burrows, M.T., Donat, M.G., Feng, M., Holbrook, N.J., 2016. A hierarchical approach to defining marine heatwaves. *Prog. Oceanogr., 141*, 227-238.

Hoell, A., Funk, C., Magadzire, T., Zinke, J., Husak, G., 2015. El Niño-Southern Oscillation diversity and southern Africa teleconnections during austral summer. *Clim. Dyn., 45*, 1583-1599.

Hoell, A., Funk, C., Zinke, J., Harrison, L., 2017. Modulation of the Southern Africa precipitation response to the El Niño Southern Oscillation by the subtropical Indian Ocean Dipole. *Clim. Dyn., 48*, 2529-2540.

Hourdin, F.I., Musat, I., Bony, S., Braconnot, P., Codron, F., Dufresne, J-L., et al., 2006. The LMDZ4 general circulation model: Climate performance and sensitivity to parameterized physics with emphasis on tropical convection. *Clim. Dyn., 27(7-8)*, 787-813.

Howard, E., Washington, R., 2018. Characterizing the synoptic expression of the Angola Low. *J. Clim., 31(9)*, 7147-7166.

Howard, E., Washington, R., 2019. Drylines in Southern Africa: Rediscovering the Congo Air Boundary. *J. Clim., 32(23)*, 8223-8242.

Howard, E., Washington, R., 2020. Tracing future spring and summer drying in southern Africa to tropical lows and the Congo Air Boundary. *J. Clim., 33(14),* 6205-6228.

Howard, E., Washington, R., Hodges, K.I., 2019. Tropical lows in southern Africa: Tracks, rainfall contributions, and the role of ENSO. *J. Geophys. Res. Atmos., 124(21),* 11009-11032.

Huang, B., Liu, C., Banzon, V., Freeman, E., Graham, G., Hankins, B., Smith, T., Zhang, H.M., 2021. Improvements of the daily optimum interpolation sea surface temperature (DOISST) version 2.1. *J. Clim., 34(8)*, 2923-2939.

Huang, B., Thorne, P.W., Banzon, V.F., Boyer, T., Chepurin, G., Lawrimore, J.H., Menne, M.J., Smith, T.M., Vose, R.S., Zhang, H.M., 2017. Extended reconstructed sea surface temperature, version 5 (ERSSTv5): upgrades, validations, and intercomparisons. *J. Clim., 30(20)*, 8179-8205.

Huffman, G.J., Bolvin, D.T., Nelkin, E.J., Wolff, D.B., Adler, R.F., Gu, G., Hong, Y., Bowman, K.P., Stocker, E.F., 2007. The TRMM Multisatellite Precipitation Analysis (TMPA): Quasi-global, multiyear, combined-sensor precipitation estimates at fine scales. *J. Hydrometeorol., 8(1)*, 38-55.

Hughes, D.A., Kingston, D.G., Todd, M.C., 2011. Uncertainty in water resources availability in the Okavango River basin as a result of climate change. *Hydrol. Earth Syst. Sci., 15(3),* 931-941.

Hunt, K.M.R., Fletcher, J.K., 2019. The relationship between Indian monsoon rainfall and low-pressure systems. *Clim. Dyn., 53*, 1859-1871.

IPCC, 2013. Climate Change 2013: The Physical Science Basis. T.F. Stocker et al., Eds., Cambridge University Press.

IPCC, 2021. Climate Change 2021: The Physical Science Basis. V. Masson-Delmotte et al., Eds., Cambridge University Press.

James, R., Hart, N.C., Munday, C., Reason, C.J., Washington, R., 2020. Coupled climate model simulation of tropical–extratropical cloud bands over southern Africa. *J. Clim., 33(19),* 8579-8602.

Jones, P.D., Lister, D.H., Osborn, T.J., Harpham, C., Salmon, M., Morice, C.P., 2012. Hemispheric and large-scale land-surface air temperature variations: An extensive revision and an update to 2010. *J. Geophys. Res. Atmos., 117(D5).*

Jury, M.R., 2010. Climate and weather factors modulating river flows in southern Angola. *Int. J. Climatol., 30(6),* 901-908.

Jury, M.R., 2013. Climate trends in southern Africa. *S. Afr. J. Sci., 109(1),* 1-11.

Jury, M.R., Valentine, H.R., Lutjeharms, J.R.E., 1993. Influence of the Agulhas Current on summer rainfall on the southeast coast of South Africa. *J. Appl. Meteorol., 32,* 1282-1287.

Kalnay, E., Kanamitsu, M., Kistler, R., Collins, W., Deaven, D., Gandin, L., Iredell, M., Saha, S., White, G., Woollen, J., Zhu, Y., 1996. The NCEP/NCAR 40–year reanalysis project. *Bull. Am. Meteorol. Soc.*, 437-472.

Kanamitsu, M., Ebisuzaki, W., Woollen, J., Yang, S.K., Hnilo, J.J., Fiorino, M., Potter, G.L., 2002. Ncep–doe amip-ii reanalysis (r-2). *Bull. Am. Meteorol. Soc., 83(11),* 1631-1644.

Kao, H.Y., Yu, J.Y., 2009. Contrasting eastern-Pacific and central-Pacific types of ENSO. *J. Clim., 22,* 615-632.

Karypidou, M.C., Katragkou, E., Sobolowski, S.P., 2021. Precipitation over southern Africa: Is there consensus among GCMs, RCMs and observational data?. *Geosci. Model Dev. Discuss.*, 1-25.

Kendall, M.G., 1975. Rank correlation methods. London: Charles Griffin.

Kgathi, D.L., Kniveton, D., Ringrose, S., Turton, A.R., Vanderpost, C.H., Lundqvist, J., Seely, M., 2006. The Okavango; a river supporting its people, environment and economic development. *J. Hydrol., 331(1-2)*, 3-17.

Kijazi, A.L., Reason, C.J.C., 2009. Analysis of the 2006 floods over northern Tanzania. *Int. J. Climatol., 29(7)*, 955-970.

Knapp, K.R., Kruk, M.C., Levinson, D.H., Diamond, H.J., Neumann, C.J., 2010. The international best track archive for climate stewardship (IBTrACS) unifying tropical cyclone data. Bull. *Am. Meteorol. Soc., 91(3)*, 363-376.

Knapp, K.R., Ansari, S., Bain, C.L., Bourassa, M.A., Dickinson, M.J., Funk, C., Helms, C.N., Hennon, C.C., Holmes, C.D., Huffman, G.J., Kossin, J.P., 2011. Globally gridded satellite observations for climate studies. *Bull. Amer. Meteor. Soc., 92(7)*, 893-907.

Koungue, R.A.I., Rouault, M., Illig, S., Brandt, P., Jouanno, J., 2019. Benguela Niños and Benguela Niñas in forced ocean simulation from 1958 to 2015. *J. Geophys. Res., 124(8)*, 5923-5951.

Kug, J.S., Jin, F.F., An, S.I., 2009. Two types of El Niño events: Cold tongue El Niño and warm pool El Niño. *J. Clim., 22*, 1499-1515.

Kuhnel, I., 1989. Tropical-extratropical cloudband climatology based on satellite data. *Int. J. Climatol., 9*, 441-463.

Laing, A.G., Carbone, R. Levizzani, V., Tuttle, J., 2008. The propagation and diurnal cycles of deep convection in northern tropical Africa. *Quart. J. Roy. Meteor. Soc., 134(630)*, 93-109.

Lazenby, M.J., Todd, M.C., Wang, Y., 2016. Climate model simulation of the South Indian Ocean Convergence Zone: Mean state and variability. *Clim. Res., 68(1)*, 59-71.

Lazenby, M.J., Todd, M.C., Chadwick, R., Wang, Y., 2018. Future precipitation projections over central and southern Africa and the adjacent Indian Ocean: What causes the changes and the uncertainty?. *J. Clim., 31(12)*, 4807-4826.

Leroux, M., 2001. The meteorology and climate of tropical Africa. Springer Science &

Business Media.

Lima, D.C., Soares, P.M., Semedo, A., Cardoso, R.M., 2018. A global view of coastal low-level wind jets using an ensemble of reanalyses. *J. Clim., 31(4),* 1525-1546.

Lindesay, J.A., 1988. South African rainfall, the Southern Oscillation and a Southern Hemisphere semi-annual cycle. *J. climatol., 8(1),* 17-30.

Luo, N., Mao, D., Wen, B., Liu, X., 2020. Climate Change Affected Vegetation Dynamics in the Northern Xinjiang of China: Evaluation by SPEI and NDVI. *Land, 9(3),* 90.

Lyon, B., 2009. Southern Africa summer drought and heat waves: observations and coupled model behaviour. *J. Clim. 22(22),* 6033-6046.

Lyon, B., Mason, S.J., 2007. The 1997–98 summer rainfall season in southern Africa. Part I: Observations. *J. Clim., 20(20),* 5134-5148.

MacKellar, N., New, M., Jack, C., 2014. Observed and modelled trends in rainfall and temperature for South Africa: 1960-2010. *S. Afr. J. Sci., 110(7-8),* 1-13.

Macron, C., Pohl, B., Richard, Y., Bessafi., M., 2014. How do tropical temperate troughs form and develop over southern Africa? *J. Clim., 27(4),* 1633-1647.

Maddox, R.A., 1980. Mesoscale convective complexes. Bull. *Amer. Meteor. Soc., 61,* 1374-1387.

Magole, L., Thapelo, K., 2005. The impact of extreme flooding of the Okavango River on the livelihood of the molapo farming community of Tubu village, Ngamiland Sub-district, Botswana. *Botsw. Notes Rec., 7(1),* 125-137.

Mahlalela, P.T., Blamey, R.C., Reason, C.J.C., 2019. Mechanisms behind early winter rainfall variability in the southwestern Cape, South Africa. *Clim. Dyn., 53(1),* 21-39.

Mahlalela, P.T., Blamey, R.C., Hart, N.C.G., Reason, C.J.C., 2020. Drought in the Eastern Cape region of South Africa and trends in rainfall characteristics. *Clim. Dyn., 55(9)*, 2743-2759.

Malan, N., Reason, C.J.C., Loveday, B.R., 2013. Variability in tropical cyclone heat potential over the Southwest Indian Ocean. *J. Geophys. Res. Oceans, 118(12)*, 6734-6746.

Malherbe, J., Landman, W.A., Engelbrecht, F.A., 2014. The bi–decadal rainfall cycle, Southern Annular Mode and tropical cyclones over the Limpopo River Basin, southern Africa. *Clim. Dyn., 42(11-12)*, 3121–3138.

Malherbe, J., Engelbrecht, F.A., Landman, W.A., Engelbrecht, C.J., 2012. Tropical systems from the southwest Indian Ocean making landfall over the Limpopo River Basin, southern Africa: a historical perspective. *Int. J. Climatol., 32*, 1018-1032.

Malo, A.R., Nicholson, S.E., 1990. A study of rainfall and vegetation dynamics in the African Sahel using normalized difference vegetation index. *J. Arid Environ., 19(1)*, 1-24.

Manhique, A.J., Reason, C.J.C., Rydberg, L., Fauchereau, N., 2011. ENSO and Indian Ocean sea surface temperatures and their relationships with tropical temperate troughs over Mozambique and the Southwest Indian Ocean. *Int. J. Climatol., 31*, 1-13.

Manhique, A.J., Reason, C.J.C., Silinto, B., Zucula, J., Raiva, I., Congolo, F., Mavume, A.F., 2015. Extreme rainfall and floods in southern Africa in January 2013 and associated circulation patterns. *Nat. Hazards, 77(2)*, 679-691.

Mann, H.B., 1945. Nonparametric tests against trend. *Econometric, 13(3)*, 245-259.

Marshall, G.J., 2003. Trends in the Southern Annular Mode from observations and reanalyses. *J. clim., 16(24)*, 4134-4143.

Martiny, N., Philippon, N., Richard, Y., Camberlin, P., Reason, C.J.C., 2010. Predictability of NDVI in semi-arid African regions. *Theor. Appl. Climatol., 100(3)*, 467-484.

Mason, S.J., 1995. Sea-surface temperature-South African rainfall associations, 1910-1989. *Int. J. Climatol., 15*, 119-135.

Mason, S.J., Jury, M.R., 1997. Climatic variability and change over southern Africa: a reflection on underlying processes. *Prog. Phys. Geogr., 21(1)*, 23-50.

Maúre, G., Pinto, I., Ndebele–Murisa, M., Muthige, M., Lennard, C., Nikulin, G., Dosio, A., Meque, A., 2018. The southern African climate under 1.5°C and 2°C of global warming as simulated by CORDEX regional climate models. *Environ. Res. Lett., 13(6),* 065002.

Mavume, A.F., Rydberg, L., Rouault, M., Lutjeharms, J.R., 2009. Climatology and landfall of tropical cyclones in the southwest Indian Ocean. *West. Indian Ocean J. Mar. Sci., 8(1),* 15-36.

Mawren, D., Hermes, J., Reason, C.J.C., 2020. Exceptional tropical cyclone Kenneth in the far northern Mozambique Channel and ocean eddy influences. *Geophys. Res. Lett., 47(16),* e2020GL088715.

Mbaiwa, J.E., 2004. The socio–economic benefits and challenges of a community–based safari hunting tourism in the Okavango Delta, Botswana. *J. Tour. Stud.*, 15(2), 37.

Mbaiwa, J.E., 2015. Ecotourism in Botswana: 30 years later. *J. Ecotourism*, 14(2-3), 204-222.

Mbaiwa, J.E., 2017. Poverty or riches: Who benefits from the booming tourism industry in Botswana?. *J. Contemp. Afr. Stud., 35(1),* 93-112.

McCarthy, T.S., Metcalfe, J., 1990. Chemical sedimentation in the semi-arid environment of the Okavango Delta, Botswana. *Chem. Geol., 89 (1-2),* 157-178.

McCarthy, J.M., Gumbricht, T., McCarthy, T., Frost, P., Wessels, K. and Seidel, F., 2003. Flooding patterns of the Okavango wetland Botswana between 1972 and 2000. *Ambio, 32(7),* 453-457.

McGregor, J.L., Dix, M.R., 2008. An updated description of the conformal-cubic atmospheric model. In High resolution numerical modelling of the atmosphere and ocean (51-75). New York: Springer.

Mendelson, J., el Obeid, S., 2004. Okavango River: The flow of lifeline. Cape Town: Struik Publishers and Research and Information Services of Namibia (RAISON).

Meque, A., Pinto, I., Maúre, G., Beleza, A., 2022. Understanding the variability of heatwave characteristics in southern Africa. *Weather Clim. Extremes*. https://doi.org/10.1016/j.wace.2022.100498.

Moalafhi, B.D., Evans, J.P., Sharma, A., 2016. Evaluating global reanalysis datasets for provision of boundary conditions in regional climate modelling. *Clim. Dyn., 47*, 2727-2745.

MODIS, 1999. MODIS Vegetation Index (MOD 13): Algorithm Theoretical Basis Document version 3. Available: http://modis.gsfc.nasa.gov/data/atbd/atbd_mod13.pdf [2022, November 9].

Morake, D.M., Blamey, R.C., Reason, C.J.C., 2021. Long-lived mesoscale convective systems over eastern South Africa. *J. Clim., 34(15)*, 6421-6439.

Morioka, Y., Engelbrecht, F., Behera, S.K., 2015. Potential sources of decadal climate variability over southern Africa. *J. Clim., 28(22)*, 8695-8709.

Morioka, Y., Tozuka, T., Masson, S., Terray, P., Luo, J.J., Yamagata, T., 2012. Subtropical dipole modes simulated in a coupled general circulation model. *J. Clim., 25(12)*, 4029-4047.

Moses, O., Hambira, W.L., 2018. Effects of climate change on evapotranspiration over the Okavango Delta water resources. *Phys. Chem. Earth, Parts A/B/C, 105*, 98-103.

Moses, O., Ramotonto, S., 2018. Assessing forecasting models on prediction of the tropical cyclone Dineo and the associated rainfall over Botswana. *Weather Clim. Extremes, 21*, 102-109.

Moses, O., Gondwe, M., 2019. Simulation of changes in the twenty-first century maximum temperatures using the statistical downscaling model at some stations in Botswana. *MESE, 5(3)*, 843-855.

Moses, O., Blamey, R.C., Reason, C.J.C., 2022. Relationships between NDVI, river discharge and climate in the Okavango River Basin region. *Int. J. Climatol., 42(2)*, 691-713.

Mpungose, N., Thoithi, W., Blamey, R.C., Reason, C.J.C., 2022. Extreme rainfall events in southeastern Africa during the summer. *Theor. Appl. Climatol., 150(1)*, 185-201.

Mueller, B., Seneviratne, S.I., 2012. Hot days induced by precipitation deficits at the global scale. *PNAS 109(31)*, 12398-12403.

Mulenga, H.M., Rouault, M., Reason, C.J.C., 2003. Dry summers over northeastern South Africa and associated circulation anomalies. *Clim Res, 25(1)*, 29-41.

Muller, A., Reason, C.J.C., Fauchereau, N., 2008. Extreme rainfall in the Namib Desert during late summer 2006 and influences of regional ocean variability. *Int. J. Climatol., 28(8)*, 1061-1070.

Munday, C., Washington, R., 2017. Circulation controls on southern African precipitation in coupled models: The role of the Angola Low. *J. Geophys. Res., 122(2)*, 861-877.

Munday, C., Washington, R., 2019. Controls on the diversity in climate model projections of early summer drying over southern Africa. *J. Clim., 32*, 3707-3725.

Murray-Hudson, M., Wolski, P., Ringrose, S., 2006. Scenarios of the impact of local and upstream changes in climate and water use on hydro-ecology in the Okavango Delta, Botswana. *J. Hydrol., 331(1-2)*, 73-84.

Nakamura, M., 2012. Impacts of SST anomalies in the Agulhas Current system on the regional climate variability. *J. Clim., 25(4)*, 1213-1229.

Ndarana, T., Mpati, S., Bopape, M.J., Engelbrecht, F., Chikoore, H., 2021. The flow and moisture fluxes associated with ridging South Atlantic Ocean anticyclones during the subtropical southern African summer. *Int. J. Climatol., 41*, E1000-E1017.

Ndarana, T., Rammopo, T.S., Chikoore, H., Barnes, M.A., Bopape, M.J., 2020. A quasi-geostrophic diagnosis of the zonal flow associated with cut-off lows over South Africa and surrounding oceans. *Clim. Dyn., 55(9)*, 2631-2644.

New, M., Hulme, M., Jones, P., 2000. Representing twentieth century space-time climate variability. Part II: development of 1901–96 monthly grids of terrestrial surface climate. *J. Clim., 13*, 2217-2238.

New, M., Hewitson, B., Stephenson, D.B., Tsiga, A., Kruger, A., Manhique, A., Gomez, B., Coelho, C.A., Masisi, D.N., Kululanga, E., Mbambalala, E., 2006. Evidence of trends in daily climate extremes over southern and west Africa. *J. Geophys. Res. Atmos., 111(D14)*. doi:10.1029/2005JD006289.

Nguyen, P., Shearer, E.J., Tran, H., Ombadi, M., Hayatbini, N., Palacios, T., Huynh, P., Braithwaite, D., Updegraff, G., Hsu, K., Kuligowski, B., 2019. The CHRS Data Portal, an easily accessible public repository for PERSIANN global satellite precipitation data. *Sci. data, 6(1)*, 1-10.

Nicholson, S.E., 2009. A revised picture of the structure of the “monsoon” and land ITCZ over West Africa. *Clim. Dyn., 32(7-8)*, 1155-1171.

Nicholson, S.E., 2018. The ITCZ and the seasonal cycle over equatorial Africa. *Bull. Am. Meteorol. Soc., 99(2)*, 337-348.

Nicholson, S.E., Entekhabi, D., 1987. Rainfall variability in equatorial and southern Africa: Relationships with sea surface temperatures along the southwestern coast of Africa. *J. Appl. Meteorol., 26(5)*, 561-578.

Nicholson, S.E., Farrar, T.J., 1994. The influence of soil type on the relationships between NDVI, rainfall, and soil moisture in semiarid Botswana. I. NDVI response to rainfall. *Remote Sens. Environ., 50(2),* 107-120.

Nicholson, S.E., Kim, J., 1997. The relationship of the El Niño-Southern Oscillation to African rainfall. *Int. J. Climatol. 17*, 117-135.

Pinheiro, H.R., Hodges, K.I., Gan, M.A., Ferreira, N.J., 2017. A new perspective of the climatological features of upper level cutoff lows in the Southern Hemisphere. *Clim. Dyn., 48*, 541-559.

Pinzon, J.E., Tucker, C.J., 2014. A non-stationary 1981–2012 AVHRR NDVI3g time series. *Remote Sens., 6(8),* 6929-6960.

Preethi, B., Sabin, T.B., Adedoyin, J.A., Ashok, K., 2015. Impacts of the ENSO Modoki and other tropical Indo-Pacific climate-drivers on African rainfall. *Sci. Rep., 5*, 16653. https://doi.org/10.1038/srep16653.

Ramos, A.M., Trigo, R.M., Liberato, M.L., 2014. A ranking of high-resolution daily precipitation extreme events for the Iberian Peninsula. *Atmos. Sci. Lett., 15*, 328-334.

Ramos, A.M., Trigo, R.M., Liberato, M.L., 2017. Ranking of multi-day extreme precipitation events over the Iberian Peninsula. *Int. J. Climatol., 37,* 607-620.

Ramos, A.M., Martins, M.J., Tomé, R., Trigo, R.M., 2018. Extreme precipitation events in summer in the Iberian Peninsula and its relationship with atmospheric rivers. *Front. Earth Sci., 6*, 110. 10.3389/feart.2018.00110.

Rapolaki, R.S., Reason, C.J.C., 2018. Tropical storm Chedza and associated floods over south-eastern Africa. *Nat. Hazards, 93,* 189-217.

Rapolaki, R.S., Blamey, R.C., Hermes, J.C., Reason, C.J.C., 2019. A classification of synoptic weather patterns linked to extreme rainfall over the Limpopo River Basin in southern Africa. *Clim. Dyn., 53(3-4)*, 2265-2279.

Rapolaki, R.S., Blamey, R.C., Hermes, J.C., Reason, C.J.C., 2020. Moisture sources associated with heavy rainfall over the Limpopo River Basin, southern Africa. *Clim. Dyn., 55(5)*, 1473-1487.

Rapolaki, R.S., Blamey, R.C., Hermes, J.C., Reason, C.J.C., 2021. Moisture sources and transport during an extreme rainfall event over the Limpopo River Basin, southern Africa. Atmos. Res., 264. https://doi.org/10.1016/j.atmosres.2021.105849.

Ratna, S.B., Behera, S., Ratnam, J.V., Takahashi, K., Yamagata, T., 2013. An index for tropical temperate troughs over southern Africa. *Clim. Dyn., 41(2)*, 421-441.

Ratnam, J.V., Behera, S.K., Masumoto, Y., Yamagata, T., 2014. Remote effects of El Niño and Modoki events on the austral summer precipitation of southern Africa. *J. Clim., 27(10)*, 3802-3815.

Ratnam, J.V., Behera, S.K., Masumoto, Y., Takahashi, K., Yamagata, T., 2011. Anomalous climatic conditions associated with the El Niño Modoki during boreal winter of 2009. *Clim. Dyn., 39*, 227-238.

Rácz, Z., Smith, R.K., 1999. The dynamics of heat lows. *Quart. J. Roy. Meteor. Soc., 125*, 225-252.

Reason, C.J.C., 1998. Warm and cold events in the southeast Atlantic/SWIO region and potential impacts on circulation and rainfall over southern Africa. *Meteorol. Atmos. Phys.*, 69, 49-66.

Reason, C.J.C., 2001a. Subtropical Indian Ocean SST dipole events and southern African rainfall. *Geophys. Res. Lett., 28(11)*, 2225-2227.

Reason, C.J.C., 2001b. Evidence for the influence of the Agulhas Current on regional atmospheric circulation patterns. *J. Clim., 14(12)*, 2769-2778.

Reason, C.J.C., 2002. Sensitivity of the southern African circulation to dipole sea surface temperature patterns in the South Indian Ocean. *Int. J. Climatol., 22,* 377-393.

Reason, C.J.C., 2007. Tropical cyclone Dera, the unusual 2000/01 tropical cyclone season in the South West Indian Ocean and associated rainfall anomalies over Southern Africa. *Meteorol. Atmos. Phys., 97*, 181-188.

Reason, C.J.C., 2016. The Bolivian, Botswana, and Bilybara Highs and Southern Hemisphere drought/floods. *Geophys. Res. Lett., 43(3)*, 1280-1286.

Reason, C.J.C., 2019. Low-frequency variability in the Botswana High and southern African regional climate. *Theor. Appl. Climatol. 137(1)*, 1321-1334.

Reason, C.J.C., Mulenga, H., 1999. Relationships between South African rainfall and SST anomalies in the southwest Indian Ocean. *Int. J. Climatol., 19(15)*, 1651-1673.

Reason, C.J.R., Rouault, M., 2002. ENSO-like decadal patterns and South African rainfall. *Geophys. Res. Lett., 29*, 1638. doi:10.1029/2002GL014663.

Reason, C.J.C., Keibel, A., 2004. Tropical cyclone Eline and its unusual penetration and impacts over the southern African mainland. *Weather Forecast*, *19(5)*, 789-805.

Reason, C.J.C., Jagadheesha, D., 2005. A model investigation of recent ENSO impacts over southern Africa. *Meteorol. Atmos. Phys., 89(1-4)*, 181-205.

Reason, C.J.C., Rouault, M., 2005. Links between the Antarctic Oscillation and winter rainfall over western South Africa. *Geophys. Res. Lett., 32(7)*.

Reason, C.J.C., Smart, S., 2015. Tropical southeast Atlantic warm events and associated rainfall anomalies over southern Africa. *Front. Environ. Sci., 3*, 24.

Reason, C.J.C., Hachigonta, S., Phaladi, R.F., 2005. Interannual variability in rainy season characteristics over the Limpopo region of southern Africa. *Int. J. Climatol.*, 25, 1835-1853.

Reason, C.J.C., Landman, W., Tennant, W., 2006. Seasonal to decadal prediction of southern African climate and its links with variability of the Atlantic Ocean. *Bull. Am. Meteorol. Soc., 87(7),* 941-955.

Reason, C., Allan, R., Lindesay, J., Ansell, T., 2000. ENSO and climatic signals across the Indian Ocean Basin in the global context: Part I, interannual composite patterns. *Int. J. Climatol., 20(11),* 1285-1327.

Rehbein, A., Ambrizzi, T., Mechoso, C.R., 2018. Mesoscale convective systems over the Amazon basin. Part I: climatological aspects. *Int. J. Climatol., 38(1),* 215-229.

Revermann, R., Finckh, M., Stellmes, M., Strohbach, B.J., Frantz, D., Oldeland, J., 2016. Linking land surface phenology and vegetation–plot databases to model terrestrial plant α–diversity of the Okavango Basin. *Remote Sens., 8(5),* 370.

Richard, Y., Poccard, I.J.I.J.O.R.S., 1998. A statistical study of NDVI sensitivity to seasonal and interannual rainfall variations in Southern Africa. *Int. J. Remote Sens., 19(15),* 2907-2920.

Richard, Y., Martiny, N., Rouault, M., Philippon, N., Tracol, Y., Castel, T., 2012. Multi-month memory effects on early summer vegetative activity in semi-arid South Africa and their spatial heterogeneity. *Int. J. Remote Sens., 33(21),* 6763-6782.

Richard, Y., Martiny, N., Fauchereau, N., Reason, C., Rouault, M., Vigaud, N., Tracol, Y., 2008. Interannual memory effects for spring NDVI in semi-arid South Africa. *Geophys. Res. Lett., 35(13).*

Ringrose, S., Matheson, W., Boyle, T., 1988. Differentiation of ecological zones in the Okavango Delta, Botswana by classification and contextural analyses of Landsat MSS data. *Photogramm. Eng. Remote Sens., 54(5),* 601-608.

Rocha, A., Simmonds, I., 1997. Interannual variability of south-eastern African summer rainfall. Part I: Relationships with air-sea interaction processes. *Int. J. Climatol., 17(3),* 235-265.

Rockström, J., Falkenmark, M., 2000. Semiarid crop production from a hydrological perspective: gap between potential and actual yields. *Crit. Rev. Plant. Sci., 19(4)*, 319-346.

Rouault, M., Richard, Y., 2003. Intensity and spatial extension of drought in South Africa at different time scales. *Water SA, 29(4)*, 489-500.

Rouault, M., Florenchie, P., Fauchereau, N., Reason, C., 2003a. Southeast tropical Atlantic warm events and southern African rainfall. *Geophys. Res. Lett.*, 30(5).

Rouault, M., Reason, C.J.C., Lutjeharms, J.R.E., Beljaars, A., 2003b. Underestimation of latent and sensible heat fluxes above the Agulhas Current in NCEP and ECMWF analyses. *J. Clim., 16*, 776-782.

Rouault, M., Illig, S., Lübbecke, J., Koungue, R.A.I., 2018. Origin, development and demise of the 2010–2011 Benguela Niño. *J. Mar. Syst., 188*, 39-48.

Rouault, M., White, S.A., Reason, C.J.C., Lutjeharms, J.R.E., Jobard, I., 2002. Ocean–atmosphere interaction in the Agulhas current region and a South African extreme weather event. *Weather Forecast, 17(4)*, 655-669.

Shannon, L.V., Boyd, A.J., Brundrit, G.B., Taunton-Clark, J., 1986. On the existence of an El Niño-type phenomenon in the Benguela system. *J. Mar. Res., 44(3)*, 495-520.

Sillmann, J., Kharin, V.V., Zhang, X., Zwiers, F.W., Bronaugh, D., 2013. Climate extremes indices in the CMIP5 multimodel ensemble: Part 1. *J. Geophys. Res. Atmos., 118(4)*, 1716-1733.

Singleton, A.T., Reason, C.J.C., 2006. Numerical simulations of a severe rainfall event over the Eastern Cape coast of South Africa: sensitivity to sea surface temperature and topography. *Tellus A: Dyn. Meteorol., 58(3)*, 335-367.

Singleton, A.T., Reason, C.J.C., 2007. Variability in the characteristics of cut-off low pressure systems over subtropical southern Africa. *Int. J. Climatol., 27*, 295-310.

SMEC, 1986. Southern Okavango Integrated Water Development Study. Gaborone: Department of Water Affairs.

Smith, P., 1976. An outline of the vegetation of the Okavango drainage system. Gaborone: Symposium on the Okavango Delta and its future utilization.

Smith, T.M., Reynolds, R.W., Peterson, T.C., Lawrimore, J., 2008. Improvements to NOAA's historical merged land-ocean surface temperature analysis (1880-2006). *J. Clim., 21*, 2283-2296.

Ta, S., Kouadio, K.Y., Ali, K.E., Toualy, E., Aman, A., Yoroba, F., 2016. West Africa extreme rainfall events and large-scale ocean surface and atmospheric conditions in the tropical Atlantic. *Adv. Meteorol.*, 1-14.

Tadeschi, R.G., Iracema, F., Cavalcantia, A., Grimm, A.M., 2013. Influences of two types of ENSO on South American precipitation. *Int. J. Climatol., 33*, 1382-1400.

Taljaard, J.J.,1972. Synoptic meteorology of the Southern Hemisphere. Meteorology of the Southern Hemisphere, C.W. Newton, Ed., Amer. Meteor. Soc., 139-213.

Taljaard, J.J., 1986. Change of rainfall distribution and circulation patterns over southern Africa in summer. *J. Climatol., 6*, 579-592.

Taschetto, A.S., Haarsma, R.J., Sen Gupta, A., Ummenhoffer, C.C., Hill, K.J., England, M. H., 2010. Australian monsoon variability driven by a Gill–Matsuno type response to central western Pacific warming. *J. Clim., 23*, 4717-4736.

Taylor, K.E., Stouffer, R.J., Meehl, G.A., 2012. An overview of CMIP5 and the experiment design. *Bull. Am. Meteorol. Soc., 93(4)*, 485-498.

Thoithi, W., Blamey, R.C., Reason, C.J.C., 2021. Dry spells, wet days and their trends across southern Africa during the summer rainy season. *Geophys. Res. Lett., 48(5)*, e2020GL091041.

Thompson, B. W., 1965. The Climate of Africa. Oxford University Press.

Thompson, D.W.J., Wallace, J.M., 2000. Annular modes in the extratropical circulation. Part I: Month-to-month variability. *J. Clim., 13*, 1000-1016.

Todd, M.C., Washington, R., 1999. Circulation anomalies with tropical-temperate troughs in southern Africa and the south west Indian Ocean. *Clim. Dyn., 15*, 937-951.

Torrance, J.D., 1979. Upper windflow patterns in relation to rainfall in south-east central Africa. *Weather, 34*, 106-115.

Tucker, C.J., Dregne, H.E., Newcomb, W.W., 1991. Expansion and contraction of the Sahara Desert from 1980 to 1990. *Science, 253*, 299-301.

Tucker, C.J., Pinzon, J.E., Brown, M.E., Slayback, D.A., Pak, E.W., Mahoney, R., Vermote, E.F., El Saleous, N., 2005. An extended AVHRR 8-km NDVI dataset compatible with MODIS and SPOT vegetation NDVI data. *Int. J. Remote Sens., 26(20)*, 4485-4498.

Tyson, P.D., 1986. Climatic change and variability in southern Africa. USA: Oxford University Press.

Tyson, P.D., Preston-Whyte, R.A., 2000. The Weather and Climate of Southern Africa. Oxford University Press.

Tyson, P. D., Preston-Whyte, R.A., 2015. The Weather and Climate of Southern Africa. Oxford University Press.

Tyson, P.D., Dyer, T.G., Mametse, M.N., 1975. Secular changes in South African rainfall: 1880 to 1972. *Q. J. R. Meteorol. Soc., 101(430)*, 817-833.

UNESCO, 2014. Okavango Delta. Available: http://whc.unesco.org/en/list/1432 [2022, August 15].

UNICEF, 2022. Children's lives and rights at risk due to KwaZulu-Natal floods. Available: https://www.unicef.org/southafrica/press-releases/childrens-lives-and-rights-risk-due-kwazulu-natal-floods [2022, August 10].

Usman, M.T., Reason, C.J.C., 2004. Dry spell frequencies and their variability over southern Africa. *Clim. Res. 26(3)*, 199-211.

VanderPost, C., Ringrose, S., Seely, M., 2005. Preliminary land–use and land–cover mapping in the upper Okavango basin and implications for the Okavango delta. *Botsw. Notes Rec.*, *37(1)*, 236-252.

Venegas, S.A., Mysak, L.A., Straub, D.N., 1997. Atmosphere–ocean coupled variability in the South Atlantic. *J. Clim., 10(11)*, 2904-2920.

Vicente-Serrano, S.M., Beguería, S., López-Moreno, J.I., 2010. A multiscalar drought index sensitive to global warming: the standardized precipitation evapotranspiration index. *J. Clim., 23(7)*, 1696-1718.

Vicente-Serrano, S.M., Van der Schrier, G., Beguería, S., Azorin-Molina, C., Lopez-Moreno, J.I., 2015. Contribution of precipitation and reference evapotranspiration to drought indices under different climates. *J. Hydrol., 526*, 42-54.

Vigaud, N., Richard, Y., Rouault, M., Fauchereau, N., 2009. Moisture transport between the South Atlantic Ocean and southern Africa: relationships with summer rainfall and associated dynamics. *Clim. Dyn., 32(1)*, 113-123.

Wainwright, C.M., Black, E., Allan, R.P., 2021. Future changes in wet and dry season characteristics in CMIP5 and CMIP6 simulations. *J. Hydrometeorol., 22(9)*, 2339-2357.

Walker, N.D., 1990. Links between South African summer rainfall and temperature variability of the Agulhas and Benguela Current systems. *J. Geophys. Res. Oceans, 95(C3)*, 3297-3319.

Walker, N.D., Mey, R.D., 1988. Ocean/atmosphere heat fluxes within the Agulhas Retroflection region. *J. Geophys. Res., 93*, 15473-15483.

Washington, R., Todd, M., 1999. Tropical-temperate links in Southern Africa and Southwest Indian Ocean satellite-derived daily rainfall. *Int. J. Climatol., 19*, 1601-1616.

Washington, R., Preston, A., 2006. Extreme wet years over southern Africa: Role of Indian Ocean sea surface temperatures. *J. Geophys. Res., 111(D15)*.

Weinzierl, T. Schilling, J., 2013. On demand, development and dependence: a review of current and future implications of socioeconomic changes for integrated water resource management in the Okavango Catchment of Southern Africa. *Land, 2(1)*, 60–80.

Weldon, D., Reason, C.J.C., 2014. Variability of rainfall characteristics over the South Coast region of South Africa. *Theor. Appl. Climatol., 115(1)*, 177-185.

Weng, H., Behera, S.K., Yamagata, T., 2009. Anomalous winter climate conditions in the Pacific rim during recent El Niño Modoki and El Niño events. *Clim. Dyn., 32*, 663-674.

White, F., 1984. The Vegetation of Africa: A Descriptive Memoir to Accompany the Unesco/Aetfat/Unso Vegetation Map of Africa and Map. Paris: United Nations Educational.

Wilk, J., Kniveton, D., Andersson, L., Layberry, R., Todd, M., Hughes, D., Ringrose, S., Vanderpost, C., 2006. Estimating rainfall and water balance over the Okavango River basin for hydrological applications. *J. Hydrol., 331(1-2)*, 18-29.

Wingate, V.R., Phinn, S.R., Kuhn, N., 2019a. Mapping precipitation corrected NDVI trends across Namibia. *Sci. Total Environ., 684*, 96-112.

Wingate, V.R., Kuhn, N.J., Phinn, S.R., van der Waal, C., 2019b. Mapping trends in woody cover throughout Namibian savanna with MODIS seasonal phenological metrics and field inventory data. *Biogeosciences Discuss.*, 1-37.

Wolski, P., 2009. Assessment of hydrological effects of climate change in the Okavango Basin. OKACOM/EPSMO, Maun, Botswana.

Wolski, P., Murray-Hudson, M., 2006a. Flooding dynamics in a large low-gradient alluvial fan, the Okavango Delta, Botswana, from analysis and interpretation of a 30-year hydrometric record. *Hydrol. Earth Syst. Sci., 10(1),* 127-137.

Wolski, P., Murray-Hudson, M., 2006b. Recent changes in Xudum distributary of the Okavango Delta and Lake Ngami, Botswana. *S. Afr., 102,* 173-175.

Wolski, P., Murray-Hudson, M., 2008. "Alternative futures" of the Okavango Delta simulated by a suite of global climate and hydro-ecological models. *Water SA, 34(5),* 605-610.

Wolski, P., Savenije, H.H.G., Murray-Hudson, M., Gumbricht, T., 2006. Modelling of the hydrology of the Okavango Delta. *J. Hydrol., 331(1),* 58-72.

Wolski, P., Todd, M.C., Murray-Hudson, M.A., Tadross, M., 2012. Multi-decadal oscillations in the hydroclimate of the Okavango River system during the past and under a changing climate. *J. Hydrol., 475,* 294-305.

Wolski, P., Stone, D., Tadross, M., Wehner, M., Hewitson, B., 2014. Attribution of floods in the Okavango basin, Southern Africa. *J. Hydrol., 511,* 350-358.

Xie, P., Arkin, P.A., 1997. Global precipitation: A 17-year monthly analysis based on gauge observations, satellite estimates, and numerical model outputs. *Bull. Amer. Meteor., 78(11),* 2539-2558.

Yang, Y., Wang, S., Bai, X., Tan, Q., Li, Q., Wu, L., Tian, S., Hu, Z., Li, C., Deng, Y., 2019. Factors affecting long-term trends in global NDVI. *Forests, 10(5),* 372.

Ye, L., Shi, K., Xin, Z., Wang, C., Zhang, C., 2019. Compound droughts and heat waves in China. *Sustainability, 11(12),* 3270.

Yeh, S.W., Kug, J.S., Dewitte, B., Kwon, M.H., Kirtman, B.P. and Jin, F.F., 2009. El Niño in a changing climate. *Nature, 461(7263),* 511-514.

Yu, M., Li, Q., Hayes, M.J., Svoboda, M.D., Heim, R.R., 2014. Are droughts becoming more frequent or severe in China based on the standardized precipitation evapotranspiration index: 1951-2010?. *Int. J. Climatol., 34(3),* 545-558.

Yue, S., Wang, C.Y., 2002. Applicability of prewhitening to eliminate the influence of serial correlation on the Mann-Kendall test. *Water Resour. Res., 38(6),* 4-1.

Yue, S., Pilon, P., Phinney, B., Cavadias, G., 2002. The influence of autocorrelation on the ability to detect trend in hydrological series. *Hydrol. Process, 16(9),* 1807-1829.

Zhang, Q., Körnich, H., Holmgren, K., 2013. How well do reanalyses represent the southern African precipitation? *Clim. Dyn., 40(3-4),* 951-962.

Zhang, X., Alexander, L., Hegerl, G.C., Jones, P., Tank, A.K., Peterson, T.C., Trewin, B., Zwiers, F.W., 2011. Indices for monitoring changes in extremes based on daily temperature and precipitation data. *Wiley Interdiscip. Rev. Clim. Change, 2(6),* 851-870.